



Universidade do Minho
Escola de Ciências

Maria Solange Dantas de Carvalho

**New heterocyclic bioactive fluorescent
compounds: spectroscopic studies of DNA
interactions and encapsulation in
nanoliposomes**

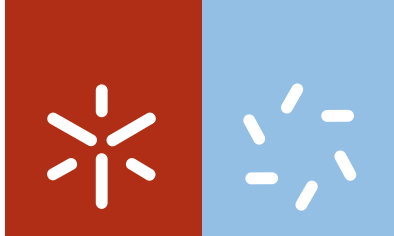
**New heterocyclic bioactive fluorescent compounds: spectroscopic
studies of DNA interactions and encapsulation in nanoliposomes**

Maria Solange Dantas de Carvalho

UMinho | 2013

agosto de 2013





Universidade do Minho

Escola de Ciências

Maria Solange Dantas de Carvalho

**New heterocyclic bioactive fluorescent
compounds: spectroscopic studies of DNA
interactions and encapsulation in
nanoliposomes**

Tese de Doutoramento em Ciências
Especialidade em Química

Trabalho realizado sob a orientação da

Doutora Maria-João Ribeiro Peixoto de Queiroz
(Investigadora Coordenadora)

e da

Doutora Elisabete Maria Santos Castanheira Coutinho
(Professora Auxiliar)

É autorizada a reprodução integral desta tese apenas para efeitos de investigação, mediante declaração escrita da interessada, que a tal se compromete.

Universidade do Minho, 06 de Agosto de 2013

Assinatura: _____

“Quand les mystères sont très malins, ils se cachent dans la lumière.”

Jean Giono

*Ao Rui,
à Luana e ao Gil,
os amores da minha vida*

Acknowledgements

Não poderia terminar esta etapa importante da minha vida sem agradecer a todas as pessoas que me apoiaram ao longo deste caminho.

As minhas primeiras palavras são para a Doutora Elisabete Coutinho e para a Doutora Maria-João Queiroz por quem tenho uma profunda admiração, não só por serem excelentes orientadoras científicas mas também excelentes pessoas. À Doutora Elisabete agradeço a amizade mas também a paciência e a disponibilidade demonstradas em tirar todas as minhas incessantes dúvidas ao longo destes anos! À Doutora Maria-João agradeço ter apostado em mim sem me conhecer, já lá vão oito anos! Desde esse dia, nunca deixou de me apoiar, tanto profissionalmente como pessoalmente, estando presente nos momentos felizes mas também nos momentos mais tristes e difíceis. Nunca sonhava que o facto de as conhecer me levaria à conclusão de um mestrado e de um doutoramento, mais uma vez muito obrigada!

À Fundação para a Ciência e Tecnologia (FCT), ao POPH-QREN e ao FSE, pela Bolsa de Doutoramento (SFRH/BD/47052/2008) que me foi concedida; ao FEDER e ao QREN pelo apoio financeiro à Escola de Ciências; ao CFUM [Projeto estratégico PEst-C/FIS/UI0607/2011 (F-COMP-01-0124-FEDER-022711) e ao CQ/UM [Projeto estratégico PEst-C/QUI/UI0686/2011 (FCOMP-01-0124-FEDER-022716)], assim como ao projeto de investigação PTDC/QUI/81238/2006 (FCOMP-01-0124-FEDER-007467) também financiado pelo COMPETE/QREN/EU.

Aos Diretores dos Departamentos e Centros de Química e de Física da Universidade do Minho, pelo acolhimento e as facilidades concedidas na utilização dos laboratórios e dos equipamentos indispensáveis à concretização do meu trabalho.

Agradeço ao Doutor Paulo Coutinho, pela gentileza e disponibilidade demonstradas em ajudar-me sempre que surgiu algum problema técnico e pelos cálculos de mecânica quântica molecular.

Agradeço à colega e amiga Ana Sofia Abreu, pelos bons conselhos, ajuda e apoio ao longo deste trabalho.

Ao Rui, minha cara metade, pelo incentivo, apoio e paciência demonstrados ao longo destes anos, e à Luana e ao Gil, os meus tesourinhos que são a minha fonte de energia! Os três juntos constituem o meu motor e o desejo de sentir que têm orgulho em mim é que me leva a tentar ultrapassar-me cada dia mais.

Aos meus pais, Manuel e Maria, pelo amor, amizade, ajuda e incentivo demonstrados ao longo de toda a minha vida. Ensinarão-me a lutar sempre pelos meus sonhos, riscando a palavra “desistir” do meu vocabulário. Sem essa educação, nunca teria chegado tão longe...

Ao meu irmão mas também melhor amigo, Daniel, a quem posso dizer tudo e que sempre me apoiou e aconselhou objetivamente tendo em mente o melhor para mim.

Aos restantes membros da minha família e amigos, agradeço todo o apoio e amizade demonstrados ao longo destes anos. Sentir-me rodeada e apoiada por tanta gente foi um fator-chave para terminar esta longa caminhada.

Sem estas pessoas todas, nada teria sido possível...



Abstract

New heterocyclic bioactive fluorescent compounds: spectroscopic studies of DNA interactions and encapsulation in nanoliposomes

Spectroscopic studies (absorption and steady-state fluorescence) of potential antitumoral heteroaryl and heteroannulated indoles, benzothienopyran-1-ones, methyl 3-amino-6-heteroarylthieno[3,2-*b*]pyridine-2-carboxylates, tetracyclic thieno[3,2-*b*]pyridine derivatives and benzothienoquinolines, synthesized in our research group, were performed in solvent of different polarities. Generally, all the compounds presented a solvent sensitive emission with significant red-shifts in polar solvents, pointing out for their potential use as solvatochromic probes.

The antitumoral potential of some of the compounds was evaluated by the growth inhibition of human tumor cell lines in collaboration with the Faculty of Pharmacy of the University of Porto.

The spectroscopic properties of the compounds were also evaluated when incorporated in liposomes of neat lipids and lipid mixtures of different formulations, including, Egg-PC (egg yolk phosphatidylcholine), DPPC (dipalmitoyl phosphatidylcholine), DPPG (dipalmitoyl phosphatidylglycerol), DMPG (dimyristoyl phosphatidylglycerol), DOPE (dioleoyl phosphatidylethanolamine), DSPE-PEG (Distearoyl phosphatidylethanolamine-polyethylene glycol), DODAB (Dioctadecyldimethylammonium bromide) and cholesterol.

Fluorescence steady-state anisotropy measurements allowed monitoring the location and behaviour of the compounds in the liposomes. In most cases, they showed to be located mainly in the hydrophobic region of the lipid bilayers, experiencing differences in fluidity between the rigid gel and the liquid-crystalline phases. These studies of the antitumoral compounds encapsulation were made having in mind future drug delivery applications.

The mean size, size-distribution and zeta-potential of the liposomes incorporating the most promising antitumoral compounds, were determined by DLS (Dynamic Light

Scattering). Almost all the liposomes with the incorporated compounds have shown diameters under 165nm and, with some formulations like DPPC:DMPG:DSPE-PEG (1:1:0.1), small diameters (below 100nm), low polydispersity and reasonable negative zeta-potential values were obtained for two of the methyl 3-amino-6-heteroarylthieno[3,2-*b*]pyridine-2-carboxylates studied.

In order to evaluate the interaction with nucleic acids, the binding modes of the tetracyclic planar fluorescent thieno[3,2-*b*]pyridine derivatives and of the benzothienoquinolines to salmon sperm DNA and/or to synthetic double-stranded (*ds*) heteropolynucleotides were studied using spectroscopic methods which allowed the determination of intrinsic binding constants (K_i) and binding site sizes (n). Fluorescence quenching experiments with iodide ion were also performed in order to distinguish between the different binding modes of the compounds to the nucleic acids studied, since intercalated molecules are less accessible to anionic quenchers due to electrostatic repulsion with negatively charged nucleic acids. All the compounds interact with DNA and polynucleotides either by intercalation or groove binding. The latter seems to be the main type of interaction of these compounds with nucleic acids.

Resumo

Novos compostos heterocíclicos bioativos fluorescentes: estudos espectroscópicos de interação com DNA e incorporação em nanolipossomas.

Foram realizados estudos espectroscópicos (absorção e fluorescência em estado estacionário) de heteroarilindoles e indoles heteroanelados, benzotienopiran-1-onas, 3-amino-6-heteroariltieno[3,2-*b*]piridina-2-carboxilatos de metilo, derivados tetracíclicos de tieno[3,2-*b*]piridinas e benzotienoquinolinas com potencial antitumoral, sintetizados no nosso grupo de investigação, em solventes de diferentes polaridades.

De um modo geral, todos os compostos apresentaram uma emissão sensível ao solvente com significativos desvios para vermelho em meios polares, indicando a sua potencial utilização como sondas solvatocrómicas.

O potencial antitumoral de alguns dos compostos foi avaliado através da inibição do crescimento de linhas celulares tumorais humanas em colaboração com a Faculdade de Farmácia da Universidade do Porto.

As propriedades espectroscópicas foram também avaliadas para os compostos incorporados em lipossomas de lípidos puros e misturas lipídicas de diferentes formulações, incluindo, Egg-PC (fosfatidilcolina do ovo), DPPC (dipalmitoilfosfatidilcolina), DPPG (dipalmitoilfosfatidilglicerol), DMPG (dimiristoilfosfatidilglicerol), DOPE (dioleoilfosfatidiletanolamina), DSPE-PEG (Distearoil fosfatidiletanolamina-polietilenoglicol), DODAB (Brometo de dioctadecildimetilamónio) e colesterol.

Medidas de anisotropia de fluorescência em estado estacionário permitiram monitorizar a localização dos compostos nos lipossomas. Na maioria dos casos, os compostos mostraram estar localizados maioritariamente na região hidrofóbica da bicamada lipídica, sentindo diferenças de fluidez entre a fase-gel e a fase líquido-cristalina dos lípidos. Estes estudos de encapsulação dos compostos antitumorais foram realizados tendo em vista aplicações futuras de libertação de fármacos.

O tamanho médio, distribuição de tamanhos e potencial-zeta dos lipossomas incorporando os compostos antitumorais mais promissores foram avaliados através de medidas de DLS (Difusão de Luz Dinâmica). A maioria dos lipossomas mostrou possuir diâmetros menores que 165nm e, algumas formulações como DPPC:DMPG:DSPE-PEG (1:1:0.1), exibiram tamanhos menores que 100nm e baixa polidispersividade. Valores de potencial-zeta razoavelmente negativos foram obtidos para dois dos 3-amino-6-heteroariltieno[3,2-*b*]piridina-2-carboxilatos de metilo estudados.

Para avaliar a interação com os ácidos nucleicos, os modos de ligação dos derivados tetracíclicos fluorescentes planares de tieno[3,2-*b*]piridinas e de benzotienoquinolinas ao DNA de esperma de salmão e heteropolinucleótidos sintéticos de cadeia dupla, foram estudados usando métodos espectroscópicos que permitiram a determinação das constantes de ligação (K_i) e tamanho dos sítios de ligação (n).

Medidas de inibição de fluorescência pelo ião iodeto foram também realizadas para distinguir entre os diferentes modos de ligação dos compostos aos ácidos nucleicos estudados, uma vez que as moléculas intercaladas estão menos acessíveis a inibidores aniônicos devido às repulsões eletrostáticas com os ácidos nucleicos carregados negativamente. Todos os compostos interatuam com o DNA e polinucleótidos ou por intercalação, ou por ligação nos sulcos (*grooves*). Este modo de ligação parece ser o tipo de interação predominante dos compostos com os ácidos nucleicos.

General index

Acknowledgements.....	vii
Abstract	ix
Resumo.....	xi
General Index.....	xiii
Figures index.....	xvii
Schemes Index	xxi
Tables index.....	xxiii
Abbreviations list	xxv
Thesis outline.....	xxix
Compounds list	xxxii

Chapter 1 – New potential antitumoral fluorescent heterocyclic compounds

1. Introduction	5
2. Heteroaryl and heteroannulated indoles.....	6
3. Benzothienopyranones	12
4. Thienopyridines	16
5. Benzothienoquinolines.....	20
6. References	22

Chapter 2 – Compounds /DNA interaction

1. Deoxyribonucleic acid (DNA)	31
2. DNA binding modes.....	36
2.1. Outside-edge binding.....	38
2.2. Intercalation/bisintercalation	38
2.3. Minor and major DNA grooves binding interaction	41
2.4. Thermodynamics of drug-DNA interactions	42
2.5. Methods to determine the DNA-drug binding modes	43
3. References	45

Chapter 3 – Compounds encapsulation in nanoliposomes

1. Nanocarriers for drug delivery	53
2. Liposomes	57
2.1. Lipids as structural components of liposomes	57
2.2. Molecular Self-assembly	59
2.3. Different types of liposomes	60
2.4. Liposomes preparation	61
3. Liposomes as drug delivery systems	63
4. Determination of the size and zeta-potential of the liposomes with incorporated compounds	67
5. References	71

Chapter 4 – Molecular Fluorescence spectroscopy

1. Introduction	81
2. Fluorescence as a particular case of Luminescence.....	85
3. Absorption of UV-Visible light	89
3.1. Molecular orbitals and electronic transitions	89
3.2. Selection rules for electronic transitions	91
3.4. Probability of transitions. The Beer-Lambert law	95
4. De-excitation processes of excited molecules.....	101
5. Characteristics of fluorescence emission	108
5.1. Fluorescent probes	108
5.2. Lifetimes and quantum yields	109
5.3. Emission and excitation spectra	112
5.4. Effects of molecular structure on fluorescence	115
5.5. Solvent and environmental effects on fluorescence emission spectra.....	117
5.5.1. Effects of solvent polarity and viscosity	118
5.5.2. Compounds submitted to photoinduced Intramolecular Charge Transfer (ICT) and internal rotation	129
5.5.3. Changes in the non-radiative decay rates	130
5.5.4. Changes in the radiative decay rates.....	131
5.5.5. Probe-probe interactions.....	132

5.6. Resolution of Fluorescence spectra.....	132
6. Quenching of fluorescence.....	133
6.1. Quenchers of fluorescence.....	134
6.2. Collisional quenching (dynamic quenching).....	135
6.3. Static quenching.....	138
6.4. How to distinguish between dynamic and static quenching.....	140
6.5. Simultaneous dynamic and static quenching.....	141
6.6. Some applications of quenching.....	142
6.7. Experimental considerations in quenching.....	143
7. Fluorescence anisotropy.....	145
7.1. Polarization ratio and emission anisotropy.....	147
7.2. Relation between anisotropy and the absorption and emission dipoles orientation.....	150
7.2.1. Parallel absorption and emission transition moments.....	150
7.2.2. Non-parallel absorption and emission transition moments.....	153
7.3. Causes of depolarization.....	154
7.3.1. Resonance Energy Transfer (RET).....	155
7.3.2. Rotational Brownian motion: the Perrin equation.....	156
7.3.3. Experimental causes of depolarization.....	158
7.4. Applications of fluorescence polarization.....	159
8. References.....	161

Chapter 5- Results and discussion as a compilation of articles

5.1. Fluorescence Studies on Potential Antitumoral Heteroaryl and Heteroannulated Indoles in Solution and in Lipid Membranes.....	171
5.2. Fluorescence Studies on New Potential Antitumoral Benzothienopyran-1-ones in Solution and in Liposomes.....	183
5.3. New potential antitumoral fluorescent tetracyclic thieno[3,2-<i>b</i>]pyridine derivatives: interaction with DNA and nanosized liposomes.....	197
5.4. Fluorescence studies on potential antitumor 6-(hetero)arylthieno[3,2-<i>b</i>]pyridine derivatives in solution and in nanoliposomes.....	207

5.5. Benzothienoquinolines: new one pot synthesis and fluorescence studies of their interaction with DNA and polynucleotides	221
Chapter 6 – Conclusions and future perspectives.....	241

Figures index

Chapter 1 - New potential antitumoral fluorescent heterocyclic compounds

Figure 1.1. Indole, L-Tryptophan and Serotonin structures	6
Figure 1.2. General structures of 2-pyrones and isocoumarins.....	12
Figure 1.3. Isomeric thienopyridine structures	16

Chapter 2 – Compounds / DNA interaction

Figure 2.1. Double-helix DNA structure	32
Figure 2.2. 2-Deoxyribose molecule (a) and 2-Deoxyribose residue in DNA (b)	32
Figure 2.3. DNA structure	33
Figure 2.4. Structure of DNA nucleobases, purines and pyrimidines.....	33
Figure 2.5. Complementary base pairing in DNA	34
Figure 2.6. Three views of DNA structure: schematic representation (a), atomic model (b), computer model (c)	34
Figure 2.7. Summary of mechanism of action of anticancer drugs	36
Figure 2.8. Drug-DNA non-covalent interactions a) schematic representation b) computer model	37
Figure 2.9. Structures of two outside-edge electrostatic DNA binding ligands, spermine and spermidine	38
Figure 2.10. Several DNA-intercalators which act as antitumoral drugs	39
Figure 2.11. A flexibly linked bisintercalator formed from two dimethylaminoethylacridine-4-carboxamide moieties	40
Figure 2.12. Schematic representation of the mechanism of cytotoxicity of a DNA-Intercalator	40
Figure 2.13. Distamycin A and Mithramycin A structures	41
Figure 2.14. (a) Atomistic structure of daunomycin. Constructed and equilibrated structures of (b) the intercalated state and (c) the minor groove-bound state.....	42

Chapter 3 – Compounds encapsulation in nanoliposomes

Figure 3.1. Typical structure of a phospholipid.....	57
Figure 3.2. Different self-organized structures.	60
Figure 3.3. Unilamellar liposome structure	60
Figure 3.4. Schematic representation of different liposomes	61
Figure 3.5. Active and passive targeting of cells for drug targeting using liposomes....	64
Figure 3.6. Schematic representation of zeta-potential	68
Figure 3.7. Different rates of the Brownian motion of particles according to their size and respective size-distribution curves	69

Chapter 4 – Molecular Fluorescence Spectroscopy

Figure 4.1. Plane-polarized electromagnetic radiation travelling along the x-axis.....	81
Figure 4.2. Regions of the electromagnetic spectrum	82
Figure 4.3. Types of luminescence processes and respective ways of molecule's excitation.....	87
Figure 4.4. Types of bonding and antibonding molecular orbitals	90
Figure 4.5. Illustration of the Franck-Condon principle.....	94
Figure 4.6. Potential energy diagrams with vertical transitions and respective absorption spectra	95
Figure 4.7. Illustration of the Beer-Lambert law	96
Figure 4.8. Integrated absorption coefficient of a transition	97
Figure 4.9. Naphthalene and anthracene with their absorption transition moments ..	99
Figure 4.10. A π (a) and a π^* (b) molecular orbital of ethylene.....	99
Figure 4.11. Definition of the Stokes shift	105
Figure 4.12. Shift to higher wavelengths of the fluorescence spectrum relative to the absorption spectrum due to interaction with solvent.....	106
Figure 4.13. Solvatochromic effects on fluorescence spectra	119

Figure 4.14. Lippert-Mataga plots for <i>N</i> -phenyl- <i>N</i> -methyl-2-aminonaphthalene-6-sulfonate and 2-aminonaphthalene-6-sulfonate	124
Figure 4.15. Fluorescence spectra of 2-acetylanthracene in methanol–hexane mixtures at 20°C	125
Figure 4.16. Effect of solvent composition on the emission maximum of 2-acetylanthracene	125
Figure 4.17. Stokes shifts of methyl 8-(2-anthroyl) octanoate in organic solvents and water	127
Figure 4.18. Normalized fluorescence emission spectra of 2-anilinonaphthalene in solvents and bound to vesicles of dimyristoyl-L- α -phosphatidylcholine (DMPC)	128
Figure 4.19. Stokes shifts and quantum yields for Coumarin-151 in various solvents	130
Figure 4.20. Sphere of effective quenching	138
Figure 4.21. Comparison between dynamic and static quenching	140
Figure 4.22. Simultaneous dynamic and static quenching by formation of a non-fluorescent complex.....	141
Figure 4.23. Natural, linearly polarized and partially polarized light	145
Figure 4.24. Transition moments and photoselection	146
Figure 4.25. Schematic diagram for measurement of fluorescence anisotropies	147
Figure 4.26. System of coordinates for characterizing the emission dipole orientation of one molecule	150
Figure 4.27. Excitation polarization spectra of fluorescein in propylene glycol at -50°C	156

Schemes index

Chapter 1 – New potential antitumoral fluorescent heterocyclic compounds

Scheme 1.1. Synthesis of the bis-Suzuki coupling products 1 and 2 , and their intramolecular C-N cyclization to the tetracyclic compounds 3 and 4	7
Scheme 1.2. General catalytic cycle of the Suzuki cross-coupling reaction for formation of Ar-Ar'	8
Scheme 1.3. Intramolecular C–N cyclization of the Suzuki cross-coupling products 1 and 2 , to the compounds 3 and 4	9
Scheme 1.4. Synthesis of heteroaryl and heteroannulated indoles 7-10 from the pure stereoisomers Suzuki cross-coupling products 5-E , 5-Z , 6-E and 6-Z	10
Scheme 1.5. Synthesis of the 3-arylbenzothieno[2,3- <i>c</i>]pyran-1-ones 11a-d	13
Scheme 1.6. General catalytic cycle of the copper-cocatalyzed Sonogashira reaction .	14
Scheme 1.7. Proposed intramolecular cyclization of the Sonogashira products using TFA	14
Scheme 1.8. Some of the methyl 3-amino-6-heteroarylthieno[3,2- <i>b</i>]pyridine-2-carboxylates synthesized by our research group by Suzuki-Miyaura cross-coupling	16
Scheme 1.9. Synthesis of compound 12d by a BSC reaction	17
Scheme 1.10. Catalytic cycle proposed for the boronation C-B using pinacolborane and Et ₃ N	18
Scheme 1.11. Synthesis of the tetracyclic thienopyrimidine derivatives 13	19
Scheme 1.12. One pot synthesis of benzothieno[3,2- <i>b</i>]quinoline 14 and benzothieno[2,3- <i>c</i>]quinoline 15	20

Chapter 3 – Compounds encapsulation in nanoliposomes

Scheme 3.1. Different methods for liposomes preparation	62
--	----

Chapter 4 – Molecular Fluorescence Spectroscopy

Scheme 4.1. Energy levels of molecular orbitals and possible allowed electronic transitions	90
Scheme 4.2. Energy levels of molecular orbitals and distinction between singlet and triplet state using formaldehyde as an example	93
Scheme 4.3. Perrin-Jablonski diagram, illustration of the relative positions of absorption, fluorescence and phosphorescence spectra and characteristic times for each transition process	102
Scheme 4.4. Absorption and de-excitation processes and respective rate constants	112
Scheme 4.5. Jablonski diagram for fluorescence with solvent relaxation	119
Scheme 4.6. Jablonski diagram and respective emission spectra for solvent relaxation	129
Scheme 4.7. The effects of polarity-induced inversion of $n-\pi^*$ and $\pi-\pi^*$ states.....	131
Scheme 4.8. Interaction of an excited molecule M^* and another molecule Q and respective rate constants	133
Scheme 4.9. Illustration of dynamic quenching	135
Scheme 4.10. Illustration of static quenching by formation of a ground-state non-fluorescent complex.....	139

Tables index

Chapter 1 – New potential antitumoral fluorescent heterocyclic compounds

Table 1.1. Heteroaryl and heteroannulated indoles **7-10** prepared via scheme 1.2 10

Chapter 3 – Compounds encapsulation in nanoliposomes

Table 3.1. Types of nanocarriers for drug delivery 55

Table 3.2. Structure, electric charge and phase transition temperature, T_m , of some lipids 58

Table 3.3. Liposome classification based on structural parameters 61

Chapter 4 – Molecular Fluorescence Spectroscopy

Table 4.1. Colour, frequency and energy of infrared, visible and ultraviolet light 83

Table 4.2. Deviation from linearity in the relation between fluorescence intensity and absorbance 114

Table 4.3. Parameters of the π^* scale of polarity 121

Table 4.4. Dielectric constant (at 20°C), refractive index (at 20°C) and orientational polarizability Δf of some solvents 122

Table 4.5. Relationship between the angular displacement of transition moments (β) and the fundamental anisotropy (r_0) or polarization (p_0) 154

Abbreviations list

A	adenine
2-AA	2-acetylanthracene
Ac	acetone
AcOH	acetic acid
2-AN	2-anilinonaphthalene
A(λ)	absorbance
Ar	aryl
B	benzene
BISC	back intersystem crossing
Boc	<i>tert</i> -butoxycarbonyl
BSC	borylation and Suzuki coupling
C	cytosine
CH	cyclohexane
Ch	chloroform
cm	centimeter
CPK	Corey-Pauling-Koltun
CRT	cathode ray tube
Cu(OAc) ₂	copper acetate
DEE	diethyl ether
DLS	dynamic light scattering
DME	dimethoxyethyl
DMF	<i>N,N</i> -dimethylformamide
DMPG	1,2-dimyristoyl- <i>sn</i> -glycero-3-[phospho- <i>rac</i> -(1-glycerol)] (sodium salt)
DMSO	dimethyl sulfoxide
DNA	deoxyribonucleic acid
DODAB	dioctadecyldimethylammonium bromide
DOPE	1,2-Dioleoyl- <i>sn</i> -glycero-3-phosphoethanolamine
DPPC	1,2-Dipalmitoyl- <i>sn</i> -glycero-3-phosphocholine

DPPG	1,2-dipalmitoyl- <i>sn</i> -glycero-3-[phospho- <i>rac</i> -(1-glycerol)] (sodium salt)
<i>ds</i>	double-stranded
DSPE-PEG	1,2-Distearoyl- <i>sn</i> -glycero-3-phosphoethanolamine- <i>N</i> -[methoxy(polyethylene glycol)-2000] (ammonium salt)
EA	Ethanol
EB	Ethidium bromide
Egg-PC	1,2-diacyl- <i>sn</i> -glycero-3-phosphocholine from egg yolk
EPR	electronic paramagnetic resonance
equiv.	equivalents
ESR	electron spin resonance
Et ₃ N	triethylamine
eV	electron volt
F	Franck-Condon state
G	Guanine
GHz	Gigahertz
GI ₅₀	Concentration that inhibits 50% of the cell growth
H	<i>n</i> -hexane
HBA	hydrogen bond acceptor
HBD	hydrogen bond donor
HDL	high-density lipoprotein
HetAr	heteroaryl
HOMO	highest occupied molecular orbital
IC	internal conversion
ICT	intramolecular charge transfer
IR	infrared
ISC	intersystem crossing
LUMO	lowest unoccupied molecular orbital
LUV	large unilamellar vesicle
M ₇₀ D ₃₀	70% 2-methylpentane and 30% dioxane
MDR	multidrug resistance
Me	methanol

M ₆₀ EA ₄₀	60% 2-methylpentane and 40% ethyl acetate
MLV	multilamellar vesicle
mm	millimeter
μm	micrometer
2-MP	2-methylpentane
MVV	multivesicular vesicle
nm	nanometer
NMR	nuclear magnetic resonance
OLV	oligo lamellar vesicle
PdCl ₂ (PPh ₃) ₂	bis(triphenylphosphane)dichloropalladium (II)
Pd(dppf) ₂ Cl ₂	1,1-bis(diphenylphosphane)ferrocen dichloropalladium (II)
Pd(OAc) ₂	palladium (II) acetate
PEG	polyethylene glycol
Q	quencher or quenching
R	relaxed state
ref.	reference
RES	reticuloendothelial system
RET	resonance energy transfer
RNA	ribonucleic acid
s	second
SARs	Structure-activity relationships
SNPs	single nucleotide polymorphisms
SUV	small unilamellar vesicle
T	thymine
<i>t</i>	<i>tert</i>
TFA	trifluoroacetic acid
THF	tetrahydrofuran
TICT	twisted intramolecular charge transfer
T(λ)	transmittance
T _m	melting temperature
Topos	topoisomerases

UV	ultraviolet
VR	vibrational relaxation
W	water
xantphos	9,9-dimethyl-4,5-bis(diphenylphosphane)xanthene

Thesis outline

The present dissertation is divided into six chapters and a description of each chapter is outlined.

Chapters 1, 2, 3 and 4 represent an introduction to the work presented. In **chapter 1**, the synthesis of the compounds studied is presented and discussed. In **chapters 2 and 3** are based on a literature review of recent years, in the areas of the interaction with DNA and encapsulation in nanoliposomes of biologically active compounds. **Chapter 4** is dedicated to theoretical concepts of molecular fluorescence spectroscopy. The organization of these four chapters is as follows:

Chapter 1 - New potential antitumoral fluorescent heterocyclic compounds

Chapter 2 - Compounds/DNA interaction

Chapter 3 - Compounds encapsulation in nanoliposomes

Chapter 4 - Molecular Fluorescence Spectroscopy

Chapter 5 comprises a compilation of articles published in international scientific journals and a manuscript to be submitted for publication, in the scope of this thesis. Each article/manuscript is presented as a sub-chapter. The organization of this chapter is as follows:

5.1. Fluorescence Studies on Potential Antitumoral Heteroaryl and Heteroannulated Indoles in Solution and in Lipid Membranes.

Elisabete M. S. Castanheira, Ana S. Abreu, M. Solange D. Carvalho, Maria-João R. P. Queiroz, Paula M. T. Ferreira, *J. Fluoresc.*, **2009**, *19*, 501-509.

5.2. Fluorescence Studies on New Potential Antitumoral Benzothienopyran-1-ones in Solution and in Liposomes.

Elisabete M. S. Castanheira, M. Solange D. Carvalho, Daniel J. G. Soares, Paulo J. G. Coutinho, Ricardo C. Calhelha, Maria-João R. P. Queiroz, *J. Fluoresc.*, **2011**, *21*, 911-922.

5.3. New potential antitumoral fluorescent tetracyclic thieno[3,2-*b*]pyridine derivatives: interaction with DNA and nanosized liposomes.

Elisabete M.S. Castanheira, Maria Solange D. Carvalho, Ana Rita O. Rodrigues, Ricardo C. Calhelha, Maria-João R.P. Queiroz, *Nanoscale Research Letters*, **2011**, *6*, 379-386.

5.4. Fluorescence studies on potential antitumor 6-(hetero)arylthieno[3,2-*b*]pyridine derivatives in solution and in nanoliposomes.

M. Solange D. Carvalho, Ana C.L. Hortelão, Ricardo C. Calhelha, Ana S. Abreu, Paulo J.G. Coutinho, Maria-João R.P. Queiroz, Elisabete M.S. Castanheira, *J. Photochem. Photobiol. A: Chem.*, **2013**, *264*, 56-66.

5.5. Benzothienoquinolines: new one pot synthesis and fluorescence studies of their interaction with DNA and polynucleotides.

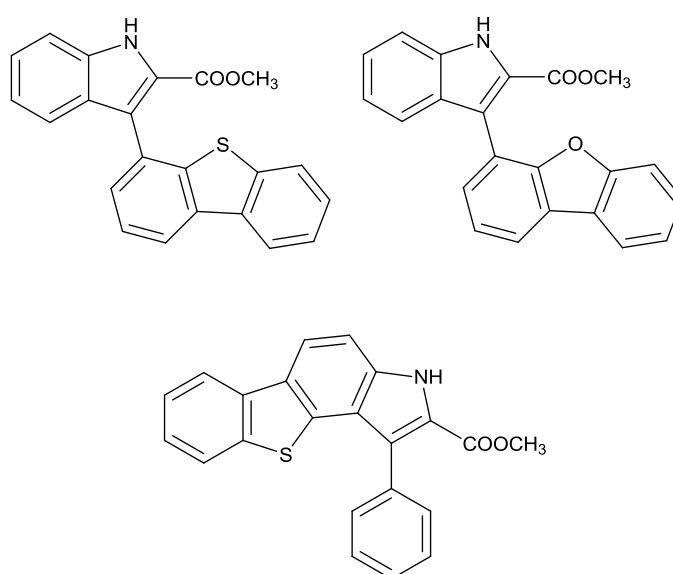
M.Solange D. Carvalho, A. Rita O. Rodrigues, João A.V. Cardoso, Ricardo C. Calhelha, Elisabete M.S. Castanheira, Maria-João R.P. Queiroz, manuscript to be submitted for publication.

Chapter 6 presents the conclusions of the research reported in this dissertation and considerations for future work.

Compounds list

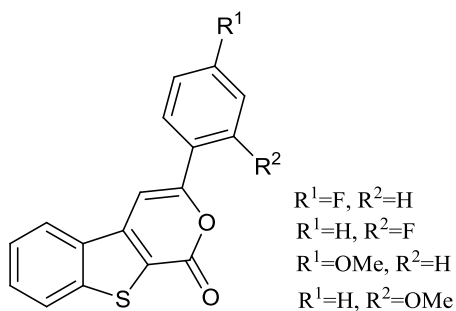
Chapter 5.1. Fluorescence Studies on Potential Antitumoral Heteroaryl and Heteroannulated Indoles in Solution and in Lipid Membranes.

Elisabete M. S. Castanheira, Ana S. Abreu, M. Solange D. Carvalho, Maria-João R. P. Queiroz, Paula M. T. Ferreira, *J. Fluoresc.*, **2009**, *19*, 501-509.



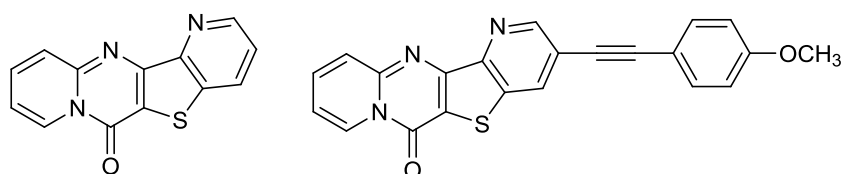
5.2. Fluorescence Studies on New Potential Antitumoral Benzothienopyran-1-ones in Solution and in Liposomes.

Elisabete M. S. Castanheira, M. Solange D. Carvalho, Daniel J. G. Soares, Paulo J. G. Coutinho, Ricardo C. Calhelha, Maria-João R. P. Queiroz, *J. Fluoresc.*, **2011**, *21*, 911-922.



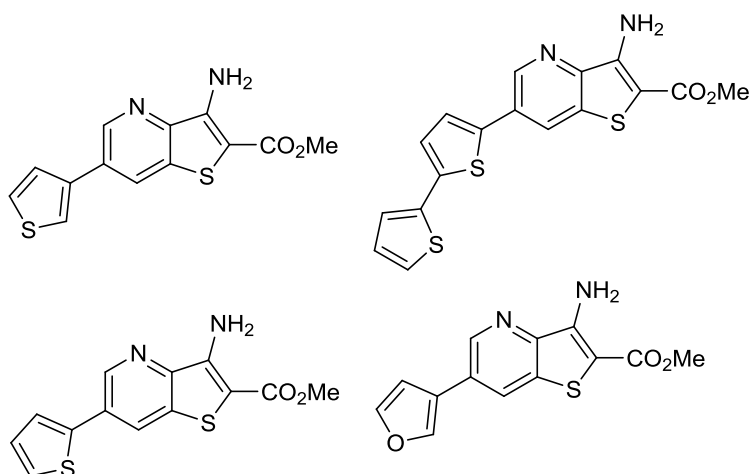
5.3. New potential antitumoral fluorescent tetracyclic thieno[3,2-*b*]pyridine derivatives: interaction with DNA and nanosized liposomes.

Elisabete M.S. Castanheira, Maria Solange D. Carvalho, Ana Rita O. Rodrigues, Ricardo C. Calhelha, Maria-João R.P. Queiroz, *Nanoscale Research Letters*, **2011**, 6, 379-386.



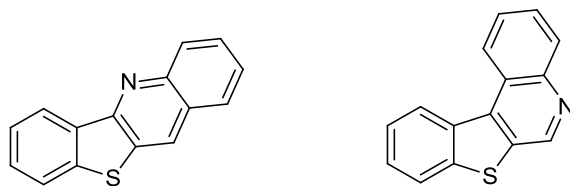
5.4. Fluorescence studies on potential antitumor 6-(hetero)arylthieno[3,2-*b*]pyridine derivatives in solution and in nanoliposomes.

M. Solange D. Carvalho, Ana C.L. Hortelão, Ricardo C. Calhelha, Ana S. Abreu, Paulo J.G. Coutinho, Maria-João R.P. Queiroz, Elisabete M.S. Castanheira, *J. Photochem. Photobiol. A: Chem.*, **2013**, 264, 56-66.



5.5. Benzothienoquinolines: new one pot synthesis and fluorescence studies of their interaction with DNA and polynucleotides.

M.Solange D. Carvalho, A. Rita O. Rodrigues, João A.V. Cardoso, Ricardo C. Calhelha, Elisabete M.S. Castanheira, Maria-João R.P. Queiroz, manuscript to be submitted for publication.



Chapter 1

New potential antitumoral fluorescent heterocyclic compounds

INDEX

1. Introduction	5
2. Heteroaryl and heteroannulated indoles	6
3. Benzothienopyranones	12
4. Thienopyridines	16
5. Benzothienoquinolines.....	20
6. References.....	22

1. Introduction

The therapy of tumors is being currently achieved by surgical intervention, radiation treatment and chemotherapy. The drawbacks of this latter are mainly due to the toxicity of the drugs, which is usually not limited to the cancer cells, and to the acquired resistance of the cancer cells to some of the most widely used drugs, which reduces the long-term efficacy of the therapy. For these reasons, there is a strongly need in the oncology field for new compounds endowed with antitumour activity. Thus, the chemistry and biological study of heterocyclic and/or heteroaromatic compounds has been an interesting field for a long time in medicinal chemistry, namely in anti-cancer chemistry^{1,2}. One way to avoid the toxicity and to decrease the therapeutic dose of the antitumoral compounds is to encapsulate them in liposomes^{3,4}. The study of the antitumoral mechanism of action of the compounds is also an important issue for cancer treatment.

For some years now, our research group has been interested in the synthesis of heterocyclic antitumoral compounds, using several synthetic methodologies and different starting materials.

In this work, several classes of compounds synthesized in our research group were studied due to their fluorescence properties and their potential antitumoral activity: heteroaryl and heteroannulated indoles, benzothienopyranones, heteroaryl and tetracyclic thienopyridine derivatives and benzothienoquinolines. These compounds were shown to be fluorescent in several solvents with different polarity and this important feature allowed us to study their location when encapsulated in liposomes of different lipid composition, and DNA interactions of some of them (including intercalation and groove binding) using natural double-stranded (*ds*) salmon sperm DNA and/or synthetic *ds*-polynucleotides.

2. Heteroaryl and heteroannulated indoles

A number of heterocyclic derivatives containing nitrogen atom serve as a unique and versatile scaffolds for experimental drug design. Indole along with their several derivatives finds a prominent place in synthetic organic chemistry, as they found to be potent pharmacophores. Indole derivatives have displayed versatile pharmacological properties such as anti-inflammatory, anticancer, antidiabetic, antimalarial, antibacterial, antifungal, anticonvulsant and cardiovascular activities. Notably, the indolic amino acid tryptophan is the precursor of the neurotransmitter serotonin (5-hydroxytryptamine) (Figure 1.1.). In addition, the indole ring is present in various marine or terrestrial natural compounds, which have useful biological properties. The name indole is deriving from the words indigo and oleum, since indole was first isolated by treatment of the indigo dye with oleum. Indole is an aromatic heterocyclic organic compound, having a bicyclic structure, consisting of a six-membered benzene ring fused to a five-membered nitrogen containing pyrrole ring, i.e., indole is a benzopyrrole (Figure 1.1)⁵.

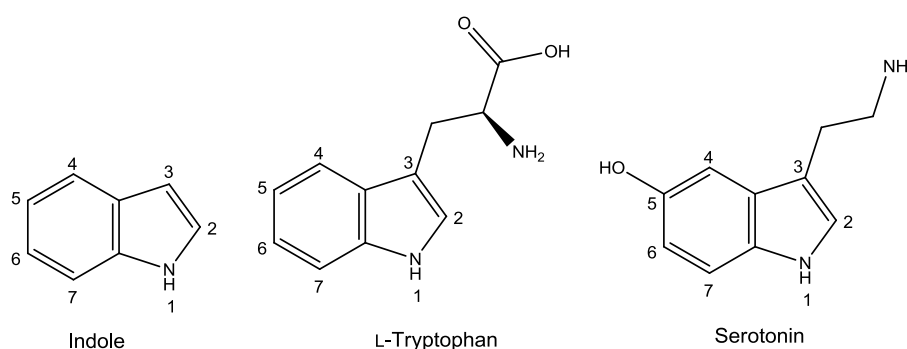
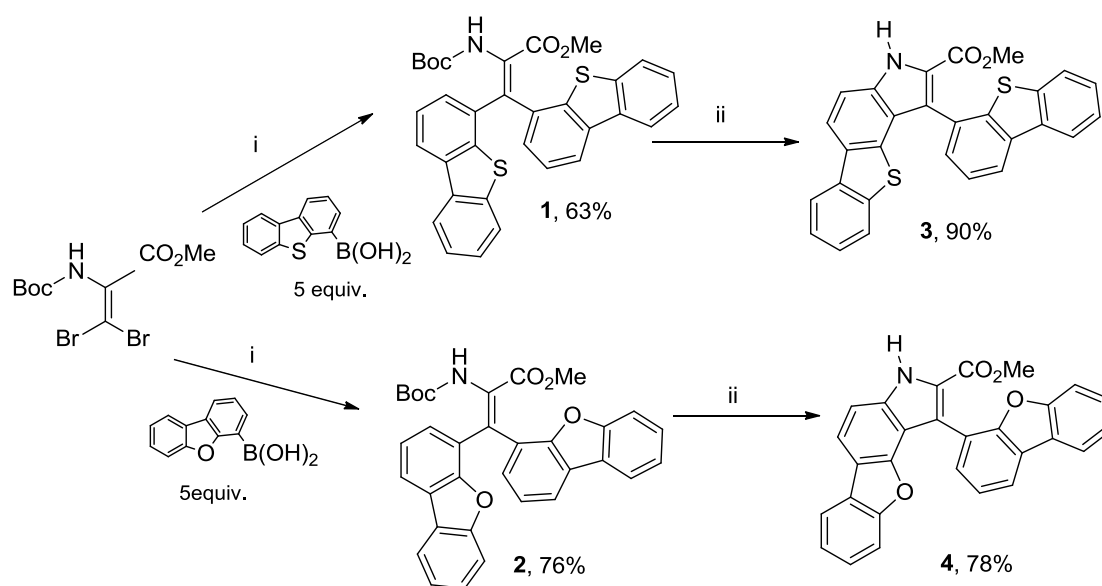


Figure 1.1. Indole, L-Tryptophan and Serotonin structures.

Several recent reviews⁶⁻⁸ represent some synthesized indole derivatives and their pharmacological profiles, namely anticancer, which may contribute in future to synthesize various analogs and to develop new pharmacologically less toxic medicines. Furthermore, many planar heteroaromatic derivatives have shown anti-proliferative activity in vitro and some of them are important anticancer drugs².

Keeping these observations in mind and the interest of our research group in the synthesis of new biologically active heterocycles, namely antitumoral compounds, it was planned to synthesize several fluorescent planar indole derivatives including heteroannulated ones.

Thus, in an earlier work^{9,10}, β,β -diaryldehydroamino acids **1** and **2** were obtained by palladium-catalyzed Suzuki (C-C) cross-couplings¹¹ of the methyl ester of *N*-(*t*-butoxycarbonyl)- β,β -dibromodehydroalanine with dibenzothien-4-yl and dibenzofur-4-yl boronic acids and were cyclized to new tetracyclic heteroaromatic compounds, the methyl 1-(dibenzothien-4-yl)-3*H*-benzothieno[2,3-*e*]indole-2-carboxylate **3**, and the methyl 1-(dibenzofuro-4-yl)-3*H*-benzofuro[2,3-*e*]indole-2-carboxylate **4** in high yields, by a novel metal assisted (palladium (II) and copper) C-N intramolecular cyclization developed by us¹²⁻¹⁵ (Scheme 1.1).

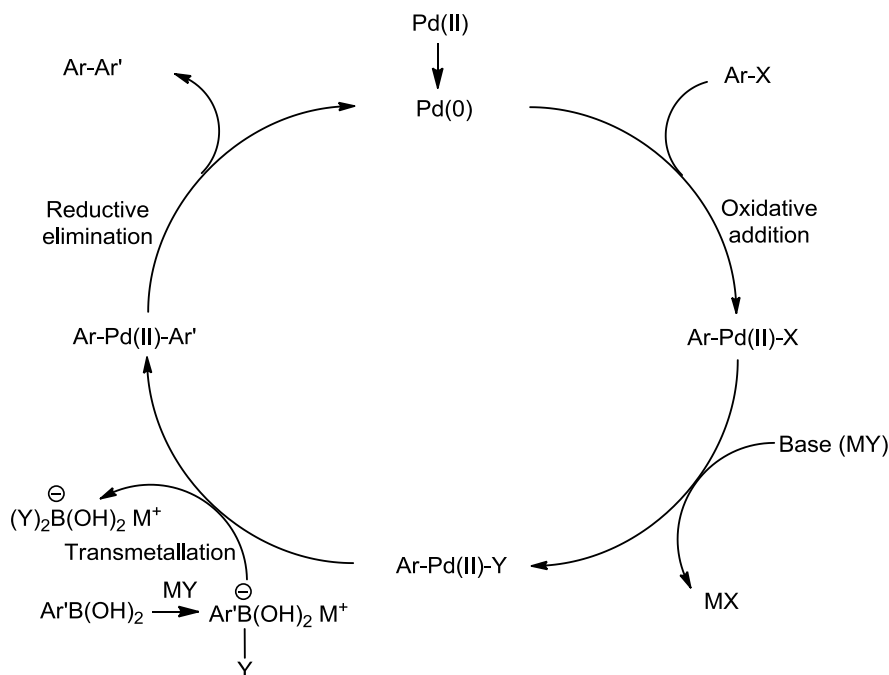


i) Pd(dppf)Cl₂·CH₂Cl₂ 1:1 (20 mol%), Cs₂CO₃ (1.4 equiv.), THF/H₂O (1:1), 80 °C, 1h 30min.

ii) Pd(OAc)₂ (50 mol%), Cu(OAc)₂·H₂O (3 equiv.), DMF, 130 °C, 3h.

Scheme 1.1. Synthesis of the bis-Suzuki coupling products **1** and **2**, and their intramolecular C-N cyclization^{9,10} to the tetracyclic compounds **3** and **4**.

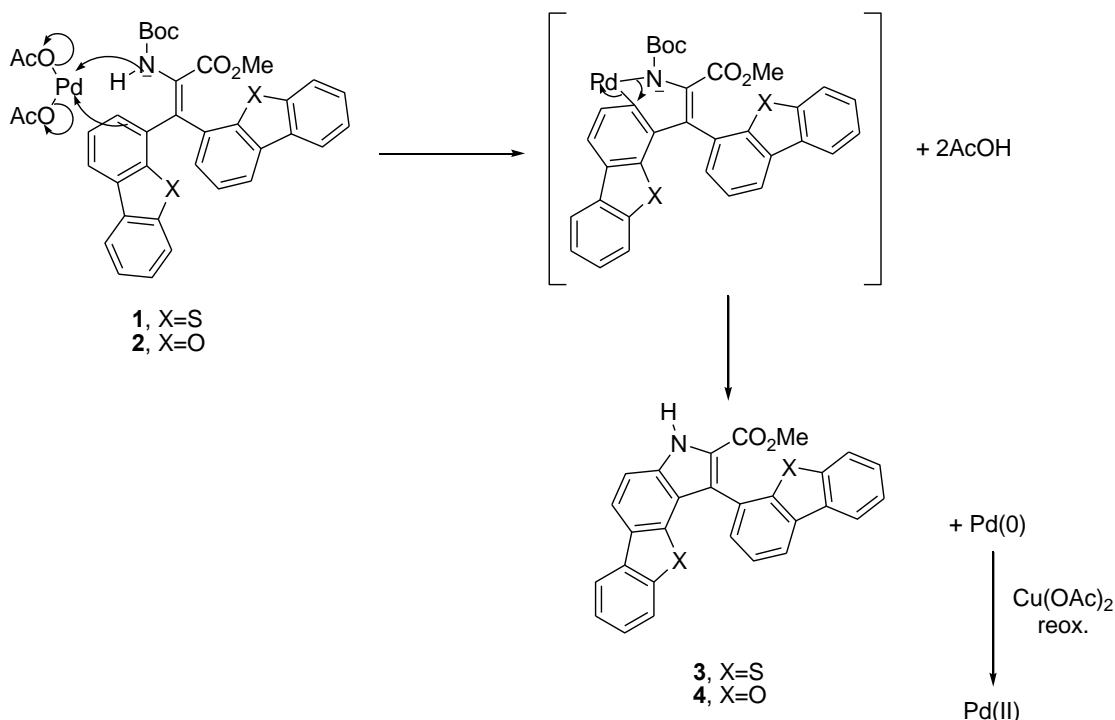
The general catalytic cycle for the Suzuki (C-C) cross coupling involves three steps: oxidative addition, transmetalation and reductive elimination (Scheme 1.2)¹¹.



Scheme 1.2. General catalytic cycle of the Suzuki cross-coupling reaction for formation of Ar-Ar'.

The first step is the oxidative addition of an organic (aryl, heteroaryl or vinyl) halide to the Pd(0), occurring the formation of an organopalladium (II) halide. Then, the halide ion of the palladium (II) complex can be removed by the metal of the base, yielding an organopalladium alkoxide or hydroxide (more reactive than the organopalladium halide as the Pd-O bond is more polar than the Pd-X bond). In the electrophilic transmetallation step, the boron organometallic compound reacts with the palladium complex (Ar-Pd(II)-Y), giving rise to the diorganometallic complex (Ar-Pd(II)-Ar'). For that, the boronic acid must be activated by the base converting in a boron tetravalent compound. Finally, the reductive elimination of Pd(0) occurs and the C-C bond (Ar-Ar') is formed.

The mechanism for the intramolecular C-N cyclization of the Suzuki cross-coupling products proposed by our research group involves the formation of a palladacycle. After extrusion of Pd(0), the pyrrole ring is formed, and it is thought that Cu(OAc)₂ reoxidizes it to Pd(II), avoiding the use of a stoichiometric amount of Pd(OAc)₂. As acetic acid is formed, the Boc group is removed¹² (Scheme 1.3).

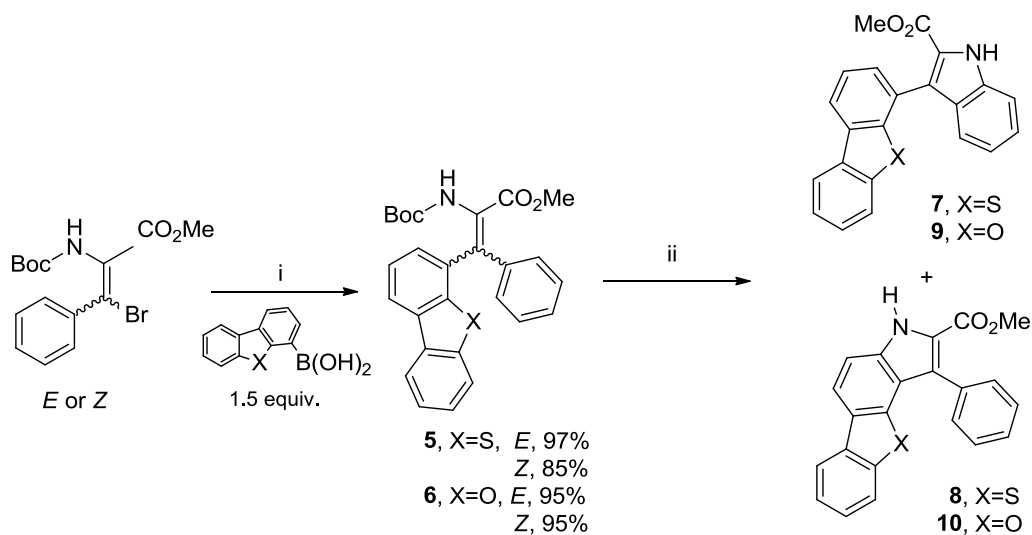


Scheme 1.3. Intramolecular C–N cyclization of the Suzuki cross-coupling products **1** and **2**, to the compounds **3** and **4** (adapted from ref.12).

Compounds **3** and **4** were prepared as potential new DNA targets and their absorption and fluorescence properties in different solvents and in the presence of natural double-stranded (*ds*) salmon sperm DNA were studied. The results in several solvents showed that either compound **3** or compound **4** can be used as fluorescence solvent sensitive probes. Spectroscopic studies of the interaction of both compounds with *ds*DNA allowed the determination of the binding constant (K_i) values and binding site sizes (n). Fluorescence quenching experiments using iodide ion allowed the determination of the accessibilities to the quencher, showing that intercalation is the preferred mode of binding of these molecules to DNA, compound **3** being the most intercalative showing also the highest affinity to DNA.

Following the same strategy in a posterior work¹, we synthesized the β -heteroaryldehydrophenylalanines **5** and **6** (*E* and *Z*) by Suzuki (C–C) cross-couplings of the methyl ester of *N*-(*t*-butoxycarbonyl)-(*E* or *Z*)- β -bromodehydrophenylalanine¹⁶ with dibenzothien-4-yl and dibenzofur-4-yl boronic acids, in excellent yields maintaining the stereochemistry of the starting material. The intramolecular metal-assisted (Pd/Cu) C–N cyclization of the Suzuki coupling products **5-E**, **5-Z**, **6-E** and **6-Z** gave, in all cases, two new heterocyclic compounds, the 3-(dibenzothien-4-yl)indole **7** and the

phenylbenzothienoindole **8** or the 3-(dibenzofur-4-yl)indole **9** and the phenylbenzofuroindole **10** in different ratios depending on the starting stereoisomer. These compounds result either from direct cyclisation or cyclization after isomerization of the Suzuki coupling products and were separated by column chromatography (Scheme 1.4, Table 1.1).



Scheme 1.4. Synthesis of heteroaryl and heteroannulated indoles **7-10** from the pure stereoisomers Suzuki cross-coupling products¹ **5-E**, **5-Z**, **6-E** and **6-Z**.

Table 1.1. Heteroaryl and heteroannulated indoles **7-10** prepared via scheme 1.4.

Starting material	Cyclized products (ratios, yields)	Time and temperature
5-E	7/8 (3:1, 41%/14%)	3h30min, 130°C + 3h30min, 160°C
5-E	7/8 (1.5:1, 37%/26%)	5h, 130°C + 2h, 160°C
5-Z	7/8 (2:1, 20%/10%)	12h, 160°C
6-E	9/10 (6:1, 30%/5%)	5h, 160°C
6-Z	9/10 (5:1, 49%/10%)	3h, 160°C

Compounds **7**, **8** and **9** were evaluated in collaboration with other research group of the Faculty of Pharmacy of the University of Porto, for their capacity to inhibit the in vitro growth of three human tumor cell lines, MCF-7 (breast adenocarcinoma, 1.5×10^5 cells/mL), NCI-H460 (non-small cell lung cancer, 0.75×10^5 cells/mL), and SF-268 (CNS

cancer, 1.5×10^5 cells/mL) after a continuous exposure of 48h. Compound **7** showed to be the most potent presenting GI_{50} (50% of cell growth inhibition) values of 11, 13 and 17 μ M, respectively, whereas compound **9** exhibited only a low inhibitory effect against the tumor cell lines tested with GI_{50} values of 27, 18 and 35 μ M, respectively. Compound **8** presented a weak growth inhibitory effect (GI_{50} values of 73, 40 and 50 μ M, respectively). Comparing the activities of the heteroarylindoles **7** and **9**, the oxygen isostere **9** presented a weaker growth inhibitory effect, although the results in NCI-H460 cell line are comparable¹.

Due to these results, the fluorescence properties in several solvents and in lipid membranes of these three indole derivatives were studied in the present work (Chapter 5.1).

3. Benzothienopyranones

In the last years, several lactones have shown to be potent anticancer agents¹⁷⁻²⁰. Additionally, promising pharmacological activities of 3-substituted isocoumarins²¹⁻²³ and 4-alkynyl substituted 2-pyrones²⁴ (Figure 1.2) and the fact that thiophene moiety is common in many bioactive agents and drugs²⁵ lead our research group to synthesize new potential antitumoral benzothienopyranones²⁶.

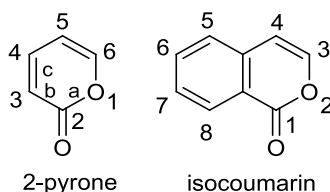
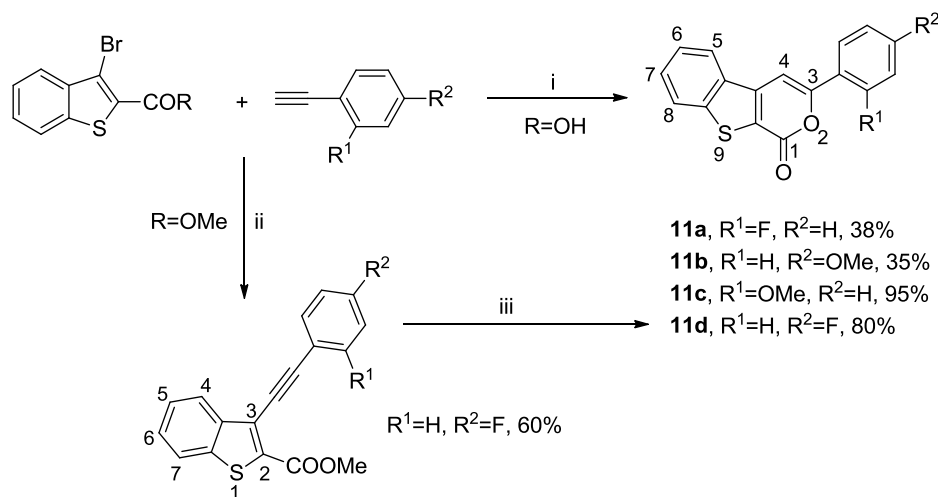


Figure 1.2. General structures of 2-pyrones and isocoumarins.

Thus, several 3-arylbenzothieno[2,3-*c*]pyran-1-ones, including compounds **11a** and **11b** were prepared in our research group, through a tandem one-pot procedure of Sonogashira coupling followed by a regioselective 6-*endo*-dig intramolecular lactonization from the commercial 3-bromobenzo[*b*]thiophene-2-carboxylic acid and different arylacetylenes (Scheme 1.5)²⁶.

As the product yields of the one-pot procedure were not high, Sonogashira couplings²⁷ of the methyl 3-bromobenzo[*b*]thiophene-2-carboxylate²⁸ with several arylacetylenes were performed. The Sonogashira coupling products were obtained in good yield, using conditions similar to those of the one-pot procedure, but 1.5 equiv. of the arylacetylene were needed to completely consume the brominated compound. Several compounds, including compound **11d** were obtained by a 6-*endo*-dig cyclization of methyl 3-(arylethynyl)benzo[*b*]thiophene-2-carboxylates, using TFA (trifluoroacetic acid) as a Brønsted acid at room temperature (Scheme 1.5).

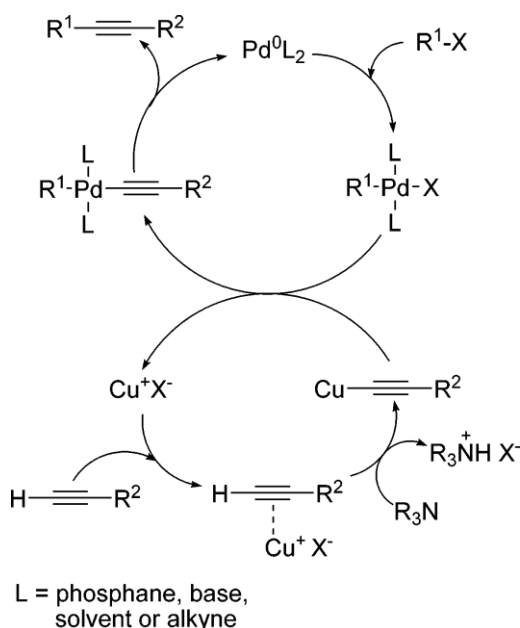


- i) PdCl₂(PPh₃)₂ (5 mol%), CuI (3 mol%), arylacetylene (1.1 equiv.), NEt₃ (3 equiv.), dry DMF, 100°C, 1h30min.
 ii) PdCl₂(PPh₃)₂ (5 mol%), arylacetylene (1.5 equiv.), CuI (3 mol%), NEt₃ (3 equiv.), dry DMF, Ar, 100°C, 1.5 h.
 iii) TFA (2 mL), 2 h, 50°C.

Scheme 1.5. Synthesis of the 3-arylbenzothieno[2,3-c]pyran-1-ones 11a–d.

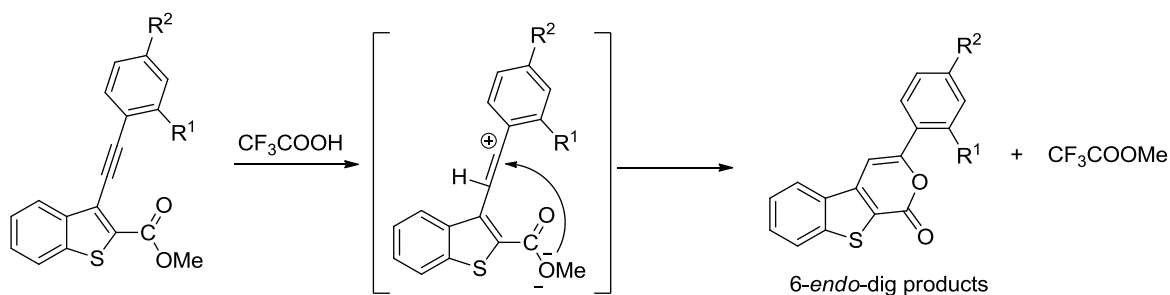
The copper-cocatalyzed Sonogashira reaction is believed to take place through two independent catalytic cycles (Pd-cycle and Cu-cycle) as shown in Scheme 1.6, where a tertiary amine is represented as base. The generally accepted catalytic cycle for the palladium catalysis (the Pd-cycle) is based on a usually fast oxidative addition of R¹-X (R¹ = aryl, heteroaryl, vinyl; X = I, Br, Cl, OTf) to the real catalyst generated from the initial palladium complex. The next step in the Pd-cycle would connect with the cycle of the copper cocatalyst (the Cu-cycle). Thus, a usually rate-determining transmetalation from the copper acetylide formed in the Cu-cycle would generate a R¹Pd(-C≡CR²)L₂ species, which gives the final coupled alkyne after reductive elimination with regeneration of the catalyst. In the Cu-cycle, the base is supposed to abstract the acetylenic proton of the terminal alkyne, thus forming a copper acetylide in the presence of the copper(I) salt. It should be pointed out that the generally employed amines are usually not basic enough to deprotonate the alkyne in order to generate the anionic nucleophile that should form the copper acetylide. Therefore, a π-alkyne-Cu complex as shown in Scheme 1.6 could be involved in the cycle, thus making the alkyne proton more acidic for easier abstraction. These copper acetylides could also be involved in the formation of the initial Pd(0)L₂ catalytic species by reaction with the starting palladium(II) complexes, thus forming Pd(-C≡CR²)₂L₂, which

after reductive elimination would afford active $\text{Pd}(0)\text{L}_2$ and some amounts of a diacetylene byproduct.



Scheme 1.6. General catalytic cycle of the copper-cocatalyzed Sonogashira reaction²⁷.

A plausible mechanism for the intramolecular cyclization of the Sonogashira products using TFA is polarization of the triple bond of the 3-(arylethynyl)benzo[*b*]thiophene-2-carboxylates with H^+ enhancing the electrophilicity of the alkyne (Scheme 1.7).



Scheme 1.7. Proposed intramolecular cyclization of the Sonogashira products using TFA.

The effect of the cyclized products (tricyclic lactones) on the *in vitro* growth of three tumor cell lines, namely MCF-7 (1.5×10^5 cells/mL), SF-268 (1.5×10^5 cells/mL) and NCI-H460 (0.75×10^5 cells/mL), was evaluated after exposure of 48h. The compounds have shown ability to inhibit the growth of all the cell lines tested, with GI_{50} values in the μM range, and it was possible to establish some structure–activity relationships, namely related to the presence and position of substituents (OMe or F) in the phenyl

ring, compound **11a** (*ortho*-fluorinated compound) showing clearly the best results, with quite low GI₅₀ values (19, 12 and 15 μ M, respectively) for the three tumor cell lines mentioned above²⁶.

As the lactone compound with an *ortho*-fluorinated phenyl ring relative to the C–C bond showed the highest antitumoral activity, it was decided in this work, to perform fluorescence studies in solution and in liposomes of compounds with a fluor atom (**11a** and **11d**) and with a methoxy group in the same positions, for comparison (**11b** and **11c**). The latter was synthesized in the present work by the same methodology used for the synthesis of compounds **11a-b** (scheme 1.5). Fluorescence (steady-state) anisotropy measurements were also performed in order to obtain further information about the location of these compounds in liposomes (Chapter 5.2).

4. Thienopyridines

Among pyridine derivatives, its fused analogs, namely thienopyridines, are often of much greater interest from the standpoint of biological activity than the corresponding constituent monocyclic compounds²⁹. Six isomeric thienopyridine structures characterized by different annelation modes are known (Figure 1.3): thieno[2,3-*b*]pyridine (A), thieno[3,2-*b*]pyridine (B), thieno[2,3-*c*]pyridine (C), thieno[3,2-*c*]pyridine (D), thieno[3,4-*b*]pyridine (E), and thieno[3,4-*c*]pyridine (F).

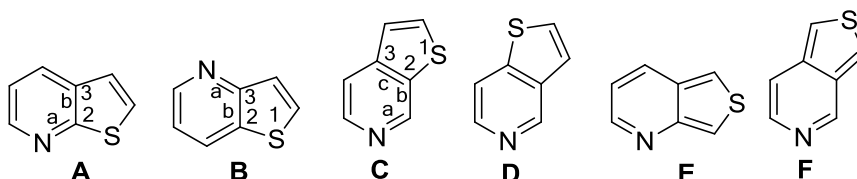
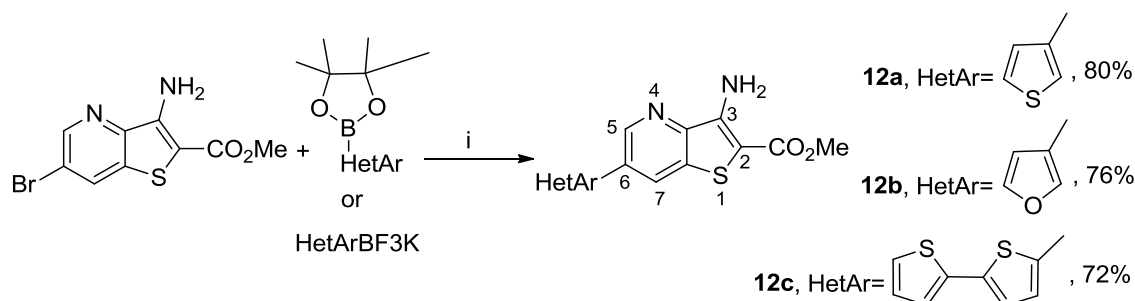


Figure 1.3. Isomeric thienopyridine structures²⁹.

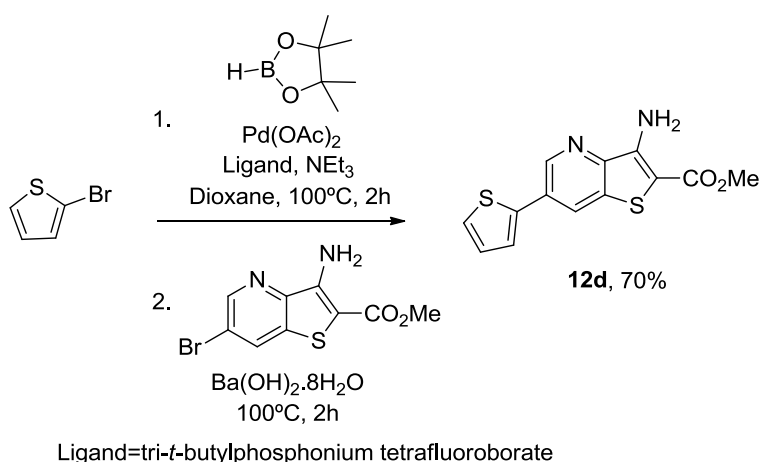
The diversity of biological activities of the thieno[3,2-*b*]pyridine system lead our research group to synthesize several methyl 3-amino-6-(hetero)arylthieno[3,2-*b*]pyridine-2-carboxylates³⁰ by Suzuki-Miyaura cross-coupling of the methyl 3-amino-6-bromothieno[3,2-*b*]pyridine-2-carboxylate³¹ with several (hetero)arylboronated pinacolboranes³² (for example, in the synthesis of **12b** and **12c**) or potassium trifluoroborates³³ (for example in the synthesis of **12a**), in high yields. These boron compounds are easier to handle than the boronic acids due to their insensitivity to air and moisture. Furthermore the corresponding boronic acids did not react with the methyl 3-amino-6-bromothieno[3,2-*b*]pyridine-2-carboxylate under the conditions used. Some of the compounds prepared are presented in scheme 1.8.



i) PdCl₂(dppf).CH₂Cl₂ (1:1) 2 mol%, K₂CO₃ (6 equiv.), DME/H₂O (3:1), 1-3h, 90°C

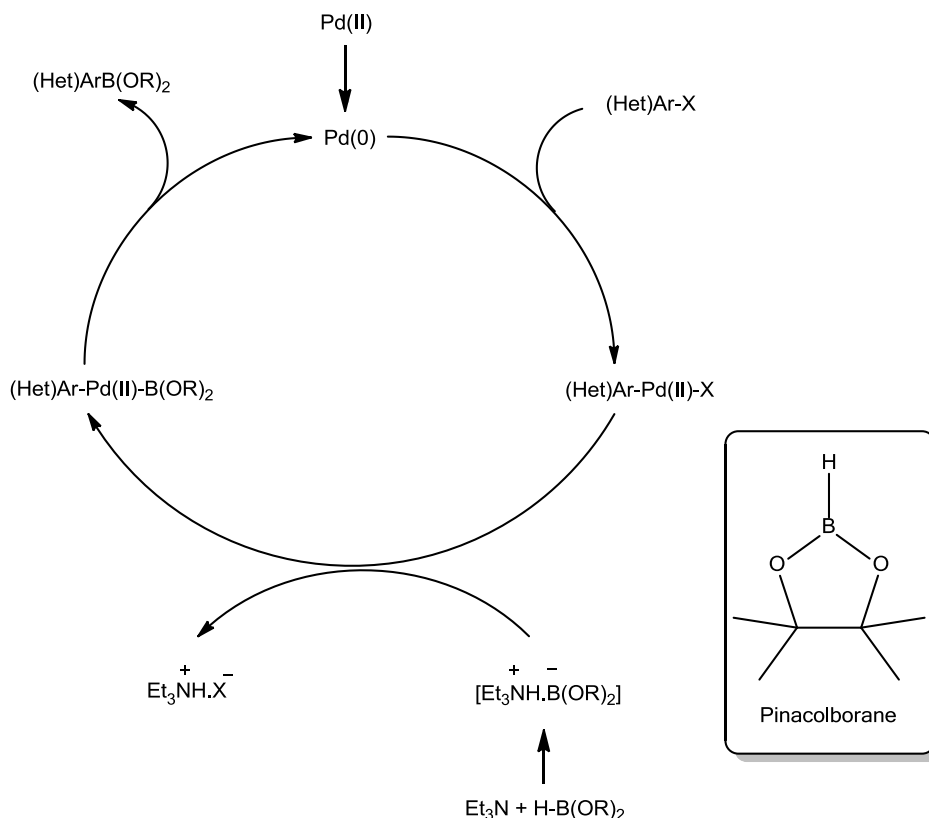
Scheme 1.8. Some of the methyl 3-amino-6-heteroarylthieno[3,2-*b*]pyridine-2-carboxylates synthesized by our research group by Suzuki-Miyaura cross-coupling³⁰.

According to the fact that neither the 2-thienyl pinacolborane ester nor the corresponding potassium trifluoroborate salt are commercially available, the methyl 6-(thiophen-2-yl)thieno[3,2-*b*]pyridine-2-carboxylate **12d** was synthesized by a one-pot palladium-catalyzed two steps, borylation with pinacolborane followed by Suzuki coupling (BSC) with the methyl 3-amino-6-bromothieno[3,2-*b*]pyridine-2-carboxylate (Scheme 1.9). Due to the electron-rich character of the thiophene ring, compound **12d** was only obtained using tri-*t*-butylphosphonium tetrafluoroborate³⁴ as the ligand, in 70% yield. To our knowledge it was the first time that this ligand was used in a BSC reaction.



Scheme 1.9. Synthesis of compound **12d** by a BSC reaction³⁰.

The C-B catalytic cycle begins with the (Het)Ar-X oxidative addition to the Pd(0) catalyst, yielding an arylpalladium(II) species [(Het)Ar-Pd(II)-X]. Then the X atom of the [(Het)Ar-Pd(II)-X] complex is removed by the boron anion, forming the intermediate [(Het)Ar-Pd(II)-B(OR)₂]. A reductive elimination of Pd(0) regenerates the catalyst and originates the heteroarylboronated compound. The use of Et₃N in the coupling is very effective, preventing the formation of Ar-H, and facilitating the formation of the C-B bond (Scheme 1.10)³⁵.



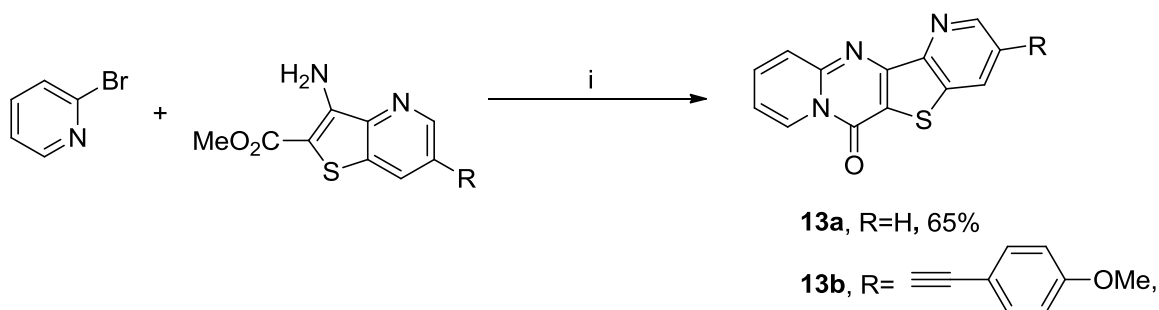
Scheme 1.10. Catalytic cycle proposed for the boronation C-B using pinacolborane and Et₃N³⁵.

The advantages of these BSC sequences are the use of two halogenated reagents and to perform an *in situ* borylation, yielding a C-B bond, without isolating the boronated intermediate, followed by a Suzuki-Miyaura cross-coupling (C-C) when the other halide reagent and the other base are added.

The growth inhibitory effect of the coupling products was evaluated against three human tumor cell lines MCF-7 (1.5×10^5 cells/mL), A375-C5 (melanoma, 0.75×10^5 cells/mL), and NCI-H460 (0.75×10^5 cells/mL), after 48 h of continuous exposure. From the results it was possible to establish some structure-activity relationships. The most active compound was **12c** (the 2,2'-bithiophene derivative) with selectivity against MCF-7 and NCI-H460 cell lines presenting very low GI₅₀ values (1 and 0.7 μ M, respectively). For this reason, compound **12c** was selected to be further studied regarding its influence on the cell cycle distribution of the NCI-H460 cells and it was shown that this compound induce a cell cycle arrest in the G₀/G₁ phases.

Due to these results, the spectroscopic properties in solvents of different polarity and in nanoliposomes of compound **12c**, as well as of the other thiophene derivatives **12a**

and **12d** and of the furan derivative **12b** for comparison (although for the latter, the results in the cell lines were not good), were studied in the present work (Chapter 5.4). Our research group has also synthesized fused thienopyridines with pyrimidones. Thus, the tetracyclic compound **13a** and **13b** were synthesized by a tandem C–N coupling of the methyl 3-amino-thieno[3,2-*b*]pyridine-2-carboxylate or of the methyl 3-amino-6-[2-(4-methoxyphenyl)ethynyl]thieno[3,2-*b*]pyridine-2-carboxylate with 2-bromopyridine followed by intramolecular cyclization involving the nucleophilic attack of the pyridine nitrogen on the carbonyl of the ester group with loss of MeOH³¹ (Scheme 1.11). This type of reaction was already performed by us in the benzo[*b*]thiophene series³⁶.



i) Pd(OAc)₂ 15 mol %, xantphos 18 mol %, 2 equiv Cs₂CO₃, dry dioxane, overnight, 120°C.

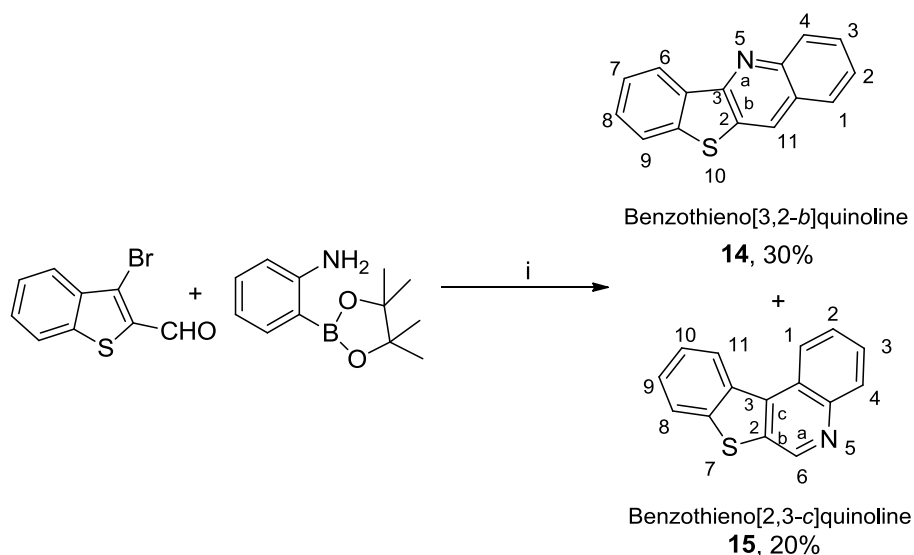
Scheme 1.11. Synthesis³¹ of the tetracyclic thienopyrimidine derivatives **13**.

The methyl 3-amino-6-[2-(4-methoxyphenyl)ethynyl]thieno[3,2-*b*]pyridine-2-carboxylate was prepared by a Sonogashira coupling of the methyl 3-amino-6-bromothieno[3,2-*b*]pyridine with the 4-methoxyphenylacetylene^{31,36}.

The interactions with DNA and nanosized liposomes of the fluorescent planar tetracyclic compounds **13a** and **13b** as potential new antitumorals were studied in the present work (Chapter 5.3).

5. Benzothienoquinolines

Benzothieno[3,2-*b*]quinoline **14**³⁷ and benzothieno[2,3-*c*]quinoline **15**³⁸ are known for their anti-plasmodic and anti-infectious activities, acting mainly through intercalation between DNA base pairs when used in their salt form. These compounds were earlier synthesized by separated reactions and in several steps^{37,38}, but our research group recently was able to obtain the two compounds in a one pot procedure. Thus, the reaction of the commercial available 3-bromobenzo[*b*]thiophene-2-carbaldehyde with 2-aminophenylpinacolborane under Suzuki coupling conditions using a stereochemically hindered ligand, 2-(cyclohexylphosphane)biphenyl³⁹, gave compounds **14** and **15** which were separated by column chromatography (Scheme 1.12).



i) Pd(OAc)₂ (5 mol%), 2-(cyclohexylphosphane)biphenyl (20 mol%), Ba(OH)₂·8H₂O (3 equiv.), dioxane, 100 °C, 5h.

Scheme 1.12. One pot synthesis of benzothieno[3,2-*b*]quinoline **14** and benzothieno[2,3-*c*]quinoline **15**.

The obtainment of the benzothieno[3,2-*b*]quinoline **14** was unexpected using these reaction conditions. It seems that it is the result of a Pd-catalyzed C-N coupling followed by an intramolecular cyclization that may perhaps occur by nucleophilic attack of the activated *ortho* position of the diarylamine intermediate on the carbonyl of the aldehyde, after deboronation. In the synthesis of the expected compound **15** a

Suzuki cross-coupling and a nucleophilic attack of the amino group on the aldehyde occurred.

Despite these compounds have already been synthesized by others in several steps we were able to prepare them in a one pot procedure which is very advantageous to economize reagents and time.

In this work, the interaction of the synthesized benzothienoquinolines **14** and **15** with natural double-stranded salmon sperm DNA and with synthetic *ds*-polyheteronucleotides was investigated by fluorescence emission measurements. These studies are important due to the biological relevance of both compounds as potential antitumorals (Chapter 5.5).

6. References

1. M.-J.-R.P. Queiroz, A.S. Abreu, M.S.D. Carvalho, P.M.T. Ferreira, N. Nazareth, M.S.J. Nascimento, Synthesis of new heteroaryl and heteroannulated indoles from dehydrophenylalanines: Antitumor evaluation, *Bioorg. Med. Chem.*, **2008**, *16*, 5584–5589.
2. S.P. Dholakia S. P, B.N. Suhagia, A.K. Patel, P.P. Kapupara, D.K. Sureja, Review: Novel Target for Cancer Therapy, *J. Chem. Pharm. Res.*, **2011**, *3(4)*, 315-332.
3. C. Kwangue, X. Wang, S. Nie, Therapeutic Nanoparticles for Drug Delivery in Cancer, *Clin. Cancer Res.*, **2008**, *14*, 1310-1316.
4. T.L. Andresen, S.S. Jensen, K. Jorgensen, Advanced Strategies in Liposomal Cancer Therapy: Problems and Prospects of Active and Tumor Specific Drug Release, *Progress in Lipid Research*, **2005**, *44*, 68-97.
5. H. Patel, N. Darji, J. Pillai, B. Patel, Recent advance in anti-cancer activity of indole derivatives, *Int. J. Drug Res. Tech.*, **2012**, *2(3)*, 225-230.
6. S. Biswal, U. Sahoo, S. Sethy, H.K.S Kumar, M. Banerjee, Indole: the molecule of diverse biological activities, *Asian J. Pharm. Clin. Res.*, **2012**, *5(1)*, 1-6.
7. K. Lalit, B. Shashi, J. Kamal, The Diverse Pharmacological Importance of Indole Derivatives: A Review, *Int. J. Res. Pharm. Science*, **2012**, *2(2)*, 23-33.
8. H. Patel, N. Darji, J. Pillai, B. Patel, Recent advance in anti-cancer activity of indole derivatives, *Int. J. Drug Res. Tech.*, **2012**, *2(3)*, 225-230.
9. M.-J.-R.P. Queiroz, E.M.S. Castanheira, M.S.D. Carvalho, A.S. Abreu, P.M.T. Ferreira, H. Karadeniz, A. Erdem, New tetracyclic heteroaromatic compounds based on dehydroamino acids: photophysical and electrochemical studies of interaction with DNA, *Tetrahedron*, **2008**, *64*, 382–391.
10. Maria Solange Dantas Carvalho, Síntese de novos compostos tetracíclicos heteroaromáticos como potenciais antitumorais, por ciclização intramolecular assistida por metais, de β,β -diarildesidroaminoácidos. Estudos de absorção e fluorescência em vários solventes e em presença de ADN, Dissertação de Mestrado, Departamento de Química, Escola de Ciências, Universidade do Minho, Braga, Fevereiro **2007**.

11. For a recent review on the Suzuki reaction see: F. Alonso, I.P. Belestskaya, M. Yus, Non-conventional methodologies for transition-metal catalysed carbon-carbon coupling: a critical overview. Part 2: The Suzuki reaction, *Tetrahedron*, **2008**, *64*, 3047-3101.
12. A.S. Abreu, P.M.T. Ferreira, M.-J.R.P. Queiroz, I.C.F.R. Ferreira, R.C. Calhelha, L.M. Estevinho, Synthesis of β -benzo[*b*]thienyldehydrophenylalanine derivatives by one-pot palladiumcatalyzed borylation and Suzuki coupling (BSC) and metal-assisted intramolecular cyclization—Studies of fluorescence and antimicrobial activity, *Eur. J. Org. Chem.*, **2005**, 2951–2957.
13. M.-J.R.P. Queiroz, A.S. Abreu, E.M.S. Castanheira, P.M.T. Ferreira, Synthesis of new 3-arylindole-2-carboxylates using β,β -diaryldehydroamino acids as building blocks. Fluorescence studies, *Tetrahedron*, **2007**, *63*, 2215–2222.
14. A.S. Abreu, N.O. Silva, P. M. T. Ferreira, M.-J. R. P. Queiroz, Synthesis and intramolecular cyclization of novel β,β -bis-(benzo[*b*]thienyl)dehydroalanine derivatives, *Tetrahedron Lett.*, **2003**, *44*, 3377–3379.
15. A.S. Abreu, N.O. Silva, P. M. T. Ferreira, M.-J. R. P. Queiroz, M. Venanzi, New β,β -bis(benzo[*b*]thienyl)dehydroalanine derivatives: Synthesis and cyclization, *Eur. J. Org. Chem.*, **2003**, 4792–4796.
16. A.S. Abreu, P.M.T. Ferreira, L.S. Monteiro, M.-J.R.P. Queiroz, I. C. F. R. Ferreira, R.C. Calhelha, L.M. Estevinho, Synthesis of pure stereoisomers of benzo[*b*]thienyl dehydrophenylalanines by Suzuki cross-coupling. Preliminary studies of antimicrobial activity, *Tetrahedron*, **2004**, *60*, 11821–11828.
17. L. Jurd, New antitumor agents. 1.Heterocyclic benzodioxole lactones, *J. Heterocyclic Chem.*, **1997**, *33*, 1227-1232.
18. K. Sun, X. Li, W. L, J. Wang, J. Liu, Y. Sha, Two New Lactones and One New Aryl- β -oxa-bicyclo[3,2,1]oct-3-en-2-one from *Descurainia sophia*, *Chem. Pharm. Bull.*, **2004**, *52(12)*, 1483–1486.
19. M. Romero, P. Renard, D.-H. Caignard, G. Atassi, X. Solans, P. Constans, C. Bailly, M.D. Pujol, Synthesis and Structure-Activity Relationships of New Benzodioxinic Lactones as Potential Anticancer Drugs, *J. Med. Chem.*, **2007**, *50*, 294-307.
20. X.W.K. Nakagawa-Goto, K.F. Bastow, M.-J. Don, Y.-L. Lin, T.-S. Wu, K.-H. Lee, Antitumor Agents. 254. Synthesis and Biological Evaluation of Novel Neo-

- tanshinlactone Analogues as Potent Anti-Breast Cancer Agents, *J. Med. Chem.*, **2006**, *49*, 5631-5634.
21. A. Kurume, Y. Kamata, M. Yamashita, Q. Wang, H. Matsuda, M. Yoshikawa, I. Kawasaki, S. Ohta, Synthesis of 3-substituted isocoumarins and their inhibitory effects on degranulation of RBL-2H3 cells induced by antigen, *Chem. Pharm. Bull.*, **2008**, *56(9)*, 1264–1269.
 22. R.M. Salloum, N.T. Jaskowiak, H.J. Maureci, S. Seetharam, M.A. Beckett, A.M. Koons, D.M. Hari, V.K. Gupta, C. Reimer, R. Kalluri, M.C. Posner, S. Hellman, D.W. Kufe, R.R. Weichselbaum, NM-3, an isocoumarin, increases the antitumor effects of radiotherapy without toxicity, *Cancer Res.*, **2000**, *60(24)*, 6958–6963.
 23. T. Kawano, N. Agata, S. Kharbanda, D. Avigan, D. Kufe, A novel isocoumarin derivative induces mitotic phase arrest and apoptosis of human multiple myeloma cells, *Cancer Chemother. Pharmacol.*, **2007**, *59(3)*, 329–335.
 24. I.J.S. Fairlamb, L.R. Marrison, J.M. Dickinson, F.J. Lu, J.P. Schmidt, 2-Pyrones possessing antimicrobial and cytotoxic activities, *Bioorg. Med. Chem.*, **2004**, *12(4)*, 4285–4299.
 25. M.A. Shaaban, M.M. Ghorab, H.I. Heiba, M.M. Kamel, N.H. Zaher, M.I. Mostafa, Novel Thiophenes, Thienopyrimidines, and Triazolothienopyrimidines for the Evaluation of Anticancer and Augmentation Effects of γ -Radiation, *Arch. Pharm. Chem. Life Sci.*, **2010**, *343*, 404 – 410.
 26. M.-J.-R.P. Queiroz, R.C. Calhelha, L.A. Vale-Silva, E. Pinto, M.S.-J. Nascimento, Synthesis of novel 3-(aryl)benzothieno[2,3-*c*]pyran-1-ones from Sonogashira products and intramolecular cyclization: antitumoral activity evaluation, *Eur. J. Med. Chem.*, **2009**, *44*, 1893–1899.
 27. For a recent review on the Sonogashira reaction see: R. Chinchilla, C. Nájera, The sonogashira reaction: A booming methodology in synthetic organic chemistry, *Chem. Rev.*, **2007**, *107*, 874–922.
 28. M.-J.-R.P. Queiroz, A. Begouin, I.C.F.R. Ferreira, G. Kirsch, R.C. Calhelha, S. Barbosa, L.M. Estevinho, Palladium-catalyzed amination of electron-deficient or relatively electron-rich benzo[*b*]thienyl bromides - Preliminary studies of antimicrobial activity and SARs, *Eur. J. Org. Chem.*, **2004**, 3679–3685.

29. V.P. Litvinov, V.V. Dotsenko, S.G. Krivokolyskob, Thienopyridines: synthesis, properties, and biological activity, *Russ. Chem. Bull., Int. Ed.*, **2005**, *54(4)*, 864–904.
30. M.-J.R.P. Queiroz, R.C. Calhelha, L.A. Vale-Silva, E. Pinto, R.T. Lima, M.H. Vasconcelos, Efficient synthesis of 6-(hetero)arylthieno[3,2-*b*]pyridines by Suzuki-Miyaura coupling. Evaluation of growth inhibition in human tumor cell lines, SARs and effects on the cell cycle, *Eur. J. Med. Chem.*, **2010**, *45*, 5628–5634.
31. R.C. Calhelha, M.-J.R.P. Queiroz, Synthesis of new thieno[3,2-*b*]pyridine derivatives by palladium-catalyzed couplings and intramolecular cyclizations, *Tetrahedron Lett.*, **2010**, *51*, 281-283.
32. M. Murata, T. Oyama, S. Watanabe, Y. Masuda, Palladium-catalyzed borylation of aryl halides or triflates with dialkoxyborane: A novel and facile synthetic route to arylboronates, *J. Org. Chem.*, **2000**, *65*, 164-168.
33. For a recent review on organotrifluoroborates see: H.A. Stefani, R. Cella, A.S. Vieira, Recent advances in organotrifluoroborates chemistry, *Tetrahedron*, **2007**, *63*, 3623-3658.
34. S.A. Al-Trawneh, M.M. El-Abadelah, J.A. Zahra, S.A. Al-Taweel, F. Zani, M. Incerti, A. Cavazzoni, P. Vicini, Synthesis and biological evaluation of tetracyclic thienopyridones as antibacterial and antitumor agents, *Bioorg. Med. Chem.*, **2011**, *19*, 2541-2548.
35. a) M. Murata, S. Watanabe, Y. Masuda, Novel Palladium(0)-Catalyzed Coupling Reaction of Dialkoxyborane with Aryl Halides: Convenient Synthetic Route to Arylboronates, *J. Org. Chem.* **1997**, *62*, 6458-6459. b) M. Murata, T. Oyama, S. Watanabe, Y. Masuda, Palladium-Catalyzed Borylation of Aryl Halides or Triflates with Dialkoxyborane: A Novel and Facile Synthetic Route to Arylboronates, *J. Org. Chem.*, **2000**, *65*, 164-168.
36. M.-J.R.P. Queiroz, R.C. Calhelha, L.A. Vale-Silva, E. Pinto, G.M. Almeida, M.H. Vasconcelos, Synthesis and evaluation of tumor cell growth inhibition of methyl 3-amino-6-[(hetero)arylethynyl]thieno[3,2-*b*]pyridine-2-carboxylates. Structure-activity relationships, effects on the cell cycle and apoptosis, *Eur. J. Med. Chem.*, **2011**, *46(1)*, 236-240.

37. X.Y. Zhu, L.G. Mardenborough, S. Li, A. Khan, W. Zhang, P. Fan, M. Jacob, S. Khan, L. Walker, S.Y. Ablordeppey, Synthesis and evaluation of isosteres of N-methyl indolo[3,2-*b*]-quinoline (cryptolepine) as new antiinfective agents, *Bioorg. Med. Chem.*, **2007**, *15*, 686–695.
38. a) J.D. McKenney Jr., R.N. Castle, The synthesis of [1]benzothieno[2,3-*c*]quinolines, [1]benzothieno[2,3-*c*][1,2,4]triazolo[4,3-*a*]quinoline, and [1]benzothieno[2,3-*c*]tetrazolo[1,5-*a*]quinoline, *J. Heterocycl. Chem.*, **1987**, *24*, 1525-1529. b) A.S. Zektzer, M.J. Quast, G.S. Linz, G.E. Martin, J.D. McKenney, M.D. Johnston Jr, R.N. Castle, New pulse sequence for long-range two-dimesional heteronuclear NMR chemical shift correlation, *Magn. Reson. Chem.*, **1986**, *24*, 1083-1088.
39. W.J. Thompson, J.H. Jones, P.A. Lyle, J.E. Thies, An efficient synthesis of arylpyrazines and bipyridines, *J. Org. Chem.*, **1988**, *53*, 2052–2055.

Chapter 2

Compounds / DNA interaction

INDEX

1. Deoxyribonucleic acid (DNA)	31
2. DNA binding modes.....	36
2.1. Outside-edge binding.....	38
2.2. Intercalation/bisintercalation	38
2.3. Minor and major DNA grooves binding interaction	41
2.4. Thermodynamics of drug-DNA interactions	42
2.5. Methods to determine the DNA-drug binding modes	43
3. References	45

1. Deoxyribonucleic acid (DNA)

DNA, or deoxyribonucleic acid, is the hereditary material in humans and almost all other organisms. DNA contains the instructions needed for an organism to develop, survive and reproduce. To carry out these functions, DNA sequences must be converted into messages that can be used to produce proteins, which are the complex molecules that do most of the work in our bodies.

Most of the DNA is found inside a special area of the cell called the nucleus (*nuclear DNA*). Because the cell is very small, and because organisms have many DNA molecules per cell, each DNA molecule must be tightly packaged. This packaged form of the DNA is called a chromosome. Each DNA sequence that contains instructions to make a protein is known as a gene. The size of a gene may vary greatly, ranging from about 1,000 bases to 1 million bases in humans. The complete set of nuclear DNA, or genome, for a human contains about 3 billion bases and about 20,000 genes on 23 pairs of chromosomes¹.

The DNA sequences from everyone in the world are more than 99% identical. That means that only 1% of our DNA sequence is unique. Single nucleotide polymorphisms (*SNPs*) represent the 1% where we differ from each other. These differences influence why some people have a greater risk for cancer, or respond poorly to a particular medication².

The German biochemist Frederich Miescher first observed DNA in the late 1800s³. But the importance of DNA became clear only in 1953 due to the work of James Watson, Francis Crick, Maurice Wilkins and Rosalind Franklin. By studying X-ray diffraction patterns and building models, the scientists figured out the *double helix* structure of DNA⁴. The term *double helix* is used to describe DNA's winding, double-stranded chemical structure. This shape - which looks much like a twisted ladder - gives DNA the power to pass along biological instructions with great precision (Figure 2.1).

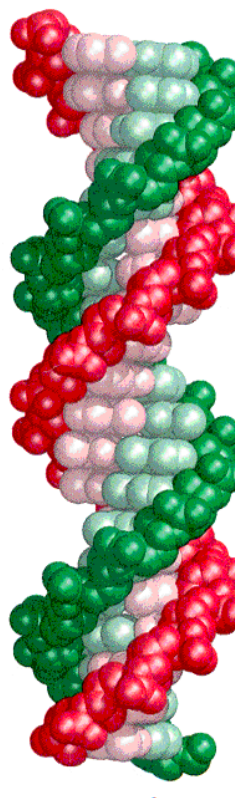


Figure 2.1. Double-helix DNA structure (computer model, one strand illustrated with green color and the other strand illustrated with red color; the weak colors represent nucleobases).

DNA is a polymer. The monomer units of DNA are nucleotides, and the polymer is known as a "polynucleotide". Each nucleotide consists of a 5-carbon (pentose) sugar (2-deoxyribose, Figure 2.2), a nitrogen containing base-covalently bonded to the 1'-carbon of the deoxyribose (*nucleobase* or *base*), and a phosphate group⁵.

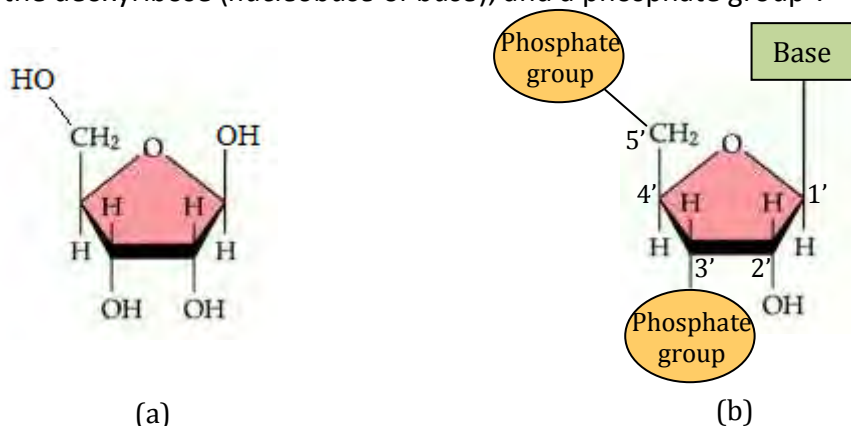


Figure 2.2. 2-Deoxyribose molecule (a) and 2-Deoxyribose residue in DNA (b).

The sugars are joined together by phosphate groups that form phosphodiester bonds. The two polynucleotide chains are held together by weak thermodynamic forces (hydrogen bonds between the bases), to form a DNA molecule (Figure 2.3)⁶.

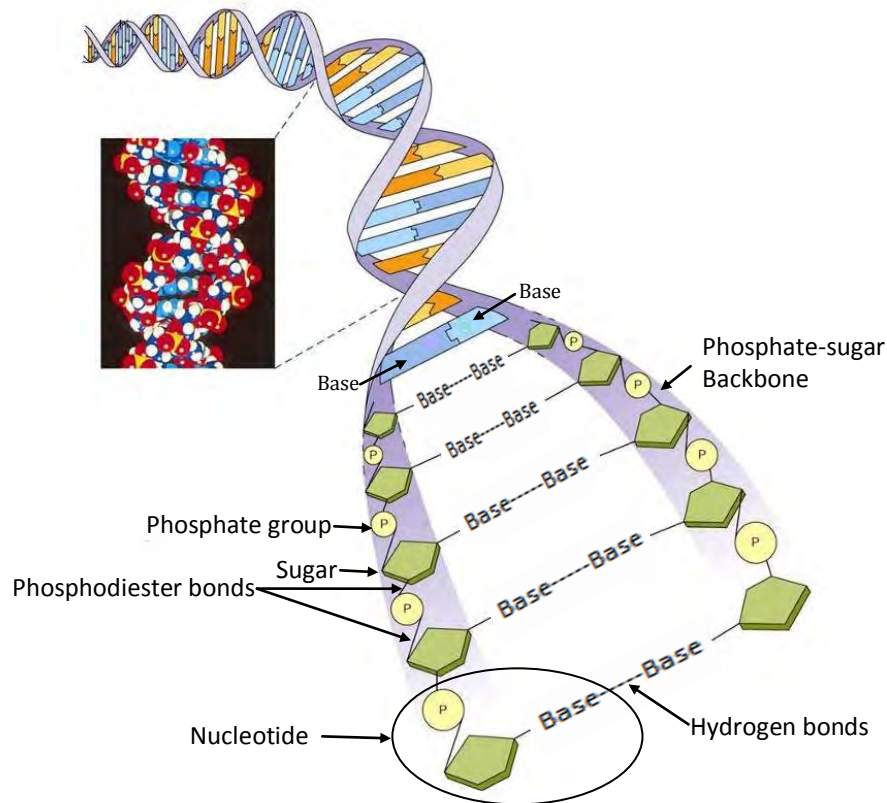


Figure 2.3. DNA structure (adapted from ref. 6).

There are two types of nitrogen bases found in nucleotides (Figure 2.4):

- purines: adenine (A) or guanine (G)
- pyrimidines: cytosine (C) or thymine (T)

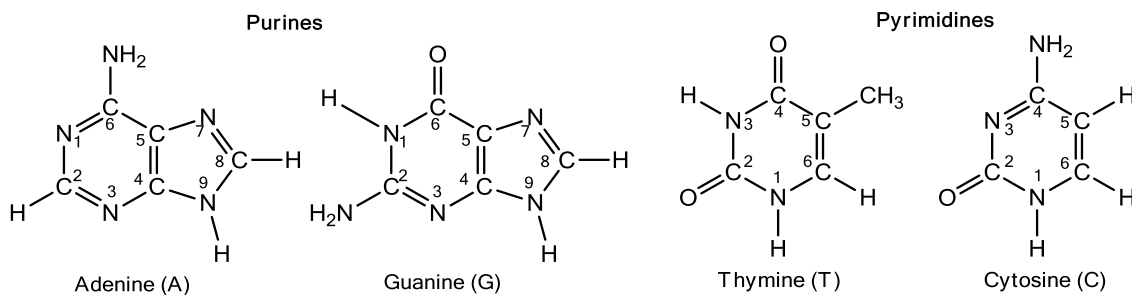


Figure 2.4. Structure of DNA nucleobases, purines and pyrimidines.

The order, or sequence, of these bases determines what biological instructions are contained in a strand of DNA. For example, the sequence ATCGTT might instruct for blue eyes, while ATCGCT might instruct for brown.

In a DNA double helix, each type of nucleobase on a strand binds with just one type of nucleobase on the other strand. This is called *complementary base pairing*. Here, purines form hydrogen bonds to pyrimidines, with adenine bonding only to thymine in

two hydrogen bonds, and cytosine bonding only to guanine in three hydrogen bonds. This arrangement of two nucleotides binding together across the double helix is called a base pair (Figure 2.5)⁷.

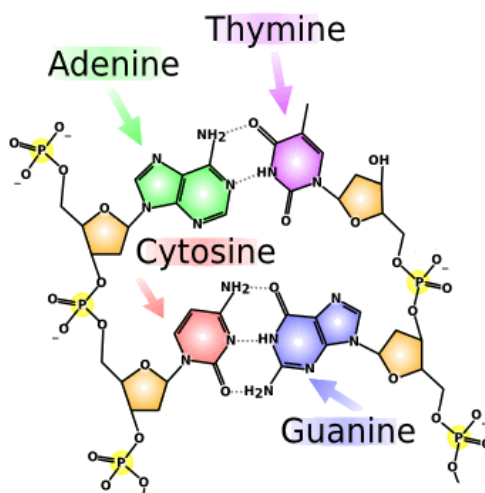


Figure 2.5. Complementary base pairing in DNA⁷.

In the double helix, the direction of the nucleotides in one strand is opposite to their direction in the other strand because the phosphodiester bonds occur between the third and fifth carbon atoms of adjacent sugar rings. Thus, these asymmetric bonds mean that a strand of DNA has a direction and we say that the strands are *antiparallel*. The asymmetric ends of DNA strands are called the 5' (*five prime*) and 3' (*three prime*) ends, with the 5' end having a terminal phosphate group and the 3' end a terminal hydroxyl group (Figure 2.6)⁸.

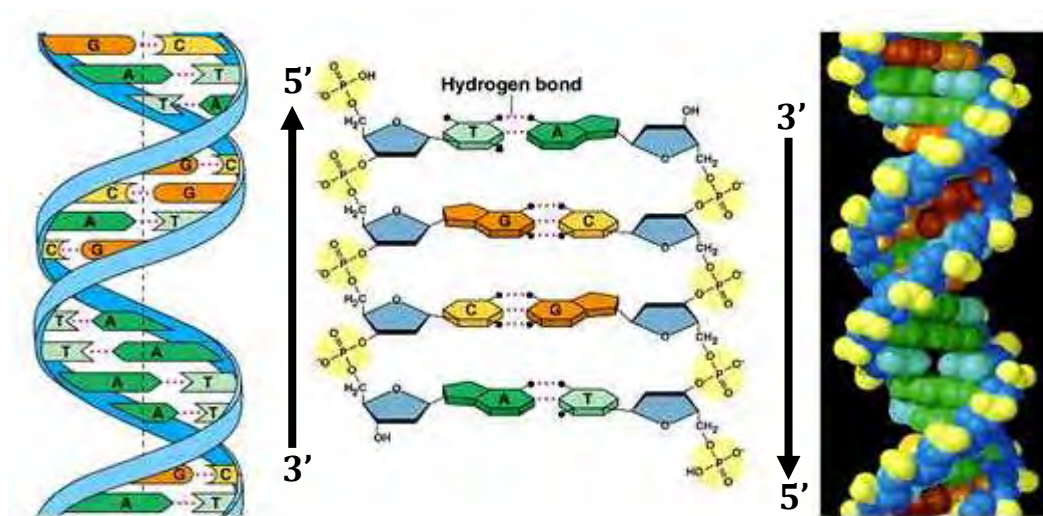


Figure 2.6. Three views of DNA structure: schematic representation (a), atomic model (b), computer model (c) (adapted from ref. 8).

As hydrogen bonds are not covalent, they can be broken and rejoined relatively easily. The two strands of DNA in a double helix can therefore be pulled apart like a zipper, either by a mechanical force or high temperature⁹. As a result of this complementarity, all the information in the double-stranded sequence of a DNA helix is duplicated on each strand, which is vital in DNA replication. Indeed, this reversible and specific interaction between complementary base pairs is critical for all the functions of DNA in living organisms¹⁰.

2. DNA binding modes

Many small molecules that bind to DNA are effective pharmaceutical agents, especially in cancer chemotherapy. Understanding the DNA binding of such drugs is essential for understanding their mode of action and for the development of design principles to guide the synthesis of new, improved compounds with enhanced or more selective activity¹¹.

The interaction of the anticancer drugs with DNA occurs mainly by three different ways^{12, 13, 14} (Figure 2.7). The first one is through control of transcription factors and polymerases in which drug interacts with proteins that bind to DNA, namely topoisomerases^{15,16}. The second is through RNA (*Ribonucleic Acid*) binding either to the DNA double helix to form nucleic acid triple helix structures or to exposed DNA single strand forming DNA–RNA hybrids that may interfere with transcriptional activity. The third type of interaction involves the covalent/cross-linking or non-covalent binding of small aromatic ligand molecules to DNA double helical structures¹⁷.

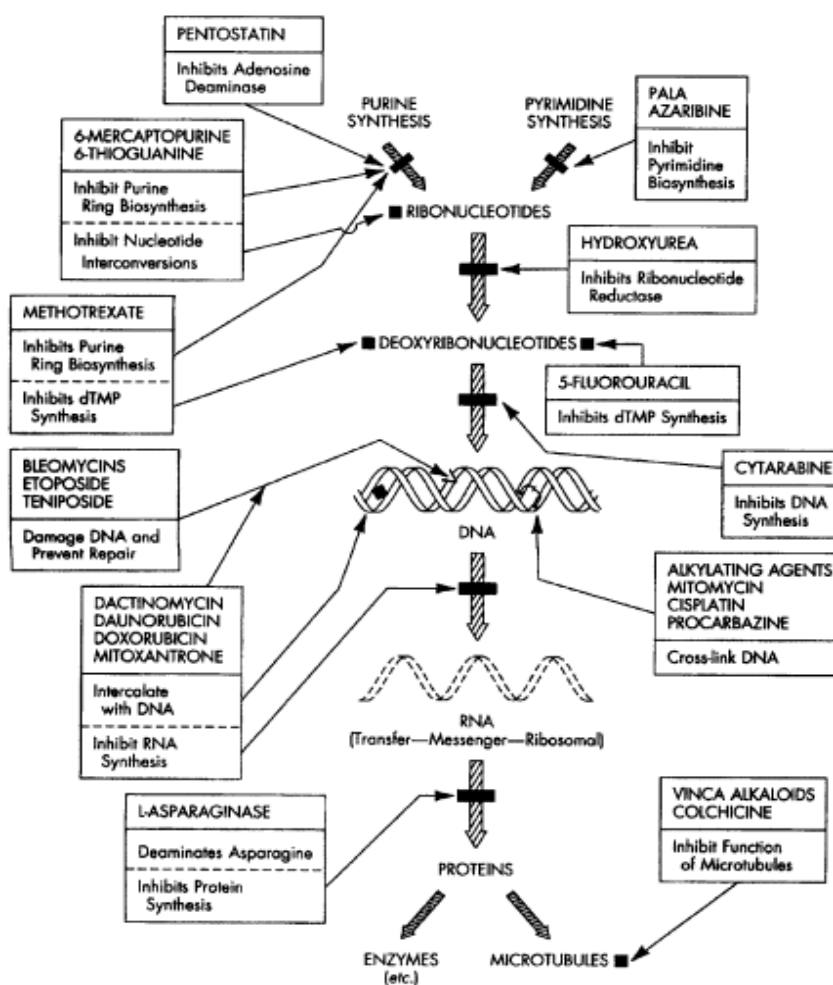


Figure 2.7. Summary of mechanism of action of anticancer drugs¹⁷.

The non-covalent interaction between small molecules and DNA generally follows three models¹² (Figure 2.8):

- (i) Outside-edge binding: This involves ligand binding (e.g. Na^+ , Mg^{2+} or polyamines, Section 2.2.1.) to the outside of the helix through non-specific, primarily electrostatic interactions with the sugar-phosphate backbone.
- (ii) Intercalation/Bisintercalation: A planar (or near planar) aromatic ring system inserts in between two adjacent base pairs, perpendicular to the helical axis (section 2.2.2).
- (iii) Groove binding: A bound ligand makes direct molecular contacts with functional groups on the edges of the bases that protrude into either the major or minor grooves (section 2.2.3.).

Compounds that have the potential to be clinically useful are normally either intercalators or groove binders. However, outside-edge, electrostatic interactions are also important, not least because the association of positively charged counterions with the DNA polyanion has a large effect on DNA conformation and stability¹². Thus, some antitumoral compounds have shown to be minor groove binders but, although they are toxic, nonselective, and sometimes expensive, at the present time DNA intercalators are among the most important drugs for treating cancer¹⁶.

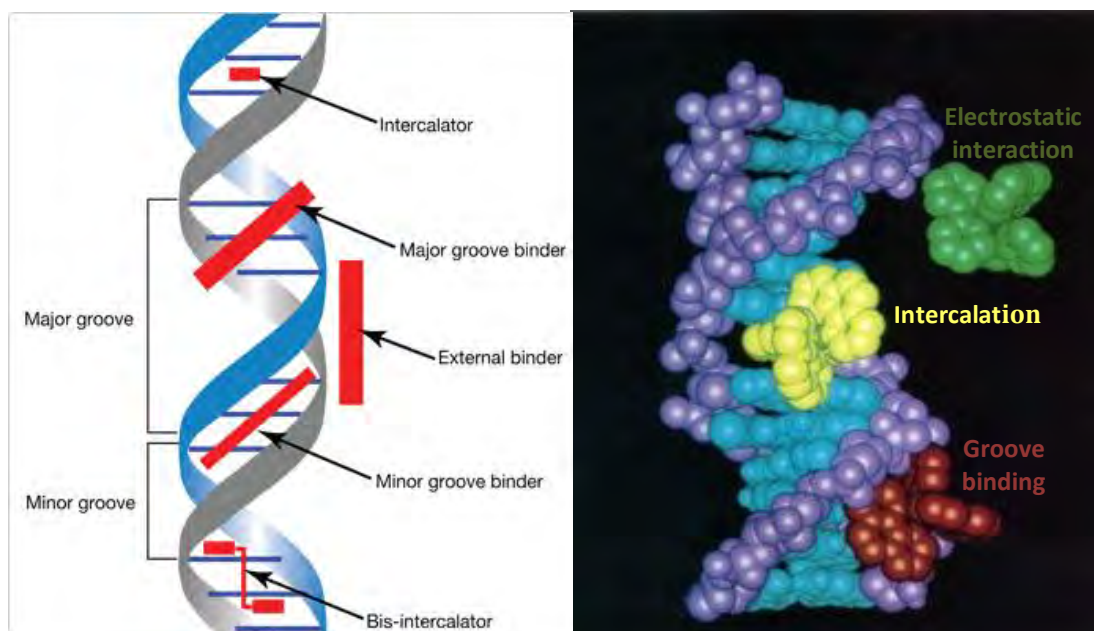


Figure 2.8. Drug-DNA non-covalent interactions a) schematic representation b) computer model.

2.1. Outside-edge binding

It is an electrostatic interaction with the negatively charged nucleic acid sugar-phosphate structure (which is generally non-specific)¹⁷. The archetypal outside-edge binding drugs are the polyamines, spermine and spermidine which play an analogous role to histones, in that they may neutralize some of the negative charges on the DNA backbone and hence promote DNA packaging (Figure 2.9)¹².

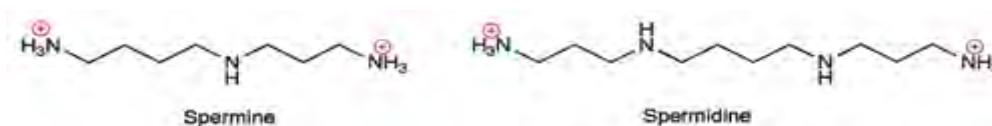


Figure 2.9. Structures of two outside-edge electrostatic DNA binding ligands, spermine and spermidine.

2.2. Intercalation/bisintercalation

Planar organic molecules containing several aromatic condensed rings often bind to DNA in an intercalative mode between base pairs^{18,19}. Ligand intercalation is associated with favourable enthalpic contributions to free energy arising from the formation of noncovalent interactions between the drug and base pairs. These noncovalent interactions involve several different forces, such as the hydrophobic effect, reduction of coulombic repulsion, Van der Waals interactions, π -stacking, and hydrogen bonding¹². Several acridines (e.g. C-1311), alkaloids (e.g. diplamine), anthracyclines (e.g. doxorubicin), anthracenediones (e.g. mitoxantrone), arylaminoalcohols (elinafide), coumarins (e.g. 9-methyl-2,3-dihydrocyclopenta[*c*]furo[3,2-*g*]chromen-4(1*H*)-one), phenanthridines (e.g. ethidium bromide), quinolines (e.g. fascaplysin), indoles (e.g. AT2433-B1), and quinoxalines (e.g. Triostin A) have shown to be intercalating antitumoral drugs¹⁶ (Figure 2.10).

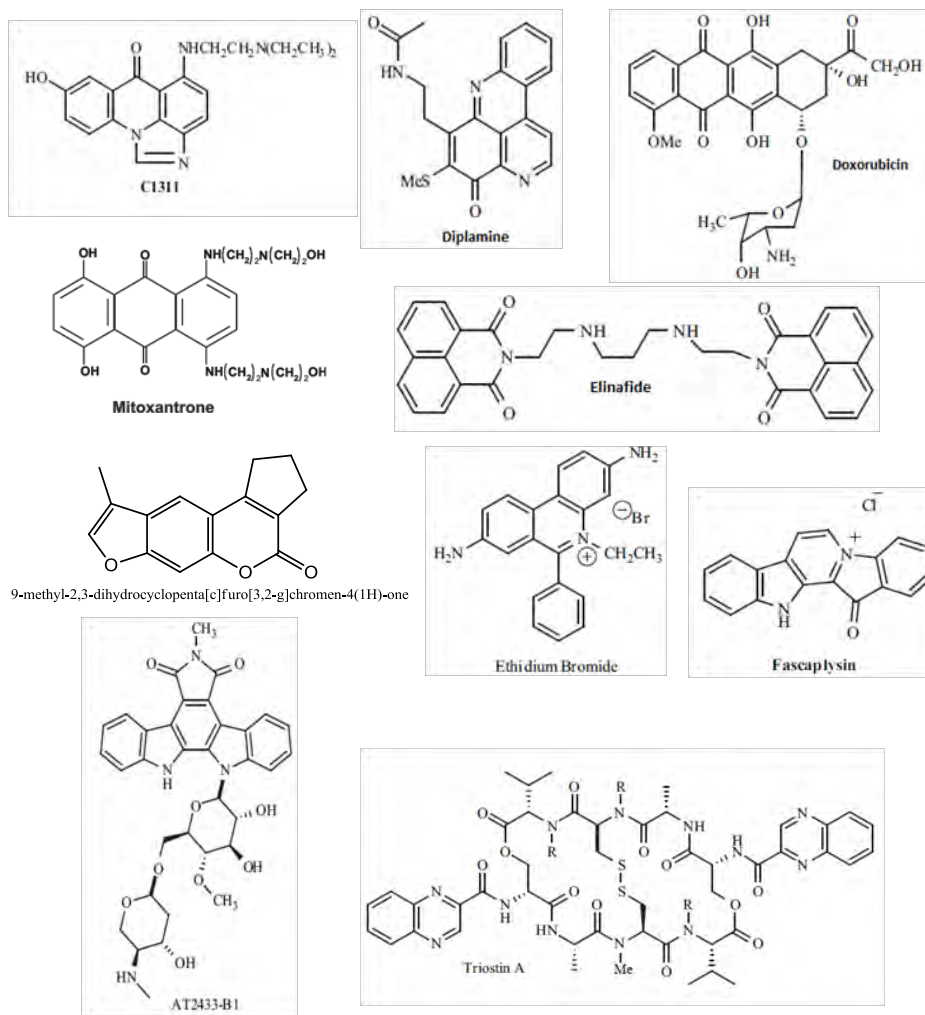


Figure 2.10. Several DNA-intercalators which act as antitumor drugs¹⁶.

Bisintercalators (e.g. bisacridine, Figure 2.11) are bifunctional molecules that possess two planar intercalating aromatic ring systems covalently linked by chains of varying length. A good reason for designing and synthesising a bisintercalator is that it should have a significantly higher affinity and much slower dissociation kinetics than the monointercalator equivalents. The binding constant for a bisintercalator should be approximately the square of the monomer binding constant. Since the biological activity is often closely correlated with binding affinity, bisintercalators should also have enhanced medical application¹².

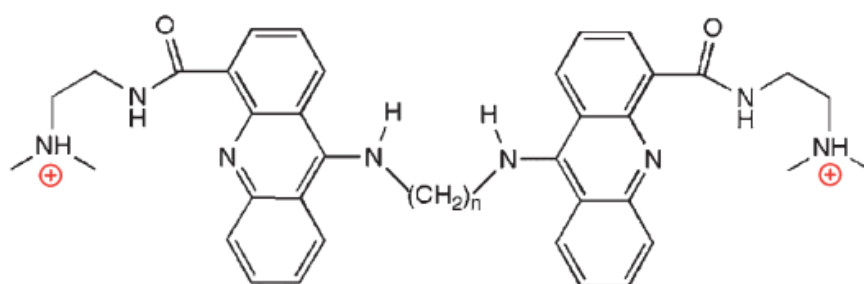


Figure 2.11. A flexibly linked bisintercalator formed from two dimethylaminoethylacridine-4-carboxamide moieties¹².

The spatial arrangement of DNA before, during, and after replication is essential to a high-quality cell-division process. In this way, DNA topology is governed by Topoisomerases (*Topos*)²⁰. Topos can be classified in two main classes: Topo I, which breaks only one strand of the DNA²¹, although both strands are involved in the interaction with the enzyme²², and Topo II²³, which breaks both strands of the duplex^{24,25}. A DNA intercalator has cytotoxic activity when it poisons the Topo by stabilizing the ternary, DNA–intercalator–Topo complex in such a way that the enzymatic process cannot continue forward or backward. Once the enzyme–DNA complexes are poisoned by intercalators, the ternary complex is detected by the cell as a damaged portion, which triggers a series of events; one of the more important events involves p53 protein, which induces cell apoptosis (programmed cell death) (Figure 2.12)²⁶⁻²⁸.

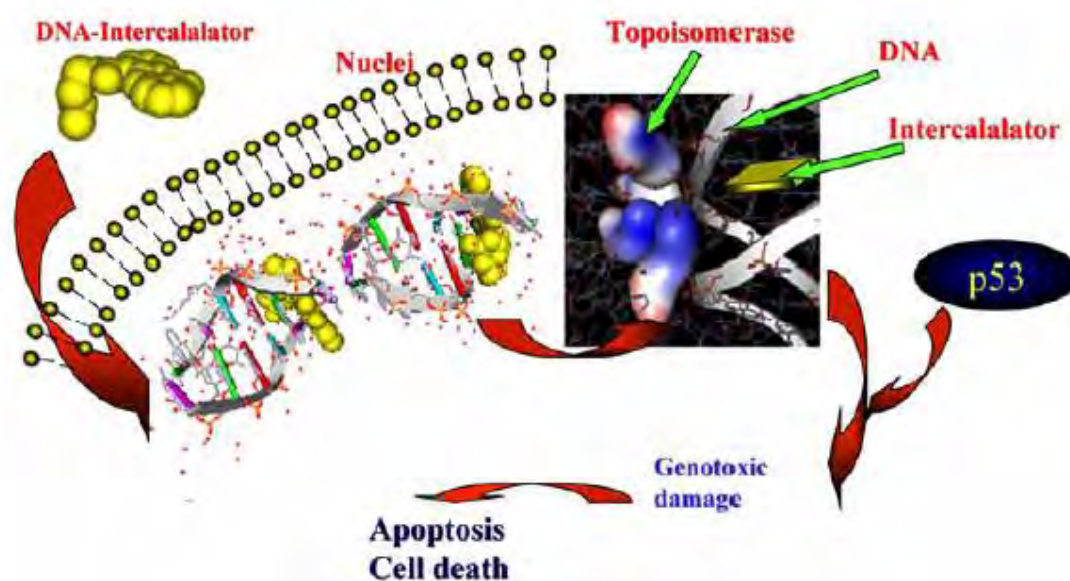


Figure 2.12. Schematic representation of the mechanism of cytotoxicity of a DNA-Intercalator¹⁶.

Since Topos are ubiquitous in eukaryotic cells, both healthy and damaged cells can be affected during treatment with this class of poisons²⁹, although cells that are constantly and frequently replicating (i.e., tumor cells) will be affected more than healthy cells¹⁶.

2.3. Minor and major DNA grooves binding interaction

The drugs which bind to DNA minor or major grooves are typically composed of several aromatic rings such as pyrrole, furan, or benzene that are connected by bonds possessing torsional freedom¹⁹. Minor groove binding makes intimate contacts with the walls of the groove, and as a result of this interaction numerous hydrogen bonding and electrostatic interactions occur between anticancer drugs and DNA (DNA bases and the phosphate backbone). Major groove binding occurs via the hydrogen bonding to the DNA and can form a DNA triple helix.

A large number of functional groups of the DNA bases are accessible in the wide major groove compared to the narrow minor groove. However, many small molecules interact with DNA in the minor groove. The major and minor grooves differ in electrostatic potential, hydrogen-bonding characteristics, steric effects, and hydration. In general, small groove-binding molecules exhibit a preference for the minor groove, not least because this site of interaction provides better Van der Waals contacts. Distamycin A and mithramycin A are antitumoral compounds which bind to DNA in the minor grooves (Figure 2.13)¹⁷.

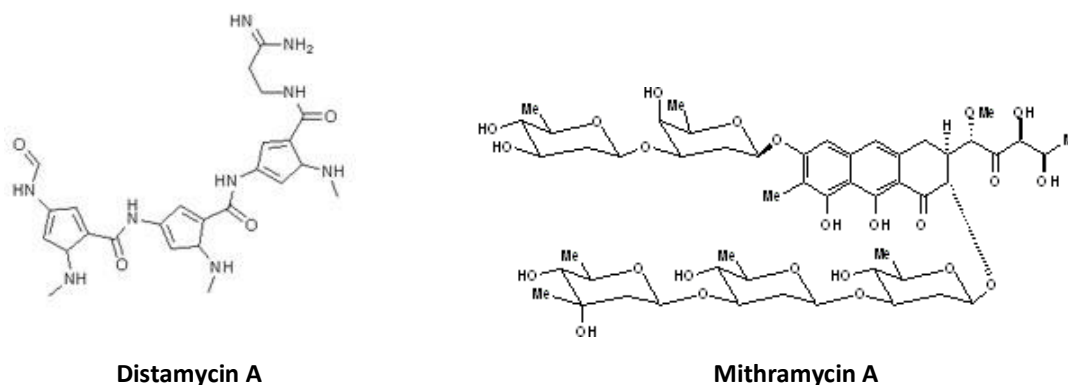


Figure 2.13. Distamycin A and Mithramycin A structures.

Different modes of binding can occur simultaneously with the same antitumoral compound³⁰. For example, mitomycin is a groove binder but also a cross-linker and

daunomycin is able to bind to the minor groove and intercalate between the DNA base pairs (Figure 2.14). Note that many minor groove-binding ligands prefer A-T sites compared to intercalators, which generally exhibit a G-C preference¹².

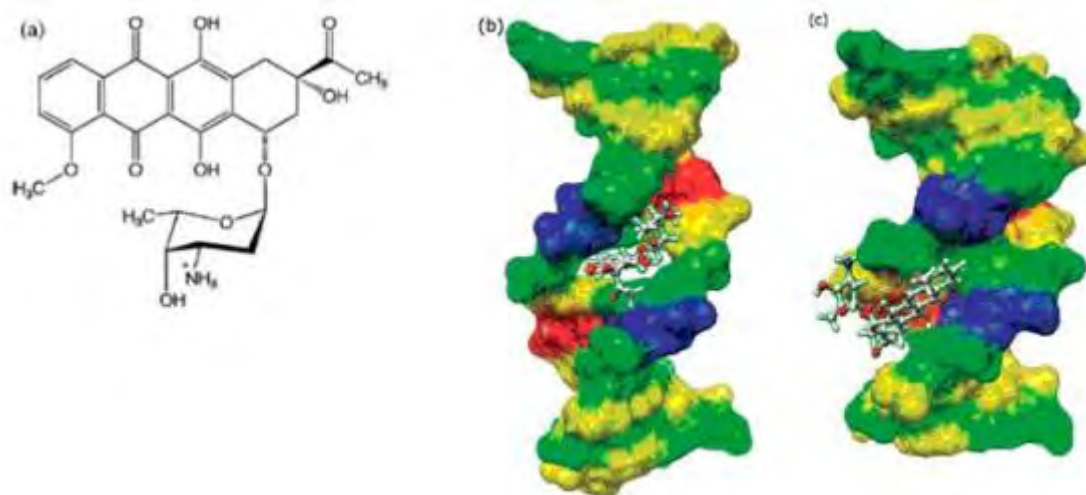


Figure 2.14. (a) Atomistic structure of daunomycin. Constructed and equilibrated structures of (b) the intercalated state and (c) the minor groove-bound state. In both figures, DNA is shown in a semitransparent surface representation including ball and stick atom models and residue-based color (yellow for C, green for G, red for A and blue for T), whereas daunomycin is represented via a ball and stick model with element-based CPK color³⁰.

2.4. Thermodynamics of drug-DNA interactions

A classical equation for the determination of binding parameters (more specifically, the association constant) for the non-cooperative binding is the modified form of Scatchard plot, proposed by McGhee and von Hippel¹²:

$$\frac{r}{C_f} = K(1 - nr) \left[\frac{(1 - nr)}{1 - (n - 1)r} \right]^{n-1} \quad (2.1)$$

where r is the binding ratio (defined as the ratio of the concentration of bound drug (C_b) over the total concentration of DNA binding sites (S), C_f the concentration of free drug, K the equilibrium binding constant for all sites, i.e. any sequence dependence for drug binding is ignored, and n the binding site size, i.e. the number of base pairs occupied by a bound drug. C_b and C_f can be calculated by

$$C_b = \frac{I_{F,0} - I_F}{I_{F,0} - I_{F,b}} \times C_{\text{total}} \quad (2.2)$$

$$\text{and } C_{\text{total}} = C_f + C_b \quad (2.3)$$

where $I_{F,0}$ is the fluorescence intensity of the free compound and $I_{F,b}$ the fluorescence intensity of the bound compound at total binding.

When a complex between DNA and drug is formed, changes in the thermodynamic stability and the functional properties of DNA occur¹⁷. Although there is a significant free energy cost for the establishment of the intercalation cavity (approximately 4 kcal mol⁻¹), favorable contributions (hydrophobic, ionic, hydrogen bonding, and Van der Waals) result in association constants of 10⁵ to 10¹¹ M⁻¹. Groove binders are stabilized by intermolecular interactions and typically have larger association constants than intercalators (approximately 10¹¹ M⁻¹), since a cost in free energy is not required for creation of the binding site¹⁵.

2.5. Methods to determine the DNA-drug binding modes

Determination of DNA binding modes of small molecules is crucial for revealing their potential genotoxicity. Drug–DNA binding may result in changes in gene expression and influence cell proliferation^{31,32}. Thus, understanding drug–DNA binding mechanisms is crucial for predicting the consequences of these interactions in the human body³³. Groove binding typically results in only subtle changes in structure, and the DNA remains in the same form. In contrast, intercalation, in which a planar ligand moiety is inserted between adjacent base pairs, results in a substantial change in DNA structure, and causes lengthening, stiffening, and unwinding of the helix. These changes result in a pronounced alteration of the hydrodynamic properties of DNA for intercalation, but not for groove binding. Furthermore, for intercalation, the planar chromophore is in close contact with the DNA base pairs, and is oriented roughly perpendicular to the DNA helix axis. Thus, techniques that can evaluate the orientation of the ligand chromophore and its proximity to the DNA bases, can potentially distinguish intercalation from groove binding³⁴.

Many techniques have been applied for investigation of the interaction of DNA with small molecules including X-ray diffraction, Nuclear Magnetic Resonance, Mass Spectrometry, Footprinting, UV-Visible Spectroscopy, Circular Dichroism Spectroscopy, Calorimetry, Gel electrophoresis, Dynamic Viscosity, Single Molecule Force Spectroscopy, Docking Studies, FT-IR and Raman Spectroscopy, Molecular Modeling Techniques, Equilibrium Dialysis, Electric Linear Dichroism, Surface Plasmon Resonance

and Electrochemical Techniques^{15,16,17,18,33,34}. Standard fluorescence methods, such as intensity measurements, polarization, and solute quenching studies have also been applied. Indeed, many molecules exhibit a large fluorescence enhancement^{15,33} and an increased polarization value³⁴ on binding to DNA. Fluorescence quenching assays allow distinguishing between DNA binding modes³⁵ since intercalators are less accessible to anionic quenchers than groove binders, due to electrostatic repulsion with the negatively charged sugar-phosphate DNA backbone³⁶.

3. References

1. International Human Genome Sequencing Consortium, Initial sequencing and analysis of the human genome, *Nature*, **2001**, *409*(6822), 860–921.
2. G. Gibson, S.V. Muse, *A Primer of Genome Science, Second Edition*, Sinauer Associates, **2004**.
3. R. Dahm, Discovering DNA: Friedrich Miescher and the early years of nucleic acid research, *Hum. Genet.*, **2008**, *122*(6), 565–581.
4. J.D. Watson, F.H.C. Crick, A Structure for Deoxyribose Nucleic Acid, *Nature*, **1953**, *171*, 737-738.
5. P. Atkins, J. de Paula, *Physical Chemistry for the life sciences*, Oxford University Press: United Kingdom, **2006**.
6. J.B. Losos, K.A. Mason, S.R. Singer, P.H. Raven, G.B. Johnson, *Biology*, Boston: McGraw-Hill Higher Education, **2008**.
7. A. Hongjie, J. Bo, Prospects of nanoparticle–DNA binding and its implications in medical biotechnology, *Biotechnology Advances*, **2012**, *30*(6), 1721–1732.
8. B. Alberts, D. Bray, K. Hopkin, A. Johnson, J. Lewis, M. Raff, K. Roberts, P. Walter *Essential cell biology, Third Edition*, New York: Garland Science, **2009**.
9. H. Clausen-Schaumann, M. Rief, C. Tolksdorf, H. Gaub, Mechanical stability of single DNA molecules, *Biophys. J.*, **2000**, *78*(4), 1997–2007.
10. B. Alberts, A. Johnson, J. Lewis, M. Raff, K. Roberts, P. Walters, *Molecular Biology of the Cell, Fourth Edition*. New York and London: Garland Science, **2002**.
11. J.B. Chaires, Energetics of drug–DNA interactions, *Biopolymers*, **1997**, *44*, 201-215.
12. G.M. Bleckburn, M.N. Gait, *Nucleic Acids in Chemistry and Biology*, IRL Press: New York, **1990**.
13. D.E. Graves, L.M. Velea, Intercalative Binding of Small Molecules to Nucleic Acids, *Curr. Org. Chem.*, **2000**, *4*, 915–929.
14. D. Duan, Pharmacology 601, Sec VII: Chemotherapy (lecture notes), Department of Pharmacology, University of Nevada, **2004**, p. 61.

15. R. Palchaudhuri, P.J. Hergenrother, DNA as a target for anticancer compounds: methods to determine the mode of binding and the mechanism of action, *Current Opinion in Biotechnology*, **2007**, *18*, 497–503.
16. R. Martínez, L. Chacón-García, The Search of DNA-Intercalators as Antitumoral Drugs: What it Worked and What did not Work, *Current Medicinal Chemistry*, **2005**, *12*, 127-151.
17. S. Rauf, J.J. Gooding, K. Akhtar, M.A. Ghauri, M. Rahman, M.A. Anwar, A.M. Khalid, Electrochemical approach of anticancer drugs–DNA interaction, *Journal of Pharmaceutical and Biomedical Analysis*, **2005**, *37*, 205–217.
18. D. Khare, R. Pande, Experimental and molecular docking study on dna binding interaction of N-phenylbenzohydroxamic acid, *Der Pharma Chemica*, **2012**, *4(1)*, 66-75.
19. Ihtshamul Haq, Part II: The Thermodynamics of Drug–Bipolymer Interaction- Thermodynamics of drug–DNA interactions, *Archives of Biochemistry and Biophysics*, **2002**, *403*, 1–15.
20. H. Lodish, D. Baltimore, A. Berk, S.L. Zipursky, P. Matsudaira, J. Darnell, *Molecular Cell Biology*, New York, **1999**, pp. 110-111.
21. L. Stewart, M.R. Redinbo, X. Qiu, W.W.J. Holo, J.J. Champoux, A model for the mechanism of human topoisomerase I, *Science*, **1998**, *279(5356)*, 1534-1541.
22. K. Christiansen, A.V. Dirac, A.H. Anderson, O. Westergaard, Eukaryotic topoisomerase I-Mediated cleavage requires bipartite DNA interaction - cleavage of dna substrates containing strand interruptions implicates a role for topoisomerase-I in illegitimate recombination, *J. Biol. Chem.*, **1993**, *268(13)*, 9690-9701.
23. J.M. Berger, S.J. Gamblin, S.C. Harrison, J.C. Wang, Structure and mechanism of DNA topoisomerase II, *Nature*, **1996**, *379(6562)*, 225-232.
24. J.C. Wang, DNA topoisomerases, *Annu. Rev. Biochem.*, **1996**, *65*, 635-692.
25. J.M. Berger, Structure of DNA topoisomerases, *Biochim. Biophys. Acta*, **1998**, *1400*, 3-18.

26. T.G. Cotter, S.V. Lennon, J.G. Glynn, S.J. Martin, Cell-death via apoptosis and its relationship to growth, development and differentiation of both tumor and normal-cells, *Anticancer Research*, **1990**, *10*, 1153-1159.
27. P. Calabresi, B.A. Chabner, *Goodman and Gilman's The Pharmacological Basis of Therapeutics*, 9th ed., Hardman, J. G., Goodman Gilman, A., Limbird, L. E., Eds., Mc. Graw Hill, **1996**, pp. 1225-1232.
28. E. Solary, R. Bertrand, Y. Pommier, Apoptosis induced by dna topoisomerase-i and topoisomerase-II inhibitors in human leukemic HL-60 cells, *Leuk. Lymph.*, **1994**, *15*, 21-32.
29. G. Boos, H. Stopper, Genotoxicity of several clinically used topoisomerase II inhibitors, *Toxicology Lett.*, **2000**, *116*, 7-16.
30. A. Mukherjee, R. Lavery, B. Bagchi, J.T. Hynes, On the Molecular Mechanism of Drug Intercalation into DNA: A Simulation Study of the Intercalation Pathway, Free Energy, and DNA Structural Changes, *J. Am. Chem. Soc.*, **2008**, *130*(30), 9747–9755.
31. P.R. Turner, W.A. Denny, The genome as a drug target: sequence specific inor groove binding ligands, *Curr. Drug Targets*, **2000**, *1*, 1–14.
32. M. Zihlif, D.R. Catchpoole, B.W. Stewart, L.P. Wakelin, Effects of DNA minor groove binding agents on global gene expression, *Cancer Genet. Proteomics*, **2010**, *7*, 323–330.
33. A.K. Williams, S.C. Dasilva, A. Bhatta, B. Rawal, M. Liu, E.A. Korobkova, Determination of the drug–DNA binding modes using fluorescence-based assays, *Analytical Biochemistry*, **2012**, *422*, 66–73.
34. D. Suh, J.B. Chaires, Criteria for the Mode of Binding of DNA Binding Agents, *Bioorganic & Medicinal Chemistry*, **1995**, *3*(6), 723-728.
35. C.V. Kumar, E.H. Asuncion, DNA-binding studies and site-selective fluorescence sensitization of an anthryl probe, *J. Am. Chem. Soc.*, **1993**, *115*(19), 8547-8553.
36. C.V. Kumar, E.H.A. Punzalan, W.B. Tan, Adenine-thymine base pair recognition by an anthryl probe from the DNA minor groove, *Tetrahedron*, **2000**, *56*(36), 7027-7040.

Chapter 3

Compounds encapsulation in nanoliposomes

INDEX

1. Nanocarriers for drug delivery	53
2. Liposomes	57
2.1. Lipids as structural components of liposomes	57
2.2. Molecular Self-assembly	59
2.3. Different types of liposomes	60
2.4. Liposomes preparation	61
3. Liposomes as drug delivery systems	63
4. Determination of the size and zeta-potential of the liposomes with incorporated compounds	67
5. References	71

1. Nanocarriers for drug delivery

The last years have seen an explosion of interest for the area of science and technology known as “nanotechnology”. Nanotechnologies are defined as technologies which include components that have at least one dimension between 1-100 nm, and display unique characteristics due to being at this scale. Unlike previous high-technology waves, nanotechnology covers a diverse field of sciences and engineering, crosses boundaries between them and aims to utilize the very fundamental characteristics of matter by manipulation and control at the nanoscale in order to create new material and devices with functional characteristics different from the common materials¹.

Bionanotechnology is one of the most promising areas of nanotechnology and in the present it is directly related with the use of biological systems, like cells and cellular components, to create functional nanodevices made of organic and inorganic materials for biological activity. This is an area in permanent expansion and a lot of studies about new fabrication methods and characterization techniques arise constantly.

Bionanotechnology includes many important areas such as nanomedicine, diagnosis and therapy with the development of new drugs. One of the most promising research areas of bionanotechnology is the development of systems for controlled drug delivery by nanoencapsulation of drugs, to solve several limitations of conventional drug delivery systems, such as nonspecific biodistribution and targeting, lack of water solubility, poor oral bioavailability, and low therapeutic indices, namely due to resistance of the cancer cells².


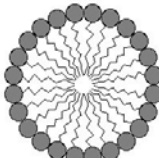

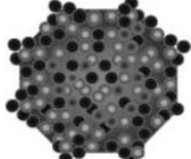

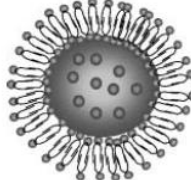
The use of nanocarriers as systems for drug delivery has many advantages when compared with other conventional methods, since they can potentially overcome solubility, pharmacokinetics, in vivo stability and toxicity problems³⁻⁵, more precisely:

- The biodistribution of cancer drugs is improved as nanoparticles have optimal size and surface characteristics which increase their circulation time in the bloodstream;
- The nature and the composition of the vehicles protect and prevent the decomposition of the drug;
- Nanocarriers allow a secure administration of the drug without local inflammatory reactions;

- More effective therapy and decrease of the number of the doses due to the gradual and controlled release of the drug;
- Nanocarriers can enhance the intracellular concentration of drugs in cancer cells while avoiding toxicity in normal cells, by using both passive targeting strategies (such as the acidic environment of tumor cells or the enhanced permeability and retention effects of tumors due to their leaky vasculature and their lack of an effective lymphatic drainage system) and active targeting strategies (using ligands or antibodies directed against selected tumor targets)^{2,6,7}.
- When nanocarriers bind to specific receptors and then enter the cell, they are usually enveloped by endosomes via receptor-mediated endocytosis, thereby bypassing the recognition of P-glycoprotein, one of the main drug resistance mechanisms⁸.

There are many different submicron-sized (3-200nm) devices being used for drug delivery, namely devices made of polymers (polymeric nanoparticles, micelles, or dendrimers), viruses (viral nanoparticles), organometallic compounds (carbon nanotubes) or lipids (liposomes). Each of these systems has specific peculiarities that should be considered in the choice of the delivery system² (Table 3.1).

Table 1. Types of nanocarriers for drug delivery (adapted from ref. 2).

System	Structure	Characteristics
Polymeric nanoparticles (polymer-drug conjugates) 	Drugs are encapsulated in a polymer or conjugated to the side chain of a linear polymer with a linker (cleavable bond).	a) Water-soluble, nontoxic, biodegradable; b) Surface modification (pegylation); c) Selective accumulation and retention in tumor tissue (EPR effect); d) Specific targeting of cancer cells while sparing normal cells- receptor mediated targeting with a ligand.
Polymeric micelles 	Amphiphilic block copolymers assemble and form a micelle with a hydrophobic core (reservoir for hydrophobic drugs) and hydrophilic shell which stabilizes the core and renders the polymer to be water-soluble.	a) Suitable carrier for water-insoluble drug; b) Biocompatible, self-assembling, biodegradable; c) Ease of functional modification; d) Targeting potential.
Dendrimers 	Radially-emerging hyperbranched synthetic polymer with regular pattern and repeated units.	a) Biodistribution and pK can be tuned; b) High structural and chemical homogeneity; c) Ease of functionalization, high ligand density; d) Controlled degradation; e) Multifunctionality.
Viral nanoparticles 	Protein cages, which are multivalent, self-assembled structures.	a) Surface modification by mutagenesis or bioconjugation – multivalency; b) Specific tumor targeting, multifunctionality; c) Defined geometry and remarkable uniformity; d) Biological compatibility and inert nature.
Carbon nanotubes 	Carbon cylinders composed of carbon atoms in a hexagonal arrangement.	a) Water-soluble and biocompatible through chemical modification (organic functionalization); b) Multifunctionality.
Liposomes 	Self-assembling closed colloidal structures composed of lipid bilayers in which an aqueous volume is entirely enclosed by a membranous lipid bilayer.	a) Amphiphilic, biocompatible; b) Ease of modification; c) Targeting potential.

However, although nanoparticles offer many advantages as drug carrier systems, there are still many limitations to be solved such as poor oral bioavailability, instability in circulation, inadequate tissue distribution, and toxicity².

2. Liposomes

2.1. Lipids as structural components of liposomes

Lipids constitute a group of naturally occurring molecules that include fats, waxes, sterols (such as cholesterol), fat-soluble vitamins (such as vitamins A, D, E, and K), monoglycerides, diglycerides, triglycerides, phospholipids, and others. The main biological functions of lipids include energy storage, signaling, and acting as structural components of cell membranes^{9,10}. Lipids have found applications in cosmetic and food industries, as well as in nanotechnology, e.g. acting as structural components of liposomes¹¹.

Phospholipids play a central role in the biochemistry of all living cells. These molecules constitute the lipid bilayer defining the outer confines of a cell, but also serve as the structural entities which confine subcellular components¹². Furthermore, phospholipids are the widely used structural components of liposomes. A phospholipid is composed of two fatty acid chains, a glycerol unit, a phosphate group and a polar molecule (e.g. choline, glycerol, etc). Phospholipids are amphipathic/amphiphilic compounds in a way that the phosphate group and polar head region of the molecule is hydrophilic, while the fatty acid tail region is hydrophobic (Figure 3.1).

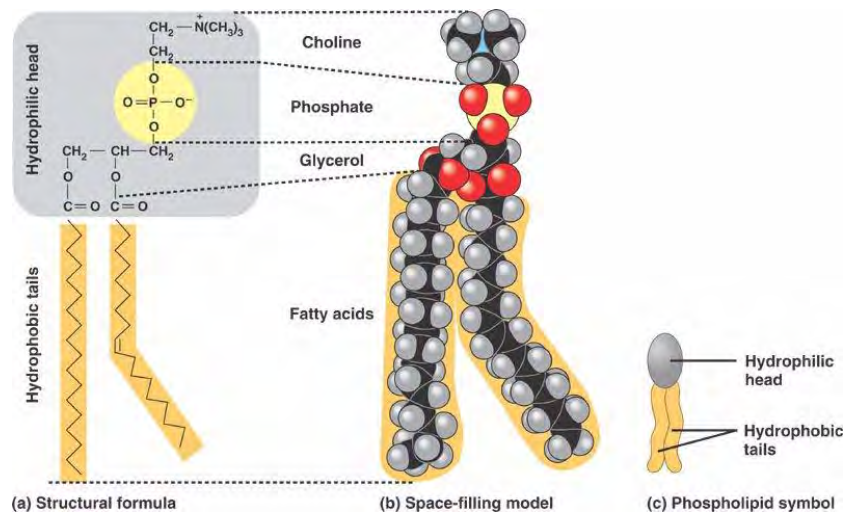


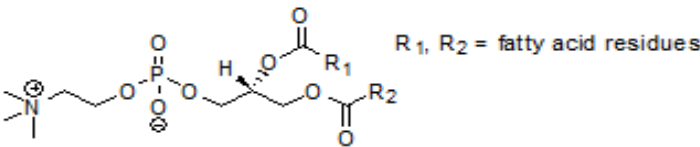
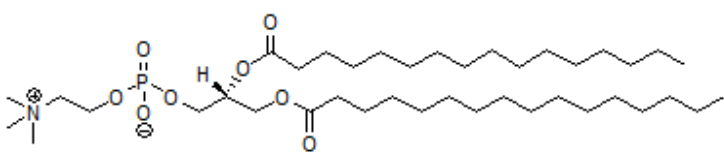
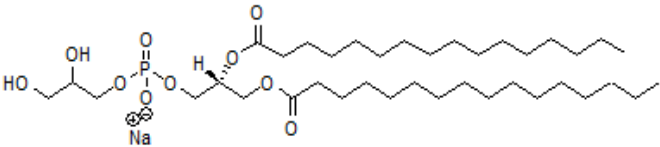
Figure 3.1. Typical structure of a phospholipid.

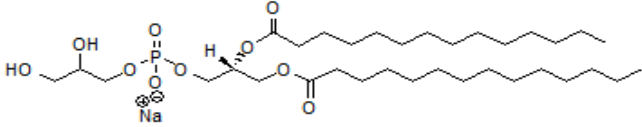
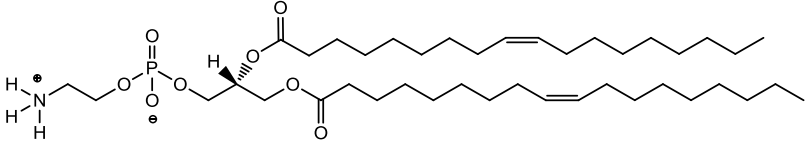
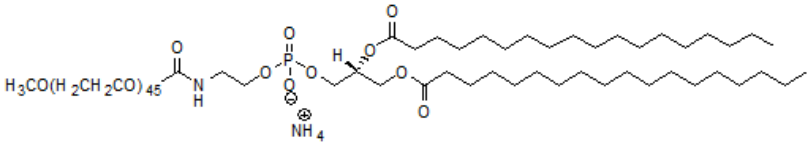
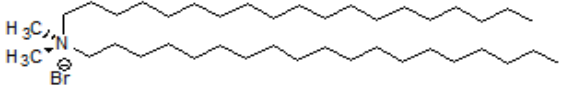
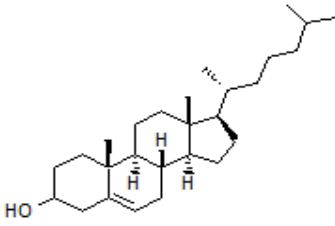
Lipids are characterized by the phase transition temperature (or melting temperature), T_m , which is defined as the temperature required to induce a change in the lipid physical state from the ordered gel phase, where the hydrocarbon chains are fully

extended and closely packed, to the disordered liquid crystalline phase, where the hydrocarbon chains are randomly oriented and fluid. There are several factors which directly affect the phase transition temperature including hydrocarbon length, unsaturation, charge, and headgroup species. As the hydrocarbon length is increased, van der Waals interactions become stronger requiring more energy to disrupt the ordered packing, thus the phase transition temperature increases. Likewise, introducing a *cis* double bond into the acyl group puts a kink in the chain which requires much lower temperatures to induce an ordered packing arrangement.

Relatively to the electric charge, lipids can be ionic (cationic or anionic) molecules, neutral molecules or zwitterionic molecules (both positive and negative charge, in different atoms). Table 3.2 shows some lipids structures, as well as their electric charge and phase transition temperature.

Table 3.2. Structure, electric charge and phase transition temperature, T_m , of some lipids.

Structure	Electric charge	T_m /°C
<p>Egg-PC 1,2-diacyl-<i>sn</i>-glycero-3-phosphocholine from egg yolk</p>  <p>$R_1, R_2 = \text{fatty acid residues}$</p>	Zwitterionic	Very low
<p>DPPC 1,2-Dipalmitoyl-<i>sn</i>-glycero-3-phosphocholine</p> 	Zwitterionic	41 (Ref. 13)
<p>DPPG 1,2-dipalmitoyl-<i>sn</i>-glycero-3-[phospho-<i>rac</i>-(1-glycerol)] (sodium salt)</p> 	Anionic	40 (Ref. 14)

<p style="text-align: center;">DMPG 1,2-dimyristoyl-<i>sn</i>-glycero-3-[phospho-<i>rac</i>-(1-glycerol)] (sodium salt)</p> 	Anionic	23 (Ref. 15)
<p style="text-align: center;">DOPE 1,2-Dioleoyl-<i>sn</i>-glycero-3-phosphoethanolamine</p> 	zwitterionic	Very low
<p style="text-align: center;">DSPE-PEG 1,2-Distearoyl-<i>sn</i>-glycero-3-phosphoethanolamine-<i>N</i>-[methoxy(polyethylene glycol)-2000] (ammonium salt)</p> 	Anionic	12.8
<p style="text-align: center;">DODAB dioctadecyldimethylammonium bromide</p> 	Cationic	45 (Ref. 16)
<p style="text-align: center;">Cholesterol</p> 	Neutral	Very low

2.2. Molecular Self-assembly

Molecular self-assembly is the process by which molecules adopt a defined arrangement without guidance or management from an outside source. When phospholipids are suspended in water they tend to self-orient in order to avoid any

contact between the non-polar tails and water (energetically unfavorable) and to maintain the contact between water and the polar head of the molecules. In this way, amphiphilic molecules can form a variety of structures, such as bilayers, micelles or liposomes, due to hydrophilic/hydrophobic interactions but also electrostatic and Van der Waals interactions (Figure 3.2).

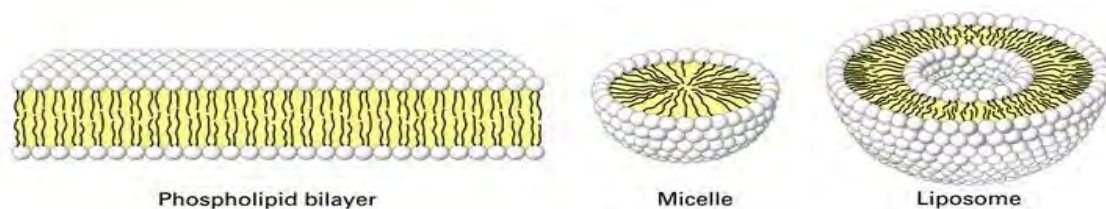


Figure 3.2. Different self-organized structures.

2.3. Different types of liposomes

Liposomes were discovered in 1965 by Bangham, who found that when phospholipids were dispersed in water, vesicular structures of hydrated bilayers with an aqueous cavity are formed spontaneously¹⁷.

Liposomes are vesicles composed of one or more lipid bilayer membranes. The unique ability of liposomes to entrap drugs both in an aqueous and a lipid phase make such delivery systems attractive for hydrophilic and hydrophobic drugs¹⁸. Because lipids are amphipathic in aqueous media, their thermodynamic phase properties and self-assembling characteristics evoke entropically driven sequestration of their hydrophobic regions into spherical bilayers. Those layers are referred to as *lamellae*¹⁹ (Figure 3.3). Liposomes can be unilamellar (with only one bilayer surrounding the aqueous core) or multilamellar (with several bilayers oriented concentrically around an aqueous core)²⁰.

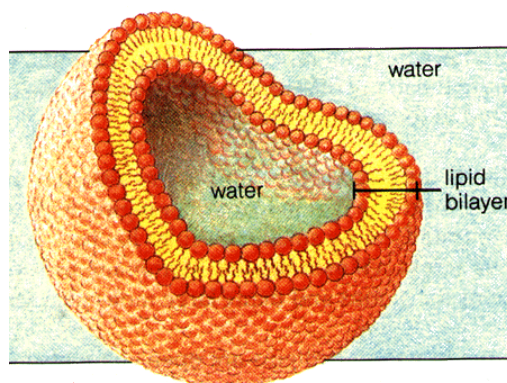


Figure 3.3. Unilamellar liposome structure.

According to size and number of lamellae, liposomes are divided into different subcategories (table 3.3 and figure 3.4).

Table 3.3. Liposome classification based on structural parameters²⁰.

Vesicle Types	Abbreviation	Diameter Size	Number of Lipid Bilayers
Small Unilamellar Vesicles	SUV	20 - 100 nm	One
Large Unilamellar Vesicles	LUV	> 100 nm	One
Multilamellar Vesicles	MLV	> 0.5 μm	Five to Twenty
Oligolamellar Vesicles	OLV	0.1 - 1 μm	Approximately five
Multivesicular Vesicles	MVV	> 1 μm	Multicompartmental Structure

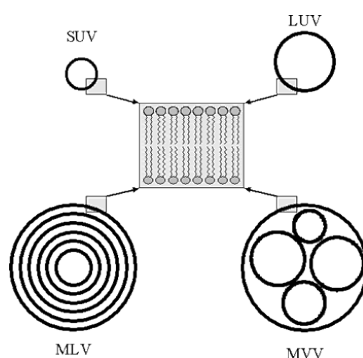
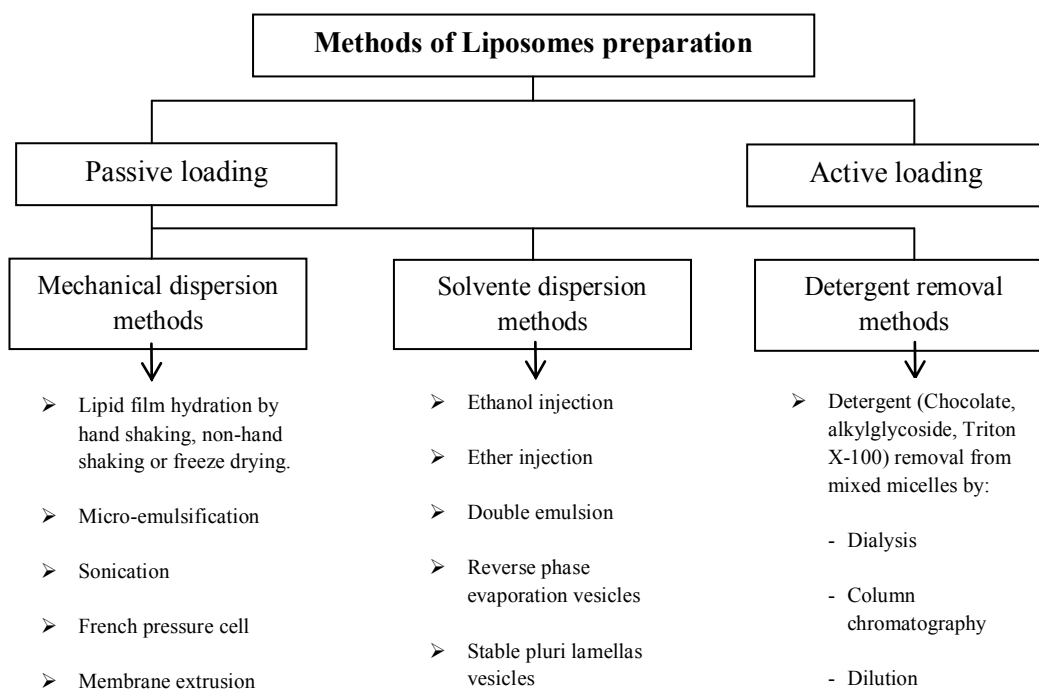


Figure 3.4. Schematic representation of different liposomes²¹.

2.4. Liposomes preparation

In contrast to other surfactant aggregates such as micelles, liposomes do not form spontaneously in aqueous media and are therefore not thermodynamically stable structures²². Formation of liposomes requires energy. Depending on which type of liposome is produced, the required energy input can greatly vary. MLVs form readily when bilayer-forming polar lipids are dispersed in aqueous media under mild agitation. In order to produce LUVs and SUVs, substantial energy inputs are required that are sufficient to disrupt MLV and MVV structures and force the generation of unimodal vesicles²³. Generally, liposomes are only stable for a defined period of time; i.e. they are said to be “kinetically stable” similar to emulsions. Because of this, many of the principles of emulsion formation also apply to the formation of liposomes and the techniques used to produce emulsions may often be used to produce liposomes²⁴.

Liposomes can be obtained by means of several different methods (Scheme 3.1). Normally, the entrapped agents are loaded before or during the manufacturing procedure (passive loading). However, certain type of compounds with ionizable groups, and those which display both lipid and water solubility, can be introduced into the liposomes after the formation of intact vesicles (active loading)²⁵.



Scheme 3.1. Different methods for liposomes preparation²⁵.

The adequate choice of liposome preparation method depends on the following parameters^{26,27}:

- 1) the physicochemical characteristics of the material to be entrapped and those of the liposomal ingredients;
- 2) the nature of the medium in which the lipid vesicles are dispersed;
- 3) the effective concentration of the entrapped substance and its potential toxicity;
- 4) additional processes involved during application/delivery of the vesicles;
- 5) optimum size, polydispersity and shelf-life of the vesicles for the intended application and
- 6) batch-to-batch reproducibility and possibility of large-scale production of safe and efficient liposomal products.

3. Liposomes as drug delivery systems

Liposomes were suggested as drug carriers in cancer chemotherapy by Gregoriadis et al.²⁸ in 1974. Since then, liposomes have been extensively used as carriers for pharmaceutical, diagnostic and cosmetic agents, with already a few commercially available products^{29,30}. As an example, Doxil[®] is a liposomal formulation of the anthracycline drug doxorubicin used to treat cancer in AIDS-related Kaposi sarcoma and multiple myeloma. Its advantages over free doxorubicin are greater efficacy and lower cardiotoxicity³¹. Nevertheless, liposomes still have not attained their full potential, and improvements must be made in terms of design, functionality and stability to allow the drugs to reach and to be transferred to the target site²⁰ and to combat the increasing problem of *multidrug resistance* (MDR) acquired by cancers³¹.

To reach the target site, the liposomes must remain time enough in the circulatory system without being disintegrated by high-density lipoproteins (HDLs) in the plasma (which were found to remove phospholipid molecules rapidly from the bilayers of vesicles) or without being intercepted by the fixed macrophages of the reticuloendothelial system (RES)³².

The selective delivery of drugs into disease sites is generally achieved by extravasation into the interstitial space from the bloodstream³¹ (Figure 3.5). This can be achieved by either passive or active targeting^{3,29}. Active targeting requires some kind of ligand to bind the liposome surface to the pathological cells and passive targeting uses the physical properties of the liposomes together with the microanatomy and the microenvironment of the target tissue to obtain selective localization²⁰. For example, liposomes can be designed to release their entrapped contents under certain controlled pH or temperature conditions¹⁸. In solid tumors, the extracellular pH tends to be significantly more acidic (6.5) than the pH of the blood at 37 °C, which is (7.5); so, it is possible to engineer vehicles for drugs with the adequate composition so that the delivery occurs in these specific sites. On the other hand, temperature can also be exploited, using a delivery system that releases the drug at temperatures above 37 °C (e.g. using lipids with $T_m > 37$ °C in the liposomes preparation)²⁰.

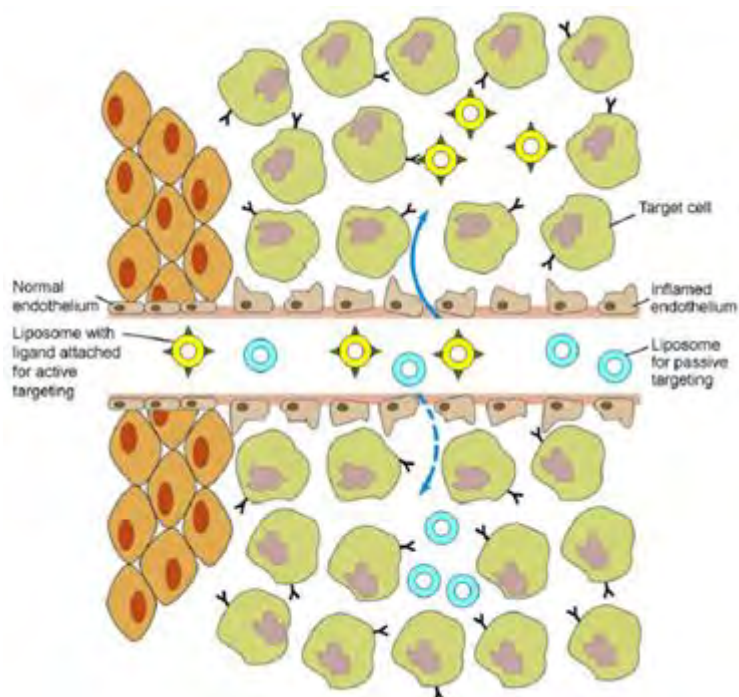


Figure 3.5. Active and passive targeting of cells for drug targeting using liposomes. At sites of pathology, where the endothelium layer is inflamed, mediators such as bradykinin, vascular endothelium growth factor, and prostaglandins increase the endothelial permeability. Underlying pathology includes cancer, rheumatoid arthritis and infection. Liposomes extravasate through the gaps between cells and enter the interstitial fluid. Active targeting is achieved by conjugating ligands to the liposome that bind to a specific target cell receptor, leading to internalization or release of the drug. Passive targeting can be mediated by internalization or local high-concentration release of the drug³¹.

To effectively deliver drug to the targeted tumor tissue, liposomes must have the ability to remain in the bloodstream for a considerable time without being eliminated. Conventional liposomes are usually caught in the circulation by the reticuloendothelial system, such as the liver and the spleen, depending on their size and composition/surface characteristics³³.

Size

The size of nanoliposomes used in a drug delivery system should be large enough to prevent their rapid leakage into blood capillaries but small enough to escape capture by fixed macrophages that are lodged in the reticuloendothelial system, such as the liver and spleen. The size of the sinusoid in the spleen and fenestra of the Kuffer cells in the liver varies from 150 to 200 nm³⁴ and the size of gap junction between endothelial cells of the leaky tumor vasculature may vary from 100 to 600 nm³⁵. Consequently, the size of nanoliposomes should be up to 100 nm to reach tumor tissues by passing through these two particular vascular structures².

Composition/surface characteristics

The phospholipid DMPG have shown to provide the formation of perforations (pores) across the lipid membrane in the intermediate phase (between the turbid gel and fluid membrane phases). This behavior might be a characteristic of charged membranes in general: they could exhibit a “melting regime” (temperature interval where the melting process evolves) instead of a unique melting transition. Thus, a high local concentration of charged lipids could help the formation/stabilization of transient pores across the membrane, which would enable a controlled material transport across biological membranes³⁶. Furthermore, the opening of pores across the membrane tuned by ionic strength, temperature, and pH, is likely to have biological relevance and could be used in applications for controlled release from nanocompartments³⁷.

The addition of cholesterol to the liposomes composition will prevent substance release as it will decrease liposome permeability and improve their chemical stability (higher membrane rigidity)^{38,39}. Egg-PC (egg yolk phosphatidylcholine) liposomes with cholesterol, in (7:3) proportion, are commonly used as models of cell membranes^{40,41}.

Nanoliposomes should ideally have a hydrophilic surface to escape macrophage capture and enhance their life span in the circulatory system⁴². This can be achieved by coating the liposome with the synthetic polymer polyethyleneglycol (PEG)^{18,43-45}. The pegylated liposomes are long circulating in blood due to a highly hydrated and protected liposome surface, constituted by the hydrophilic polymers that inhibit protein adsorption and opsonization of the liposomes. PEG provides the liposomes with up to 72 hours half-life in blood²⁰.

Grafting specific ligands to the liposome surface facilitates the fusion of the liposome with target cells by endocytosis, thus releasing material to be delivered¹⁸. This can be achieved by coupling liposomes to specific antibodies or coating the liposomes with ligands targeting proteins expressed on cancer cell membranes or endothelial cells lining the newly generated blood vessels in the tumor²⁰.

In terms of the liposomes charge, cationic liposomes, unlike their anionic and electroneutral counterparts, have been shown to target tumor vessels to a significant extent over vessels in normal healthy tissues, targeting approximately 25 and 5% of vessel areas respectively⁴⁶ (electrostatic interactions between positively charged

liposomes and the negatively charged cell membranes facilitate cell uptake). However, cationic liposomes can cause cytotoxicity limiting their safety for clinical use. Consequently, interest for drug delivery has turned to neutral and anionic liposomes and the latter have shown to have enhanced macrophage internalisation⁴⁷. Additionally, there is a relationship between surface charge and stability. This relationship can be evaluated by zeta-potential measurements: in general, particles with zeta potentials more positive than +30mV or more negative than -30mV are normally considered stable, with no tendency to aggregate, due to the electrostatic repulsion between the particles.

In conclusion, it can be stated that liposomes are just beginning to make an impact in chemotherapy owing to the promising effects in the reduction of toxicity and side effects of existing therapies and in the increase efficacy by selective targeting of tumors. However, the full potential of these emerging technologies has not yet been fully realized. The toxicology of nanomaterials in humans still needs to be fully studied and evaluated. The studies already performed have been small and limited to short-term exposure and should focus on long-term exposure in humans, animals and the environment. Further, *in vivo* studies are needed to determine the efficacy of these new drug formulations, and the reproducibility of batches of drug formulations also needs to be refined³¹.

4. Determination of the size and zeta-potential of the liposomes with incorporated compounds

The fate of intravenously injected liposomes used as drug delivery systems is determined by a number of properties, two of the most important being particle size and zeta potential. The size is one of the most important physical properties of lipid vesicles with incorporated compounds because this parameter has a direct influence in many other properties such as reactivity, stability and efficacy of drug delivery. Unless the sample to characterize is perfectly monodisperse, i.e. every single particle has exactly the same dimensions, it will consist of a statistical distribution of particles of different sizes. It is common practice to represent this distribution in the form of a frequency distribution curve, or a cumulative (undersize) distribution curve (*size distribution*)⁴⁸.

Zeta-potential is another important parameter that affects the stability of the liposomes. It represents a measure of the magnitude of the electrostatic or charge repulsion or attraction between particles, and its measurement brings detailed insight into the causes of dispersion, aggregation or flocculation, and can be applied to improve the liposomes formulation.

The development of a net charge at the particle surface affects the distribution of ions in the surrounding interfacial region, resulting in an increased concentration of counter ions, ions of opposite charge to that of the particle, close to the surface. Thus, an electrical double layer exists around each particle. The liquid layer surrounding the particle exists as two parts; an inner region (Stern layer), where the ions are strongly bound, and an outer (diffuse) region where they are less firmly associated. Within the diffuse layer, there is a notional boundary inside which the ions and particles form a stable entity. When a particle moves (e.g. due to gravity), ions within the boundary move with it. Those ions beyond the boundary stay with the bulk dispersant. The potential at this boundary (surface of hydrodynamic shear) is the zeta potential (Figure 3.6)⁴⁹.

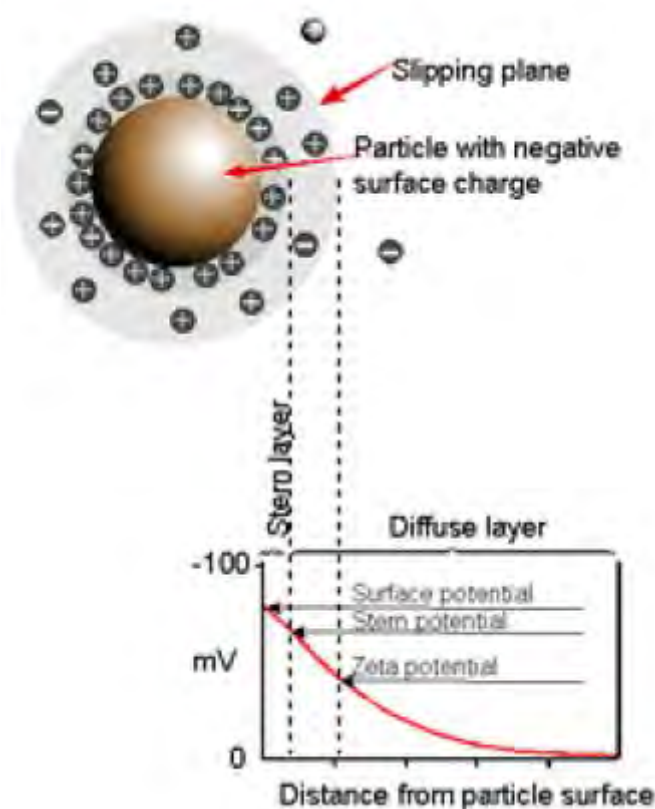


Figure 3.6. Schematic representation of zeta-potential⁴⁹.

The magnitude of the zeta potential gives an indication of the potential stability of the colloidal system. If all the particles in suspension have a large negative or positive zeta potential, then they will tend to repel each other and there will be no tendency for the particles to come together. However, if the particles have low zeta potential values, then there will be no force to prevent the particles coming together and flocculating. The general dividing line between stable and unstable suspensions is generally taken at either +30 or -30 mV. Particles with zeta potentials more positive than +30 mV or more negative than -30 mV are normally considered stable.

Particles size, size distribution and zeta-potential of particles, typically in the submicron region, suspended in a liquid can be evaluated by DLS (Dynamic Light Scattering), a non-invasive and well-established technique with many advantages, such as⁵⁰:

- Accurate, reliable and repeatable particle size analysis in one or two minutes.

- Measurement in the native environment of the material.
- Mean size only requires knowledge of the viscosity of the liquid.
- Simple or no sample preparation, low concentration, turbid samples can be measured directly.
- Simple set up and fully automated measurement.
- Size measurement of particles typically in the submicron region down to 1nm nanometre.
- Low volume requirement (as little as 2 μL).

The Brownian motion of particles or molecules in suspension causes laser light to be scattered at different intensities. Analysis of these intensity fluctuations yields the velocity of the Brownian motion (random movement of particles due to the bombardment by the solvent molecules that surround them). The larger the particle, the slower the Brownian motion will be. Smaller particles are “kicked” further by the solvent molecules and move more rapidly (Figure 3.7).

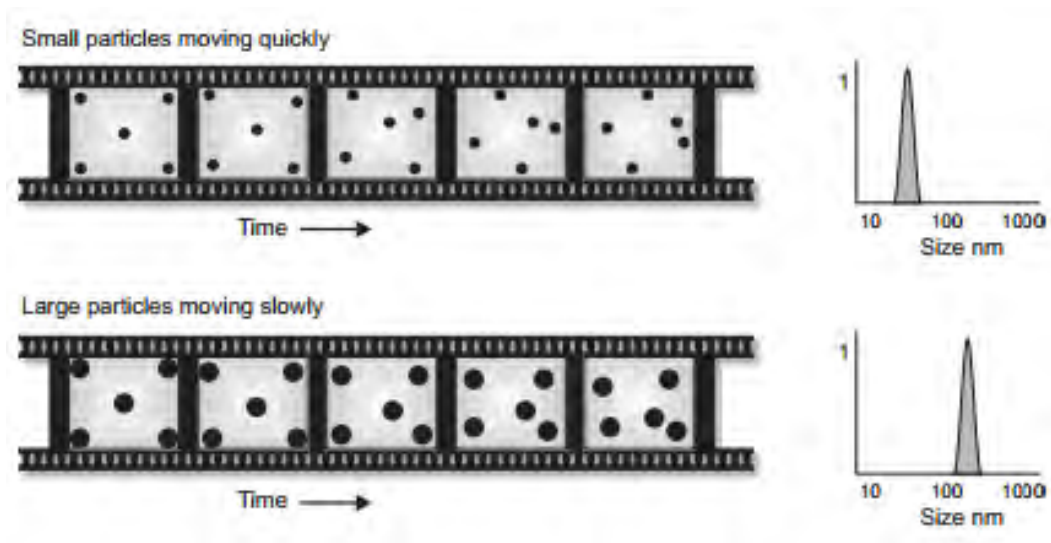


Figure 3.7. Different rates of the Brownian motion of particles according to their size and respective size-distribution curves.

An accurately known temperature is necessary for DLS, because knowledge of the viscosity is required (the viscosity of a liquid is related to its temperature). The temperature also needs to be stable, otherwise convection currents in the sample will cause non-random movements, that will ruin the correct interpretation of size. The velocity of the Brownian motion is defined by a property known as the translational

diffusion coefficient, D , and the size of the particles is calculated from this coefficient, by using the Stokes-Einstein relationship:

$$D = \frac{kT}{6\pi\eta R} \quad (3.1)$$

where k is Boltzmann's constant, T is the absolute temperature, η is the solvent viscosity, and R is the molecular radius.

Note that the diameter that is measured in DLS is a value that refers to how a particle diffuses within a fluid, so it is referred to as a hydrodynamic diameter. The diameter that is obtained by this technique is the diameter of a sphere that has the same translational diffusion coefficient as the particle⁵⁰.

If the particles are small compared to the wavelength of the laser used (typically, less than $d = \lambda/10$, or around 60 nm for a He-Ne laser), then the scattering from a particle illuminated by a vertically polarised laser will be essentially isotropic, i.e. equal in all directions. The Rayleigh approximation tells us that $I \propto d^6$ and also that $I \propto 1/\lambda^4$, where I is the intensity of light scattered, d is the particle diameter and λ is the laser wavelength. The d^6 term tells us that a 50nm particle will scatter one million times as much light as a 5nm particle. Hence, there is a danger that the light from the larger particles will swamp the scattered light from the smaller ones. This d^6 factor also means that it is difficult to measure a mixture of 1000 nm and 10 nm particles with DLS, because the contribution to the total light scattered by the small particles will be extremely small. The inverse relationship to λ^4 means that a higher scattering intensity is obtained as the wavelength of the laser used decreases⁵⁰.

A conventional dynamic light scattering instrument consists of a laser light source, which converges to a focus in the sample using a lens. Light is scattered by the particles at all angles and a single detector, traditionally placed at 90° to the laser beam, collects the scattered light intensity. The intensity fluctuations of the scattered light are converted into electrical pulses, which are fed into a digital correlator. This generates the autocorrelation function, from which the particle size is calculated⁴⁸.

5. References

1. D. K. R. Robinson, A. Rip, V. Mangematin, Technological agglomeration and the emergence of clusters and networks in nanotechnology, *Research Policy*, **2007**, *36*, 871-879.
2. C. Kwangue, X. Wang, S. Nie, Therapeutic Nanoparticles for Drug Delivery in Cancer, *Clin. Cancer Res.*, **2008**, *14*, 1310-1316.
3. T.L. Andresen, S.S. Jensen, K. Jorgensen, Advanced Strategies in Liposomal Cancer Therapy: Problems and Prospects of Active and Tumor Specific Drug Release, *Progress in Lipid Research*, **2005**, *44*, 68-97.
4. N.A. Ocheke, P.O. Olorunfemi, N.C. Ngwuluka, Nanotechnology and drug delivery. Part 1: Background and applications, *Tropical J. Pharm. Res.*, **2009**, *8*, 265-274.
5. N.A. Ocheke, P.O. Olorunfemi, N.C. Ngwuluka, Nanotechnology and drug delivery. Part 2: Nanostructures for Drug Delivery, *Tropical J. Pharm. Res.*, **2009**, *8*, 275-287.
6. H. Maeda, The enhanced permeability and retention (EPR) effect in tumor vasculature: the key role of tumor-selective macromolecular drug targeting, *Adv. Enzyme Regul.*, **2001**, *41*, 189-207.
7. T.M. Allen, Ligand-targeted therapeutics in anticancer therapy, *Nat. Rev. Cancer*, **2002**, *2*, 750-763.
8. A.K. Larsen, A.E. Escargueil, A. Skladanowski, Resistance mechanisms associated with altered intracellular distribution of anticancer agents, *Pharmacol. Ther.*, **2000**, *85*, 217- 229.
9. E. Fahy, S. Subramaniam, R. Murphy, M. Nishijima, C. Raetz, T. Shimizu, F. Spener, G. Van Meer, M. Wakelam, E.A. Dennis, Update of the LIPID MAPS comprehensive classification system for lipids, *Journal of Lipid Research*, **2009**, *50(Supplement)*, S9-S14.
10. S. Subramaniam, E. Fahy, S. Gupta, M. Sud, R.W. Byrnes, D. Cotter, A.R. Dinasarapu, M.R. Maurya, Bioinformatics and Systems Biology of the Lipidome, *Chemical Reviews*, **2011**, *111(10)*, 6452-6490.

11. S. Mashaghi, T. Jadidi, G. Koenderink, A. Mashaghi, Lipid Nanotechnology, *Int. J. Mol. Sci.*, **2013**, *2013(14)*, 4242–4282.
12. M. Pulfer, R.C. Murphy, Electrospray mass spectrometry of phospholipids, *Mass Spectrom. Rev.*, **2003**, *22(5)*, 332-364.
13. B.R. Lentz, Membrane “fluidity” as detected by diphenylhexatriene probes, *Chem. Phys. Lipids*, **1989**, *50*, 171-190.
14. J.S. Vincent, S.D. Revak, C.D. Cochrane, I.W. Levin, Interactions of model human pulmonary surfactants with a mixed phospholipid bilayer assembly: Raman spectroscopic studies, *Biochemistry*, **1993**, *32*, 8228-8238.
15. M.T. Lamy-Freund, K.A. Riske, The peculiar thermo-structural behavior of the anionic lipid DMPG, *Chem. Phys. Lipids*, **2003**, *122*, 19-32.
16. E. Feitosa, P.C.A. Barreleiro, G. Olofsson, Phase transition in dioctadecyldimethylammonium bromide and chloride vesicles prepared by different methods, *Chem. Phys. Lipids*, **2000**, *105*, 201-213.
17. A.D. Bangham, M.M. Standish, J.C. Watkins, Diffusion of univalent ions across the lamellae of swollen phospholipids, *Journal of Molecular Biology*, **1965**, *13*, 238-252.
18. S.S. Chrai, R. Murari, I. Ahmad. Liposomes (a review), part two: drug delivery systems, *Biopharm*, **2002**, *15(1)*, 40, 42-43, 49.
19. S.S. Chrai, R. Murari, I. Ahmad. Liposomes (a review), part one: Manufacturing issues, *Biopharm*, **2001**, *14(11)*, 10-14.
20. M.R. Faria, *Development and Characterization of Magnetoliposomes for Drug Delivery Applications*, Instituto Superior Técnico de Lisboa, **2011**.
21. R. Daniel, Galenic principles of Modern Skin Care Products, *Skim Care Forum*, **2001**, issue 25.
22. A.D. Bangham, M.W. Hill, N.G.A. Miller, *Methods in Membrane Biology*, New York, NY: Korn, Plenum Press, **1974**, 1-68.
23. R.R.C. New, Preparation of Liposomes. In *Liposomes: A Practical Approach*, New York, NY: New, Oxford University Press, **1990**, 33-104.
24. T.M. Taylor, J. Weiss, P.M. Davidson, B.D. Bruce, Liposomal Nanocapsules in Food Science and Agriculture, *Food Science and Nutrition*, **2005**, *45(7-8)*, 587-605.

25. J.S. Dua, A.C. Rana, A.K. Bhandari, Liposome: methods of preparation and applications, *International Journal of Pharmaceutical Studies and Research*, **2012**, 3(2), 14-20.
26. A. Gomez-Hens, J.M. Fernandez-Romero, Analytical methods for the control of liposomal delivery systems, *Trends Anal. Chem.*, **2006**, 25,167–178.
27. E. Wisse, F. Braet, D. Luo, R. DeZanger, D. Jans, E. Crabbe, A. Vermoesen, Structure and function of sinusoidal lining cells in the liver, *Toxicol. Pathol.*, **1996**, 24, 100-111.
28. G. Gregoriadis, E.J. Willis, C.P. Swain, A.S. Tavill, Drug-Carrier Potential of Liposomes in Cancer Chemotherapy, *The Lancet*, **1974**, 1, 1313-1316.
29. Barenholz, Yechezkel, Liposome Application: problems and prospects, *Current Opinion in Colloid & Interface Science*, **2001**, 6, 66-77.
30. P.D. Marcato, N. Dur'an, New Aspects of Nanopharmaceutical Delivery Systems, *Journal of Nanoscience and Nanotechnology*, **2008**, 8, 1-14.
31. Y. Malam, M. Loizidou, A.M. Seifalian, Liposomes and nanoparticles: nanosized vehicles for drug delivery in cancer, *Trends in Pharmacol. Sci.*, **2009**, 30, 592-599.
32. G. Gregoriadis, Engineering liposomes for drug delivery: progress and problems, *Trends Biotechnol.*, **1995**, 13, 527-537.
33. S.M. Moghimi, A.C. Hunter, J.C. Murray, Long-circulating and target-specific nanoparticles: theory to practice, *Pharmacol. Rev.*, **2001**, 53, 283-318.
34. E. Wisse, F. Braet, D. Luo, R. DeZanger, D. Jans, E. Crabbe, A. Vermoesen, Structure and function of sinusoidal lining cells in the liver, *Toxicol. Pathol.*, **1996**, 24, 100-111.
35. F. Yuan, M. Dellian, D. Fukumura, M. Leunig, D.A. Berk, V.P. Torchilin, R.K. Jain, Vascular permeability in a human tumor xenograft: molecular size dependence and cutoff size, *Cancer Res.*, **1995**, 55, 3752-3756.
36. K.A. Riske, L.Q. Amaral, H.-G. Döbereiner, M.T. Lamy, Mesoscopic structure in the chain-melting regime of anionic phospholipid vesicles: DMPG, *Biophys. J.*, **2004**, 86, 3722-3733.
37. R.P. Barroso, K.R. Perez, I.M. Cuccovia, M.T. Lamy, Aqueous dispersions of DMPG in low salt contain leaky vesicles, *Chem. Phys. Lipids*, **2012**, 165, 169-177.

38. K. Rebolj, B. Bakrac, M. Garvas, K. Ota, M. Sentjurc, C. Potrich, M. Coraiola, R. Tomazzolli, M.D. Serra, P. Macek, K. Sepcic, EPR and FTIR studies reveal the importance of highly ordered sterol-enriched membrane domains for ostreolysin activity, *Biochimica et Biophysica Acta*, **2010**, *1798*, 891-902.
39. L. Zhao, S. Feng, Effects of cholesterol component on molecular interactions between paclitaxel and phospholipid within the lipid monolayer at the air-water interface, *Journal of Colloid and Interface Science*, **2006**, *300*, 314-326.
40. C. Toniolo, M. Crisma, F. Formaggio, C. Peggion, V. Monaco, C. Goulard, S. Rebuffat, B. Bodo, Effect of N-acyl chain length on the membrane-modifying properties of synthetic analogs of the lipopeptaibol trichogin GA I, *Journal of the American Chemical Society*, **1996**, *118*, 4952-4958.
41. A. Crisma, F. Barazza, B. Formaggio, B.Q. Kaptein, J. Broxterman, C. Kamphuis, C. Toniolo, Peptaibolin: synthesis, 3D-structure, and membrane modifying properties of the natural antibiotic and selected analogues, *Tetrahedron*, **2001**, *57*, 2813-2825.
42. S.M. Moghimi, J. Szebeni, Stealth liposomes and long circulating nanoparticles: critical issues in pharmacokinetics, opsonization and protein-binding properties, *Prog. Lipid Res.*, **2003**, *42*, 463-478.
43. M.L. Immordino, F. Dosio, L. Cattel, Stealth Liposomes: Review of the Basic Science, Rationale, and Clinical Applications, Existing and Potential, *International Journal of Nanomedicine*, **2006**, *1(3)*, 297-315.
44. N. Nuytten, M. Hakimhashemi, T. Ysenbaert, L. Defour, J. Trekker, S.J.H. Soenen, P.V. Meeren, M. Cuyper, PEGylated lipids impede the lateral diffusion of adsorbed proteins at the surface of (magneto)liposomes, *Colloids and Surfaces B: Biointerfaces*, **2010**, *80*, 227-231.
45. Y. Ran, S.H. Yalkowsky, Halothane, a novel solvent for the preparation of liposomes containing 2-4'-amino-3'-methylphenyl benzothiazole (AMPB), an anticancer drug: A technical note, *AAPS Pharm. Sci. Tech.*, **2003**, *4*, article 20.
46. S. Dandamudi, R.B. Campbell, Development and characterization of magnetic cationic liposomes for targeting tumor microvasculature, *Biochim. Biophys. Acta (BBA) – Biomembranes*, **2007**, *3*, 427-438.

47. C. Kelly, C. Jefferies, S.-A. Cryan, Targeted Liposomal Drug Delivery to Monocytes and Macrophages, *Journal of Drug Delivery*, **2011**, 2011, 727241-727252.
48. Malvern Instruments, "A Basic guide to particle characterization", MRK1806-01, **2012**.
49. Malvern Instruments, "Zeta-potential: an introduction in 30 min", zetasizer nanoseries technical note, MRK654-01.
50. Malvern Instruments, "Dynamic Light Scattering: an introduction in 30 min", DLS technical note, MRK656-01.

Chapter 4

Molecular Fluorescence Spectroscopy

INDEX

1. Introduction	81
2. Fluorescence as a particular case of Luminescence.....	85
3. Absorption of UV-Visible light.....	89
3.1. Molecular orbitals and electronic transitions	89
3.2. Selection rules for electronic transitions	91
3.4. Probability of transitions. The Beer-Lambert law	95
4. De-excitation processes of excited molecules.....	101
5. Characteristics of fluorescence emission	108
5.1. Fluorescent probes	108
5.2. Lifetimes and quantum yields	109
5.3. Emission and excitation spectra	112
5.4. Effects of molecular structure on fluorescence	115
5.5. Solvent and environmental effects on fluorescence emission spectra.....	117
5.5.1. Effects of solvent polarity and viscosity	118
5.5.2. Compounds submitted to photoinduced Intramolecular Charge Transfer (ICT) and internal rotation	129
5.5.3. Changes in the non-radiative decay rates	130
5.5.4. Changes in the radiative decay rates.....	131
5.5.5. Probe-probe interactions.....	132
5.6. Resolution of Fluorescence spectra.....	132
6. Quenching of fluorescence	133
6.1. Quenchers of fluorescence	134
6.2. Collisional quenching (dynamic quenching)	135
6.3. Static quenching	138
6.4. How to distinguish between dynamic and static quenching	140
6.5. Simultaneous dynamic and static quenching	141
6.6. Some applications of quenching	142
6.7. Experimental considerations in quenching.....	143
7. Fluorescence anisotropy.....	145

7.1. Polarization ratio and emission anisotropy	147
7.2. Relation between anisotropy and the absorption and emission dipoles orientation	150
7.2.1. Parallel absorption and emission transition moments	150
7.2.2. Non-parallel absorption and emission transition moments.....	153
7.3. Causes of depolarization	154
7.3.1. Resonance Energy Transfer (RET).....	155
7.3.2. Rotational Brownian motion: the Perrin equation	156
7.3.3. Experimental causes of depolarization.....	158
7.4. Applications of fluorescence polarization	159
8. References	161

1. Introduction

Spectroscopy is basically related with the absorption, emission or scattering of electromagnetic radiation by atoms or molecules. Electromagnetic radiation covers a wide wavelength range, from radio waves to γ -rays. As the name implies, it contains both an electric and a magnetic component, which are best illustrated by considering plane-polarized (also known as linearly polarized) radiation. Figure 4.1 illustrates one photon of such radiation travelling along the x -axis. The electric component of the radiation is in the form of an oscillating electric field of magnitude E , and the magnetic component is in the form of an oscillating magnetic field of magnitude H . These oscillating fields are at right angles to each other. The plane of polarization is conventionally taken to be the plane containing the direction of E and that of propagation; in Figure 4.1 this is the xy -plane. The reason for this choice is that interaction of electromagnetic radiation with matter is more commonly through the electric component¹.

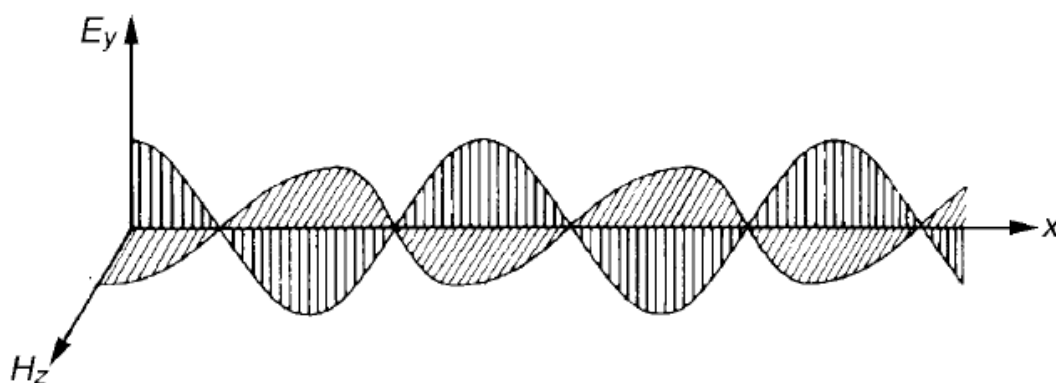


Figure 4.1. Plane-polarized electromagnetic radiation travelling along the x -axis; E_y is the electric component; H_z is the magnetic component¹.

In vacuum, all electromagnetic radiations travel at the same speed, the speed of light c ($2.99792458 \times 10^8 \text{ ms}^{-1}$), and may be characterized by its wavelength, λ , in air or vacuum, or by its wavenumber, $\bar{\nu}$, or frequency, ν , both conventionally in vacuum, where

$$\lambda_{\text{vac}} = \frac{c}{\nu} = \frac{1}{\bar{\nu}} \quad (4.1)$$

Figure 4.2 illustrates the extent of the electromagnetic spectrum and the processes that may occur in an atom or molecule exposed to radiation. Indications of region boundaries, which should not be regarded as clear cut, are given in wavelength (mm,

μm or nm), frequency (GHz) and wavenumber (cm^{-1}). In addition, in the high-energy regions the energy is indicated in electron volts (eV) where

$$1 \text{ eV} = 1.60218 \times 10^{-19} \text{ J} \quad (4.2)$$

A molecule may undergo rotational, vibrational, electronic or ionization processes, in order of increasing energy (typical ranges are indicated in Figure 4.2). A molecule may also scatter light in a Raman process, and the light source for such an experiment is usually in the visible or near-ultraviolet region. An atom may undergo only an electronic transition or ionization since it has no rotational or vibrational degrees of freedom. Nuclear magnetic resonance (NMR) and electron spin resonance (ESR) processes involve transitions between nuclear spin and electron spin states, respectively, but these spectroscopies need the sample to be located between the poles of a magnet.

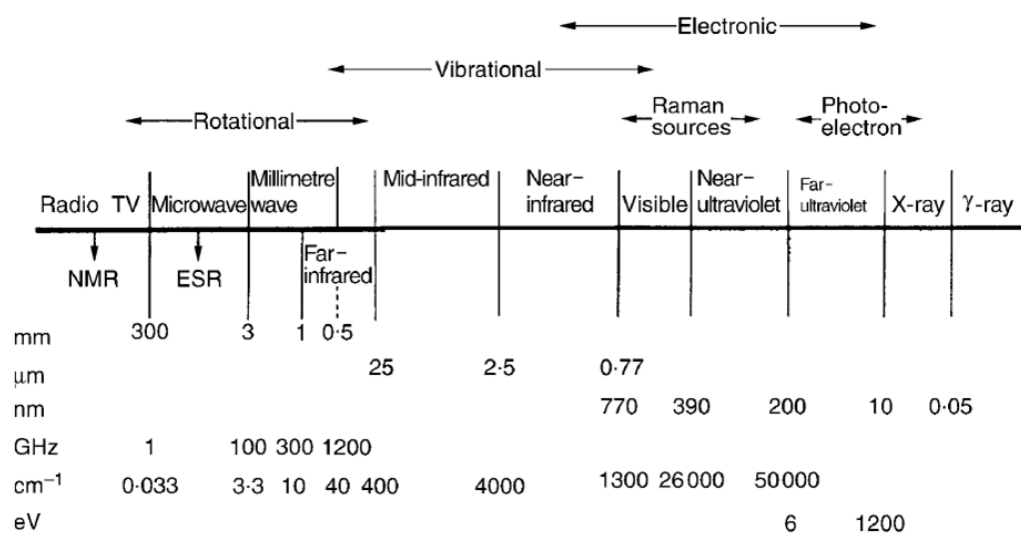


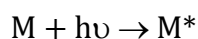
Figure 4.2. Regions of the electromagnetic spectrum¹.

When an atom or molecule is exposed to a radiation of frequency ν , it passes from a state m to a state n separated by

$$\Delta E = h\nu = hc\bar{\nu} = \frac{hc}{\lambda} \quad (4.3)$$

where h is the Planck constant ($h=6.62606876 \times 10^{-34}\text{Js}$). This can occur by three possible processes¹:

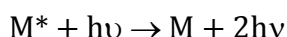
- Induced absorption, where the molecule (or atom) M absorbs a quantity of radiation and is excited from state m to state n :



- Spontaneous emission, in which M^* (in state n) spontaneously emits a quantum of radiation:



- Induced, or stimulated, emission. This is a different type of emission in which a quantum of radiation is required to induce, or stimulate, M^* to go from state n to state m :



The populations of the states m and n (respectively, N_m and N_n) are related, at equilibrium, through the Boltzmann distribution law:

$$\frac{N_n}{N_m} = \frac{g_n}{g_m} \exp\left(-\frac{E}{kT}\right) \quad (4.4)$$

where g_n and g_m are the degrees of degeneracy of the states n and m respectively, T is the absolute temperature (K) and k is the Boltzmann constant ($k = 1.3806503 \times 10^{-23} \text{ JK}^{-1}$).

Molecular Fluorescence is a spontaneous emission after induced absorption involving electronic transitions. The energies needed to change the electron distributions of molecules are of the order of several electron volts. Consequently, the photons emitted or absorbed when such changes occur lie in the visible and ultraviolet regions of the spectrum (Figure 4.2, Table 4.1)².

Table 4.1. Colour, frequency and energy of infrared, visible and ultraviolet light².

Colour	λ / nm	ν / (10^{14} Hz)	E / kJ mol ⁻¹
Infrared	>1000	<3.0	<120
Red	700	4.3	170
Yellow	580	5.2	210
Blue	470	6.4	250
Ultraviolet	<300	>10	>400

Molecular Fluorescence has many applications in physical, chemical, material, biological and medical sciences. It was first used as an analytical tool to determine the concentrations of several species, but is also the best method for the detection of analytes with a very high sensitivity (considerably improved due to the progress in

instrumentation) and a powerful tool for the investigation of structures and dynamics of matter or living systems at a molecular or supramolecular level. Biological membranes are examples in which it is possible to determine some parameters such as polarity, fluidity, order, molecular mobility and electrical potential by the use of fluorescent probes³.

2. Fluorescence as a particular case of Luminescence

According to The Fluorescent Mineral Society, "Light is a form of energy. To create light, another form of energy must be supplied". Luminescence is "cold light" (vs incandescence which is "hot light") that can be emitted at normal and lower temperatures. In luminescence, some energy source kicks an electron out of its lowest energy "ground" state into a higher energy "excited" state; then, the electron returns the energy in the form of light, so it can fall back to its "ground" state. With few exceptions, the excitation energy is always larger than the energy (wavelength, color) of the emitted light.

There are several types of luminescence, each named according to the mode of excitation⁴:

Chemiluminescence is luminescence where the energy is supplied by chemical reactions. The glow-in-the-dark plastic tubes sold in amusement parks are examples of chemiluminescence.

Bioluminescence is luminescence caused by chemical reactions in living things; it is a form of chemiluminescence. Fireflies glow by bioluminescence.

Electroluminescence is luminescence caused by electric current.

Sonoluminescence is luminescence caused by a micron size gas bubble which is both spatially trapped and oscillated by an acoustic field in such a way that, on each compression of the bubble, a small burst of light is emitted.

Cathodoluminescence is electroluminescence caused by electron beams; this is how television pictures were formed on a CRT (Cathode Ray Tube). Other examples of electroluminescence are neon lights, the auroras, and lightning flashes. This should not be confused for what occurs with the ordinary incandescent electric lights, in which the electricity is used to produce heat, and it is the heat that in turn produces light.

Radioluminescence is luminescence caused by nuclear radiation. Older glow-in-the-dark clock dials often used a paint with a radioactive material (typically a radium compound) and a radioluminescent material.

Triboluminescence is luminescence triggered by mechanical action or electroluminescence excited by electricity generated by mechanical action. Some

minerals glow when hit or scratched, e.g. by banging two quartz pebbles together in the dark.

Thermoluminescence is luminescence caused by temperatures above a certain threshold. This should not be confused with incandescence, which occurs at higher temperatures. In thermoluminescence, heat is not the primary source of the energy, only the trigger for the release of energy that originally came from another source.

Photoluminescence is luminescence where the energy is supplied by electromagnetic radiation. The mode of excitation is absorption of a photon which brings the absorbing species into an excited state and the photoluminescence is the emission of photons accompanying de-excitation process.

Fluorescence, delayed fluorescence and phosphorescence are particular cases of photoluminescence.



Figure 4.3. Types of luminescence processes and respective ways of molecules excitation (adapted from ref. 3).

Phosphorescence is delayed luminescence or "afterglow" (the term phosphorescence comes from the Greek: $\phi\omega\zeta$ = light and $\phi\sigma\rho\epsilon\iota\nu$ = to bear; therefore, *phospor* means "which bears light"). Many minerals are phosphorescent. The most famous is the *Bolognian phosphor* discovered by a cobbler of Bologna in 1602 during a walk in the Monte Paterno: he picked up some strange heavy stones and, after calcination with

coal, he observed that the stones glowed in the dark after exposure to light (the stones contained barium sulfate, which, upon reduction by coal, led to barium sulfide, a phosphorescent compound). Today, many glow-in-the-dark products, especially toys for children, involve substances that receive energy from light, and emit the energy again as light later.

Fluorescence is seen in fluorescent lights, amusement parks and movie special effects, the redness of rubies in sunlight, "day-glo" or "neon" colors, and in emission nebulae seen with telescopes in the night sky. The first reported observation of fluorescence was made by a Spanish physician, Nicolas Monardes, in 1565: he observed that an infusion of a wood called *Lignum Nephriticum* exhibits a wonderful blue color. In his famous paper "On the change of refrangibility of light" (1852), Stokes⁵ reinvestigated this fact and demonstrated that the phenomenon was an emission of light after absorption of light.

A basic distinction between fluorescence and phosphorescence based on experiment was made in the nineteenth century: Fluorescence disappears with the end of excitation, whereas phosphorescence persists after the end of excitation. Now, we know there are long-lived fluorescence and short-lived fluorescence and Francis Perrin was the first who theoretically distinguished fluorescence and phosphorescence, in 1929⁶: a molecule emits phosphorescence when it passes, between absorption and emission, through an intermediate state and it is not able to reach the fundamental state without receiving some energy from the medium.

3. Absorption of UV-Visible light

3.1. Molecular orbitals and electronic transitions

A molecular orbital is a mathematical function describing the wave-like behavior of an electron in a molecule⁷. It represents regions in a molecule where an electron is likely to be found. Molecular orbitals arise from allowed interactions between atomic orbitals (which predict the location of an electron in an atom), which are allowed if the symmetries are compatible. Efficiency of atomic orbital interactions is determined from the overlap (a measure of how well two orbitals constructively interact with one another) between two atomic orbitals, which is significant if the atomic orbitals are close in energy. When atomic orbitals interact, the resulting molecular orbital can be of three types⁸: bonding (σ or π orbitals), antibonding (σ^* or π^* orbitals), or nonbonding (n orbitals):

- Bonding molecular orbitals: Constructive (in-phase) interactions between atomic orbitals lead to bonding molecular orbitals. These molecular orbitals are lower in energy than the atomic orbitals that combine to produce them. They can be σ orbitals or π orbitals: σ orbitals are formed either from two s atomic orbitals, or from one s and one p atomic orbital, or from two p atomic orbitals having a collinear axis of symmetry; π orbitals are formed from two p orbitals which overlap laterally.
- Antibonding molecular orbitals: Destructive (out-of-phase) interactions between atomic orbitals lead to antibonding molecular orbitals. They can be σ^* or π^* molecular orbitals and are higher in energy than the atomic orbitals that combine to produce them.
- Nonbonding molecular orbitals (n orbitals): they are the result of no interaction between atomic orbitals because of lack of compatible symmetries. Normally, these molecular orbitals are located on heteroatoms such as oxygen or nitrogen and have the same energy as the atomic orbitals of these atoms in the molecule.

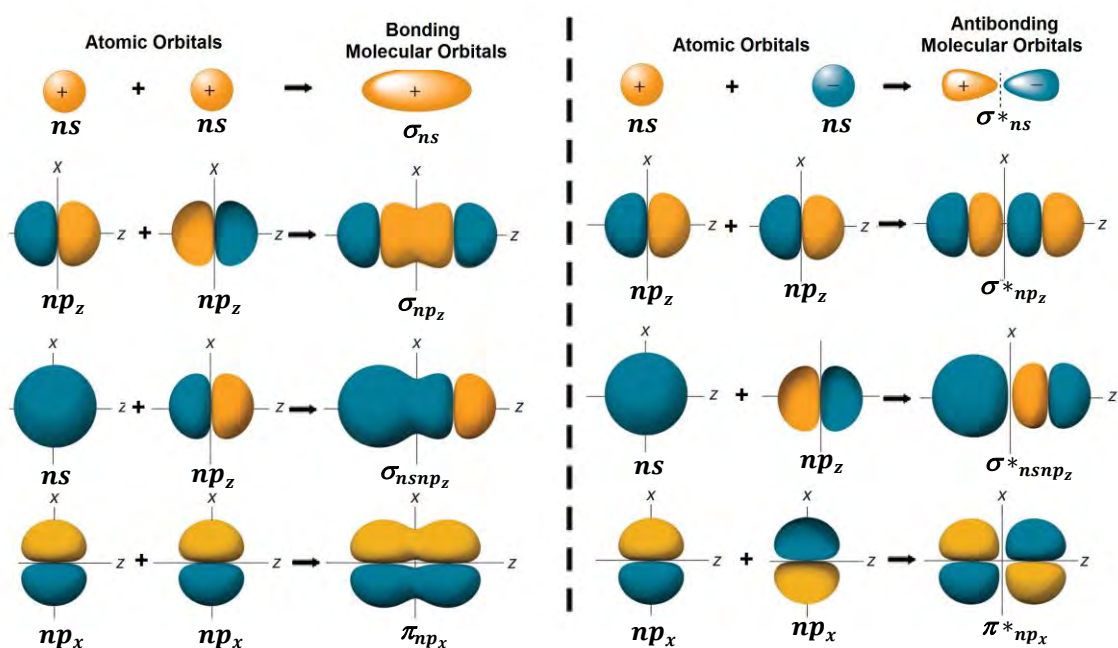
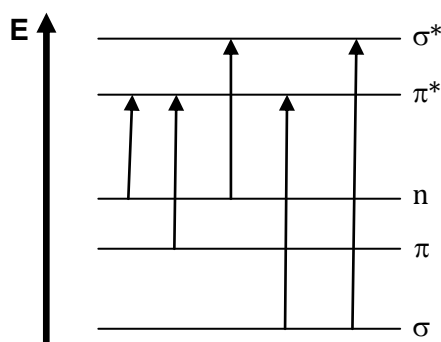


Figure 4.4. Types of bonding and antibonding molecular orbitals.

A molecule is in an excited state when an electronic transition occurs, i.e. when one electron passes from an orbital of the molecule in the ground state to an unoccupied orbital by absorption of a photon. Normally, σ orbitals are more stable than π orbitals and, for molecules with heteroatoms, π orbitals are more stable than n orbitals. The lower is the bonding molecular orbital, the higher is the respective antibonding molecular orbital.



Scheme 4.1. Energy levels of molecular orbitals and possible electronic transitions.

From scheme 4.1, it can be seen that the lowest energy (the longest wavelength) transitions are from a non-bonding orbital n to a π^* antibonding orbital (transition $n-\pi^*$). Normally, it corresponds to the near UV and visible region. Hereafter come the $\pi-\pi^*$ transitions, $n-\sigma^*$ transitions, $\sigma-\pi^*$ transitions and finally $\sigma-\sigma^*$ transitions, which normally occur below 200nm ⁹:

$$E_{n-\pi^*} < E_{\pi-\pi^*} < E_{n-\sigma^*} < E_{\sigma-\pi^*} < E_{\sigma-\sigma^*}$$

Following both the Pauli exclusion principle and Hund's rule, electrons fill in orbitals of increasing energy. Thus, for molecules with heteroatoms, the HOMO (Highest Occupied Molecular Orbital) - LUMO (Lower Unoccupied Molecular Orbital) transition is a $n-\pi^*$ transition.

In conjugated systems, overlap of the π orbitals allows the electrons to be delocalized over the whole system (resonance effect) and not only between pairs of atoms. As there is no overlap between σ and π orbitals, the π electron system is independent of the σ bonds and the higher its extent, the lower the energy of the $\pi-\pi^*$ transition (i.e., the larger the wavelength of the absorption band)³.

3.2. Selection rules for electronic transitions

There are two principal rules for electronic transitions:

- Symmetry rule: some transitions are forbidden for symmetry reasons. This is the case, for example, of $n-\pi^*$ transitions. However, a symmetry-forbidden transition can become weakly allowed when the molecular vibrations cause some departure from perfect symmetry (*vibronic coupling*). The intensity of a band indicates if the respective transition is allowed (high probability to occur) or forbidden (low probability to occur). Consequently, we can observe such bands although with low intensities, in electronic spectra.
- $S=0$: transitions between states of different multiplicity are forbidden².

The multiplicity of a term is the $2S+1$ value. S is the total spin angular momentum quantum number. S is a non-negative integer or a half integer and is obtained by coupling the individual spin angular momenta by using the Clebsch-Gordan series:

$$S = |s_1-s_2|, |s_1-s_2|+1, \dots, s_1+s_2 \quad (4.5)$$

As each electron has $s=\pm\frac{1}{2}$, S can be 1 or 0 for two electrons. If there are three electrons, the third spin must be coupled to each value of S , which results in $S = \frac{1}{2}, \frac{3}{2}$.

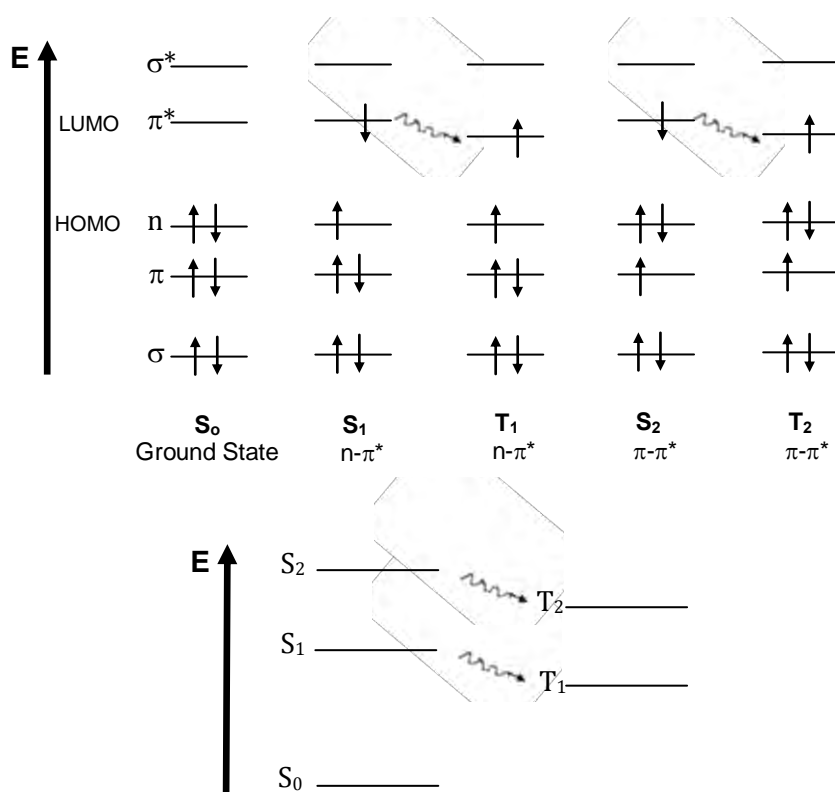
When $S=0$ (for a closed shell), the electrons are all paired, $2S+1=1$, which gives rise to a singlet term S (there is only one possible value for M_S , the total spin magnetic quantum number: $M_S=0$). When there are two unpaired electrons, $S=1$, thus

$2S+1=3$, which gives rise to a triplet term T (there are three possible values for M_S : $M_S=-1, 0, 1$).

Note: it is important to distinguish S , the total spin angular momentum quantum number from S , which designate a singlet term³.

The ground state is normally a singlet state (denoted S_0) because the total spin angular momentum quantum number S is equal to 0 and the multiplicity ($2S+1$) is equal to 1. When one electron is promoted to a molecular orbital of higher energy during a $n-\pi^*$ transition or a $\pi-\pi^*$ transition, etc., its spin is in principle unchanged and the corresponding excited states are also singlet states (denoted S_1, S_2 , etc...). In this case, the electronic transition is called a “singlet-singlet” transition. If the spin of the electron is changed during the transition, the reached state is called triplet state because the total spin angular momentum quantum number S is 1 and the multiplicity ($2S+1$) is equal to 3, which leaves three possible values for the total spin magnetic quantum number M_S , namely -1, 0, 1 (three states of equal energy). In this case, the electronic transition is called a “singlet-triplet” transition and is spin-forbidden ($S \neq 0$). Spin-forbidden transitions can be observed, although with very small molar absorption coefficients due to *spin-orbit coupling*, which is the interaction of the spin magnetic moment with the magnetic field arising from the orbital angular momentum of the electron. As this coupling increases sharply with atomic number (as Z^4), such forbidden transitions are favored by the presence of heavy atoms.

Direct formation of a triplet is a very improbable process, since both the orbit and spin of the electron would have to change simultaneously. Normally, triplet states are lower in energy than singlet states because the electrons have an electronic and magnetic part due to the spin correlation effect. If the spins are in the same direction, there is a magnetic repulsion and the electrons are farther. This gives a less electronic repulsion, thus a lower energy state (Hund’s rule)².



Scheme 4.2. Energy levels of molecular orbitals and distinction between singlet and triplet state using formaldehyde as an example (only higher energy orbitals are shown) (adapted from ref. 3).

3.3. The Franck-Condon principle

To account for the vibrational structure in electronic spectra of molecules, we apply the *Franck-Condon principle*, which is a consequence of the Born-Oppenheimer approximation²: according to this approximation, the nuclei of a molecule, being so much heavier than the electrons, move very slowly comparatively with the electrons and thus may be treated as stationary. Indeed, promotion of an electron to an antibonding orbital after excitation takes about 10^{-15} s, while the characteristic times for molecular vibrations are about $10^{-10} - 10^{-12}$ s. Thus, the Franck Condon principle states that an electronic transition is most likely to occur without change of nuclear positions and momenta. In other words, in a vibronic transition, the nuclei have very nearly the same position and velocity before and after the transition. Thus, upon excitation, the molecule is assumed to be initially in the *Franck-Condon state* (F)^{1,10}.

Figure 4.5a) shows potential curves for the lower state (which is the ground state if we are considering an absorption process) and the upper state, as a function of the nuclear configuration (internuclear distance in the case of diatomic molecules). The curves have been drawn so that $r'_e > r''_e$. When the lower state is the ground state,

this is very often the case, since the electron promotion involved is often from a bonding orbital to an orbital which is less bonding, or even antibonding. Before the absorption, at room temperature, most of the molecules are in the lowest vibrational level of the ground state (according to the Boltzmann distribution, see equation 4.4). In absorption, from point A of the ground state, the transition will be to point B of the upper state. The requirement that the nuclei have the same position before and after the transition means that the transition is between points which lie on a vertical line in the figure: this means that r remains constant and such a transition is often referred to as a vertical transition. The second requirement, that the nuclei have the same velocity before and after the transition, means that a transition from A, where the nuclei are stationary, must go to B, as this is the classical turning point of a vibration, where the nuclei are also stationary. A transition from A to C is highly improbable because, although the nuclei are stationary at A and C, there is a large change of r . An A to D transition is also unlikely because, although r is unchanged, the nuclei are in motion at the point D.

Figure 4.5b) illustrates the case where $r'_e \approx r''_e$. Here the most probable transition is from A to B with no vibrational energy in the upper state. The transition from A to C maintains the value of r but the nuclear velocities are increased due to their having kinetic energy equivalent to the distance BC.

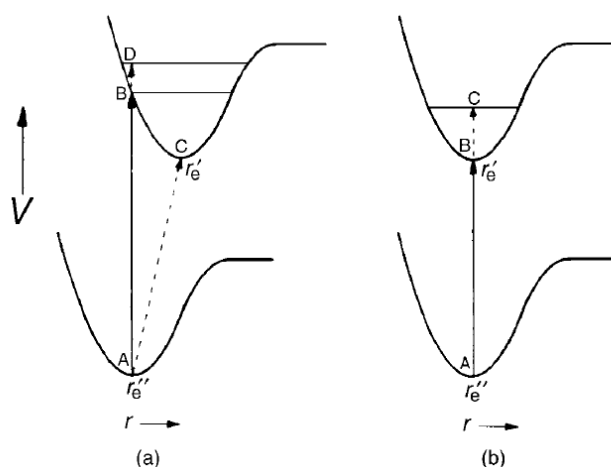


Figure 4.5. Illustration of the Franck-Condon principle for (a) $r'_e > r''_e$ and (b) $r'_e \approx r''_e$. The vibronic transition A–B is the most probable (and so the most intense) in both cases¹.

In addition to the most probable transition, there are several vibronic transitions whose intensities depend on the relative position and shape of the potential energy

curves. The width of the bands depends is the result of two factors: homogeneous and inhomogeneous broadening. Homogeneous broadening is due to the existence of continuous set of vibrational sublevels in each electronic state. Inhomogeneous broadening results from the fluctuations of the structure of the solvation shell³ (Figure 4.6).

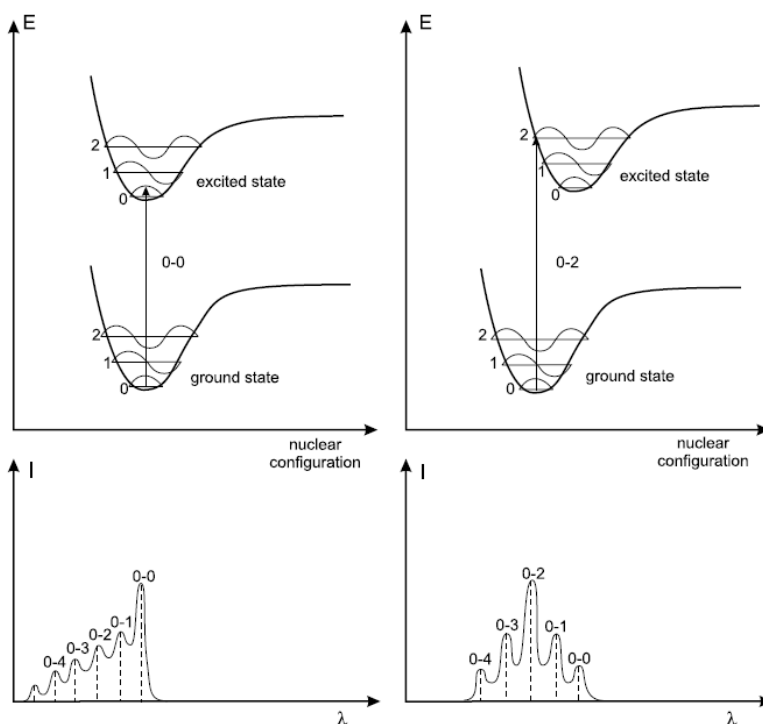


Figure 4.6. Potential energy diagrams with vertical transitions and respective absorption spectra; the vertical broken lines represent the absorption lines that are observed for a vapor, whereas the solid lines represent the expected broadening of the spectra in solution³.

3.4. Probability of transitions. The Beer-Lambert law

The absorbance $A(\lambda)$ and the Transmittance $T(\lambda)$ represent the efficiency of light absorption by a sample, for a given wavelength λ and are defined as:

$$A(\lambda) = \log \frac{I_0}{I} = -\log T(\lambda) \quad (4.6)$$

and

$$T(\lambda) = \frac{I}{I_0} \quad (4.7)$$

or

$$A(\lambda) = \frac{\ln\left(\frac{I_0}{I}\right)}{\ln 10} \approx \frac{1}{2.3} \ln \frac{I_0}{I} \quad (4.8)$$

where I_0 and I are the light intensities of the beams before and after passing through the sample.

In many cases, namely in the absence of aggregate formation at high concentrations, in the absence of other absorbing species or in the absence of instrument deviations, as described hereafter, the absorbance of a solution follows the Beer-Lambert law:

$$A(\lambda) = \varepsilon(\lambda)Cl \quad (4.9)$$

or
$$I = I_0 \exp(-2.3\varepsilon Cl) \quad (4.10)$$

where $\varepsilon(\lambda)$ is the molar absorption coefficient (in $\text{L mol}^{-1}\text{cm}^{-1}$) (it expresses the ability of a molecule to absorb light in a given solvent at a given wavelength); C is the concentration of absorbing species (in mol L^{-1}); l is the path length (thickness of the cuvette in cm).

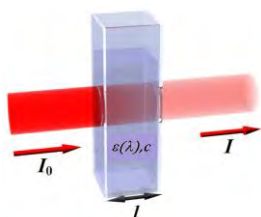


Figure 4.7. Illustration of the Beer-Lambert law¹¹.

As referred above, under certain circumstances, the Beer-Lambert relationship breaks down and gives a non-linear relationship. These deviations from the Beer-Lambert law can be classified into three categories¹¹:

1. **Real Deviations** - These are fundamental deviations due to the limitations of the law itself: Beer-Lambert law is capable of describing absorption behavior of solutions containing relatively low amounts of solutes dissolved in it ($< 10^{-2}$ M). When the concentration of the analyte in the solution is higher, the analyte begins to behave differently due to interactions with the solvent and other solute molecules and can form aggregates.
2. **Chemical Deviations** - These deviations occur due to chemical phenomenon involving the analyte molecules due to association, dissociation and interaction

with the solvent (for example, hydrogen bonding interactions) to produce a product with different absorption characteristics.

3. **Instrument Deviations** - These are deviations which occur due to the way the absorbance measurements are made. They can be due to polychromatic radiation, to mismatched cells in reference and sample, to the presence of scattered radiation (mainly with samples of macromolecules or other large aggregates), or to fluorescence of the sample.

The optical density resulting from scatter is proportional to $1/\lambda^4$ (Rayleigh scattering) and may thus be easily recognized as a background absorption which increases rapidly with decreasing wavelengths¹².

If the absorbing species is fluorescent, the emitted light can reach the detector but, as the fluorescence is omnidirectional whereas the incident light is collimated along an axis, this effect can be minimized by keeping the detector distant from the sample and thereby by decreasing the efficiency with which the fluorescence emission is collected.

The maximum value of the molar absorption coefficient, ϵ_{\max} , is an indication of the intensity of a transition. However, as absorption bands generally spread over a range of wavenumbers, quoting the absorption coefficient at a single wavenumber might not give a true indication of the intensity of a transition. The integrated absorption coefficient, ϵ_T , is the integral over the entire band (Figure 4.8), and corresponds to the area under the plot of the molar absorption coefficient against wavenumber²:

$$\epsilon_T = \int_{\text{Band}} \epsilon(\bar{\nu}) d\bar{\nu} \quad (4.11)$$

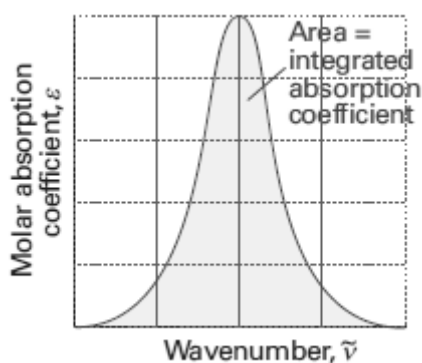


Figure 4.8. Integrated absorption coefficient of a transition².

If the absorption is due to an electronic transition, then f_{nm} , the oscillator strength, is often used to quantify the intensity and is related to the area under the curve by¹

$$f_{nm} = \frac{4\varepsilon_0 m_e c^2 \ln 10}{N_A e^2} \int_{\bar{\nu}_1}^{\bar{\nu}_2} \varepsilon(\bar{\nu}) d\bar{\nu} \quad (4.12)$$

where ε_0 is the vacuum permittivity ($\varepsilon_0 = 8.854187816 \times 10^{-12} \text{ C}^2 \text{ J}^{-1} \text{ m}^{-1}$), m_e and e are the electron mass and charge, respectively ($m_e = 9.10938188 \times 10^{-31} \text{ kg}$ and $e = -1.602176462 \times 10^{-19} \text{ C}$), c is the speed of light ($c = 2.99792458 \times 10^8 \text{ ms}^{-1}$) and N_A is the Avogadro's number ($N_A = 6.02214199 \times 10^{23} \text{ mol}^{-1}$).

The quantity f_{nm} is dimensionless and represents the ratio of the strength of the transition to that of an electric dipole transition between two states of an electron, oscillating in three dimensions in a simple harmonic way, and its maximum value is usually 1 (completely allowed transition).

For $n \rightarrow \pi^*$ transitions, the values of ε are in the order of a few hundreds or less, and those of f_{nm} are no greater than 10^{-3} . For $\pi \rightarrow \pi^*$ transitions, the values of ε and f_{nm} are in principle much higher (except for symmetry-forbidden transitions): f_{nm} is close to 1 for some compounds, which corresponds to values of ε that are of the order³ of $100000 \text{ M}^{-1} \text{ cm}^{-1}$.

To characterize the displacement of charges during a transition between an initial and a final state, a vector quantity called *transition moment*, R^{nm} , is introduced (note that it is not strictly a dipole moment): in most cases, it can be drawn as a vector in the coordinate system defined by the location of the nuclei of the atoms. This concept is very important in all experiments carried out with polarized light, because the molecules whose absorption transition moments are parallel to the electric vector of a linearly polarized incident light are preferentially excited. The probability of excitation is proportional to the square of the scalar product of the transition moment and the electric vector. This probability is thus maximum when the two vectors are parallel and zero when they are perpendicular.

For $\pi \rightarrow \pi^*$ transitions of aromatic hydrocarbons, the absorption transition moments are in the plane of the molecule. The direction with respect to the molecular axis depends on the electronic state attained on excitation. For example, in naphthalene

and anthracene, the transition moment is oriented along the short axis for the $S_0 \rightarrow S_1$ transition and along the long axis for the $S_0 \rightarrow S_2$ transition.

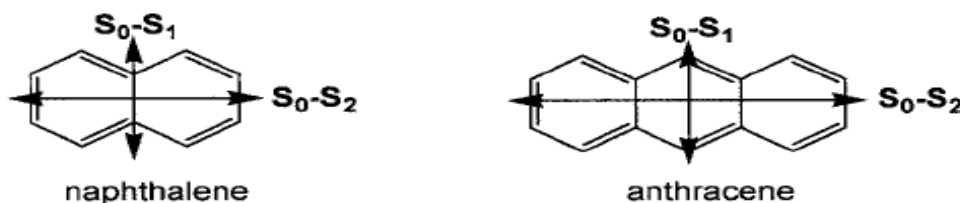


Figure 4.9. Naphthalene and anthracene with their absorption transition moments.

The transition moment can be defined by

$$R^{nm} = \int \psi_n^* \mu \psi_m d\tau \quad (4.13)$$

for interaction with the electric component of the radiation. The quantity μ is the electric dipole moment operator,

$$\mu = \sum_i q_i r_i \quad (4.14)$$

where q_i and r_i are the charge and position vector of the i -th particle (electron or nucleus).

The transition moment can be thought as the oscillating electric dipole moment due to the transition. Figure 4.10 shows the π and π^* molecular orbitals of ethylene and, if an electron is promoted from π to π^* in an electronic transition, there is a corresponding non-zero transition moment. This example illustrates the important point that a transition moment may be non-zero even though the permanent electric dipole moment is zero in both the states m and n ¹.

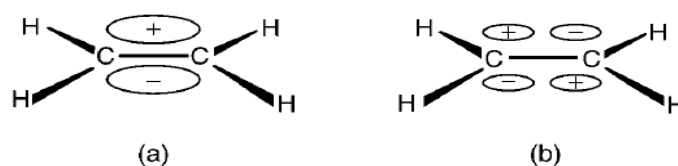


Figure 4.10. A π (a) and a π^* (b) molecular orbital of ethylene.

The square of the magnitude of R^{nm} is the transition probability, $|R^{nm}|^2$. It is related to selection rules in spectroscopy: it is zero for a forbidden transition and non-zero for an allowed transition. The electric dipole moment operator, μ , has components along the cartesian axes:

$$\mu_x = \sum_i q_i x_i \quad \mu_y = \sum_i q_i y_i \quad \mu_z = \sum_i q_i z_i \quad (4.15 - 4.17)$$

where q_i and x_i are, respectively, the charge and x -coordinate of the i -th particle, and so on. Similarly, the transition moment can be resolved into three components:

$$R_x^{nm} = \int \psi_n^* \mu_x \psi_m dx \quad R_y^{nm} = \int \psi_n^* \mu_y \psi_m dy \quad R_z^{nm} = \int \psi_n^* \mu_z \psi_m dz \quad (4.18 - 4.20)$$

and the transition probability is related to these by

$$|R^{nm}|^2 = (R_x^{nm})^2 + (R_y^{nm})^2 + (R_z^{nm})^2 \quad (4.21)$$

4. De-excitation processes of excited molecules

When a molecule has been promoted to an excited state, it does not remain there for a long time, and has many ways to return to the ground state. We may classify de-excitation processes to two broad categories⁹:

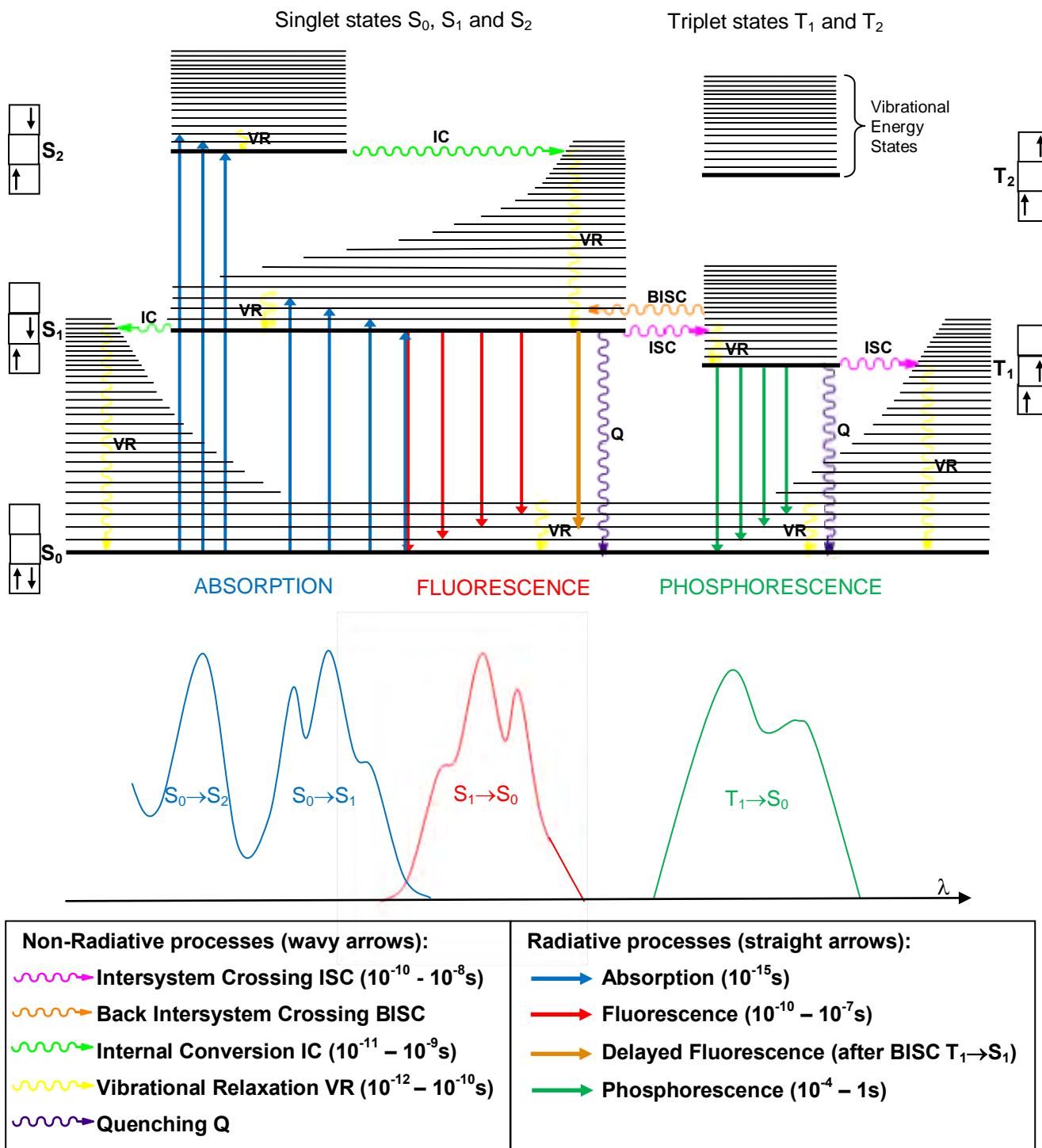
A. Photophysical deactivation processes, e.g. photoluminescence (normal or delayed fluorescence and phosphorescence), vibrational/rotational transitions, internal conversion (IC), intersystem crossing (ISC) and quenching (Q).

B. Photochemical deactivation processes, i.e. de-excitation resulting from excited state photochemical reactions, implying bond breaking and formation of new bonds, so that the ground state of the molecule is not recovered (photodecomposition, photoaddition, photosubstitution, etc.). Some of these processes may lead to fluorescent species whose emission can be higher than that of the initial one.

Photochemical deactivation processes, as well as vibrational/rotational transitions, internal conversion (IC), intersystem crossing (ISC) and quenching (Q) are radiationless processes (heat emission, i.e., the excess energy is transferred into the vibration, rotation, and translation of the surrounding molecules), whereas normal or delayed fluorescence and phosphorescence are radiant processes (the molecule discards its excitation energy as a photon).

The time that a molecule spends in the excited state is determined by the inverse of the sum of the kinetic constants of all de-excitation processes. Fluorescence competes with the other de-excitation pathways and can be observed if its rate constant, k_F , is higher than that sum.

The Perrin-Jablonski diagram (scheme 4.3) shows the absorption process as well as the different possible de-excitation processes. The radiative processes are represented by straight arrows. The non-radiative decays are represented by wavy arrows. Vibrational levels are represented for each electronic state. Note that fluorescence and phosphorescence always occur from the lowest vibrational level of the excited state because if the molecule is on a non-zero vibrational level, it is subjected to collisions with the surrounding molecules and gives up energy, until arise the zero vibrational level by vibrational relaxation, before emitting fluorescence or phosphorescence.



Scheme 4.3. Perrin-Jablonski diagram, illustration of the relative positions of absorption, fluorescence and phosphorescence spectra and characteristic times for each transition process (adapted from ref. 3).

Absorption of a photon can bring a molecule to one of the vibrational levels of S_1, S_2, \dots and the subsequent de-excitation processes may be^{3,9}:

- **Internal Conversion:**

Internal Conversion is a non-radiative transition between two states of the same spin multiplicity that occurs with a time-scale of $10^{-11} - 10^{-9}$ s. When a molecule is excited to a singlet state higher than S_1 , internal conversion leads the molecule to the S_1 state. Internal conversion from S_1 to S_0 is also possible, but is less efficient than conversion from S_2 to S_1 , because of the much larger energy gap between S_1 and S_0 . Furthermore, internal conversion from S_1 to S_0 competes with other de-excitation processes (fluorescence, intersystem crossing to the triplet state, etc.).

- **Vibrational Relaxation:**

It is a non-radiative transition between two different vibrational levels of the same electronic state. When a molecule is on a non-zero vibrational level of the ground state or of the excited state, the excess vibrational energy is transferred to the solvent during collisions of the molecule with the surrounding solvent molecules. This process is called *Vibrational Relaxation* and occurs with a time-scale of $10^{-12} - 10^{-10}$ s.

- **Intersystem Crossing:**

Intersystem Crossing is a non-radiative transition between two isoenergetic vibrational levels belonging to electronic states of different multiplicities. When a molecule is in the lowest vibrational level of the S_1 state, it can move to the isoenergetic vibrational level of the T_n state. Then, internal conversion and vibrational relaxation bring it to the lowest vibrational level of the T_1 state. This process occurs with a time-scale of $10^{-10} - 10^{-8}$ s. Thus, it is fast enough to compete with other pathways of de-excitation.

Normally, crossing between states of different multiplicity is forbidden (selection rule $S=0$, see section 3.2.2.), but spin-orbit coupling may be large enough (especially with the presence of heavy atoms) to make it possible. The probability of intersystem crossing depends on the singlet and triplet states involved. For example, if the transition $S_0 \rightarrow S_1$ is of $n \rightarrow \pi^*$ type (symmetry forbidden transition), intersystem crossing is often efficient.

- **Back Intersystem Crossing:**

Back Intersystem Crossing is a reverse Intersystem Crossing $T_1 \rightarrow S_1$, that can occur when the energy difference between S_1 and T_1 is small and when the lifetime of T_1 is long enough. Normally, it is followed by delayed fluorescence (fluorescence emission with the same spectral distribution as normal fluorescence, but with a much longer decay time constant, because the molecule stay in the triplet state before emitting from S_1).

- **Quenching:**

Quenching is any non-radiative intermolecular process responsible for de-excitation of molecules which decrease the fluorescence or phosphorescence intensity: energy transfer, electron transfer, proton transfer, complex formation and collisional quenching.

In these cases, the fluorescence and/or phosphorescence characteristics (decay time and/or fluorescence/phosphorescence quantum yields) of the molecules are affected by the presence of a quencher, as a result of competition between the intrinsic de-excitation and these intermolecular processes.

- **Fluorescence:**

Fluorescence is the emission of photons accompanying the $S_1 \rightarrow S_0$ relaxation. The downward electronic transition is vertical (according to the Franck-Condon principle) and the fluorescence spectrum has a vibrational structure characteristic of the lower electronic state.

The absorption spectrum arises from 0–0, 0–1, 0–2,... transitions, that occur at progressively higher wavenumbers and with intensities governed by the Franck-Condon principle. The fluorescence spectrum arises from 0–0, 0–1, 0–2,... downward transitions that hence occur with decreasing wavenumbers, i.e., the wavelength of a fluorescence emission should always be higher than that of absorption. This was empirically observed by Stokes before the knowledge of the Perrin-Jablonski diagram and, for that reason, this statement is called “Stokes rule”. The vivid oranges and greens of fluorescent dyes are an everyday manifestation of this effect: they absorb in the ultraviolet and blue, and fluoresce in the visible. The gap (expressed in

wavenumbers) between the maximum of the first absorption band and the maximum of fluorescence is called “Stokes shift” (Figure 4.11) and can provide useful information on the excited states because it is a result of several dynamic processes. These processes include energy losses due to dissipation of vibrational energy, redistribution of electrons in the surrounding solvent molecules induced by the generally increased dipole moment of the excited fluorophore, reorientation of the solvent molecules around the excited state dipole, and specific interactions (like hydrogen bonding and formation of charge transfer complexes) between the fluorophore and the solvent.

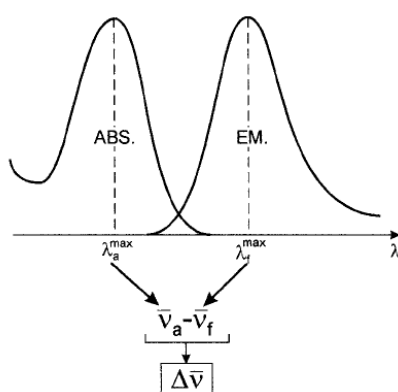


Figure 4.11. Definition of the Stokes shift³.

Despite the Stokes rule, in most cases, the absorption spectrum partly overlaps the fluorescence spectrum, i.e., a fraction of light is emitted at shorter wavelengths than the absorbed light. It can be explained by the fact that at room temperature, a small fraction of molecules is in a vibrational level higher than level 0 in the ground state, as well as in the excited state. At low temperature, this departure from the Stokes law should disappear.

Normally, the fluorescence spectrum resembles the first absorption band (“mirror image” rule) because the differences between the vibrational levels are similar in the ground and excited states.

The 0-0 transitions are usually the same for absorption and fluorescence, but sometimes they are not exactly coincident because the solvent may interact differently with the solute in the ground and excited states (for instance, the hydrogen bonding pattern might differ). Absorption of light occurs in about 10^{-15} s, a very short time. For that reason, the solvent molecules do not have time to rearrange during the transition. Thus, absorption spectra are less sensitive to solvent polarity because the molecule is

exposed to the same local environment in the ground and excited states. In contrast, the emitting fluorophore is exposed to the relaxed environment, which contains solvent molecules oriented around the dipole moment of the excited state (Figure 4.12). The mechanism also suggests that the intensity of the fluorescence ought to depend on the ability of the solvent molecules to accept the electronic and vibrational quanta. It is indeed found that a solvent composed of molecules with widely spaced vibrational levels (such as water) can in some cases accept the large quantum of electronic energy and so extinguish, or quench, the fluorescence.

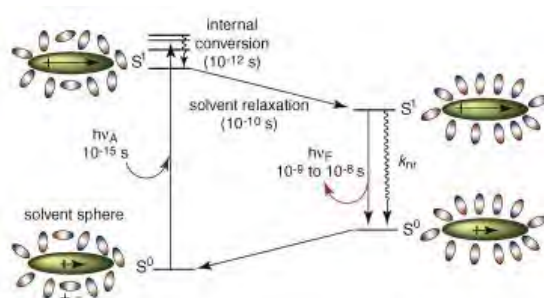


Figure 4.12. Shift to higher wavelengths of the fluorescence spectrum relative to the absorption spectrum due to interaction with solvent¹³.

- **Delayed Fluorescence:**

Delayed Fluorescence is similar to normal fluorescence but with a longer decay time constant, because the molecule is subjected to an intersystem crossing from a singlet to a triplet state, stay in the triplet state and is subjected to a back intersystem crossing from the triplet to the singlet state, before emitting fluorescence.

- **Phosphorescence:**

Phosphorescence is the emission of photons accompanying the $T_1 \rightarrow S_0$ relaxation after an intersystem crossing $S_1 \rightarrow T_1$. Once a molecule is in a triplet state, it continues to deposit energy into the surroundings. However, it is now stepping down the triplet's vibrational ladder, and, at the lowest energy level, it is trapped because the triplet state is at a lower energy than the corresponding singlet (that is why the phosphorescence spectrum is located at higher wavelengths than the fluorescence spectrum). The solvent cannot absorb the final, large quantum of electronic excitation energy, and the molecule cannot radiate its energy because return to the ground state is spin-forbidden. However, the radiative transition is not totally forbidden because the

spin-orbit coupling, that was responsible for the intersystem crossing, also breaks the selection rule. The molecules are therefore able to emit weakly, and the emission may continue long after the original excited state was formed.

Phosphorescence competes with non-radiative de-excitation processes from the triplet state. In solution, at room temperature, as the transition $T_1 \rightarrow S_0$ is spin-forbidden, the radiative rate constant is very low (10^3 s^{-1} or less), and during such a process, the numerous collisions with solvent molecules (or oxygen and impurities) favor non-radiative processes (intersystem crossing, vibrational relaxation and quenching, with radiationless rate constants about 10^9 s^{-1}). On the contrary, at low temperatures and/or in a rigid medium (e.g. polymer), the lifetime of the triplet state may be long enough to observe phosphorescence.

5. Characteristics of fluorescence emission

5.1. Fluorescent probes

Fluorescence is a powerful investigative tool in the study of the structure and dynamics of matter or living systems due to its high sensitivity, its specific characteristics according to the microenvironment of the emitting molecules (e.g. polarity, hydrogen bonds, pH, pressure, viscosity, temperature, quenchers, electric potential and ions) and its ability to provide spatial and temporal information. As a consequence, fluorescent molecules are very often used as probes for the investigation of matter and living systems³.

Fluorescent probes (also called *fluorophores* or simply *dyes*) have been used for nearly a century to study cellular processes, due to their exquisite sensitivity and selectivity. Their high sensitivity arises in part because, unless a fluorophore is irreversibly destroyed in the excited state by photobleaching, the same fluorophore can be repeatedly excited and detected. This allows a single fluorophore to generate many thousands of detectable photons. Fluorescent probes have also gained in popularity as safety and environmental concerns over the use of radioactive probes have grown¹⁴. In contrast to radioactive tracers or EPR (Electronic Paramagnetic Resonance) probes, which are used in relatively few applications, fluorescent probes can be used in the study of innumerable systems like polymers, solid surfaces, surfactant solutions, biological membranes, vesicles, proteins, nucleic acids or living cells. They can also be used in fluoroimmunoassays³.

There are two principal classes of fluorescent probes⁹:

- A. Intrinsic probes: occur naturally in the systems under study such as aromatic amino acids, neurotransmitters, porphyrins, and green fluorescent protein.
- B. Extrinsic probes: synthetic fluorescent probes that are added to a species to produce fluorescence with specific spectral properties. These probes may be covalently attached (*markers*) or non-covalently attached probes³.

The advantage of markers *versus* non-covalently attached probes is that, in the first type, we know the location of the probe. However, as the synthesis of covalently-bound probes is difficult, most of the experiments are carried out with non-covalently attached probes.

In the choice of a probe, it is important to consider its sensitivity to a particular property of its microenvironment (or not, e.g. in fluorescence polarization or in energy transfer experiments).

The main clause criticism to the use of extrinsic probes is the possible perturbation induced by the probe itself; hence, attention must be paid to the size and the shape of the probe with respect to the probed region¹².

5.2. Lifetimes and quantum yields

The fluorescence lifetimes and quantum yields of fluorescent molecules are frequently measured, because they represent the most important characteristics of a fluorophore. The lifetime (τ) determines the time available for the fluorophore to interact with or diffuse in its environment, and the quantum yield (Φ_F) is the number of emitted photons relative to the number of absorbed photons.

The lifetime τ of the excited state is defined by the average time the molecule spends in the excited state prior to return to the ground state³:

$$\tau = \frac{1}{k_R + k_{NR}} \quad (4.22)$$

where k_R and k_{NR} are the rate constants for radiative (fluorescence) and non-radiative (internal conversion and intersystem crossing) decays, respectively.

The lifetime of a homogeneous population of fluorophores is very often independent of the excitation wavelength, because internal conversion and vibrational relaxation are always very fast in solution and emission arises from the lowest vibrational level of S_1 state.

The lifetime of the molecule in the absence of non-radiative processes is called the *intrinsic lifetime* or *radiative lifetime* (τ_0), and is given by³

$$\tau_0 = \frac{1}{k_R} \quad (4.23)$$

The radiative lifetime can be theoretically calculated from the absorption and fluorescence spectra, using the Strickler-Berg relation²²:

$$\begin{aligned} \frac{1}{\tau_0} &= \frac{8\pi \times 230cn^2}{N_a} \frac{\int F_{\bar{\nu}}(\bar{\nu}_F) d\bar{\nu}_F}{\int \bar{\nu}_F^3 F_{\bar{\nu}}(\bar{\nu}_F) d\bar{\nu}_F} \int \frac{\varepsilon(\bar{\nu}_A)d\bar{\nu}_A}{\bar{\nu}_A} \\ &= 2.88 \times 10^{-9}n^2 \frac{\int F_{\bar{\nu}}(\bar{\nu}_F) d\bar{\nu}_F}{\int \bar{\nu}_F^3 F_{\bar{\nu}}(\bar{\nu}_F) d\bar{\nu}_F} \int \frac{\varepsilon(\bar{\nu}_A)d\bar{\nu}_A}{\bar{\nu}_A} \end{aligned} \quad (4.24)$$

where n is the refractive index, c is the speed of light, ε is the molar absorption coefficient, N_a is the Avogadro's number and $F_{\bar{\nu}}(\bar{\nu}_F) d\bar{\nu}_F$ is the fluorescence spectrum, defined by

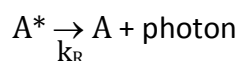
$$\int_{\infty}^0 F_{\bar{\nu}}(\bar{\nu}_{em}) d\bar{\nu}_{em} = \Phi_F = \int_0^{\infty} F_{\lambda}(\lambda_{em}) d\lambda_{em} \quad (4.25)$$

Thus, quantum yields (and radiative lifetimes) are usually determined by integration of the fluorescence spectrum (and subsequent normalization using a standard of known fluorescence quantum yield, in order to get rid of the instrumental factor).

Attention should be paid to the method of integration; from a theoretical point of view, $\int F_{\bar{\nu}}(\bar{\nu}_{em}) d\bar{\nu}_{em}$ is equivalent to $\int F_{\lambda}(\lambda_{em}) d\lambda_{em}$. However, from a practical point of view, because all spectrofluorometers are equipped with grating monochromators, calculation of the integral must be made with the wavelength form³.

The Strickler-Berg equation yields values of τ that are often in agreement with the experimental ones, but it fails in a number of cases, especially when the interactions with the solvent cannot be ignored and when there is a change in the excited-state geometry. An important consequence of this equation is that the lower the molar absorption coefficient, the longer the radiative lifetime, i.e. the lower the rate of the radiative process.

The fluorescence intensity is defined as the amount of photons emitted per unit time and per unit volume of solution, according to³



The fluorescence intensity, i_F , at time t , after excitation by a very short pulse of light at time 0, is proportional, at any time, to the instantaneous concentration of molecules still excited $[A^*]$; the proportionality factor is the rate constant for radiative de-excitation, k_R :

$$i_F(t) = k_R [A^*] = k_R [A^*]_0 \exp\left(-\frac{t}{\tau}\right) \quad (4.26)$$

$i_F(t)$, the δ -pulse response of the system, decreases according to a single exponential. In any practical measurement of fluorescence intensity, the measured quantity is proportional to i_F , the proportionality factor depending on instrumental conditions. The “measured” fluorescence intensity will be denoted I_F and its numerical value is obtained on an arbitrary scale, depending on the experimental settings.

The fraction of fluorophores which decay through emission, and hence the fluorescence quantum yield, Φ_F , is given by³

$$\Phi_F = \frac{k_R}{k_R + k_{NR}} = k_R \tau = \frac{\tau}{\tau_0} \quad (4.27)$$

The quantum yield can be close to the unity if the radiationless decay or deactivation is much smaller than the rate of radiative decay, that is $k_{NR} \ll k_R$, but it is always less than unity because of the Stokes losses.

It is interesting to note that when the fluorescence quantum yield and the excited state lifetime of a fluorophore are measured under the same conditions, the non-radiative and radiative rate constants can be easily calculated by means of the following relations:

$$k_R = \frac{\Phi_F}{\tau} \quad (4.28)$$

$$k_{NR} = \frac{1}{\tau} (1 - \Phi_F) \quad (4.29)$$

Following an external perturbation, the fluorescence quantum yield can remain proportional to the excited state lifetime (e.g. in the case of dynamic quenching: section 6.2), variation in temperature, etc.). However, such a proportionality may not be valid if de-excitation pathways – different from those described above – result from interactions with other molecules. A typical case where the fluorescence quantum yield is affected without any change in excited-state lifetime is the formation of a ground-state complex that is non-fluorescent (static quenching; section 6.3).

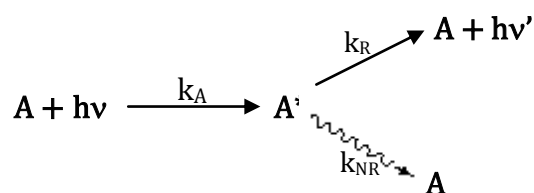
It is well known that atmospheric oxygen quenches fluorescence (and phosphorescence) (section 6.1), but its effect on quantum yields and lifetimes strongly depends on the nature of the compound and the medium. Oxygen quenching is a collisional process and, therefore, is diffusion-controlled. Consequently, compounds of long lifetime, such as naphthalene and pyrene, are particularly sensitive to the

presence of oxygen. Moreover, oxygen quenching is less efficient in media of high viscosity.

Generally, an increase in temperature results in a decrease in the fluorescence quantum yield and lifetime, because the non-radiative processes related to thermal agitation (collisions with solvent molecules, intramolecular vibrations and rotations, etc.) are more efficient at higher temperatures. Experiments are often in good agreement with the empirical linear variation of $\ln\left(\frac{1}{\Phi_F} - 1\right)$ versus $\frac{1}{T}$.

5.3. Emission and excitation spectra

Emission and excitation spectra are recorded using a spectrofluorometer. The light source is a lamp emitting a constant photon flow, i.e. a constant amount of photons per unit time, whatever their energy. Let us denote by N_0 the constant amount of incident photons entering, during a given time, a unit volume of the sample where the fluorophore concentration is $[A]$ (N_0 and $[A]$ in mol L^{-1}). αN_0 represents the amount of absorbed photons per unit volume involved in the excitation process



Scheme 4.4. Absorption and de-excitation processes and respective rate constants.

The rate constant for absorption, k_A , is very large ($k_A \approx 10^{15} \text{ s}^{-1}$) comparing with the radiative and non-radiative de-excitation rate constants (k_R and $k_{NR} \approx 10^7 - 10^{10} \text{ s}^{-1}$).

Under continuous illumination, the concentration $[A^*]$ remains constant, which means that A is in a steady state. Measurements under these conditions are then called *steady-state measurements*.

The rate of change of $[A^*]$ is equal to zero:

$$\frac{d[A^*]}{dt} = 0 = k_A \alpha N_0 - (k_R + k_{NR})[A^*] \quad (4.30)$$

$k_A \alpha N_0$ represents the amount of absorbed photons per unit volume and per unit time. It can be rewritten as αI_0 where I_0 represents the intensity of the incident light (in moles of photons per liter and per second).

The constant concentration $[A^*]$ is thus given by

$$[A^*] = \frac{\alpha I_0}{k_R + k_{NR}} \quad (4.31)$$

The amount of fluorescence photons emitted per unit time and per unit volume, i.e. the steady-state fluorescence intensity, is then given by

$$i_F = k_R[A^*] = \alpha I_0 \frac{k_R}{k_R + k_{NR}} = \alpha I_0 \Phi_F \quad (4.32)$$

This expression shows that the steady-state fluorescence intensity per absorbed photon, $\frac{i_F}{\alpha I_0}$, is the fluorescence quantum yield.

We saw (equation 4.25) that $\Phi_F = \int_0^\infty F_\lambda(\lambda_{em}) d\lambda_{em}$, where Φ_F is the fluorescence quantum yield and $F_\lambda(\lambda_{em})$ represents the *fluorescence spectrum* (or *emission spectrum*): it represents the probability of the various transitions from the lowest vibrational level of S_1 to the various vibrational levels of S_0 . The emission spectrum is characteristic of a given compound and may be used in some cases for the identification of species, especially when the spectrum exhibits vibronic bands (e.g. in the case of aromatic hydrocarbons), but the spectra of most fluorescent probes (in the condensed phase) exhibit broad bands.

In practice, the steady-state fluorescence intensity, $I_F(\lambda_{em})$, measured at wavelength λ_{em} , is proportional to $F_\lambda(\lambda_{em})$ and to the number of photons absorbed at the excitation wavelength λ_{ex} ,

$$\begin{aligned} I_F(\lambda_{ex}\lambda_{em}) &= k F_\lambda(\lambda_{em}) I_A(\lambda_{ex}) = k F_\lambda(\lambda_{em}) (I_0(\lambda_{ex}) - I(\lambda_{ex})) \\ \Leftrightarrow I_F(\lambda_{ex}\lambda_{em}) &= k F_\lambda(\lambda_{em}) I_0(\lambda_{ex}) [1 - \exp(-2.3\varepsilon(\lambda_{ex})Cl)] \end{aligned} \quad (4.33)$$

where k is an instrumental factor, $\varepsilon(\lambda_{ex})$ is the molar absorption coefficient of the fluorophore at wavelength λ_{ex} (in $L \text{ mol}^{-1} \text{ cm}^{-1}$), C is the concentration in mol L^{-1} , l is the optical path in the sample (cm), $F_\lambda(\lambda_{em})$ is the fluorescence spectrum, and $I_A(\lambda_{ex})$ is the absorbed intensity, defined as the difference between the intensity of the incident light, $I_0(\lambda_{ex})$, and the intensity of the transmitted light, $I(\lambda_{ex})$.

So, measurement of I_F as a function of λ_{em} for a fixed excitation wavelength, λ_{ex} , provides the fluorescence spectrum. As the proportional instrumental factor k is

normally unknown, the measured intensity I_F has no meaning and is expressed in arbitrary units.

In the case of low concentrations, the following expansion of $[1 - \exp(-2.3\varepsilon(\lambda_{ex})Cl)]$ can be used:

$$1 - \exp(-2.3\varepsilon(\lambda_{ex})Cl) = 2.3\varepsilon(\lambda_{ex})Cl - \frac{1}{2}(2.3\varepsilon(\lambda_{ex})Cl)^2 + \dots \quad (4.34)$$

As the term of higher order become negligible for highly diluted solutions, we obtain

$$I_F(\lambda_{ex}, \lambda_{em}) \simeq k F_\lambda(\lambda_{em}) I_0(\lambda_{ex}) [2.3\varepsilon(\lambda_{ex})Cl] = 2.3k F_\lambda(\lambda_{em}) I_0(\lambda_{ex}) A(\lambda_{ex}) \quad (4.35)$$

where $A(\lambda_{ex})$ represents the absorbance at wavelength λ_{ex} (according to the Beer-Lambert law).

This relation shows that the fluorescence intensity is proportional to concentration only for low absorbances: deviations from a linear variation increase with increasing absorbance, Table 4.2. Furthermore, when the concentration is high, inner filter effects reduce the fluorescence intensity, depending on the observation conditions. In particular, the photons emitted at wavelengths corresponding to the overlap of the absorption and emission spectra can be reabsorbed. That is the reason why, in practice, the fluorescence spectra are recorded for samples of low absorbances (< 0.1), i.e. diluted solutions.

Table 4.2. Deviation from linearity in the relation between fluorescence intensity and absorbance³.

Absorbance	Deviation (%)
10^{-3}	0.1
10^{-2}	1.1
0.05	5.5
0.10	10.6
0.20	19.9

The *excitation spectra* represent the variations in fluorescence intensity as a function of the excitation wavelength, λ_{ex} , for a fixed observation wavelength, λ_{em} . If we look to the last expression, these variations reflect the evolution of the product $I_0(\lambda_{ex})A(\lambda_{ex})$. As the wavelength dependence of the incident light, $I_0(\lambda_{ex})$, can be compensate, the

only term to be taken in account is $A(\lambda_{ex})$. The corrected excitation spectrum is thus identical in shape to the absorption spectrum, unless several species (or a species in different forms like aggregates, complexes, etc.) are present in the ground state.

5.4. Effects of molecular structure on fluorescence

➤ Extent of π -electron system

Most fluorescent compounds are aromatic. Generally speaking, an increase in the extent of the π -electron system (high degree of conjugation), leads to a shift of the absorption and fluorescence spectra to longer wavelengths (*red shift*) and to an increase in the fluorescence quantum yields.

The lowest-lying transitions of aromatic hydrocarbons are of $\pi \rightarrow \pi^*$ type and are characterized by high molar absorption coefficients and fluorescence quantum yields. If a heteroatom is involved (for instance, in azo compounds or compounds containing carbonyl groups and/or nitrogen heterocycles), the lowest-lying transition may be of $n \rightarrow \pi^*$ type. Such transitions are characterized by molar absorption coefficients that are, at least, 100 times smaller than those of $\pi \rightarrow \pi^*$ transitions, because these transitions are symmetry-forbidden (see section 3.2.). As a consequence, the radiative rate constant is much smaller than the non-radiative rate constant and the fluorescence quantum yields are low.

➤ Substitution effects on aromatic hydrocarbons

Generally, the presence of internal heavy atoms increase spin-orbit coupling (which has a Z^4 dependence) and thus the probability of intersystem crossing, unless the fluorescence rate constant is much higher, or much smaller, than other de-excitation rate constants, or unless there is no triplet state energetically close to the singlet emitting state.

➤ Electron-donating substituents (-OH, -OR, -NH₂, -NHR₁, -NR₂)

The presence of electron-donating substituents induce an increase in the molar absorption coefficient and the fluorescence quantum yield, as well as a *bathochromic effect* (*red shift*) in both absorption and fluorescence spectra, which become often broad and structureless, compared to the parent non-substituted compound^{15,16}. This

can be explained by the significant intramolecular charge transfer due to the lone pairs of electrons on oxygen and/or nitrogen atoms, which are involved directly in π -bonding with the aromatic system (that is why the $\pi \rightarrow \pi^*$ nature of the parent molecule transitions is not affected by the oxygen or nitrogen atom). This intramolecular charge transfer decreases the $S_0 \rightarrow S_1$ energy transition, which explains the observed effects. If the aromatic amines or alcohols are planar, the observed effects are more intense than if the amino or the alcohol group is twisted out of the plane of the aromatic ring for steric reasons, because the degree of conjugation is decreased.

Note that the absorption and fluorescence spectra of aromatic amines and alcohols are pH-dependent.

➤ **Electron-withdrawing substituents: carbonyl and nitro compounds**

The lone-pairs of electrons of carbonyl or nitro substituents are not directly involved in π -bonding with the aromatic system. Thus, many aromatic compounds with carbonyl or nitro substituents have a low-lying $n \rightarrow \pi^*$ excited state. As these transitions are symmetry-forbidden, such compounds are submitted to an efficient intersystem crossing process and exhibit low fluorescence quantum yields.

Normally, the fluorescence of nitroaromatics is not even detectable and they are rather phosphorescent. In some cases, as the $-\text{NO}_2$ group has a very strong electron-withdrawing power, such compounds have a considerable charge-transfer character and the absence of fluorescence (and phosphorescence) is thus rather due to $S_1 \rightarrow S_0$ internal conversion than to $S_1 \rightarrow T_1$ intersystem crossing.

In some cases (if the $n \rightarrow \pi^*$ and $\pi \rightarrow \pi^*$ states are close in energy), aromatic carbonyl compounds can exhibit high fluorescence quantum yields. When the polarity and the hydrogen bonding power of the solvent increases, the $n \rightarrow \pi^*$ state shifts to higher energy, whereas the $\pi \rightarrow \pi^*$ state shifts to lower energy. Therefore, intense fluorescence can be observed in polar solvents and weak fluorescence in non-polar solvents.

Conformational changes of aromatic molecules with a carboxylic group can lead to different absorption and fluorescence spectra for the acidic ($-\text{COOH}$) and the basic

(-COO⁻) forms. Normally, the carboxylate group (-COO⁻) is almost perpendicular to the ring, so that the π aromatic system is only slightly perturbed. On the contrary, the carboxylic group is in a position close to the coplanarity of the ring. The resulting interaction induces an intramolecular charge-transfer character to the $\pi \rightarrow \pi^*$ transition, which leads to broad and structureless fluorescence bands.

➤ Heterocyclic compounds

Heterocyclic compounds have a heteroatom involved in the π -system of electrons. For that reason, the low-lying transition is of $n \rightarrow \pi^*$ type (symmetry-forbidden transition), which explains the low fluorescence quantum yields of such compounds.

However, in protic solvents such as alcohols, hydrogen bonds can be formed between the heteroatoms and the solvent molecules. In this case, the n-orbitals are more stabilized than the π^* orbitals (the electron density on the heteroatom is reduced on the excited state) and there is an inversion of the $n \rightarrow \pi^*$ and $\pi \rightarrow \pi^*$ states: the lowest-lying transition becomes of $\pi \rightarrow \pi^*$ type. As a consequence, the spectra of these compounds exhibit a bathochromic effect and the fluorescence quantum yields are increased from non-polar to polar solvents.

If the heteroatom is singly bonded to carbon atoms of the heterocycle, the transitions involving the non-bonding electrons have similar properties to those of $\pi \rightarrow \pi^*$ transitions. In fact, as the non-bonding orbital is perpendicular to the plane of the ring, the lone pair of electrons are involved in π -bonding of the aromatic system by overlapping the π -orbitals of the adjacent carbon atoms.

5.5. Solvent and environmental effects on fluorescence emission spectra

We saw that the principal cause of the Stokes shift is that, after absorption, the excess vibrational energy is rapidly lost to the solvent (section 4, scheme 4.3). Solvent polarity and the local environment have strong effects on the emission spectral properties of fluorophores and are another origin of the Stokes shift. These effects are complex and are due to several factors. Typically, more than one effect will simultaneously affect the fluorophore and it can be difficult to know which effect is dominant.

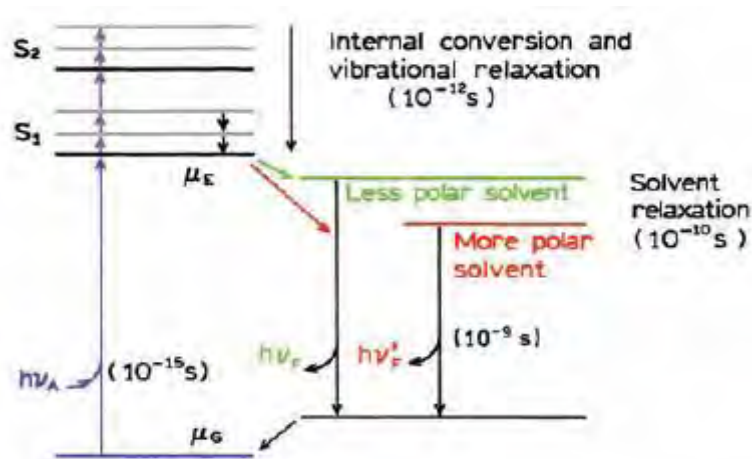
At the simplest level, solvent-dependent emission spectra are interpreted in terms of the Lippert-Mataga equation (section 5.5.1.). These general solvent effects occur

whenever a fluorophore is dissolved in any solvent, and are independent of the chemical properties of the fluorophore and the solvent. However, this theory is often inadequate for explaining the detailed behavior of fluorophores in a variety of environments. For example, indole displays a structured emission spectrum in cyclohexane but, after addition of a small amount of the polar solvent ethanol (1 to 5%), we note a loss of the structured emission and a spectral shift to higher wavelengths. As the amount of ethanol is too small to significantly change the solvent polarity, the observed effects are rather due to hydrogen bonding of ethanol to the imino nitrogen on the indole ring than to general solvent effects. In addition to such general and specific solvent effects (section 5.5.1.), solvent relaxation may be accompanied by internal rotation within the fluorophore, leading to a Twisted Intramolecular Charge Transfer (TICT), from which emission occurs (section 5.5.2.). Additionally, the quantum yield can be altered due to a conformational change in the fluorophore or due to a change in the rate of radiative or non-radiative decay (Sections 5.5.3. and 5.5.4.). Finally, a fluorophore may display a large spectral shift due to excimer or exciplex formation (the fluorophore may be fluorescent or non-fluorescent in these different states, see section 5.5.5.). In summary, no single theory can be used for a quantitative interpretation of the effects of environment on fluorescence³.

5.5.1. Effects of solvent polarity and viscosity

The fluorescence emission spectra of many fluorophores, especially those containing polar substituents on the aromatic rings are sensitive to the polarity of their surrounding environment. As the excitation process induces the movement of an electron from one orbital to another, it is normally accompanied by an increase in the dipole moment of the fluorescent molecule. In other words, the fluorophore has a larger dipole moment in the excited state (μ^*) than in the ground state (μ). If the molecule has both an electron-donating and an electron-withdrawing group, this increase can be quite large. Thus, if the medium is sufficiently fluid, the solvent molecules rotate until the solvation shell is in equilibrium with the fluorophore (*solvent relaxation*) and a relaxed intramolecular charge transfer (ICT) state is reached. Normally, when we increase solvent polarity, this effect becomes larger and results in

shifts (*solvatochromic shifts*) of the emission spectrum to longer wavelengths (*red shifts*) which are often, but not always, accompanied by decrease in the quantum yield of the fluorophore (Figures 4.12, 4.13 and scheme 4.5). As the emission of a fluorescence photon is quasi-instantaneous, the solute recovers its ground state dipole moment and a new relaxation process leads to the most stable initial configuration of the solute–solvent system in the ground state. Note that, if the medium is sufficiently fluid, the time required for the reorganization of solvent molecules around the solute is short comparatively to the excited-state lifetime and fluorescence will essentially be emitted from molecules in equilibrium with their solvation shell. Conversely, if the medium is too viscous to allow solvent molecules to reorganize, emission arises from a state close to the Franck–Condon state (F) (as in the case of a non-polar medium) and no shift of the fluorescence spectrum will be observed¹⁷.



Scheme 4.5. Jablonski diagram for fluorescence with solvent relaxation¹⁷.

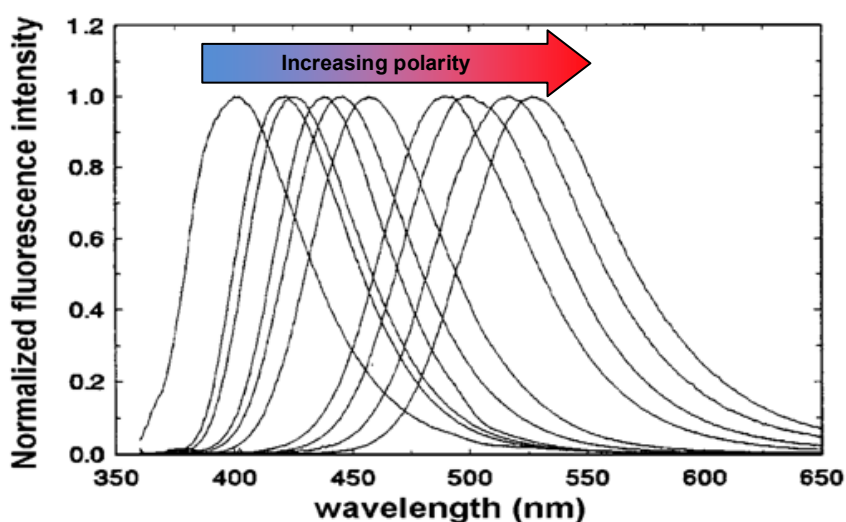


Figure 4.13. Solvatochromic effects on fluorescence spectra.

One common use of solvent effects is to determine the polarity of the probe binding site on a macromolecule. This is accomplished by comparison of the emission spectra and/or quantum yields when the fluorophore is bound to the macromolecule or dissolved in solvents of different polarity.

The observed shifts result from both the interactions of the dipole moment of the fluorophores with the reactive fields induced in the surrounding solvent (*General Solvent Effects*), and from the specific chemical interactions between the fluorophores and one or more solvent molecules (*Specific Solvent Effects*). General Solvent Effects (non-specific dielectric interactions) result from the refractive index (n) and the dielectric constant (ϵ), i.e. the physical constants which reflect the freedom of movement of the electrons in the solvent molecules and the dipole moment of these molecules. Specific solvent effects (specific interactions) refer to specific chemical interactions between the fluorophores and the solvent molecules, such as hydrogen bonding and complexation. General solvent effects are expected to always be present whereas specific solvent effects depend upon the chemical structures of the solvent and the fluorophore. Normally, general solvent effects lead to higher spectral shifts¹⁷.

Polarity and solvatochromism

Compounds are called *solvatochromic* when the location of their absorption (and emission) spectra depends on solvent polarity. A *bathochromic (red)* shift and a *hypsochromic (blue)* shift with increasing solvent polarity pertain to *positive* and *negative solvatochromism*, respectively. Such shifts of appropriate solvatochromic compounds in solvents of various polarities were used to construct several empirical polarity scales^{18,19}. The π^* scale of Kamlet and Taft²⁰ deserves special recognition because it has been successfully applied to the positions or intensities of maximal absorption in IR, NMR, ESR and UV–visible absorption and fluorescence spectra, and many other physical or chemical parameters (reaction rate, equilibrium constant, etc.). It is remarkable that the π^* scale has been established from the averaged spectral behavior of numerous solutes. It offers the distinct advantage of taking into account both non-specific and specific interactions³.

Table 4.3. Parameters of the π^* scale of polarity, where π^* is a measure of the polarity/polarizability effects of the solvent; the α scale is an index of solvent HBD (hydrogen bond donor) acidity and the β scale is an index of solvent HBA (hydrogen bond acceptor) basicity³.

Solvent	π^*	α	β
Cyclohexane	0.00	0.00	0.00
<i>n</i> -Hexane, <i>n</i> -heptane	-0.08	0.00	0.00
Benzene	0.59	0.10	0.00
Toluene	0.54	0.11	0.00
Dioxane	0.55	0.00	0.37
Tetrahydrofuran	0.58	0.00	0.55
Acetone	0.71	0.08	0.48
Carbon tetrachloride	0.28	0.00	0.00
1,2-Dichloroethane	0.81	0.00	0.00
Diethyl ether	0.27	0.00	0.47
Ethyl acetate	0.55	0.00	0.45
Dimethylsulfoxide	1.00	0.00	0.76
<i>N,N</i> -Dimethylformamide	0.88	0.00	0.69
Acetonitrile	0.75	0.19	0.31
Ethanol	0.54	0.83	0.77
Methanol	0.60	0.93	0.62
<i>n</i> -Butanol	0.47	0.79	0.88
Trifluoroethanol	0.73	1.51	0.00
Ethylene glycol	0.92	0.90	0.52
Water	1.09	1.17	0.18

General Solvent Effects on fluorescence spectra: the Lippert-Mataga equation

A variety of equations have been proposed to describe the effects of the physical properties of solvents on emission spectra. In these equations, the solvent is considered as a continuum in which the fluorophore is contained. This simplifying assumption limits the applicability of the equations since specific fluorophore-solvent interactions which can have substantial effects upon the emission spectra are not considered. Nevertheless, as the general solvent effects are always present, a quantitative prediction of these effects provides a framework within which one can analyze the experimental data. The most widely used expression was previously presented by Lippert and others²¹⁻²³. As the interactions between the solvent and fluorophore molecules affect the energy difference between the ground and the excited state, the Lippert-Mataga equation represents this energy difference:

$$\bar{\nu}_a - \bar{\nu}_{em} = \frac{1}{4\pi\epsilon_0} \frac{2}{hc} \left(\frac{\epsilon - 1}{2\epsilon + 1} - \frac{n^2 - 1}{2n^2 + 1} \right) \frac{(\mu^* - \mu)^2}{R^3} + \text{const.} \quad (4.36)$$

where $\bar{\nu}_a$ and $\bar{\nu}_{em}$ are the wavenumbers of the absorption and emission, respectively (thus, the difference $\bar{\nu}_a - \bar{\nu}_{em}$ represents the energy difference between the ground and the excited state); ϵ_0 is the vacuum permittivity; h is the Planck's constant; c is the speed of light; R is the radius of the cavity in which the fluorophore resides (considering the fluorophore a point dipole at the center of a spherical cavity immersed in the homogeneous solvent); $\mu^* - \mu$ is the difference in the dipole moment of solute molecule between excited (μ^*) and ground (μ) states.

The term in brackets is called the *orientation polarizability* (f). Then, the Lippert-Mataga equation can be written³

$$\bar{\nu}_a - \bar{\nu}_{em} = \frac{1}{4\pi\epsilon_0} \frac{2}{hc} (\mu^* - \mu)^2 R^{-3} \Delta f + \text{const.} \quad (4.37)$$

f ranges from -0.001 in cyclohexane to 0.320 in water (Table 4.4).

This equation is only an approximation but there is a reasonable correlation between the observed and calculated energy losses in nonprotic solvents (those not having hydroxyl groups or other groups capable of hydrogen bonding). In this case, a linear behaviour is observed which allows us to determine the increase in dipole moment $\mu = \mu^* - \mu$, provided that a correct estimation of the cavity radius is possible.

This sensitivity of the Stokes shift to solvent polarity is the reason why fluorescence emission spectra are frequently used to estimate the polarity of the environment surrounding the fluorophore.

Table 4.4. Dielectric constant (at 20°C), refractive index (at 20°C) and orientational polarizability f of some solvents³.

Solvent	ϵ	n^{20}	f
Cyclohexane	2.023	1.4266	-0.001
Benzene	2.284	1.5011	0.003
Toluene	2.379	1.4961	0.013
Dioxan	2.218	1.4224	0.021
Chloroform	4.806	1.4459	0.149
Diethyl ether	4.335	1.3526	0.167
Butyl acetate	5.01	1.3941	0.171
Dichloromethane	9.08	1.4242	0.219
Dimethylsulfoxide	48.9	1.4770	0.265
N,N-Dimethylformamide	37.6	1.4305	0.275
Acetonitrile	38.8	1.3442	0.306
Ethanol	25.07	1.3611	0.290
Methanol	33.62	1.3288	0.309
Water ²	80.10	1.3330	0.320

Note that the Lippert-Mataga equation only considers the absolute magnitude of the charge transfer dipole moment $\mu = \mu^* - \mu$ and not the angle between the dipoles. Bakhshiev argued that the general solvent effects must also depend upon the angle between the ground and excited state dipole moments of the fluorophore and have presented an alternative expression^{24,25}. However, as other specific interactions between the solvent and the fluorophore result in substantial spectral shifts and are not conveniently accounted for within the framework of the existing theories, the use of the simplest conceptual model for general solvent effects seems justified. This simple theory is useful for interpreting experimental data and to evaluate the presence/importance of specific solvent effects. As the Lippert-Mataga equation describes the Stokes shift expected for a given fluorophore in media of varying polarity, it has two main applications:

- The sensitivity of a fluorophore to solvent polarity is expected to be proportional to $(\mu^* - \mu)^2$. Once this term is constant for a given fluorophore, we can prepare calibration curves for $(\bar{\nu}_a - \bar{\nu}_{em})$ versus f . Then, if the fluorophore is placed in an unknown environment, the polarity of this environment can be estimated from $(\bar{\nu}_a - \bar{\nu}_{em})$. An ideal polarity probe based on photoinduced charge transfer and solvent relaxation should (i) undergo a large change in dipole moment upon excitation but without change in direction; (ii) bear no permanent charge in order to avoid contributions from ionic interactions; (iii) be soluble in solvents of various polarities, from the apolar solvents to the most polar ones.
- The sensitivity of the Stokes shift to f can be used to estimate the change in dipole moment which occurs upon excitation. For that, we can trace a *Lippert-Mataga plot*, which is a plot of $(\bar{\nu}_a - \bar{\nu}_{em})$ versus the orientational polarizability, f , and evaluate the change in dipole moment μ assuming the molecular radius as the cavity radius. Fluorophores which have the largest changes in dipole moment upon excitation are more sensitive to solvent polarity. As an example, Lippert-Mataga plots for two naphthylamine derivatives are shown in Figure 4.14. The *N*-phenyl-*N*-methyl derivative is clearly more sensitive to solvent polarity than the unsubstituted derivative¹².

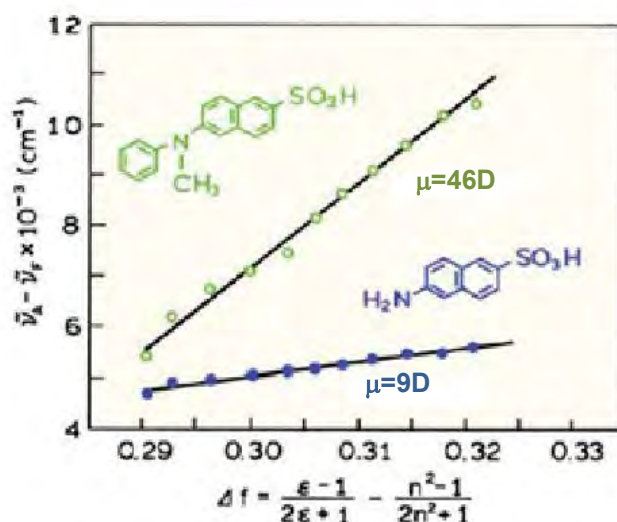


Figure 4.14. Lippert-Mataga plots for *N*-phenyl-*N*-methyl-2-aminonaphthalene-6-sulfonate (o) and 2-aminonaphthalene-6-sulfonate (●). Adapted from ref. 26.

Specific Solvent Effects on fluorescence spectra

General solvent effects are approximately described by the Lippert-Mataga equation and represent the collective influence of the entire set of surrounding solvent molecules on the fluorophore. In contrast, specific interactions are produced by one or a few neighboring molecules, and are determined by the specific chemical properties of both fluorophores and solvent^{27,28}. Specific effects can be due, for example, to hydrogen bonding, acid-base equilibrium, or charge transfer interactions and they can lead to substantial shifts.

Specific solvent effects can be identified by examining either emission spectra in a variety of solvents, or the Lippert-Mataga plots. When a substantial red shift of the emission spectrum of a fluorophore in a non-polar solvent is observed for the addition of a small percentage of a polar solvent, it can indicate that the observed shift is due to specific solvent effects. For example, the emission spectrum of 2-acetylanthracene (2-AA) in hexane shifted gradually as the percentage of dioxane was increased to 100%. These shifts are probably a result of general solvent effects. In contrast, most of the shift expected for methanol, together with a loss of structured emission, was produced by only about 1-2% methanol. This amount of alcohol is too small to affect the refractive index or dielectric constant of the solvent, and hence this shift is a result of specific solvent effects (Figures 4.15 and 4.16)¹⁷.

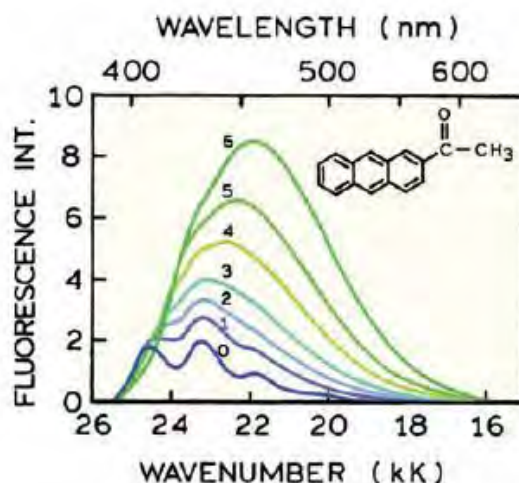


Figure 4.15. Fluorescence spectra of 2-acetylanthracene in methanol-hexane mixtures at 20°C¹⁷. Concentrations of methanol in mol dm⁻³: (0) 0, (1) 0.03, (2) 0.05, (3) 0.075, (4) 0.12, (5) 0.2, and (6) 0.34. 1 kK=1000 cm⁻¹.

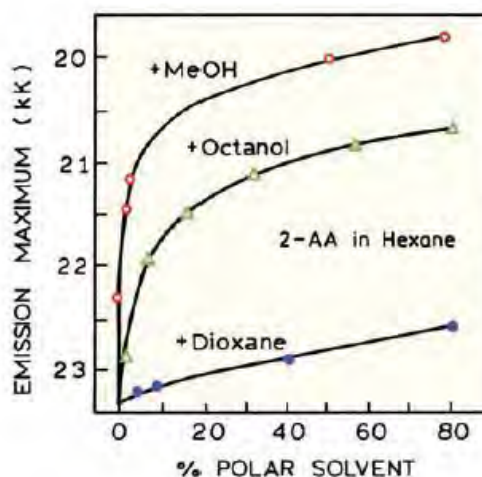


Figure 4.16. Effect of solvent composition on the emission maximum of 2-acetylanthracene (1 kK=1000 cm⁻¹)¹⁷.

Specific solvent-fluorophore interactions can occur in either the ground state or the excited state. If the interaction only occurred in the excited state, then the polar additive would not affect the absorption spectra. If the interaction occurs in the ground state, then some change in the absorption spectrum is expected.

In the case of $n-\pi^*$ transitions, the electronic density on a heteroatom like nitrogen decreases upon excitation and these transitions have a charge transfer character illustrated by an increase of the dipole moment with respect to the ground state dipole moment. It can be explained by the fact that the electron is removed from the heteroatom and goes to an π^* orbital localized half on the heteroatom, half on a

carbon atom. This results in a decrease in the capability of this heteroatom to form hydrogen bonds. The resulting effect is a blue-shift of the absorption spectrum (the higher the strength of hydrogen bonding, the larger the shift). This criterion is convenient for assigning a $n-\pi^*$ band and the spectral shift can be used to determine the energy of the hydrogen bond. The fluorescence emitted from a $n-\pi^*$ singlet state will be always less sensitive to the ability of the solvent to form hydrogen bonds than absorption because, as $n-\pi^*$ excitation of a heterocycle containing nitrogen (e.g. in solution in methanol) causes hydrogen bond breaking (e.g. $N\dots HOCH_3$), the fluorescence spectrum will only be slightly affected by the ability of the solvent to form hydrogen bonds (emission arises from an $n-\pi^*$ state without hydrogen bonds).

In the case of $\pi-\pi^*$ transitions, it is often observed that the heteroatom of a heterocycle (e.g. N) is more basic in the excited state than in the ground state. The resulting excited molecule can thus be hydrogen bonded more strongly than the ground state. $\pi-\pi^*$ fluorescence is thus more sensitive to hydrogen bonding than $\pi-\pi^*$ absorption³.

Attention must be paid to the emission spectrum of a fluorophore bound to a macromolecule. For example, a molecule like 2-acetylanthracene, when bound in a hydrophobic site on a protein, may display an emission spectrum comparable to that seen in water if only a single water molecule is near the carbonyl group.

Evidence of specific solvent effects can also be seen in the Lippert-Mataga plots. For example, the Stokes shifts observed for methyl 8-(2-anthroyl) octanoate (a 2-AA derivative) in hydrogen bonding solvents (water, methanol and ethanol) are much larger than that observed in solvents that less readily form hydrogen bonds (Figure 4.17).

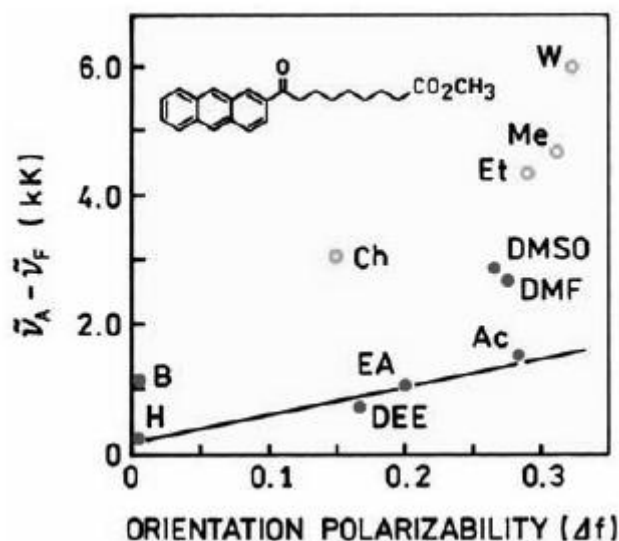


Figure 4.17. Stokes shifts of methyl 8-(2-anthroyl) octanoate in organic solvents and water. The solvents are benzene (B), *n*-hexane (H), diethyl ether (DEE), ethyl acetate (EA), acetone (Ac), *N,N*-dimethylformamide (DMF), chloroform (Ch), dimethyl sulfoxide (DMSO), ethanol (EA), methanol (Me), and water (W)¹⁷.

The presence of specific solvent effects can be problematic because these effects can prevent a quantitative interpretation of the emission spectra in terms of the orientation polarizability of the macromolecule. On the other hand, the presence of specific solvent effects can be favorable because they could reveal the accessibility of the macromolecule-bound probe to the aqueous phase.

An understanding of specific and general solvent effects can provide a basis for interpreting the emission spectra of fluorophores that are bound to macromolecules. For instance, the emission spectra of 2-anilinonaphthalene (2-AN) bound to membranes composed of dimyristoyl-L- α -phosphatidylcholine (DMPC) is considerably red shifted relative to the emission in cyclohexane, but it is blue shifted relative to water (Figure 4.18)¹⁷.

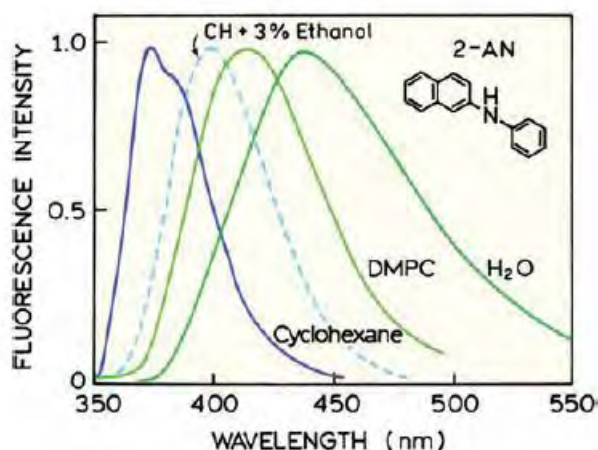
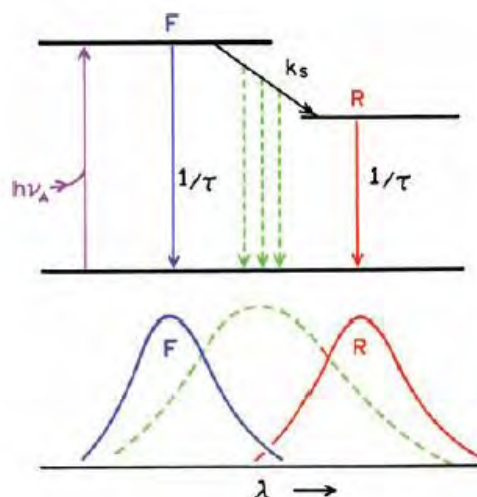


Figure 4.18. Normalized fluorescence emission spectra of 2-anilinonaphthalene in solvents and bound to vesicles of dimyristoyl-L- α -phosphatidylcholine (DMPC). The dashed line indicates the spectrum in cyclohexane (CH), which contains 3% ethanol¹⁷.

As 2-AN is highly sensitive to small concentrations of ethanol, it seems likely that cyclohexane containing more than 3% ethanol is the preferable reference solvent for a low polarity environment (in this solvent the specific effects are saturated). With this adjustment in mind, one may conclude that the environment in which the 2-AN is localized is mostly nonpolar, but that this site is accessible to water. Without consideration of specific solvent effects one might conclude that the 2-AN is in a more polar environment.

Temperature effects (solvent viscosity effects)

At low temperatures the solvent can become more viscous, and the time for solvent reorientation increases. Upon excitation, the fluorophore is assumed to be initially in the Franck-Condon state (F). Solvent relaxation proceeds with a rate k_s . If this rate is much slower than the decay rate ($1/\tau$), then one expects to observe the emission spectrum of the unrelaxed F state. If solvent relaxation is much faster than the emission rate ($k_s \gg 1/\tau$), then emission from the relaxed state (R) will be observed. At intermediate temperatures, where $k_s \approx 1/\tau$, emission and relaxation will occur simultaneously. Under these conditions, an intermediate emission spectrum will be observed (Scheme 4.6). Frequently, this intermediate spectrum (---) is broader on the wavelength scale because of contributions from both the F and R states.



Scheme 4.6. Jablonski diagram and respective emission spectra for solvent relaxation¹⁷.

Normally, internal rotations favor non-radiative de-excitation processes. That is the reason why rigid compounds are more fluorescent than similar compounds which can suffer internal rotations (e.g. phenolphthalein versus fluorescein). For the same reasons, when the temperature decreases, the environment become more rigid (because the solvent viscosity increases), the fluorophore suffers less internal rotations and, consequently, the fluorescence quantum yield increases.

5.5.2. Compounds submitted to photoinduced Intramolecular Charge Transfer (ICT) and internal rotation

Solvent relaxation may be accompanied by internal rotation within the fluorophore, leading to a Twisted Intramolecular Charge Transfer (TICT) state. Thus, highly conjugated planar molecules can sometimes completely lose the conjugation. In this case, there is a total charge separation and two bands can be observed in the fluorescence spectrum of the fluorophore in polar non-viscous solvents: one corresponding to the emission from the Franck Condon state and one to the emission from the TICT state (at higher wavelengths). Attention may be paid to the fact that internal rotation accompanying solvent relaxation or not can occur in many fluorophores, but dual fluorescence and right angle twist (required for full charge separation) are exceptional. Note that intramolecular charge transfer and internal rotation can also occur in non-polar and highly symmetric molecules³.

5.5.3. Changes in the non-radiative decay rates

Increases in quantum yield are frequently observed when fluorophores bind to biomolecules. These changes are due to solvent or environmental effects, but these changes are not explained by the Lippert equation. It seems reasonable to suggest that changes in quantum yield are due to changes in the rates of non-radiative decay (k_{NR}). One example for such a process is Coumarin-151. Figure 4.19 shows the Stokes shift and the quantum yields for Coumarin-151 in several solvents. The Stokes shift increases in a stepwise manner upon addition of the polar solvent dioxane, even though the value of Δf is almost unchanged. The quantum yield is low in nonpolar solvents and also increases stepwise when the solvent contains a polar additive. Since the excitation coefficient and radiative decay rates are usually not very sensitive to solvent polarity, the decrease in quantum yield suggests an increase in k_{NR} in nonpolar solvents¹⁷.

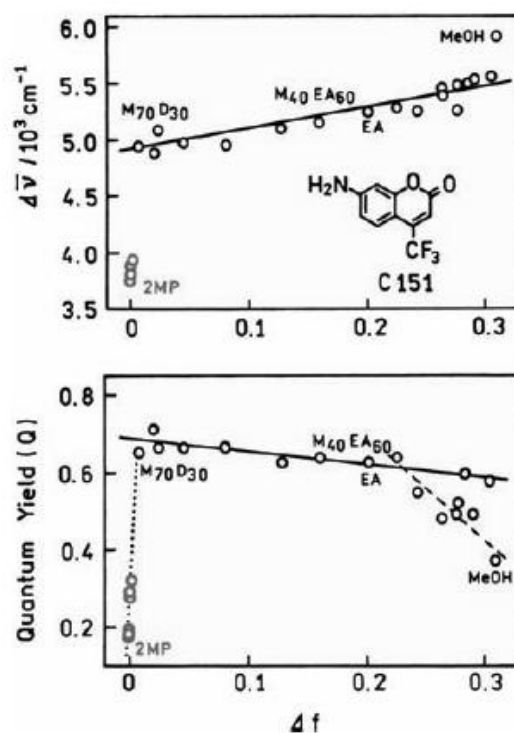
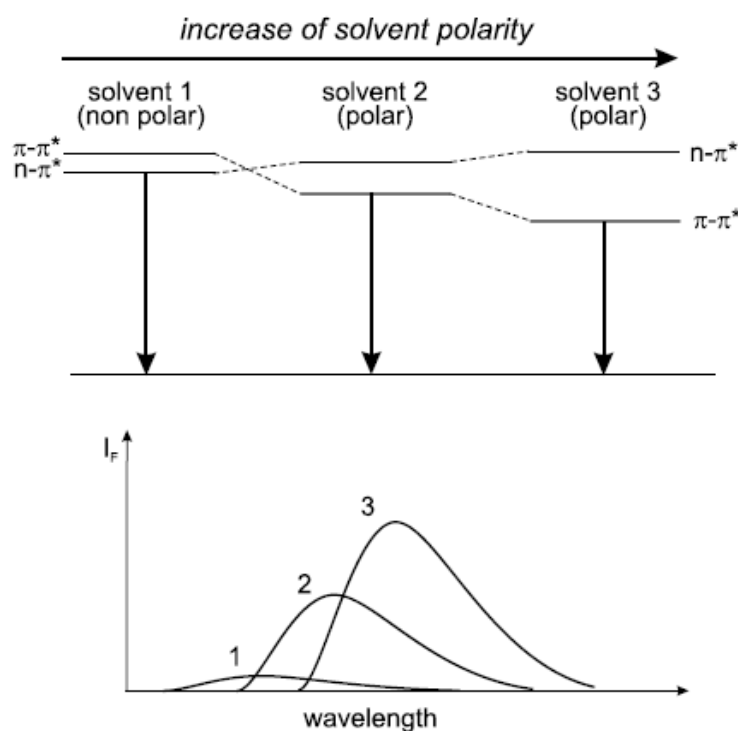


Figure 4.19. Stokes shifts and quantum yields for Coumarin-151 in various solvents. 2-MP, 2-methylpentane; M₇₀D₃₀, 70% 2-MP and 30% dioxane (D); M₆₀EA₄₀, 60% 2-MP and 40% EA, ethyl acetate; MeOH, methanol²⁹.

This fact can be explained by a polarity-induced inversion of $n-\pi^*$ and $\pi-\pi^*$ states³. A change in the ability of a solvent to form hydrogen bonds can affect the nature ($n-\pi^*$

vs $\pi-\pi^*$) of the lowest singlet state. Some aromatic carbonyl compounds often have low-lying, closely spaced $\pi-\pi^*$ and $n-\pi^*$ states (see section 5.4.). Inversion of these two states can be observed when the polarity and the hydrogen-bonding power of the solvent increases, because the $n-\pi^*$ state shifts to higher energy whereas the $\pi-\pi^*$ state shifts to lower energy. This results in an increase in fluorescence quantum yield because radiative emission from $n-\pi^*$ states is known to be less efficient than from $\pi-\pi^*$ states. The other consequence is a red-shift of the fluorescence spectrum (Scheme 4.7).



Scheme 4.7. The effects of polarity-induced inversion of $n-\pi^*$ and $\pi-\pi^*$ states³.

5.5.4. Changes in the radiative decay rates

In the previous example, the quantum yield of Coumarin-151 decreases in low polarity solvents. A more typical situation is an increase in quantum yield in low-polarity solvents. This behavior can be explained by the formation of an ICT state. In low polarity solvents, emission arises from the Franck-Condon $\pi-\pi^*$ state which is lower in energy. In high polarity solvents, the ICT state is stabilized by interaction with the solvent and thus becomes the emitting species. Thus, we can observe a redshift and, as

hydrogen bonds favor intersystem crossing, the radiative decay rates decrease as well as the fluorescence quantum yields, when the solvents polarity increases¹⁷.

5.5.5. Probe-probe interactions

In addition to interacting with solvents, fluorophores can interact with each other. One example is excimer formation due to an excited-state complex of two identical fluorophores. Excimer formation is a short-range interaction that requires molecular contact between the fluorophores. Excimer formation has found some utility in biotechnology, to detect, for example, an insertion mutation in DNA^{30,31}: a probe DNA with a insertion mutant sequence can prevent a non-fluorescent compound from intercalating into the double helix, resulting in the formation of an excimer out of the double helix that exhibits fluorescence. Another use of excimer formation is to follow self-assembly processes³² in which, according to the extent of the self-association, the fluorescence spectrum suffers spectral shifts.

5.6. Resolution of Fluorescence spectra

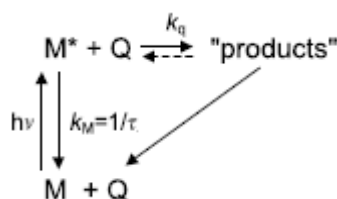
The width of a band in the emission (and/or the absorption) spectrum of a fluorophore is the result of two effects: *homogeneous* and *inhomogeneous broadening*.

Homogeneous broadening is due to the existence of a continuous set of vibrational levels. Thus, at room temperature, most emission (and absorption) spectra of moderately large and rigid fluorophores in solution are almost structureless.

Inhomogeneous broadening is due to the fluctuations in the structure of the solvation shell surrounding the fluorophore. The distribution of solute-solvent configurations leads to a distribution of the energies of the electronic transitions. Normally, the extent of inhomogeneous broadening is larger than that of homogeneous broadening, but there are several ways to reduce these effects like using solid matrices at low temperatures, or using laser excitation (whose linewidth is reduced) which allows exciting individual compounds in complex mixtures^{33,34}.

6. Quenching of fluorescence

Fluorescence quenching refers to any process that decreases the fluorescence intensity of a sample. A variety of photophysical processes can result in quenching. Most of them involve interaction of an excited molecule M^* with another molecule Q , as shown in Scheme 4.8. k_M is the sum of the rate constants of the intrinsic pathways (radiative and non-radiative) of de-excitation and is the reciprocal of the excited-state lifetime τ (equation 4.22); k_q represents the observed rate constant for the bimolecular process³.



Scheme 4.8. Interaction of an excited molecule M^* and another molecule Q and respective rate constants³.

These intermolecular photophysical processes responsible for de-excitation of molecules compete with the intrinsic de-excitation and affect the fluorescence characteristics (fluorescence intensity, decay time and/or fluorescence quantum yield) of M^* :

- (i) After excitation by a light pulse, the excited-state M^* population, and consequently the fluorescence intensity, decrease more rapidly than in the absence of excited-state interaction with Q , because quenching is an additional rate process that depopulates the excited state.
- (ii) For the same reasons, in the case of dynamic quenching (section 6.2.) the excited-state lifetime is decreased. However, in the case of static quenching (see section 6.3.) the lifetime is not decreased because only the fluorescent molecules are observed, and the uncomplex fluorophores have the unquenched lifetime τ .
- (iii) The fluorescence quantum yield is decreased because quenching depopulates the excited state without fluorescence emission. The loss of fluorescence intensity is called fluorescence quenching whatever the nature of the competing intermolecular process and even if this process leads to a fluorescent species (the word quenching applies only to the initially excited molecule)³.

The processes responsible for quenching include electron transfer, energy transfer, excimer or exciplex formation (in these cases, we talk about *dynamic quenching* or *collisional quenching*), and the formation of a non-fluorescent ground-state complex (*static quenching*). Intramolecular excited-state processes (intramolecular charge transfer, internal rotation, intramolecular proton transfer, etc.) and photochemical de-excitation (i.e. de-excitation resulting from organic photochemical reactions implying bond breaking and formation of new bonds, so that the ground state of M is not recovered) can also affect the fluorescence characteristics (we talked about some of these effects in section 5.5.).

There are numerous applications of quenching measurements. For example, quenching measurements can reveal the accessibility of fluorophores to quenchers. An example is a fluorophore bound to a protein or in a membrane. If the protein or membrane is impermeable to the quencher, and the fluorophore is located in the interior of the macromolecule/aggregate, then neither collisional nor static quenching can occur. For this reason, quenching studies can be used to reveal the localization of fluorophores in proteins and membranes, and their permeabilities to quenchers¹⁷.

6.1. Quenchers of fluorescence

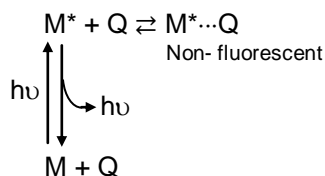
There is a large variety of substances which act as quenchers. One of the best-known collisional quenchers is molecular oxygen which quenches almost all known fluorophores. The mechanism by which oxygen quenches has been a subject of debate³⁵. The most likely mechanism is that the paramagnetic oxygen causes the fluorophore to undergo intersystem crossing to the triplet state. Under atmospheric pressure, the concentration of oxygen in most solvents is 10^{-3} – 10^{-4} mol L⁻¹. For that reason, it is frequently necessary to remove dissolved oxygen by bubbling the solutions with nitrogen or argon for example, in order to obtain reliable measurements of the fluorescence quantum yields or lifetimes.

Aromatic and aliphatic amines are also efficient quenchers of most unsubstituted aromatic hydrocarbons³⁶. Another type of quenching is due to heavy atoms such as iodide and bromide. Quenching by these larger halogens may be a result of intersystem crossing to an excited triplet state, promoted by spin–orbit coupling of the

excited (singlet) fluorophore and the halogen³⁷. There is a large variety of other quenchers and we can identify fluorophore–quencher combinations for a desired purpose. It is important to note that not all fluorophores are quenched by all the substances identified as “quenchers”. This fact occasionally allows selective quenching of a given fluorophore. The occurrence of quenching depends upon the mechanism, which in turn depends upon the chemical properties of the individual molecules. An overview of some possible quenchers for typical fluorophores can be found in reference 17.

6.2. Collisional quenching (dynamic quenching)

Collisional quenching of fluorescence results from diffusive encounters between the fluorophore and quencher during the lifetime of the excited state (*diffusion-controlled* process, scheme 4.9). This is a time-dependent process because the excited fluorophores, M^* , that are at a short distance from a quencher, Q , at the time of excitation react, on average, at shorter times than those that are more distant, because mutual approach requires a longer time before reaction occurs.



Scheme 4.9. Illustration of dynamic quenching.

As a first approach, the experimental quenching rate constant, k_q , is assumed to be time-independent. In this case, collisional quenching is described by the Stern-Volmer equation¹⁷:

$$\frac{\Phi_0}{\Phi} = \frac{I_0}{I} = 1 + k_q \tau_0 [Q] = 1 + K_{SV} [Q] \quad (4.38)$$

where Φ_0 and Φ are the fluorescence quantum yields in the absence and presence of quencher, respectively; I_0 and I are the fluorescence intensities in the absence and presence of quencher, respectively; τ_0 is the lifetime of the fluorophore in the absence of quencher; $[Q]$ is the concentration of quencher; $K_{SV} = k_q \tau_0$ is the Stern–Volmer constant. k_q is the bimolecular quenching constant which reflects the efficiency of quenching or the accessibility of the fluorophores to the quencher. Diffusion-

controlled quenching typically results in values of k_q near $10^{10} \text{ M}^{-1} \text{ s}^{-1}$. Values of k_q smaller than the diffusion-controlled value can result from steric shielding of the fluorophore or a low quenching efficiency. Apparent values of k_q larger than the diffusion-controlled limit usually indicate some type of binding interaction.

The meaning of the bimolecular quenching constant can be understood in terms of the collisional frequency between freely diffusing molecules. The collisional frequency (Z) of a fluorophore with a quencher is given by

$$Z = k_0 [Q]$$

where k_0 is the diffusion-controlled bimolecular rate constant. This constant may be calculated using the Smoluchowski equation which describes the diffusive flux of a molecule with a diffusion coefficient D through the surface of a sphere of radius R ¹⁷:

$$k_0 = \frac{4\pi N_A}{1000} RD = \frac{4\pi N_A}{1000} (R_f + R_q)(D_f + D_q) \quad (4.39)$$

where R is the collision radius (generally, it is assumed to be the sum of the molecular radii of the fluorophore R_f and quencher R_q); D is the sum of the diffusion coefficients of the fluorophore D_f and quencher D_q ; N_A is Avogadro's number (the term $N_A/1000$ converts molarity to molecules/cm³).

The collisional frequency is related to the bimolecular quenching constant by the quenching efficiency, f_Q :

$$k_q = f_Q k_0 \quad (4.40)$$

For example, if $f_Q=0.5$, then 50% of the collisional encounters are effective in quenching and k_q will be half the diffusion-controlled value, k_0 . Since k_0 can be estimated with moderate precision, the observed value of k_q can be used to judge the efficiency of quenching. Quenchers like oxygen, acrylamide, and iodide ion generally have efficiencies near unity, but the quenching efficiency of weak quenchers like succinimide depends on the solvent and/or viscosity. The efficiency of quenching can be calculated from the observed value of k_q , if the diffusion coefficients and molecular radii are known. The radii can be obtained from molecular models, or from the molecular weights and densities of the quencher in question. Diffusion coefficients may be obtained from the Stokes-Einstein equation:

$$D = \frac{kT}{6\pi\eta R} \quad (4.41)$$

where k is Boltzmann's constant, T is the absolute temperature, η is the solvent viscosity, and R is the molecular radius. Frequently, the Stokes-Einstein equation underestimates the diffusion coefficients of small molecules (this equation describes the diffusion of molecules that are larger than the solvent molecules). As an alternative method, diffusion coefficients can be obtained from nomograms based upon the physical properties of the system³⁸. Once the diffusion coefficients are known, the bimolecular quenching constant for $f_Q=1$ can be predicted using Smoluchowski equation (equation 4.39).

Generally, the ratio $\frac{I_0}{I}$ is plotted against the quencher concentration (Stern–Volmer plot). If the variation is found to be linear, the slope gives the Stern–Volmer constant. Then, k_q can be calculated if the excited-state lifetime in the absence of quencher is known. A linear Stern-Volmer plot is generally indicative of a single class of fluorophores, all equally accessible to quencher. If two fluorophore populations are present, and one class is not accessible to quencher, then the Stern-Volmer plots deviate from linearity toward the x-axis. As an example, when we study the interaction of a compound with DNA, a fraction of compound molecules can intercalate between DNA base pairs. In this case, the Stern-Volmer plot generally exhibits a downward curvature because the fraction of intercalated molecules is not accessible to the quencher. Then, the modified Stern-Volmer plot allows the determination of the fraction of compound molecules accessible to the quencher,

$$\frac{I_0}{\Delta I} = \frac{1}{f_a} + \frac{1}{f_a K_{SV}[Q]} \quad (4.42)$$

where I_0 and I are the fluorescence intensities in the absence and in the presence of quencher, respectively; $\Delta I = I_0 - I$; f_a is the fraction of molecules accessible to the quencher; K_{SV} is the Stern-Volmer constant; and $[Q]$ is the quencher concentration.

Attention must be paid to the fact that the observation of a linear Stern-Volmer do not necessarily imply that collisional quenching of fluorescence has occurred because static quenching also results in linear Stern-Volmer plots¹⁷.

6.3. Static quenching

Static quenching occurs as a result of the existence of a sphere of effective quenching or as a result of the formation of a non-fluorescent ground-state complex between the fluorophore and quencher.

- **Sphere of effective quenching**

In the case of viscous media or rigid matrices, M^* and Q cannot change their positions in space relative to one another during the excited-state lifetime of M^* . Perrin proposed a model for that cases, in which quenching of a fluorophore is assumed to be complete if a quencher molecule Q is located inside a sphere (*sphere of effective quenching, active sphere or quenching sphere*) of volume V_q surrounding the fluorophore M . If a quencher is outside the quenching sphere, it has no effect on M (Figure 4.20)³.

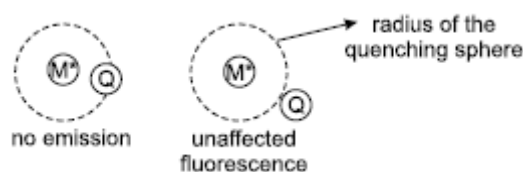


Figure 4.20. Sphere of effective quenching³.

Therefore, the fluorescence intensity of the solution is decreased by addition of Q , but the fluorescence decay after pulse excitation is unaffected:

$$\frac{I_0}{I} = \exp(V_q N_A [Q]) \quad (4.43)$$

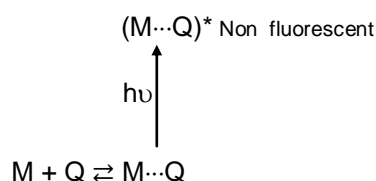
where I_0 and I are the fluorescence intensities in the absence and presence of quencher, respectively; V_q is the volume of the quenching sphere; N_A is the Avogadro's number and $[Q]$ is the concentration of quencher.

In contrast to the Stern–Volmer equation, the ratio $\frac{I_0}{I}$ is not linear and shows an upward curvature at high quencher concentrations. At low concentrations, $\exp(V_q N_A [Q]) \approx 1 + V_q N_A [Q]$, so that the concentration dependence is almost linear and a plot of $\frac{I_0}{I}$ versus $[Q]$ yields V_q . The values of $V_q N_A$ are often found to be in the range of 1–3 Lmol^{-1} . This corresponds to a quenching sphere radius of about 10Å,

which is somewhat larger than the Van der Waals contact distance between M and Q¹⁷.

- **Formation of a ground-state non-fluorescent complex**

Static quenching can also occur from the formation of non-fluorescent ground-state complex. When this complex absorbs light it immediately returns to the ground state without emission of a photon (Scheme 4.10).



Scheme 4.10. Illustration of static quenching by formation of a ground-state non-fluorescent complex.

The association constant for the complex formation is given by:

$$K_S = \frac{[M \cdots Q]}{[M][Q]} \quad (4.44)$$

where $[M \cdots Q]$ is the concentration of the complex, $[M]$ is the concentration of uncomplexed fluorophore, and $[Q]$ is the concentration of quencher.

As the total concentration of fluorophore, $[M]_0$, is given by

$$[M]_0 = [M] + [M \cdots Q] \quad (4.45)$$

substitution into equation 4.44 leads to

$$K_S = \frac{[M]_0 - [M]}{[M][Q]} = \frac{[M]_0}{[M][Q]} - \frac{1}{[Q]} \quad (4.46)$$

The fraction of uncomplexed fluorophores is thus

$$\frac{[M]}{[M]_0} = \frac{1}{1 + K_S[Q]} \quad (4.47)$$

Considering that the fluorescence intensities are proportional to the concentrations (which is valid only in dilute solutions), this relationship can be rewritten as

$$\frac{I_0}{I} = 1 + K_S[Q] \quad (4.48)$$

Note that this relation is linear, as in the case of the Stern-Volmer plot for dynamic quenching, except that the quenching constant is now the association constant.

6.4. How to distinguish between dynamic and static quenching

The value of K_S can sometimes be used to demonstrate that dynamic quenching cannot account for the decrease in intensity. However, the measurement of fluorescence lifetimes is the most definitive method to distinguish static and dynamic quenching. Static quenching removes a fraction of the fluorophores from observation. The complexed fluorophores are nonfluorescent, and the only observed fluorescence is from the uncomplexed fluorophores. The uncomplexed fraction, and thus, the lifetime τ_0 are unperturbed. Therefore, for static quenching $\frac{\tau_0}{\tau} = 1$ whereas for dynamic quenching $\frac{\tau_0}{\tau} = \frac{I_0}{I}$.

Static and dynamic quenching can also be distinguished by their differing dependence on temperature and viscosity. Higher temperatures result in faster diffusion and in the dissociation of weakly bound complexes. Consequently, there are larger amounts of collisional quenching and smaller amounts of static quenching.

One additional method to distinguish between static and dynamic quenching is by careful examination of the absorption spectra of the fluorophore. Collisional quenching only affects the excited states of the fluorophores, and thus no changes in the absorption spectra are expected. In contrast, static quenching as a result of the formation of a ground-state non-fluorescent complex will frequently result in perturbation of the absorption spectrum of the fluorophore. Attention must be paid to the fact that, at low concentrations, the absence of changes on the absorption spectrum and a linear variation of $\frac{I_0}{I}$ can lead to confusion between dynamic quenching and static quenching as a result of the existence of a quenching sphere (Figure 4.21)¹⁷.

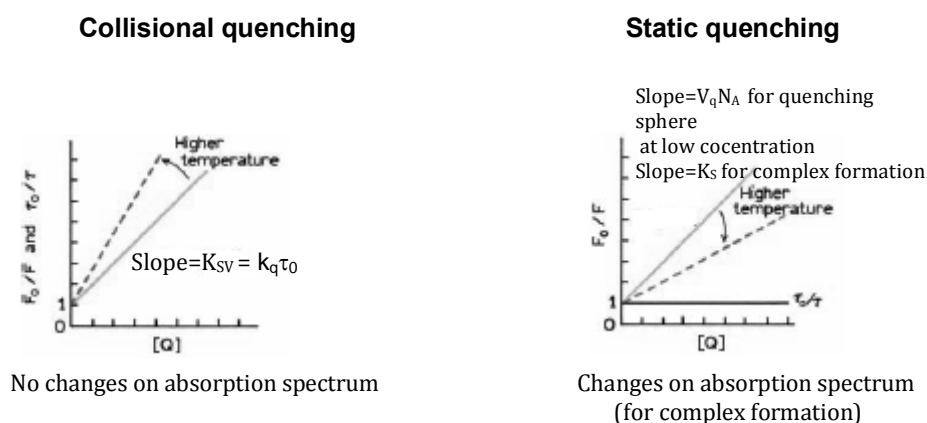


Figure 4.21. Comparison between dynamic and static quenching (adapted from ref. 17).

6.5. Simultaneous dynamic and static quenching

In many cases, the fluorophore can be quenched both by collisions and by complex formation or by a quenching sphere, with the same quencher. The characteristic feature of the Stern-Volmer plots in such circumstances is an upward curvature, concave towards the y-axis.

Let us consider first the case of static quenching by formation of a non-fluorescent complex. The ratio $\frac{I_0}{I}$ obtained for dynamic quenching must be multiplied by the fraction of fluorescent molecules (i.e. uncomplexed)¹⁷:

$$\frac{I}{I_0} = \left[\frac{I}{I_0} \right]_{\text{dyn}} \times \frac{[M]}{[M]_0} \quad (4.49)$$

Replacing $\left[\frac{I}{I_0} \right]_{\text{dyn}}$ by $\frac{1}{1+K_{SV}[Q]}$ (from the Stern-Volmer equation, equation 4.38) and $\frac{[M]}{[M]_0}$ by $\frac{1}{1+K_S[Q]}$ (static quenching by formation of a non-fluorescent complex, equation 4.47):

$$\frac{I_0}{I} = (1 + K_{SV}[Q])(1 + K_S[Q]) \quad (4.50)$$

This modified form of the Stern-Volmer equation is second order in $[Q]$, which accounts for the upward curvature observed when both static and dynamic quenching occur for the same fluorophore (Figure 4.22, left).

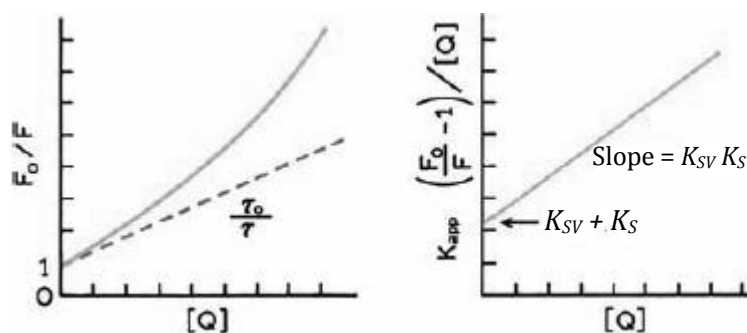


Figure 4.22. Simultaneous dynamic and static quenching by formation of a non-fluorescent complex¹⁷.

The dynamic portion of the observed quenching can be determined by lifetime measurements. That is, $\frac{\tau_0}{\tau} = 1 + K_{SV}[Q]$ (the dashed line in Figure 4.22, left). If lifetime measurements are not available, then the last equation can be modified to allow a graphical separation of K_S and K_{SV} . Multiplication of the terms in parentheses yields

$$\begin{aligned} \frac{I_0}{I} &= 1 + (K_{SV} + K_S)[Q] + K_{SV}K_S[Q]^2 \Leftrightarrow \frac{I_0}{I} = 1 + K_{app}[Q] \\ \Leftrightarrow K_{app} &= \left(\frac{I_0}{I} - 1\right) \frac{1}{[Q]} = (K_{SV} + K_S) + K_{SV}K_S[Q] \end{aligned} \quad (4.51)$$

The apparent quenching constant is calculated at each quencher concentration. A plot of $\left(\frac{I_0}{I} - 1\right) \frac{1}{[Q]} = K_{app}$ versus $[Q]$ yields a straight line with an intercept of $K_{SV} + K_S$ and a slope of $K_{SV}K_S$ (Figure 4.22, right). The individual values can also be obtained from the two solutions of the quadratic equation below.

In the case of the sphere of effective quenching model, the ratio $\frac{I_0}{I}$ obtained for dynamic quenching must be multiplied by the ratio $\frac{I_0}{I}$ obtained for static quenching by a quenching sphere¹⁷:

$$\frac{I}{I_0} = \left[\frac{I}{I_0}\right]_{dyn} \times \left[\frac{I}{I_0}\right]_{stat} \quad (4.52)$$

Replacing $\left[\frac{I}{I_0}\right]_{dyn}$ by $\frac{1}{1+K_{SV}[Q]}$ (from the Stern-Volmer equation, equation 4.38) and $\left[\frac{I}{I_0}\right]_{stat}$ by $\exp(V_q N_A [Q])$ for high concentrations or by $1 + V_q N_A [Q]$ for low concentrations (static quenching by a quenching sphere, equation 4.43) we obtain

$$\frac{I_0}{I} = (1 + K_{SV}[Q]) \exp(V_q N_A [Q]) \quad (4.53)$$

for high concentrations (upward curvature)

or

$$\frac{I_0}{I} = (1 + K_{SV}[Q]) (1 + V_q N_A [Q]) \quad (4.54)$$

for low concentrations (upward curvature)

But if we plot $\frac{I_0}{I} - 1$ versus $[Q]$ we obtain a straight line with an intercept of $K_{SV} + V_q N_A$ and a slope of $K_{SV} V_q N_A$.

6.6. Some applications of quenching

The extent of quenching can be affected by steric shielding and charge. Thus, protection against quenching is frequently observed for probes bound to macromolecules^{39,40} and even cyclodextrins⁴¹. Furthermore, charge effects are

generally present with charged quenchers such as iodide, and absent with neutral quenchers like oxygen and acrylamide.

The most dramatic effects of charge and shielding on quenching have been observed for fluorophores bound to DNA. The extent of quenching is decreased by intercalation of probes into the DNA double helix. For instance, ethidium bromide (EB) bound to DNA was found to be protected from oxygen quenching by a factor of 30 as compared to EB in solution⁴². Given the high negative charge density of DNA, one can expect the quenching to be sensitive to the charge of the quencher, the ionic strength of the solution, and the rate of quencher diffusion near the DNA helix^{43,44}.

The extent of quenching can also be affected by the charge on the quenchers. For instance, Hoechst 33258 is readily quenched by iodide when free in solution, but is not quenched when bound to DNA. Apparently, the negative charges on DNA prevent iodide from coming into contact with Hoechst 33258 when bound to DNA⁴⁵.

As the occurrence of intercalation with DNA is one of the fundamental steps for antitumoral activity⁴⁶, fluorescent quenching experiments with external quenchers are of major importance, in order to determine the DNA binding modes⁴⁷ of new potential antitumoral compounds.

6.7. Experimental considerations in quenching

When performing quenching experiments, several problems can appear:

- We should examine emission spectra under conditions of maximum quenching. In these conditions (low fluorescence intensity), the contribution from background fluorescence may begin to be significant.
- Quenchers are often used at high concentrations, and the quenchers themselves may contain fluorescent impurities.
- The intensity of the Raman and Rayleigh scattering peaks from solvent is independent of quencher concentration. Hence, the relative contribution of scattered light always increases with quenching.
- The absorption spectra of the quenchers must be taken into consideration. For example, iodide and acrylamide absorb light below 290 nm. In this case, the inner filter effect due to absorption can decrease the apparent fluorescence intensity, causing distortion on the quenching data⁴⁸. Thus, if inner filter effects

are present, the observed fluorescence intensities must be corrected, except for lifetime measurements which are relatively independent of total intensity.

- When using iodide or other ionic quenchers, it is important to maintain a constant ionic strength. This is usually accomplished by addition of KCl. It is also important to use freshly prepared solutions or to add a reducing agent, such as $\text{Na}_2\text{S}_2\text{O}_3$ (otherwise, I_2 may be formed)^{3,17}.

7. Fluorescence anisotropy

As we saw at the beginning of section 4, light is an electromagnetic wave consisting of an electric field E and a magnetic field H perpendicular to each other and to the direction of propagation, and oscillating in phase (*vd.* Figure 4.1). These fields have no preferred orientation for natural light but they oscillate along a given direction when the light is linearly polarized (the intermediate case corresponds to light which is partially polarized, Figure 4.23)³.

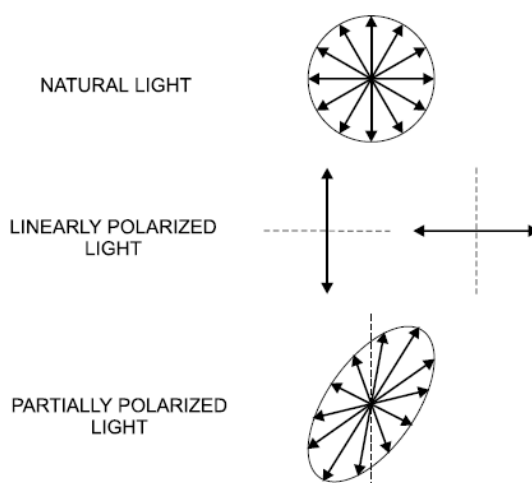


Figure 4.23. Natural, linearly polarized and partially polarized light³.

When excited with polarized light, those fluorophores that have their absorption transition moments, $\overline{R_A^{nm}}$, oriented along the electric vector of the incident light are preferentially excited. Indeed, if the incident light is linearly polarized, the probability of excitation of a chromophore is proportional to the square of the scalar product $\overline{R_A^{nm}} \cdot E$, and therefore to $\cos^2 \theta_A$, θ_A being the angle between the electric vector \vec{E} of the incident light and the absorption transition moment $\overline{R_A^{nm}}$, (Figure 4.24). This probability is maximum when \vec{E} is parallel to $\overline{R_A^{nm}}$, of the molecule; it is zero when the electric vector is perpendicular (*photoselection*)³.

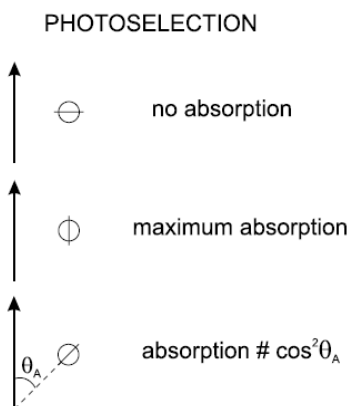


Figure 4.24. Transition moments and photoselection³.

Upon excitation with polarized light, the emission from many samples is also polarized. The extent of polarization of the emission is described in terms of the anisotropy (r). Samples exhibiting nonzero anisotropies are said to display polarized emission. Any change in direction of the transition moment during the lifetime of the excited state will cause this anisotropy to decrease, i.e. will induce a partial (or total) depolarization of fluorescence. The emission can become depolarized by a number of factors:

- Noncollinear absorption and emission transition moments¹⁷;
- Torsional vibrations;
- Light scattering, reabsorption and misalignment of the polarizers;
- Transfer of the excitation energy to another molecule with different orientation;
- Brownian motion (molecular rotation occurring between fluorophore excitation and emission).

Anisotropy measurements reveal the average angular displacement of the fluorophore that occurs between absorption and subsequent emission of a photon. This angular displacement is dependent upon the motions of the fluorophore. Therefore, the viscosity of the solvent and the size and shape of the molecule are important factors that affect anisotropy. For example, small fluorophores in low-viscosity solutions move very fast comparatively to the rate of emission. Under these conditions, the emission is depolarized and the anisotropy is close to zero. The dependence of fluorescence anisotropy upon fluorophore motions has resulted in numerous applications of this technique in biochemical research, as it provides useful information on molecular mobility, size, shape and flexibility of molecules, fluidity of a medium, and order

parameters (e.g. in a lipid bilayer). For example, the anisotropies of membrane-bound fluorophores have been used to estimate the internal viscosities of membranes and the effects of lipid composition upon the membrane phase-transition temperature¹⁷.

7.1. Polarization ratio and emission anisotropy

For most experiments of fluorescence anisotropy, the sample is excited with vertically polarized light. The electric vector of the excitation light is oriented parallel to the vertical or z -axis. The intensity of the emission is measured through a polarizer. When the emission polarizer is oriented parallel to the direction of the polarized excitation the observed intensity is called I_{VV} . Likewise, when the polarizer is perpendicular to the excitation, the intensity is called I_{VH} (Figure 4.25)¹⁷.

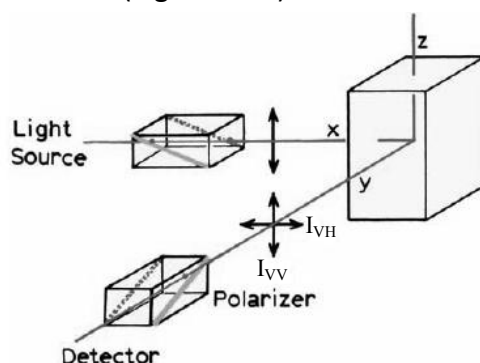


Figure 4.25. Schematic diagram for measurement of fluorescence anisotropies¹⁷.

Fluorescence can be considered as the result of three independent sources of light polarized along three perpendicular axis Ox , Oy , Oz without any phase relation between them. I_x , I_y , I_z are the intensities of these sources, and the total intensity is

$$I_T = I_x + I_y + I_z \quad (4.55)$$

For vertically polarized incident light, $I_z = I_{VV}$ and $I_x = I_y = I_{VH}$ and thus the total intensity is

$$I_T = I_{VV} + 2 I_{VH} \quad (4.56)$$

The polarization state of fluorescence is characterized either by

- the polarization ratio, p , defined as the fraction of light that is linearly polarized:

$$p = \frac{I_{VV} - I_{VH}}{I_{VV} + I_{VH}} \quad (4.57)$$

When I_{VV} or I_{VH} is 0, the polarization ratio will have values of -1 or 1, respectively. This represents the full range of polarization ratio values possible with a value of 1,

indicating a perfect alignment of emission dipoles with the orientation of the light source electric field; a value of -1 indicates an orthogonal orientation⁴⁹.

- or the emission anisotropy, r , which represents the ratio of the polarized component to the total intensity (I_T):

$$r = \frac{I_{VV} - I_{VH}}{I_{VV} + 2I_{VH}} \quad (4.58)$$

When I_{VV} or I_{VH} is 0, the emission anisotropy will have values of -0.5 or 1, respectively. This represents the full range of anisotropy values possible; a value of 1 indicates a perfect alignment of emission dipoles with the orientation of the light source and a value of -0.5 indicates an orthogonal orientation of emission dipoles⁴⁹.

The anisotropy is a dimensionless quantity that is independent of the total intensity of the sample. This is because the difference ($I_{VV} - I_{VH}$) is normalized by the total intensity ($I_T = I_{VV} + 2I_{VH}$), whereas in the expression of the polarization ratio, the denominator represents the fluorescence intensity in the direction of observation. For that reason, the use of anisotropy leads to simpler equations and is preferred to the use of polarization, except in a few situations (e.g. the study of radiative transfer).

When the sample contains a mixture of fluorophores, each has its own emission anisotropy³, r_i :

$$r_i = \frac{I_{VV_i} - I_{VH_i}}{I_{VV_i} + 2I_{VH_i}} = \frac{I_{VV_i} - I_{VH_i}}{I_{T_i}} \quad (4.59)$$

and each contributes to the total fluorescence intensity with a fraction

$$f_i = \frac{I_{T_i}}{I_T} \quad (\sum_i f_i = 1) \quad (4.60)$$

Thus, the total emission anisotropy is the weighted sum of the individual anisotropies:

$$r = \sum_i f_i r_i \quad (4.61)$$

The polarization and anisotropy values can be interchanged using

$$p = \frac{3r}{2 + r} \quad (4.62)$$

and

$$r = \frac{2p}{3 - p} \quad (4.63)$$

If the light observed through the emission polarizer is completely polarized along the transmission direction of the polarizer, then $I_{VH} = 0$ and $p = r = 1.0$. Completely

polarized emission can be observed for oriented samples, but not for homogeneous unoriented samples: in this case, the measured values are smaller due to the angular dependence of photoselection.

If the light observed through the emission polarizer is completely depolarized, then $I_{VH} = I_{VV}$ and $p = r = 0$. It is important to note that p and r are not equal for intermediate values.

For the moment, we have assumed that these intensities could be measured without interference due to the polarizing properties of the optical components, especially the emission monochromator. However, an additional factor must be introduced in order to correct this effect: in most cases, the sample is excited with vertically polarized light, and the emission is observed through a monochromator. The monochromator will usually have different transmission efficiencies for vertically and horizontally polarized light. Consequently, rotation of the emission polarizer changes the measured intensities even if the sample emits unpolarized light. The measured intensities are not the desired parallel and perpendicular intensities, but rather intensities that are also proportional to the transmission efficiencies of the monochromator for each polarized component. The objective is to measure these actual intensities, I_{VV} and I_{VH} , unbiased by the detection system¹⁷.

The measured intensity ratio I_{VV}/I_{VH} is different from the true value by a factor G , which is the ratio of the sensitivities of the detection system for vertically and horizontally polarized light (S_V and S_H , respectively). The G factor is easily measured using horizontally polarized excitation:

$$G = \frac{S_V}{S_H} = \frac{I_{HV}}{I_{HH}} \quad (4.64)$$

When the G factor is known, the polarization ratio and the anisotropy are respectively given by:

$$p = \frac{I_{VV} - GI_{VH}}{I_{VV} + GI_{VH}} \quad (4.65)$$

and

$$r = \frac{I_{VV} - GI_{VH}}{I_{VV} + 2GI_{VH}} \quad (4.66)$$

7.2. Relation between anisotropy and the absorption and emission dipoles orientation

7.2.1. Parallel absorption and emission transition moments

We will consider a population of N molecules randomly oriented and excited at time 0 by an infinitely short pulse of light polarized along Oz . At time t , the emission transition moments, $\overline{R_E^{nm}}$, of the excited molecules have a certain angular distribution. Here we assume that the absorption and emission transition moments are parallel. The orientation of these transition moments is characterized by θ , the angle with respect to the Oz axis, and by ϕ , the angle between the projection of the transition moments in the xy plane and the Ox axis (Figure 4.26)³.

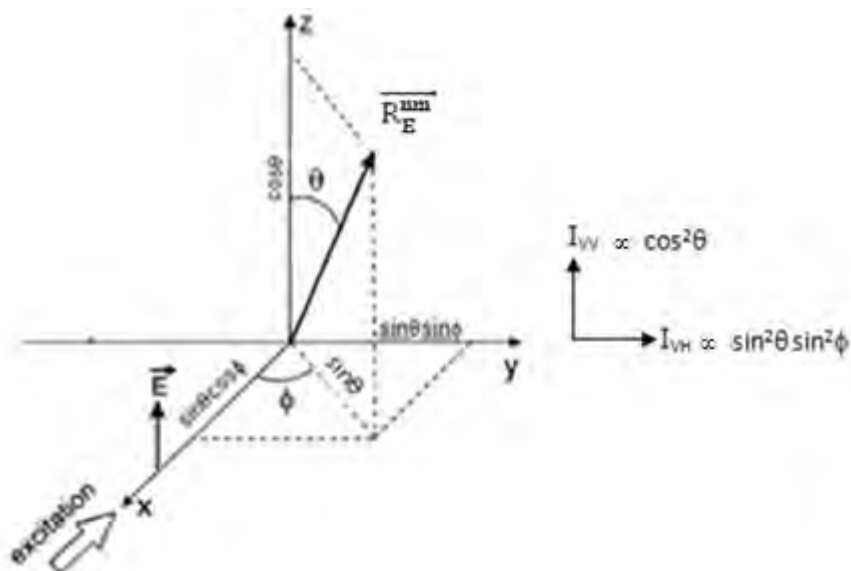


Figure 4.26. System of coordinates for characterizing the emission dipole orientation of one molecule (adapted from ref. 3).

Figure 4.26 shows I_{VV} and I_{VH} being proportional to the projection of the emission transition moment of one molecule onto the axes. This is true because the projection of the transition moment is the same as the projection of the electric field created by the fluorophore. Hence the projection of the field onto the z -axis is proportional to $\cos\theta$ and the intensity is proportional to $\cos^2\theta$. Similarly, the field along the y -axis is proportional to $\sin\theta\sin\phi$ and the intensity is proportional to $\sin^2\theta\sin^2\phi$:

$$I_{VV} \propto \cos^2\theta \quad (4.67)$$

and
$$I_{VH} \propto \sin^2\theta\sin^2\phi \quad (4.68)$$

If we consider now randomly oriented fluorophores, the anisotropy is calculated by performing the appropriate averaged intensities based on excitation photoselection. For excitation polarized along the z-axis, the population of excited molecules is oriented with values of ϕ from 0 to 2π with equal probability. Hence we can eliminate the ϕ dependence (equation 4.68) by calculating the average value of $\sin^2\phi$ with the general definition of an averaged quantity¹⁷:

$$\langle \sin^2\phi \rangle = \frac{\int_0^{2\pi} \sin^2\phi d\phi}{\int_0^{2\pi} d\phi} = \frac{1}{2} \quad (4.69)$$

Therefore,

$$I_{VV} \propto \cos^2\theta \quad (4.70)$$

and

$$I_{VH} \propto \frac{1}{2}\sin^2\theta \quad (4.71)$$

If we assume we are observing a collection of fluorophores that are oriented relative to the z-axis with a probability $f(\theta)$, the measured fluorescence intensities for this collection of molecules are

$$I_{VV} = \int_0^{\pi/2} f(\theta)\cos^2\theta d\theta = k \langle \cos^2\theta \rangle \quad (4.72)$$

and

$$I_{VH} = \frac{1}{2} \int_0^{\pi/2} f(\theta)\sin^2\theta d\theta = \frac{k}{2} \langle \sin^2\theta \rangle \quad (4.73)$$

where $f(\theta)d\theta$ is the probability that a fluorophore is oriented between θ and $\theta + d\theta$, and k is an instrumental constant.

Thus, using the identity

$$\sin^2\theta = 1 - \cos^2\theta \quad (4.74)$$

we can write

$$r = \frac{I_{VV} - I_{VH}}{I_{VV} + 2I_{VH}} = \frac{3 \langle \cos^2\theta \rangle - 1}{2} \quad (4.75)$$

This equation shows that, for a single fluorophore oriented along the z-axis with collinear transitions ($\theta=0$), $r=1.0$. However, it is not possible to obtain a perfectly oriented excited-state population with optical excitation of homogeneous solutions. Hence the anisotropies are always less than 1.0. Complete loss of anisotropy is equivalent to $\theta=54.7^\circ$. This does not mean that each fluorophore is oriented at 54.7° ,

or that they have rotated through 54.7° . Rather, it means that the average value of $\cos^2\theta$ is $1/3$.

In this expression, we assumed that the absorption and the emission transition moments are collinear. However, for almost all fluorophores, they rarely are. In addition, these anisotropies values are not taking into account the effects of photoselection¹⁷.

When a sample is illuminated with polarized light, those molecules with absorption transitions aligned parallel to the electric vector of the polarized excitation have the highest probability of excitation (photoselection) and this probability is proportional to $\cos^2\theta$. For the random ground state distribution, which must exist in a disordered solution, the number of molecules at an angle between θ and $\theta + d\theta$ is proportional to $\sin \theta d\theta$. This quantity is proportional to the surface area on a sphere within the angles θ and $\theta + d\theta$.

Hence, the probability distribution of molecules excited by vertically polarized light is given by:

$$f(\theta)d\theta = \cos^2\theta\sin\theta d\theta \quad (4.76)$$

This probability determines the maximum photoselection that can be obtained using one-photon excitation (more highly oriented populations can be obtained using multiphoton excitation).

For collinear absorption and emission transition moments, the value of $\langle \cos^2\theta \rangle$ is given by:

$$\langle \cos^2\theta \rangle = \frac{\int_0^{\pi/2} \cos^2\theta f(\theta) d\theta}{\int_0^{\pi/2} f(\theta) d\theta} = \frac{3}{5} \quad (4.77)$$

The emission anisotropy can thus be written as

$$r_0 = \frac{3 \langle \cos^2\theta \rangle - 1}{2} = \frac{2}{5} = 0.4 \quad (4.78)$$

r_0 is called the *fundamental anisotropy*, i.e. the theoretical anisotropy that is observed when the absorption and emission dipoles are collinear, and when there are no processes which result in depolarization (in practice, rotational motions can be hindered in a rigid medium). Under these conditions, the excited-state population is preferentially oriented along the z-axis and the value of I_{VH} is one-third the value of I_{VV}

($I_{VV} = 3 I_{VH}$). This value of 0.4 is considerably smaller than that possible for a single fluorophore oriented along the z -axis ($r = 1.0$).

The experimental value, called the *limiting anisotropy*, is always slightly smaller than the theoretical value (normally it ranges from 0.32 to 0.39). This difference is mainly due to torsional vibrations of the fluorophores about their equilibrium orientation⁵⁰. Consequently, a temperature dependence of the limiting anisotropy is noted^{51,52}: at low temperature (i.e. when the medium is frozen), r_0 may be considered as a constant quantity, whereas at high temperature it decreases linearly with the temperature.

It is important to remember that there are other possible origins for polarized light. These include reflections and light scattered by the sample that can interfere with anisotropy measurements: in the case of one-photon excitation, if the measured anisotropy for a randomly-oriented sample is greater than 0.4, we can infer the presence of scattered light in addition to fluorescence (for multiphoton excitation, anisotropy values can exceed 0.4)¹⁷.

7.2.2. Non-parallel absorption and emission transition moments

The situation of non-parallel absorption and emission transition moments occurs when excitation brings the fluorophores to an excited state other than the first singlet state from which fluorescence is emitted. In this case, the absorption and emission transition moments are displaced by an angle β relative to each other. We saw previously that displacement of the emission dipole by an angle θ from the z -axis resulted in a decrease in the anisotropy by a factor $(3\cos^2\theta - 1)/2$. Similarly, the displacement of the absorption and emission dipoles by an angle β results in a further loss of anisotropy. The observed anisotropy in a vitrified dilute solution is a product of the loss of anisotropy due to photoselection ($2/5$), and that due to the angular displacement of the dipoles. The fundamental anisotropy of a fluorophore is then given by

$$r_0 = \frac{2}{5} \left(\frac{3 \langle \cos^2\beta \rangle - 1}{2} \right) \quad (4.79)$$

where β is the angle between the absorption and emission transition moments³.

The fundamental anisotropy value is zero when $\beta = 54.7^\circ$. When β exceeds 54.7° the anisotropy becomes negative. The maximum negative value (-0.20) is found for

$\beta=90^\circ$. In other words, for any fluorophore randomly distributed in solution, with one-photon excitation, the value of r_0 must be within the range from -0.20 to 0.40. The values for both r_0 and p_0 are summarized in Table 4.5.

Table 4.5. Relationship between the angular displacement of transition moments (β) and the fundamental anisotropy (r_0) or polarization (p_0)¹⁷.

β (deg)	r_0	p_0
0	0.40	0.50=1/2
45	0.10	0.143=1/7
54.7	0.00	0.000
90	-0.20	-0.333=-1/3

Negative values generally correspond to $S_0 \rightarrow S_2$ transitions. A value close to -0.2 is indeed observed in the case of some aromatic molecules excited to the second singlet state whose transition moment is perpendicular to that of the first singlet state, from which fluorescence is emitted (e.g. perylene).

The measurement of the fundamental anisotropy requires special conditions. In order to avoid rotational diffusion, the probes are usually examined in solvents that form a clear glass at low temperature, such as propylene glycol or glycerol. Additionally, the solutions must be optically dilute to avoid depolarization due to radiative reabsorption and emission, or due to resonance energy transfer. One commonly used solvent for measuring fundamental anisotropies is propylene glycol at -60 to -70 °C. Under these conditions, the fluorophores remain immobile during the lifetime of the excited state. Glycerol also forms a rigid glass at low temperature. However, glycerol typically displays more autofluorescence than propylene glycol. At similar temperatures, phosphorescence from the fluorophores seems to be more common in glycerol than in propylene glycol. The anisotropy values (r_0) determined in these rigid solutions provide a measure of the angle between the absorption and emission dipoles¹⁷.

7.3. Causes of depolarization

There are several causes of depolarization. One of them is non-collinear absorption and emission transition moments, as we discussed in section 7.2.2. Another cause of depolarization can be torsional vibrations of the fluorophores about their equilibrium orientation⁵⁰ (section 7.2.1.). The two principal causes of depolarization are Resonance

Energy Transfer (RET) and rotational Brownian motion, which will be discussed in sections 7.3.1. and 7.3.2., respectively. Light scattering, reabsorption and misalignment of the polarizers represent three experimental causes of depolarization and will be examined in section 7.3.3.

7.3.1. Resonance Energy Transfer (RET)

Radiationless energy transfer in solution occurs only in concentrated solutions, where the average distance between the fluorophore molecules is comparable to a characteristic distance R_0 , which is typically near 40 Å. Millimolar fluorophore concentrations are required to obtain this average distance. This concentration is considerably larger than the usual concentrations required for fluorescence measurements, which are about 10^{-6} M. Hence, radiationless energy transfer is easily avoided by the use of dilute solutions. The solutions also need to be adequately diluted so that radiative transfer does not occur³.

The effect of RET on the anisotropy is illustrated by the excitation anisotropy spectrum of fluorescein in dilute and concentrated solution⁵³. Fluorescein is subject to radiative (emission and reabsorption) and non-radiative energy transfer because of the small Stokes shift. In this experiment (Figure 4.27), radiative transfer was avoided by using thin samples, and rotational diffusion was eliminated by using a vitrified sample. Under these experimental conditions, RET is the only mechanism that can decrease the anisotropy. In dilute solution, fluorescein displays its characteristic anisotropy spectrum, with high anisotropy for excitation above 380 nm. At high concentration, the anisotropy is decreased, due to the occurrence of RET between fluorescein molecules. In random solution, it is known that a single non-radiative transfer step reduces the anisotropy to 4% of the initial value⁵⁴⁻⁵⁷. Hence, RET is an effective mechanism of depolarization. The presence or absence of RET can usually be predicted from the concentration of the sample and the spectral properties of the probes.

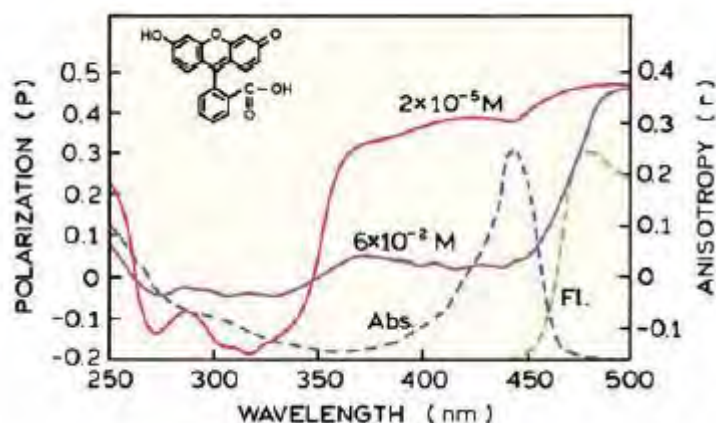


Figure 4.27. Excitation polarization spectra of fluorescein in propylene glycol at -50°C . Radiative transfer was avoided by using thin samples, 30 to 50 microns thick. Adapted from ref. 53.

7.3.2. Rotational Brownian motion: the Perrin equation

If excited molecules can rotate during the excited-state lifetime, the emitted fluorescence is partially (or totally) depolarized. Rotational diffusion of fluorophores is a dominant cause of fluorescence depolarization, and most applications depend on changes in the rate of rotation. From the extent of fluorescence depolarization, we can obtain information on the molecular motions, which depend on the size and the shape of molecules, and on the fluidity of their microenvironment. A distinction should be made between free rotation and hindered rotation. In the case of free rotation, after a δ -pulse excitation, the emission anisotropy decays from r_0 to 0, because the rotational motions of the molecules lead to a random orientation at long times. In the case of hindered rotations (not considered here), the molecules cannot become randomly oriented at long times, and the emission anisotropy does not decay to zero, but to a steady value¹⁷.

Depolarization by rotational diffusion of spherical rotors (isotropic rotations) is described by the Perrin equation⁵⁸⁻⁶⁰:

$$\frac{r_0}{r} = 1 + \frac{\tau}{\theta} = 1 + 6D\tau \quad (4.80)$$

where τ is the fluorescence lifetime, θ is the rotational correlation time, and D is the rotational diffusion coefficient. If the correlation time is much larger than the lifetime ($\theta \gg \tau$), then the measured anisotropy (r) is equal to the fundamental anisotropy

(r_0). If the correlation time is much shorter than the lifetime ($\theta \ll \tau$), then the anisotropy tends to zero.

The rotational correlation time of the fluorophore (θ) is related to the rotational diffusion coefficient by $\theta = (6D)^{-1}$ and is given by the Stokes-Einstein relation:

$$\theta = \frac{\eta V}{RT} \quad (4.81)$$

where η is the viscosity of the medium, T is the absolute temperature, R is the gas constant, and V is the volume of the rotating unit. The Stokes-Einstein relation is valid only when the microviscosity around the molecule is equal to the total viscosity of the sample.

A different version of the Perrin equation (equivalent, except for the use of polarization instead of anisotropy) is often found in literature

$$\left(\frac{1}{p} - \frac{1}{3}\right) = \left(\frac{1}{p_0} - \frac{1}{3}\right) \left(1 + \frac{\tau RT}{\eta V}\right) = \left(\frac{1}{p_0} - \frac{1}{3}\right) (1 + 6D\tau) \quad (4.82)$$

Using the Perrin equation, it is possible to calculate the anisotropy expected for fluorophores in solvents or for labelled macromolecules, assuming the molecules are spherical. For example, perylene has a lifetime of 6 ns and $r_0 = 0.36$. In ethanol, rotational diffusion is expected to decrease the anisotropy to 0.005.

The Perrin equation also allows calculating the apparent volume of a protein. Substitution of equation 4.81 into equation 4.80 yields a modified form of the Perrin equation:

$$\frac{1}{r} = \frac{1}{r_0} + \frac{\tau RT}{r_0 \eta V} \quad (4.83)$$

Normally, the protein is covalently labeled with an extrinsic fluorophore, which is chosen on the basis of its fluorescence lifetime. This lifetime should be comparable to the expected rotational correlation time of the protein (this way, the anisotropy will be sensitive to changes in the correlation time)¹⁷.

In most cases, fluorescent molecules undergo anisotropic rotations because of their asymmetry (non-spherical rotors). A totally asymmetric rotor has three different rotational diffusion coefficients. Steady-state anisotropy measurements are then

insufficient for fully characterizing rotational motions and time-resolved experiments are required.

7.3.3. Experimental causes of depolarization

Light scattering, reabsorption and misalignment of the polarizers are three experimental problems on anisotropy measurements that depend only on the optical conditions of the experiment, and do not provide useful information on the molecular properties of the sample.

Biological samples, such as aqueous suspensions of membranes, are frequently turbid. This turbidity can cause scattering of both the incident light and the emitted photons. The scattered incident light can result in excitation, and the emitted photons can be scattered prior to observation. The observed anisotropy is expected to decrease linearly with the optical density due to turbidity. It is therefore advisable to investigate the effect of turbidity for any sample which displays visible turbidity. This can be accomplished by either actual dilution of the sample or using a cuvette with smaller dimensions. If dilution does not change the anisotropy value, then there is unlikely to be significant depolarization due to scattering.

A more serious effect of scattering is the possibility that scattered light reaches the detector. This is particularly true for dilute solutions where the intensity is low and scattering from the optics and sample can be significant. Since the scattered light will be highly polarized ($r=1.0$), a small percentage of scattered light can result in significant changes in the anisotropy (normally, the measured anisotropy increases relative to its true value).

Reabsorption of emitted photons (radiative transfer) is another cause of depolarization that occurs with fluorophores with large spectral overlap (e.g. fluorescein). It is difficult to eliminate this effect since it occurs at lower concentrations than RET. Radiative transfer is more efficient in depolarization than RET since a single radiative transfer step results in an anisotropy loss of 28%, whereas a single RET step results in an anisotropy loss for 4%¹⁷.

Inefficiency of the polarizers can also result in a loss of anisotropy: for example, film polarizers become less ideal at short wavelengths. Misalignment of the polarizers can

also reduce the anisotropy, but the alignment can be easily checked and adjusted using a dilute suspension of glycogen or colloidal silica in water (it is essential to use dilute suspensions of the scatterer; otherwise multiple scattering events lead to decreased values of polarization). The scattered light is 100% polarized, that is, $r=1.0$. To accomplish alignment, the excitation polarizer is rotated to the approximate vertical position. Precise vertical alignment is not necessary since the scattered light is vertically polarized. The angular alignment of the emission polarizer is adjusted so that the minimum intensity is observed. This is the horizontal position. Rotation of the emission polarizer should now yield the maximum and minimum intensities when the polarizer is at the vertical and horizontal stops, respectively. These adjustments should be performed with the emission monochromator removed, or its wavelength chosen for approximate equal transmission efficiencies for vertically and horizontally polarized light. Otherwise, the polarizing properties of the emission monochromator could interfere with the alignment. The wavelength selection for equal transmission efficiencies can be accomplished using either horizontally polarized excitation, to obtain $I_{VV}=I_{VH}$, or a sample whose emission is not polarized. Examples of such solutions are 9-cyanoanthracene in the fluid solvent ethanol or $[\text{Ru}(\text{bpy})_3]^{2+}$ in water⁶¹. Alignment of the excitation polarizer is performed in a similar manner¹⁷.

Finally, one should always examine a blank sample that scatters approximately the same light as the sample. Background signals can be especially problematic for anisotropy measurements. The background signal may be polarized if due to scattered light, or unpolarized if due to low-molecular-weight impurities. Hence, background signals can either increase or decrease the anisotropy. In order to correct for background, it is necessary to measure the four individual intensities from the blank sample, and subtract them from each respective intensity value.

7.4. Applications of fluorescence polarization

There are several fields concerned with the applications of fluorescence polarization. For example, the study of DNA-fluorophore interactions in the field of molecular biology; the determination of fluidity and order parameters; the determination of the phase-transition temperature and the effect of additives such as cholesterol, in the field of biological membranes^{3,17}. In this work, steady-state fluorescence anisotropy

measurements were performed in order to evaluate the location and the behavior of several new potential antitumoral fluorophores into lipid membranes (Chapter 5, sections 5.1., 5.2., and 5.4.).

8. References

1. J.M. Hollas, *Modern spectroscopy*, Fourth edition, University of reading, Wiley, **2004**.
2. P. Atkins, J. di Paula, *Physical chemistry*, Eighth edition, Oxford University Press, **2006**.
3. B. Valeur, *Molecular Fluorescence: Principles and applications*, Wiley-VCH Verlag GmbH, **2001**.
4. G. F. J. Garlick, Luminescence, In *Handbuch der Physik*, vol. 26, **1958**, pp. 1-128.
5. G.G. Stokes, On the Change of Refrangibility of Light, *Philosophical Transactions of the Royal Society of London*, **1852**, 142, 463-562.
6. F. Perrin, Doctoral Thesis, Paris, *Annales de Physique*, **1929**, 12, 2252-2254.
7. R.H. Petrucci, W.S. Harwood, F.G. Herring, *General Chemistry: Principles and Modern Applications*, New Jersey: Pearson Prentice Hall, **2007**.
8. B. Averill, P. Eldredge, *General Chemistry: Principles, Patterns, and Applications*, First Edition, Prentice Hall, **2007**.
9. N.J. Turro, *Modern Molecular Photochemistry*, University Science Books, Sausalito, CA, **1991**.
10. A.M. Ellis, M. Fehér, T.G. Wright, Transition probabilities, In *Electronic and photoelectron spectroscopy: fundamentals and case studies*, Cambridge: Cambridge University Press, **2005**, pp. 51-64.
11. D.A. Skoog, D.M. West, F.J. Holler, *Analytical Chemistry: An Introduction*, 7th Edition, Saunders Golden Sunburst Series, **1999**.
12. J.R. Lakowicz, *Principles of Fluorescence Spectroscopy*, Kluwer Academic/Plenum Press, New York, **1999**.
13. G.S. Loving, M. Sainlos, B. Imperiali, Monitoring protein interactions and dynamics with solvatochromic fluorophores, *Trends in Biotechnology*, **2010**, 28(2), 73–83.
14. G. Hanson, Fluorescent probes for cellular assays, *Combinatorial chemistry & high throughput screening*, **2008**, 11(7), 505-513.
15. H. Maeda, T. Maeda, K. Mizuno, Absorption and Fluorescence Spectroscopic Properties of 1- and 1,4-Silyl-Substituted Naphthalene Derivatives, *Molecules*, **2012**, 17, 5108-5125.

16. L. Cisse, A. Tine, J.J. Aaron, Effect of electron-donating substituents on the electronic absorption and fluorescence spectra of coumarin derivatives, *Bull. Chem. Soc. Ethop.*, **1996**, *10(1)*, 33-38.
17. J. R. Lakowicz, *Principles of Fluorescence Spectroscopy*, Third edition, Springer Science/Business media, LLC, New York, **2006**.
18. C. Reichardt, *Solvent Effects in Organic Chemistry*, Verlag Chemie, Weinheim, **1988**.
19. E. Buncl, S. Rajagopal, Solvatochromism and Solvent Polarity Scales, *Acc. Chem. Res.*, **1990**, *23*, 226–231.
20. M.J. Kamlet, J.-L. Abboud, R.W. Taft, The Solvatochromic Comparison Method. 6. The py Scale of Solvent Polarities, *J. Am. Chem. Soc.*, 1977, **99**, 6027–6038.
21. V.E. Lippert, Spektroskopische Bestimmung des Dipolmomentes aromatischer Verbindungen im ersten angeregten Singluettzustand, *Z. Electrochem.*, **1957**, *61*, 962-975.
22. A. Kawski, Zur Lösungsmittelabhängigkeit der Wellenzahl von Elektronenbanden lumineszierender Moleküle and über die Bestimmung der elektrischen Dipolomente im Anregungszustand, *Acta Phys. Pol.*, **1966**, *29*, 507-518.
23. N. Mataga, Y. Kaifu, M. Koizumi, Solvent effects upon fluorescence spectra and the dipole moments of excited molecules, *Bull. Chem. Soc. Jpn.*, **1956**, *29*, 465-470.
24. N.G. Bakhshiev, Universal molecular interactions and their effects on the position of the electronic spectra of molecules in two-component solutions, *Opt. Spectrosc.*, **1962**, *12*, 309-313.
25. N.G. Bakhshiev, Universal molecular interactions and their effects on the position of the electronic spectra of molecules in two-component solutions, *Opt. Spectrosc.*, **1962**, *13*, 24-29.
26. C.J. Seliskar, L. Brand, Electronic spectra of 2-aminonaphtalene-6-sulfonate and related molecules II. Effects of solvent medium on the absorption and fluorescence spectra, *J.Am.Chem.Soc.*, **1971**, *93*, 5414-5420.
27. A.N. Perov, Energy of intermediate pair interactions as a characteristic of their nature. Theory of the solvato (fluoro) chromism of three-component solutions, *Opt.Spectrosc.*, **1980**, *49*, 371-374.

28. B.S. Neporent, N.G. Bakhshiev, On the role of universal and specific intermolecular interactions in the influence of the solvent on the electronic spectra of the molecules, *Opt.Spectrosc.*, **1960**, *8*, 408-413.
29. S. Nad, H. Pal, Unusual photophysical properties of coumarin-151, *J. Phys. Chem. A*, **2001**, *105(7)*, 1097–1106.
30. A. Okamoto, T. Ichiba, I. Saito, Pyrene-labeled oligodeoxynucleotide probe for detecting base insertion by excimer fluorescence emission, *J. Am. Chem. Soc.*, **2004**, *126*, 8364–8365.
31. K. Yamana, T. Iwai, Y. Ohtani, S. Sato, M. Nakamura, H. Nakano, Bis-pyrene-labeled oligonucleotides: sequence specificity of excimer and monomer fluorescence changes upon hybridization with DNA, *Bioconjugate Chem.*, **2002**, *13*, 1266–1273.
32. W. Wang, J.J. Han, L.Q. Wang, L.S. Li, W.J. Shaw, A.D.Q. Li, Dynamic B–B stacked molecular assemblies emit from green to red colors, *Nano Lett*, **2003**, *3(4)*, 455–458.
33. J.W. Hofstraat, C. Gooijer, N.H. Velthorst, Highly resolved molecular Luminescence Spectroscopy, In *Molecular Luminescence Spectroscopy, Part 2*, John Wiley and Sons, S.G. Schulman Ed., New York., **1988**, pp. 283–400.
34. E.L. Wehry, G. Mamantov, Low-Temperature Fluorometric Techniques and Their Application to Analytical Chemistry, in *Modern Fluorescence Spectroscopy, Vol. 4*, Plenum Press, E.L. Wehry Ed., New York, **1981**, pp. 193–250.
35. H. Kautsky, Quenching of luminescence by oxygen, *Trans. Faraday Soc.*, **1939**, *35*, 216–219.
36. H. Knibbe, D. Rehm, A. Weller, Intermediates and kinetics of fluorescence quenching by electron transfer, *Ber Bunsenges Phys. Chem.*, **1968**, *72*, 257–263.
37. M. Kasha, Collisional perturbation of spin-orbital coupling and the mechanism of fluorescence quenching: a visual demonstration of the perturbation, *J. Chem. Phys.*, **1952**, *20*, 71–74.
38. D.F. Othmer, M.S. Thakar, Correlating diffusion coefficients in liquids, *Ind. Eng. Chem. Res.*, **1953**, *45*, 589–593.
39. G. Maniara, J.M. Vanderkooi, D.C. Bloomgarden, H. Koloczek, Phosphorescence from 2-(p-toluidinyl)naphthalene-6-sulfonate and 1-anilinonaphthalene-8-

- sulfonate, commonly used fluorescence probes of biological structures, *Photochem. Photobiol.*, **1988**, *47*(2), 207–208.
40. H. Kim, S.R. Crouch, M.J. Zabik, Room-temperature phosphorescence of compounds in mixed organized media: synthetic enzyme model-surfactant system, *Anal. Chem.*, **1989**, *61*, 2475–2478.
41. M.V. Encinas, E.A. Lissi, A.M. Rufs, Inclusion and fluorescence quenching of 2,3-dimethylnaphthalene in β -cyclodextrin cavities, *Photochem. Photobiol.*, **1993**, *57*(4), 603–608.
42. J.R. Lakowicz, G. Weber, Quenching of fluorescence by oxygen: a probe for structural fluctuation in macromolecule, *Biochemistry*, **1973**, *12*, 4161–4170.
43. S.J. Atherton, P.C. Beaumont, Quenching of the fluorescence of DNA-intercalated ethidium bromide by some transition metal ions, *J. Phys. Chem.*, **1986**, *90*, 2252–2259.
44. R.F. Pasternack, M. Caccam, B. Keogh, T.A. Stephenson, A.P. Williams, E.J. Gibbs, Long-range fluorescence quenching of ethidium ion by cationic porphyrins in the presence of DNA, *J. Am. Chem. Soc.*, **1991**, *113*, 6835–6840.
45. D. Suh, J.B. Chaires, Criteria for the mode of binding of DNA binding agents, *Bioorgan. Med. Chem.*, **1995**, *3*(6), 723–728.
46. C.V. Kumar, E.H.A. Punzalan, W.B. Tan, Adenine-Thymine base pair recognition by an anthryl probe from the DNA minor groove, *Tetrahedron*, **2000**, *56*, 7027–7040.
47. C.V. Kumar, E.H. Asuncion, DNA-binding studies and site-selective fluorescence sensitization of an anthryl probe, *J. Am. Chem. Soc.*, **1993**, *115*, 8547–8553.
48. B. Fanget, O. Devos, Correction of inner filter effect in mirror coating cells for trace level fluorescence measurements, *Anal. Chem.*, **2003**, *75*, 2790–2795.
49. A. Periasamy, R.M. Clegg, Time-resolved fluorescence anisotropy, in *FLIM Microscopy in Biology and Medicine*, Chapman & Hall/CRC, **2009**.
50. A. Jablonski, Fundamental Polarization of Photoluminescence and Torsional Vibrations of Molecules, *Acta Physica Polonica*, **1950**, *10*, 193–206.
51. A.Kawski, A.Kubicki, I. Weyna and I. Janić, Temperature Dependence of Limiting Fluorescence Anisotropy of POPOP in Cellulose Acetate Film, *Z. Naturforschung*, **1985**, *40a*, 559–561.

52. V. Veissier, J.L. Viovy, L. Monnerie, Temperature-dependence of the fundamental anisotropy of anthracene-derivatives in melt polyisobutylene, *J. Phys. Chem.*, **1989**, *93*(5), 1709-1713.
53. G. Weber, M. Shinitzky, Failure of energy transfer between identical aromatic molecules on excitation at the long wave edge of the absorption spectrum, *Proc. Natl. Acad. Sci. USA*, **1970**, *65*(4), 823–830.
54. A. Kowski, *Fotoluminescencja roztworów*, Wydawnictwo Naukowe PWN, Warsaw, **1992**.
55. B.W. Van Der Meer, G. Coker III, S.-Y.S. Chen, *Resonance energy transfer theory and data*, Wiley-VCH, New York, **1991**.
56. A. Jablonski, Anisotropy of fluorescence of molecules excited by excitation transfer, *Acta Phys. Pol. A*, 1970, **38**, 453–458.
57. J. Baumann, M.D. Fayer, Excitation transfer in disordered twodimensional and anisotropic three-dimensional systems: effects of spatial geometry on time-resolved observables, *J. Chem. Phys.*, **1986**, *85*, 4087–4107.
58. F. Perrin, La fluorescence des solutions: induction moleculaire. Polarisation et durée d'emission. *Photochimie. Ann. Phys.*, **1929**, *Ser 10, 12*, 169–275.
59. F. Perrin, Polarisation de la lumière de fluorescence: vie moyenne des molécules dans l'état excité, *J. Phys. Radium V*, **1926**, *Ser 6, 7*, 390–401.
60. F. Perrin, Fluorescence: durée élémentaire d'émission lumineuse, *Conférences D'Actualités Scientifiques et Industrielles*, **1931**, *22*, 2–41.
61. R.B. Thompson, I. Gryczynski, J. Malicka, Fluorescence polarization standards for high-throughput screening and imaging, *Biotechnology*, **2002**, *32*, 34–42.

Chapter 5

Results and discussion as a compilation of articles

INDEX

- 5.1.** Fluorescence Studies on Potential Antitumoral Heteroaryl and Heteroannulated Indoles in Solution and in Lipid Membranes **171**
- 5.2.** Fluorescence Studies on New Potential Antitumoral Benzothienopyran-1-ones in Solution and in Liposomes **183**
- 5.3.** New potential antitumoral fluorescent tetracyclic thieno[3,2-*b*]pyridine derivatives: interaction with DNA and nanosized liposomes **197**
- 5.4.** Fluorescence studies on potential antitumor 6-(hetero)arylthieno[3,2-*b*]pyridine derivatives in solution and in nanoliposomes **207**
- 5.5.** Benzothienoquinolines: new one pot synthesis and fluorescence studies of their interaction with DNA and polynucleotides **221**

5.1

Fluorescence Studies on Potential Antitumoral Heteroaryl and Heteroannulated Indoles in Solution and in Lipid Membranes

Elisabete M. S. Castanheira, Ana S. Abreu, M. Solange D. Carvalho, Maria-João R. P. Queiroz, Paula M. T. Ferreira, *J. Fluoresc.*, **2009**, *19*, 501-509.

My contribution to this article was the synthesis of the compounds (published in a previous article) and the study of their spectroscopic properties in different solvents and neat liposomes.

Fluorescence Studies on Potential Antitumoral Heteroaryl and Heteroannulated Indoles in Solution and in Lipid Membranes

Elisabete M. S. Castanheira · Ana S. Abreu ·
M. Solange D. Carvalho · Maria-João R. P. Queiroz ·
Paula M. T. Ferreira

Received: 7 August 2008 / Accepted: 3 November 2008 / Published online: 29 November 2008
© Springer Science + Business Media, LLC 2008

Abstract Fluorescence properties of three potential anti-tumoral compounds, a 3-(dibenzothien-4-yl)indole **1**, a phenylbenzothienoindole **2** and a 3-(dibenzofur-4-yl)indole **3**, were studied in solution and in lipid aggregates of dipalmitoyl phosphatidylcholine (DPPC), dioleoyl phosphatidylethanolamine (DOPE) and egg yolk phosphatidylcholine (Egg-PC). The 3-(dibenzofur-4-yl)indole **3** exhibits the higher fluorescence quantum yields in all solvents studied ($0.32 \leq \Phi_F \leq 0.51$). All the compounds present a solvent sensitive emission, with significant red shifts in alcohols. The results point to an ICT character of the excited state, more pronounced for compound **1**. Fluorescence (steady-state) anisotropy measurements of the compounds incorporated in lipid aggregates of DPPC, DOPE and Egg-PC indicate that the three compounds are deeply located in the lipid bilayer, feeling the difference between the rigid gel phase and fluid phases.

Keywords Heteroaryl and heteroannulated indoles · Lipid membranes · Fluorescence anisotropy

Abbreviations

DPPC dipalmitoyl phosphatidylcholine
DOPE dioleoyl phosphatidylethanolamine

Egg-PC egg yolk phosphatidylcholine
PC phosphatidylcholine
PE phosphatidylethanolamine

Introduction

For some years now our research group has synthesized a large variety of new fluorescent planar heteroaromatic compounds from dehydroamino acid derivatives, using metal-mediated reactions [1–3] and some of them were shown to be DNA intercalators [3].

Studies of incorporation in lipid vesicles using fluorescence techniques were also performed with biological active tetracyclic planar compounds derivatives of benzo[*b*]thiophenes and pyridines, a benzothienopyridopyrimidone [4] and a thieno- δ -carboline [5], prepared by us. These studies are very useful for controlled drug release assays.

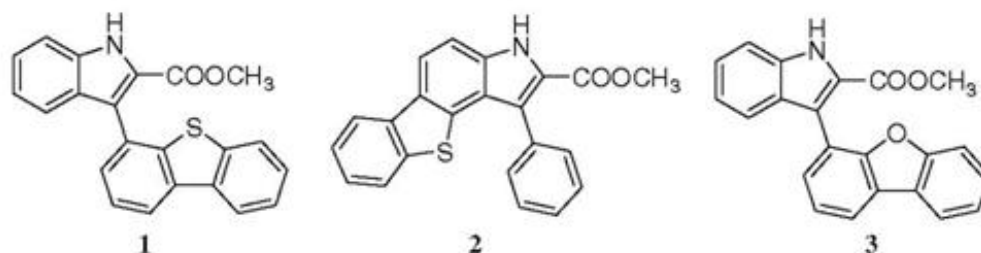
More recently, some of us have described the synthesis of new heteroaryl and heteroannulated indoles from dehydrophenylalanines, a methyl 3-(dibenzothien-4-yl)indole-2-carboxylate **1**, a methyl 1-phenyl-3*H*-benzothieno[2,3-*e*]indole-2-carboxylate **2**, a methyl 3-(dibenzofur-4-yl)indole-2-carboxylate **3** and a methyl 1-phenyl-3*H*-benzofuro[2,3-*e*]indole-2-carboxylate. Compounds **1–3** (Fig. 1) were evaluated for their capacity to inhibit the *in vitro* growth of three human tumor cell lines, MCF-7 (breast adenocarcinoma), NCI-H460 (non-small cell lung cancer) and SF-268 (CNS cancer). The indolic compounds **1** and **3** gave the best anti-proliferative results but compound **1** was shown to be the most potent with GI_{50} (50% of cell growth inhibition) values ranging from 11–17 μ M in all cell lines studied [6].

These results suggested us to perform fluorescence studies of incorporation of compounds **1–3** in lipid

E. M. S. Castanheira (✉) · A. S. Abreu
Centro de Física, Universidade do Minho,
Campus de Gualtar,
4710-057 Braga, Portugal
e-mail: ecoutinho@fisica.uminho.pt

A. S. Abreu · M. S. D. Carvalho · M.-J. R. P. Queiroz ·
P. M. T. Ferreira
Centro de Química, Universidade do Minho,
Campus de Gualtar,
4710-057 Braga, Portugal

Fig. 1 Structure of heteroarylindoles **1** and **3** and heteroannulated indole **2**

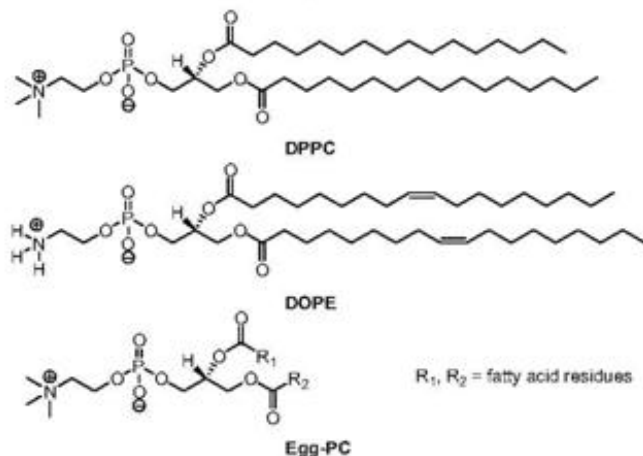


membranes. The photophysical properties in solution and in lipid aggregates of neutral phospholipid components of biological membranes, DPPC (dipalmitoyl phosphatidylcholine), DOPE (dioleoyl phosphatidylethanolamine) and Egg-PC (egg yolk phosphatidylcholine) were studied. Fluorescence (steady-state) anisotropy measurements were also performed to obtain further information about the behavior of the compounds in lipid membranes.

Experimental

Materials and methods

All the solutions were prepared using spectroscopic grade solvents and ultrapure water (Milli-Q grade). 1,2-Dipalmitoyl-*sn*-glycero-3-phosphocholine (DPPC), 1,2-Dioleoyl-*sn*-glycero-3-phosphoethanolamine (DOPE) and 1,2-Diacyl-*sn*-glycero-3-phosphocholine from egg yolk (Egg-PC) were purchased from Sigma-Aldrich (lipid structures are shown below).



For DOPE and Egg-PC membranes preparation, defined volumes of stock solutions of lipid (26.9 mM for DOPE and 34.5 mM for Egg-PC) and compound (0.235 mM for **1**, 0.229 mM for **2** and 0.282 mM for **3**) in ethanol were injected together, under vigorous stirring, to an aqueous buffer solution (10 mM Tris, 1 mM EDTA, pH = 7.4), at room temperature. A similar procedure was adopted for

DPPC vesicles, but the injection of the required amounts of stock solutions of lipid (50 mM) and compounds **1**, **2** or **3** in ethanol was done at 60°C, well above the melting transition temperature of DPPC (*ca.* 41°C) [7]. In all cases, the final lipid concentration was 1 mM, with compounds **1**, **2** or **3**/lipid molar ratio of 1:500.

Spectroscopic measurements

Absorption spectra were recorded in a Shimadzu UV-3101PC UV-Vis-NIR spectrophotometer. Fluorescence measurements were performed using a Spex Fluorolog 3 spectrofluorimeter, equipped with double monochromators in both excitation and emission and a temperature controlled cuvette holder. Fluorescence spectra were corrected for the instrumental response of the system. An excitation wavelength of 325 nm was used, near the lowest energy maximum (or shoulder) in the absorption spectrum of the compounds in all solvents studied.

For fluorescence quantum yield determination, the solutions were previously bubbled for 20 minutes with ultrapure nitrogen. The fluorescence quantum yields (Φ_s) were determined using the standard method (eq. 1) [8, 9]. 9,10-diphenylanthracene in ethanol was used as reference, $\Phi_r = 0.95$ [10].

$$\Phi_s = \frac{A_r F_s n_s^2}{A_s F_r n_r^2} \Phi_r \quad (1)$$

where A is the absorbance at the excitation wavelength, F the integrated emission area and n the refraction index of the solvents used. Subscripts refer to the reference (r) or sample (s) compound.

Results and discussion

Photophysical properties of compounds **1**, **2** and **3** in solution

The absorption and fluorescence properties of the 3-(dibenzothien-4-yl)indole **1**, the phenylbenzothienindole **2** and the 3-(dibenzofur-4-yl)indole **3** were studied in several solvents. The maximum absorption (λ_{abs}) and emission wavelengths (λ_{em}), molar extinction coefficients

(ϵ) and fluorescence quantum yields (Φ_F) of the three compounds are presented in Table 1. The normalized fluorescence spectra of compounds **1**, **2** and **3** are shown in Figs. 2, 3 and 4, respectively. Examples of absorption spectra are displayed as insets.

The near-ultraviolet absorption of indole and their derivatives has been attributed to two strongly overlapping $\pi \rightarrow \pi^*$ transitions [11–13], with an average ϵ value for unsubstituted indole of $5550\text{M}^{-1}\text{cm}^{-1}$, which also justifies its relatively high fluorescence quantum yield [14]. All the indole derivatives **1–3** have also a carboxylate group and it is known that many carbonyl compounds exhibit low fluorescence quantum yields due to the low-lying $n \rightarrow \pi^*$ state. In these new indole derivatives, it is possible that the electronic transitions $\pi \rightarrow \pi^*$ and $n \rightarrow \pi^*$ can be nearby in energy, resulting in state-mixing [15]. A predominance of $\pi \rightarrow \pi^*$ character could explain the relatively high ϵ values ($\epsilon > 9 \times 10^3\text{M}^{-1}\text{cm}^{-1}$) for compounds **1–3** (Table 1).

In emission spectra, a significant red shift can be observed from cyclohexane to more polar solvents (38 nm for compound **1**, 47 nm for compound **2**, 26 nm for compound **3**, from cyclohexane to methanol). In the absorption spectra, the red shifts are negligible for the three compounds (Table 1), indicating that solvent relaxation after photoexcitation plays an important role.

In polar solvents, a strong band enlargement and complete absence of vibrational structure is also observed (Figs. 2, 3 and 4), which is usually related to an intramolecular charge transfer (ICT) mechanism and/or to specific solvent effects [16]. This behavior was already observed in other indole

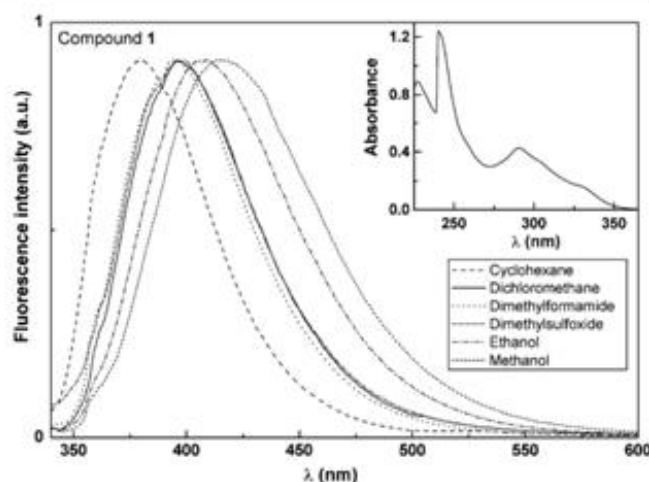


Fig. 2 Normalized fluorescence (at peak of maximum emission) spectra of 3×10^{-6} M solutions of 3-(dibenzothien-4-yl)indole **1** in several solvents ($\lambda_{exc}=325$ nm). Inset: Absorption spectrum of a 2×10^{-5} M solution of **1** in dichloromethane, as an example

derivatives previously obtained by us, namely the methyl 3-arylindole-2-carboxylates [2] and the 1-heteroaryl-3H-benzothieno or benzofuroindole-2-carboxylates [3].

Solvatochromic shifts caused by general (not specific) solvent effects are often described by the Lippert-Mataga eq. (2), which relates the energy difference between absorption and emission maxima to the orientation polarizability, [16, 17]

$$\bar{\nu}_{abs} - \bar{\nu}_{fl} = \frac{1}{4\pi\epsilon_0} \frac{2 \Delta\mu^2}{hcR^3} \Delta f + const \quad (2)$$

Table 1 Maximum absorption (λ_{abs}) and emission wavelengths (λ_{em}), molar extinction coefficients (ϵ) and fluorescence quantum yields (Φ_F) for compounds **1**, **2** and **3** in several solvents

Solvent	λ_{abs}/nm ($\epsilon/\text{M}^{-1}\text{cm}^{-1}$)			λ_{em}/nm			Φ_F^a		
	1	2	3	1	2	3	1	2	3
Cyclohexane	325 sh (9.04×10^3)	321 (1.21×10^4)							
	290 (2.45×10^4)	285 (2.81×10^4)	290 (2.74×10^4)	380	382	372	0.17	0.12	0.51
	240 (6.50×10^4)	257 (3.28×10^4)	226 (4.62×10^4)						
Dichloromethane	324 sh (9.27×10^3)	322 (1.54×10^4)							
	291 (2.14×10^4)	287 (3.92×10^4)	291 (2.42×10^4)	398	399	381	0.10	0.08	0.32
	234 (6.39×10^4)	257 (4.08×10^4)	227 (4.46×10^4)						
Dimethylformamide	325 sh (1.10×10^4)	322 (1.51×10^4)	290 (3.10×10^4) ^b						
	290 (2.21×10^4) ^b	288 (4.08×10^4) ^b		399	400	384	0.15	0.17	0.46
Dimethylsulfoxide	325 sh (1.08×10^4)	323 (1.61×10^4)							
	291 (2.09×10^4) ^b	289 (4.91×10^4) ^b	292 (2.71×10^4) ^b	400	402	390	0.05	0.09	0.49
Ethanol	325 sh (1.07×10^4)	323 (1.61×10^4)							
	290 (2.21×10^4)	287 (4.70×10^4)	290 (2.76×10^4)	408	420	393	0.14	0.12	0.47
	233 (6.94×10^4)	257 (4.39×10^4)	225 (4.96×10^4)						
Methanol	324 sh (9.95×10^3)	323 (1.41×10^4)							
	289 (2.13×10^4)	285 (4.25×10^4)	290 (2.59×10^4)	418	429	398	0.15	0.12	0.42
	233 (6.68×10^4)	255 (3.99×10^4)							

^a Relative to 9,10-diphenylanthracene in ethanol ($\Phi_F=0.95$ [12]).

^b Solvents cut-off: Dimethylformamide: 275 nm; Dimethylsulfoxide: 270 nm. sh: shoulder.

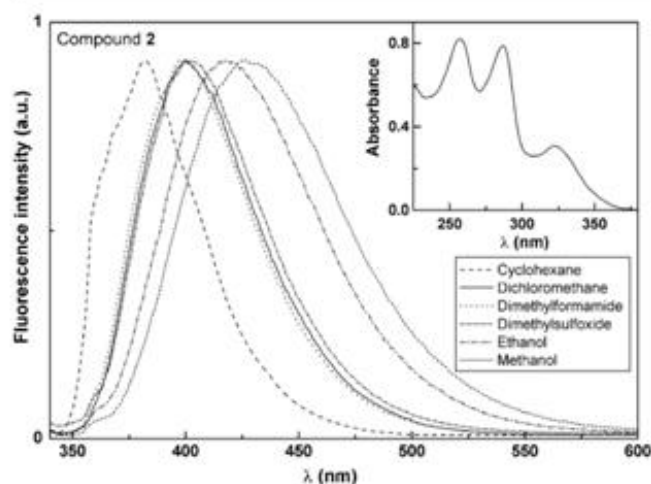


Fig. 3 Normalized fluorescence (at peak of maximum emission) spectra of 3×10^{-6} M solutions of phenylbenzothienoindeole **2** in several solvents ($\lambda_{\text{exc}}=325$ nm). Inset: Absorption spectrum of a 2×10^{-5} M solution of **2** in dichloromethane, as an example

where $\bar{\nu}_{\text{abs}}$ is the wavenumber of maximum absorption, $\bar{\nu}_{\text{fl}}$ is the wavenumber of maximum emission, $\Delta\mu = \mu_{\text{e}} - \mu_{\text{g}}$ is the difference in the dipole moment of solute molecule between excited (μ_{e}) and ground (μ_{g}) states, R is the cavity radius (considering the fluorophore a point dipole at the center of a spherical cavity immersed in the homogeneous solvent), and Δf is the orientation polarizability given by (eq. 3):

$$\Delta f = \frac{\varepsilon - 1}{2\varepsilon + 1} - \frac{n^2 - 1}{2n^2 + 1} \quad (3)$$

where ε is the static dielectric constant and n the refractive index of the solvent.

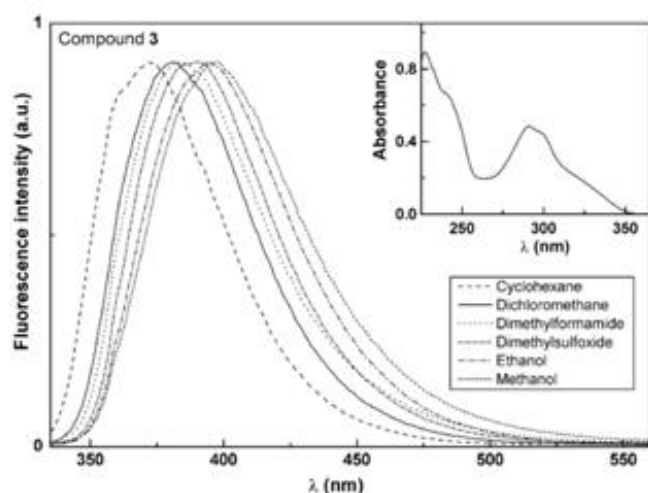


Fig. 4 Normalized fluorescence (at peak of maximum emission) spectra of 3×10^{-6} M solutions of 3-(dibenzofur-4-yl)indole **3** in several solvents ($\lambda_{\text{exc}}=325$ nm). Inset: Absorption spectrum of a 2×10^{-5} M solution of **3** in dichloromethane, as an example

The Lippert-Mataga plot for compounds **1–3**, shown in Fig. 5, is reasonably linear in non-protic solvents, alcohols exhibiting large positive deviations, especially for the heteroannulated indole **2**.

This behavior in alcohols can be due to specific solute-solvent interactions by hydrogen bonds, as all the three compounds have the capability of hydrogen bonding formation through the NH group (donor) and the ester group (acceptor). The S atom of the thiophene ring (for compounds **1** and **2**) and the oxygen atom of the furan ring (in the case of compound **3**) can also act as H-bond acceptors.

From *ab initio* molecular quantum chemistry calculations, the cavity radius (R) and the ground state dipole moment (μ_{g}) were determined for the three compounds (Table 2), through an optimized structure provided by GAMESS software [19], using a 3-21G(d) basis set [20] (Fig. 6). The optimized geometry of compound **2** shows that this molecule is almost completely planar, with the phenyl ring slightly out of the plane of the benzothienoindeole tetracyclic moiety. On the contrary, the indole ring on compounds **1** and **3** is roughly perpendicular to the dibenzothiophene moiety (compound **1**) or the dibenzofuran moiety (compound **3**).

The excited state dipole moments, estimated from the Lippert-Mataga plots, are displayed in Table 2. The μ_{e} values of the three molecules point to the presence of an intramolecular charge transfer (ICT) mechanism, more important for compound **1**. Twisted intramolecular charge transfer states (TICT) usually exhibit significantly higher excited state dipole moments (≥ 20 D) [21] than those here obtained.

Figure 7 reports the HOMO and LUMO wavefunctions of the three compounds. For compound **2**, the HOMO-LUMO transition exhibits a charge transfer from the

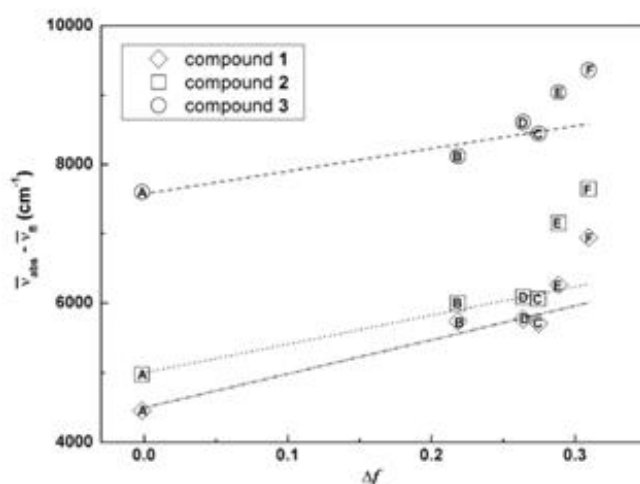
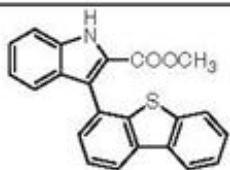
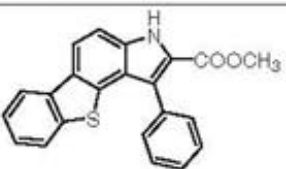
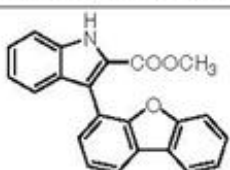


Fig. 5 Lippert-Mataga plots for compounds **1**, **2** and **3**: A: cyclohexane; B: dichloromethane; C: *N,N*-dimethylformamide; D: dimethylsulfoxide; E: ethanol; F: methanol (values of ε and n were obtained from ref. [18])

Table 2 Cavity radius (R) and ground state dipole moments (μ_g), obtained from theoretical calculations, and excited state dipole moments (μ_e) calculated from the Lippert-Mataga plots

Compound	Cavity radius, R (Å)	Ground state dipole moment, μ_g (D)	Excited state dipole moment, μ_e (D)
 1 3-(dibenzothien-4-yl)indole	7.0	1.9	14.6
 2 phenylbenzothienoindole	6.4	1.4	11.8
 3 3-(dibenzofur-4-yl)indole	6.6	2.6	12.3

benzothienoindole moiety to the carboxylate group, the S atom having no electronic density at the LUMO. In case of compound **3**, both ground and excited state electronic distributions are mainly localized at the indole moiety and the carbonyl group. The HOMO-LUMO transition shows a charge transfer from the indole ring to the carbonyl group

of the ester, the dibenzofuran moiety having no contribution to this transition. However, for compound **1**, the electronic density of HOMO is localized at the dibenzothiophene moiety and moves completely to the indole ring and to the carboxylate group upon the HOMO-LUMO transition. This justifies the higher excited state dipole moment obtained for

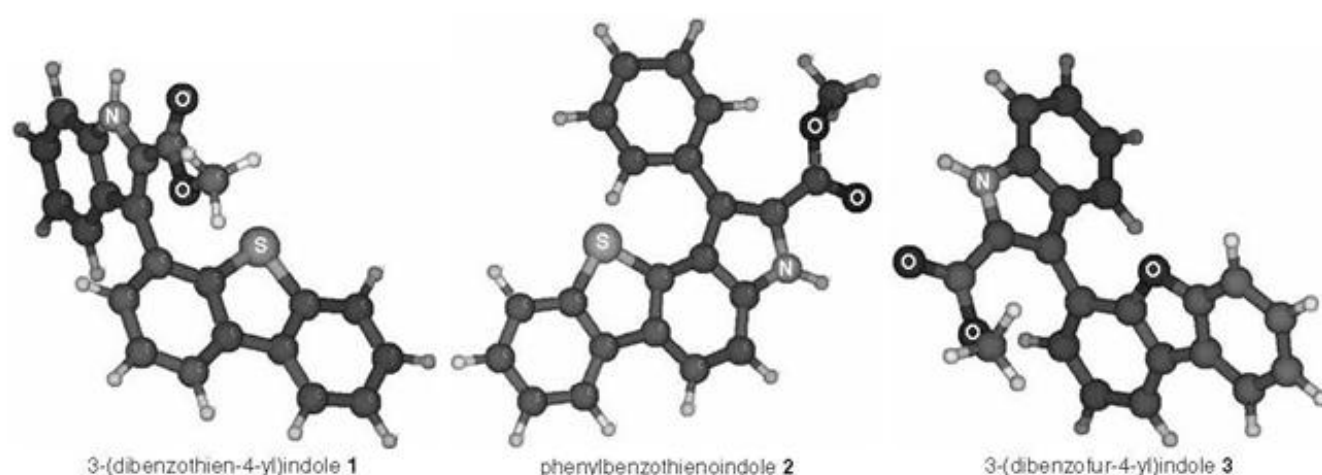
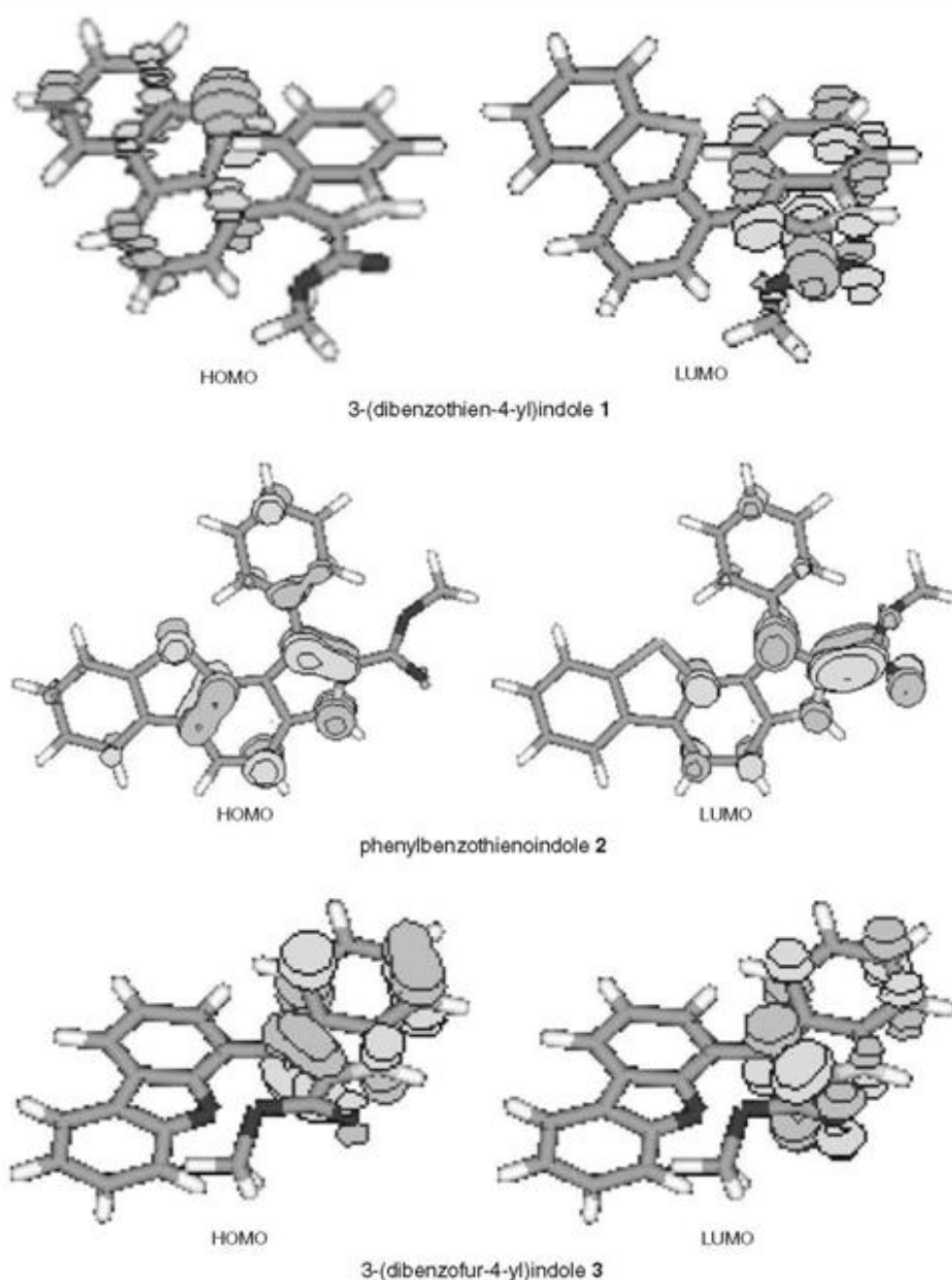
**Fig. 6** Optimized structures of heteroarylindoles **1** and **3** and heteroannulated indole **2** (obtained by GAMESS software), with indication of S, N and O atoms

Fig. 7 HOMO and LUMO electronic wavefunctions of heteroarylindoles **1** and **3** and heteroannulated indole **2**



this compound and indicates a strong influence of the S heteroatom in the dibenzothiophene system when compared to the O in the dibenzofuran moiety of compound **3**.

Compound **3** presents good fluorescence quantum yields in all solvents ($\Phi_F \geq 0.32$, Table 1), while for compounds **1** and **2**, the values are relatively low ($\Phi_F \leq 0.17$). The decrease in fluorescence quantum yields observed for the latter compounds is justified by the presence of the S atom in the thiophene ring, which can promote the intersystem crossing process by enhancement of spin-orbit coupling interaction [15, 16], as observed for other indole derivatives [2, 3]. The expected formation of hydrogen bonds between these compounds and protic solvents does not cause a

decrease (or even an increase) of Φ_F values in alcohols (Table 1), in contrast to what was observed for other indoles obtained by us [2].

Interaction of compounds **1**, **2** and **3** with lipid membranes

Due to their promising antitumoral activity [6], photo-physical studies of indoles **1–3** incorporated in lipid membranes were also performed. These studies are important to evaluate the interaction of the compounds with lipid membranes. It is also important to assess the localization of the compounds in lipid vesicles, pointing to drug delivery applications using liposomes.

Different types of phospholipid molecules, DPPC, Egg-PC and DOPE, were used for vesicle preparation. It is known that at room temperature, DPPC (16:0 PC) is in the ordered gel phase, where the hydrocarbon chains are fully extended and closely packed. Above the melting transition temperature, $T_m = 41^\circ\text{C}$ [7], DPPC attains the disordered liquid-crystalline phase. DOPE (18:1 PE) has a very low melting transition temperature ($T_m = -16^\circ\text{C}$ [22]) and presents a lamellar bilayer to inverse hexagonal ($L_\alpha\text{-H}_{II}$) phase transition at 3.3°C [23]. Finally, Egg-PC is a natural phospholipid mixture, where all molecules have the same polar head group (phosphatidylcholine) but several hydrocarbon chains, differing in length and degree of unsaturation. Egg-PC main components are 16:0 PC, 18:0 PC and 18:1 PC [24]. Therefore, at room temperature, Egg-PC is in the fluid liquid-crystalline phase.

The emission spectra of compounds 1–3 in lipid membranes are displayed in Figs. 8, 9 and 10. The maximum emission wavelengths (Table 3) of the three compounds indicate a environment of moderate polarity, slightly more polar for compound 3 (*vd.* Table 1). A small blue shift (1–3 nm) is observed for all compounds in DPPC at the rigid gel phase (at 25°C) relative to the emission in lipids at fluid phases.

In homogeneous solution, the effect of increasing temperature in the fluorescence of these indolic compounds is a ~20–30% reduction and a very small blue shift (2–3 nm) between 25°C and 55°C . The insets of Figs. 8, 9 and 10 show the emission spectra in cyclohexane and ethanol at 55°C , where it can also be seen that the spectral shape is roughly the same observed at 25°C .

The red-shifted emission of compounds 1–3 observed in lipid membranes at fluid phases (DOPE and Egg-PC at

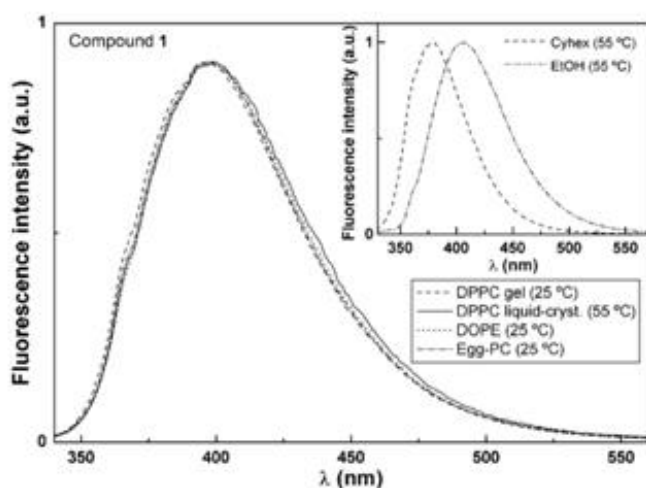


Fig. 8 Normalized fluorescence spectra of 3-(dibenzothien-4-yl)indole 1 in lipid membranes of DOPE, Egg-PC and DPPC ($\lambda_{\text{exc}} = 325$ nm). Inset: Normalized fluorescence spectra of compound 1 in cyclohexane (Cyhex) and ethanol (EtOH) at 55°C

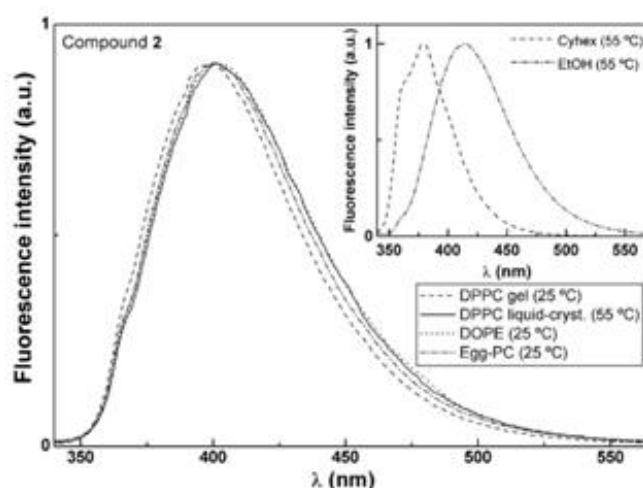


Fig. 9 Normalized fluorescence spectra of phenylbenzothienindole 2 in lipid membranes of DOPE, Egg-PC and DPPC ($\lambda_{\text{exc}} = 325$ nm). Inset: Normalized fluorescence spectra of compound 2 in cyclohexane (Cyhex) and ethanol (EtOH) at 55°C

25°C and DPPC at 55°C) points to a higher penetration of water molecules in the vesicle bilayer, as lipid hydrocarbon chains are randomly oriented and fluid. However, it is also possible that in fluid phases these indoles locate in a more polar environment.

Fluorescence anisotropy measurements can give further information about these molecules behavior in lipid membranes. The steady-state fluorescence anisotropy, r , is given by

$$r = \frac{I_{VV} - GI_{VH}}{I_{VV} + 2GI_{VH}} \quad (4)$$

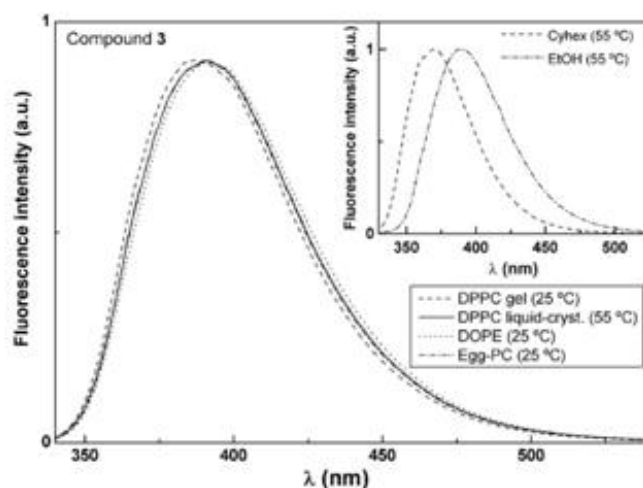


Fig. 10 Normalized fluorescence spectra of 3-(dibenzofur-4-yl)indole 3 in lipid membranes of DOPE, Egg-PC and DPPC ($\lambda_{\text{exc}} = 325$ nm). Inset: Normalized fluorescence spectra of compound 3 in cyclohexane (Cyhex) and ethanol (EtOH) at 55°C

Table 3 Steady-state fluorescence anisotropy (r) values, fluorescence quantum yields and maximum emission wavelengths (λ_{em}) of compounds **1**, **2** and **3** in lipid membranes. Values in ethylene glycol at room temperature are also shown for comparison

	Compound 1			Compound 2			Compound 3		
	λ_{em}/nm	Φ_F^a	r	λ_{em}/nm	Φ_F^a	R	λ_{em}/nm	Φ_F^a	R
DPPC (25 °C)	397	0.08	0.162	400	0.08	0.038	387	0.26	0.181
DPPC (55 °C)	399	0.02	0.115	401	0.01	0.027	390	0.04	0.089
DOPE (25 °C)	399	0.09	0.091	401	0.08	0.013	391	0.27	0.062
Egg-PC (25 °C)	397	0.07	0.156	401	0.08	0.029	390	0.28	0.151
Ethylene glycol (25 °C)	422	0.09	0.116	434	0.08	0.022	400	0.31	0.097

^a Relative to 9,10-diphenylanthracene in ethanol ($\Phi_r = 0.95$ [12]).

where I_{VV} and I_{VH} are the intensities of the emission spectra obtained with vertical and horizontal polarization, respectively (for vertically polarized excitation light), and $G = I_{HV}/I_{HH}$ is the instrument correction factor, where I_{HV} and I_{HH} are the emission intensities obtained with vertical and horizontal polarization (for horizontally polarized excitation light).

Steady-state anisotropy relates to both the excited-state lifetime and the rotational correlation time of the fluorophore [25],

$$\frac{1}{r} = \frac{1}{r_0} \left(1 + \frac{\tau}{\tau_c} \right) \quad (5)$$

where r_0 is the fundamental anisotropy, τ is the excited-state lifetime and τ_c is the rotational correlation time.

The fluorescence steady-state anisotropies and fluorescence quantum yields of the three indoles in lipid aggregates are shown in Table 3. Anisotropy and quantum yield values in ethylene glycol at room temperature were also determined for comparison. The small anisotropy value obtained for compound **2** in this viscous solvent (Table 3) points to a low fundamental anisotropy for this molecule.

For each compound, the fluorescence quantum yields are similar in all lipid aggregates and in ethylene glycol at 25 °C. Therefore, variations in fluorescence anisotropy values at this temperature can be directly related to changes in the rotational correlation time of the fluorophore and, thus, to changes in the microviscosity of the surrounding medium of the fluorescent molecule. It can be observed for all compounds that r values in DPPC at gel phase (25 °C) and in Egg-PC are higher than those obtained in ethylene glycol, indicating that compounds **1–3** are deeply located in the lipid bilayer. Indole **3** presents high anisotropy values in DPPC gel phase and in Egg-PC, similar to those of compound **1**, despite the significantly higher fluorescence quantum yields, pointing to an even deeper penetration of compound **3** in these bilayers.

In DPPC at 55 °C, a significant fluorescence quenching (Table 3) is observed for all compounds, as expected from the increase of the non-radiative deactivation pathways at higher temperatures. An increase of the steady-state

anisotropy is predicted from a decrease of the excited-state lifetime (equation 5). However, all compounds show a significant decrease in anisotropy in DPPC at 55 °C (Table 3), showing that these indoles detect the phospholipid gel to liquid-crystalline phase transition and the associated decrease of microviscosity. Anisotropies obtained in DPPC fluid phase (55 °C) are roughly similar to the values in ethylene glycol at 25 °C (Table 3). Compound **3** exhibits a larger difference in anisotropy between the gel and the liquid-crystalline phase of DPPC. It is possible that, upon DPPC membrane fluidization, this compound locates in a more hydrated environment, as indicated by the slightly higher red shift in emission from the gel to the fluid phase (Table 3).

The phospholipid DOPE, at room temperature, adopts the inverse hexagonal phase, where the lipid molecules can adopt inverse curvature at the interface, allowing the chains to expand and at the same time reduce the headgroup area at the interface [26]. The lower anisotropy values measured in DOPE (Table 3) reflect the quite different geometry of self-organized DOPE aggregates, through the mentioned chain expansion. The emission spectra (Figs. 8, 9 and 10) indicate that these indoles feel a very similar environment in DOPE to that in DPPC at the liquid-crystalline phase.

Liposomes have been widely used to deliver anticancer agents, in order to reduce the toxic effects of the drugs when given alone or to increase the drug circulation time and effectiveness [27]. Considering that compounds **1**, **2** and **3** are mainly located near the phospholipid tails and their antitumoral activity, previously shown [6], these studies are promising to the incorporation of these indoles in liposomes for controlled drug delivery systems.

Conclusions

The three potential antitumoral compounds studied, a 3-(dibenzothien-4-yl)indole **1**, a phenylbenzothienindole **2** and a 3-(dibenzofur-4-yl)indole **3**, show a solvent sensitive fluorescence emission and reasonable fluorescence quan-

tum yields in all solvents studied, compound **3** exhibiting the higher Φ_F values. The estimated excited state dipole moments point to an ICT character of the excited state, more pronounced for compound **1**, confirmed by molecular quantum chemistry calculations.

Studies of the compounds incorporation in lipid aggregates of DPPC, DOPE and Egg-PC revealed that the three indolic compounds are deeply located in the lipid bilayer and are able to report differences between the gel and liquid-crystalline phases.

Considering the already proven anti-proliferative activity of human tumor cell lines exhibited by these molecules, the results obtained here show a promising utility of compounds **1–3** as antitumoral drugs, with the possibility of being transported in the hydrophobic region of liposomes.

Acknowledgements Foundation for the Science and Technology (FCT)—Portugal and FEDER, for financial support through Centro de Física and Centro de Química of Univ. Minho, through the Project POCI/QUI/59407/2004. A.S.A. acknowledges a post-doc. grant SFRH/BPD/24548/2005.

References

- Abreu AS, Ferreira PMT, Queiroz M-JRP, Ferreira ICFR, Calheta RC, Estevinho LM (2005) Synthesis of β -benzo[*b*]thienyldehydrophenylalanine derivatives by one-pot palladium-catalyzed borylation and Suzuki coupling (BSC) and metal-assisted intramolecular cyclization—Studies of fluorescence and antimicrobial activity. *Eur J Org Chem* 2951–2957. doi:10.1002/ejoc.200500040
- Queiroz M-JRP, Abreu AS, Castanheira EMS, Ferreira PMT (2007) Synthesis of new 3-arylindole-2-carboxylates using β , β -diaryldihydroamino acids as building blocks. *Fluorescence studies*. *Tetrahedron* 63:2215–2222. doi:10.1016/j.tet.2006.12.084
- Queiroz M-JRP, Castanheira EMS, Carvalho MSD, Abreu AS, Ferreira PMT, Karadeniz H, Erdem A (2008) New tetracyclic heteroaromatic compounds based on dehydroamino acids: photophysical and electrochemical studies of interaction with DNA. *Tetrahedron* 64:382–391. doi:10.1016/j.tet.2007.10.090
- Castanheira EMS, Pinto AMR, Queiroz M-JRP (2006) Fluorescence of a Benzo[*b*]thienopyridopyrimidone in solution and in lipid vesicles. *J Fluorescence* 16:251–257. doi:10.1007/s10895-005-0050-z
- Queiroz M-JRP, Castanheira EMS, Pinto AMR, Ferreira ICFR, Begouin A, Kirsch G (2006) Synthesis of the first thieno- δ -carboline. *Fluorescence studies in solution and in lipid vesicles*. *J Photochem Photobiol Chem* 181:290–296. doi:10.1016/j.jphotochem.2005.12.010
- Queiroz M-JRP, Abreu AS, Carvalho MSD, Ferreira PMT, Nazareth N, Nascimento MSJ (2008) Synthesis of new heteroaryl and heteroannulated indoles from dehydrophenylalanines: Antitumor evaluation. *Bioorg Med Chem* 16:5584–5589. doi:10.1016/j.bmc.2008.04.004
- Lentz BR (1989) Membrane “fluidity” as detected by diphenylhexatriene probes. *Chem Phys Lipids* 50:171–190. doi:10.1016/0009-3084(89)90049-2
- Demas JN, Crosby GA (1971) The measurement of photoluminescence quantum yields. A review. *J Phys Chem* 75:991–1024. doi:10.1021/j100678a001
- Fery-Forgues S, Lavabre D (1999) Are fluorescence quantum yields so tricky to measure? A demonstration using familiar stationary products. *J Chem Educ* 76:1260–1264
- Morris JV, Mahaney MA, Huber JR (1976) Fluorescence quantum yield determinations. 9,10-Diphenylanthracene as a reference standard in different solvents. *J Phys Chem* 80:969–974. doi:10.1021/j100550a010
- Creed D (1984) The photophysics and photochemistry of the near-UV absorbing amino-acids. I. Tryptophan and its simple derivatives. *Photochem. Photobiol* 39:537–562
- Albinsson B, Kubista M, Nordén B, Thulstrup EW (1989) Near-Ultraviolet electronic-transitions of the tryptophan chromophore—linear dichroism, fluorescence anisotropy, and magnetic circular-dichroism spectra of some indole-derivatives. *J Phys Chem* 93:6646–6654. doi:10.1021/j100355a016
- Lippert H, Ritze H-H, Hertel IV, Radloff W (2004) Femtosecond time-resolved analysis of the photophysics of the indole molecule. *Chem Phys Lett* 398, 526–531. doi:10.1016/j.cplett.2004.09.111
- Tatischeff I, Klein R (1975) Influence of environment on excitation wavelength dependence of fluorescence quantum yield of indole. *Photochem Photobiol* 22:221–229. doi:10.1111/j.1751-1097.1975.tb06740.x
- Turro NJ (1978) *Modern Molecular Photochemistry*. Benjamin/Cummings Pub., Menlo Park California
- Lakowicz JR (1999) *Principles of Fluorescence Spectroscopy*. Kluwer Academic/Plenum Press, New York
- Mataga N, Kubota T (1970) *Molecular Interactions and Electronic Spectra*. Marcel Dekker, New York
- Lide DR (ed) (2002) *Handbook of Chemistry and Physics*. 83th Edition, CRC Press, Boca Raton
- Schmidt MW, Baldrige KK, Boatz JA, Elbert ST, Gordon MS, Jensen JH, Koseki S, Matsunaga N, Nguyen KA, Su S, Windus TL, Dupuis M, Montgomery JA (1993) General Atomic and Molecular Electronic Structure System. *J Comput Chem* 14:1347–1363. doi:10.1002/jcc.540141112
- Jensen F (1999) *Introduction to Computational Chemistry*. John Wiley & Sons West Sussex, England
- Grabowski ZR, Rotkiewicz K, Rettig W (2003) Structural changes accompanying intramolecular electron transfer: Focus on twisted intramolecular charge-transfer states and structures. *Chem Rev* 103:3899–4031. doi:10.1021/cr9407451
- Silvius JR (1982) Thermotropic phase transitions of pure lipids in model membranes and their modifications by membrane proteins, in *Lipid-Protein Interactions*. John Wiley & Sons, New York
- Toombes GES, Finnefrock AC, Tate MW, Gruner SM (2002) Determination of L_{α} - H_{II} Phase Transition Temperature for 1,2-Dioleoyl-*sn*-Glycero-3-Phosphatidylethanolamine. *Biophys J* 82:2504–2510
- Papahadjopoulos D, Miller N (1967) Phospholipid model membranes. I. Structural characteristics of hydrated liquid crystals. *Biochim Biophys Acta* 135:624–638. doi:10.1016/0005-2736(67)90094-6
- Valeur B (2001) *Molecular Fluorescence—Principles and Applications*. Wiley-VCH, Weinheim
- Seddon JM (1990) Structure of the inverted hexagonal (H_{II}) phase and non-lamellar phase transitions in lipids. *Biochim Biophys Acta* 1031:1–69
- Banerjee R (2001) *Liposomes Applications in medicine*. *J Biomater Appl* 16:3–21. doi:10.1106/RA7U-1V9C-RV7C-8QXL

5.2

Fluorescence Studies on New Potential Antitumoral Benzothienopyran-1-ones in Solution and in Liposomes

Elisabete M. S. Castanheira, M. Solange D. Carvalho, Daniel J. G. Soares, Paulo J. G. Coutinho, Ricardo C. Calhelha, Maria-João R. P. Queiroz, *J. Fluoresc.*, **2011**, *21*, 911-922.

My contribution to this paper was the photophysical studies of the compounds in several solvents and fluorescence measurements in liposomes.

Fluorescence Studies on New Potential Antitumoral Benzothienopyran-1-ones in Solution and in Liposomes

Elisabete M. S. Castanheira · M. Solange D. Carvalho ·
Daniel J. G. Soares · Paulo J. G. Coutinho ·
Ricardo C. Calhella · Maria-João R. P. Queiroz

Received: 27 October 2009 / Accepted: 7 February 2010 / Published online: 2 March 2010
© Springer Science+Business Media, LLC 2010

Abstract Fluorescence properties of four new potential antitumoral compounds, 3-arylbenzothieno[2,3-*c*]pyran-1-ones, were studied in solution and in lipid membranes of dipalmitoyl phosphatidylcholine (DPPC), egg yolk phosphatidylcholine (Egg-PC) and dioctadecyldimethylammonium bromide (DODAB). The 3-(4-methoxyphenyl)benzothieno[2,3-*c*]pyran-1-one (**1c**) exhibits the higher fluorescence quantum yields in all solvents studied. All compounds present a solvent sensitive emission, with significant red shifts in polar solvents for the methoxylated compounds. The results point to an ICT character of the excited state, more pronounced for compound **1c**. Fluorescence (steady-state) anisotropy measurements of the compounds incorporated in liposomes of DPPC, DODAB and Egg-PC indicate that all compounds have two different locations, one due to a deep penetration in the lipid membrane and another corresponding to a more hydrated environment. In general, the methoxylated compounds prefer hydrated environments inside the liposomes. The 3-(4-fluorophenyl)benzothieno[2,3-*c*]pyran-1-one (**1a**) clearly prefers a hydrated environment, with some molecules located at the outer part of the liposome interface. On the contrary, the preferential location of 3-(2-fluorophenyl)benzothieno[2,3-*c*]pyran-1-one (**1b**) is in the region of lipid hydrophobic tails. Compounds with a planar geometry (**1a** and **1c**) have higher mobility in the lipid membranes when phase transition occurs.

Keywords Benzothienopyran-1-ones · Antitumoral compounds · Liposomes · Fluorescence anisotropy

Abbreviations

DPPC	Dipalmitoyl phosphatidylcholine
DODAB	Dioctadecyldimethylammonium bromide
Egg-PC	Egg yolk phosphatidylcholine
PC	Phosphatidylcholine

Introduction

Our research group has been interested in the synthesis and in the photophysical behavior, in solution and in lipid membranes, of novel heteroaromatic biological active compounds [1–3].

Recently, some of us have described the synthesis of new 3-(aryl)benzothieno[2,3-*c*]pyran-1-ones from 3-bromobenzo[*b*]thiophene-2-carboxylic acid and different arylphenylacetylenes [4] (compounds **1a–c**, Fig. 1). Compound **1d**, with a methoxy group in the *ortho* position relative to the pyranone ring (Fig. 1) was synthesized in this work (Scheme 1) for comparison, and the synthesis is described below.

Compounds **1a–c** were evaluated for their capacity to inhibit the *in vitro* growth of three human tumor cell lines, MCF-7 (breast adenocarcinoma), NCI-H460 (non-small cell lung cancer) and SF-268 (CNS cancer). Compound **1b** was shown to be the most potent against the three cell lines tested, presenting low GI_{50} (the lowest concentration causing 50% of the cell growth inhibition after a continuous exposure of 48 h) values (12–19 μ M) [4].

These results suggested us to perform fluorescence studies of compounds **1a–d** incorporated in liposomes. The photophysical properties in solution and in lipid vesicles of DPPC (dipalmitoyl phosphatidylcholine), Egg-PC (egg yolk phosphatidylcholine) and of the cationic lipid DODAB (dioctadecyldimethylammonium bromide) were studied. The

E. M. S. Castanheira (✉) · M. S. D. Carvalho · D. J. G. Soares ·
P. J. G. Coutinho
Centro de Física (CFUM), Universidade do Minho,
Campus de Gualtar,
4710-057 Braga, Portugal
e-mail: ecoutinho@fisica.uminho.pt

M. S. D. Carvalho · R. C. Calhella · M.-J. R. P. Queiroz
Centro de Química (CQ-UM), Universidade do Minho,
Campus de Gualtar,
4710-057 Braga, Portugal

phospholipids DPPC and phosphatidylcholine (from egg yolk) are neutral components of biological membranes, while cationic liposomes based in DODAB have been used as vehicles for DNA transfection and drug delivery [5–7]. Fluorescence (steady-state) anisotropy measurements were also performed to obtain further information about the location of these compounds in lipid membranes.

Experimental

Synthesis

General The melting point (°C) was determined on a SMP3 Stuart apparatus. ^1H and ^{13}C NMR spectra were recorded on a Bruker Avance II⁺ at 400 and 100.6 MHz, respectively. Chemical shifts (δ) are given in ppm. MS (EI) spectrum and HRMS on the M^+ were recorded by the mass spectrometry service of the University of Vigo, Spain. Petroleum ether refers to the boiling range 40–60 °C.

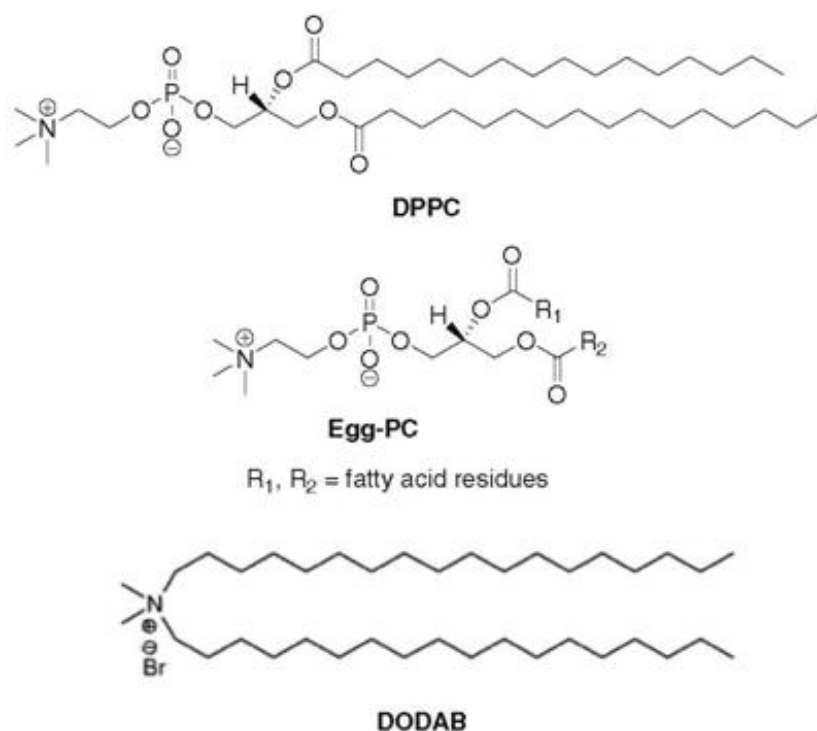
3-(2-methoxyphenyl)benzothieno[2,3-c]pyran-1-one (1d) 3-Bromo-benzo[*b*]thiophene-2-carboxylic acid (100 mg, 0.390 mmol), 2-methoxyphenylacetylene (1.2 equiv.) $\text{PdCl}_2(\text{PPh}_3)_2$ (5 mol%), CuI (3 mol%), and NEt_3 (3 equiv.) were added under argon to dry DMF (2 mL) in a dry Schlenk tube and the mixture was heated for 2 h at 100 °C. After cooling, water (5 mL) and ethyl acetate (5 mL) were added and the phases were separated. The aqueous phase

was then extracted with more ethyl acetate (3 × 5 mL) and the organic phases were collected, dried (MgSO_4) and filtered. The solvent removal gave a solid which was crystallized from CH_2Cl_2 /petroleum ether affording **1d** as a beige solid (95 mg, 80%), m.p. 191–193 °C. ^1H -NMR (400 MHz, $\text{DMSO-}d_6$) δ 3.98 (3H, s, OMe), 7.11–7.15 (1H, m, ArH), 7.23–7.25 (1H, m, ArH), 7.48–7.53 (1H, m, ArH), 7.62–7.66 (1H, m, ArH), 7.70–7.74 (1H, m, ArH), 7.80–7.83 (1H, m, ArH), 7.99 (1H, s, 4-H), 8.21–8.24 (1H, m, ArH), 8.43–8.45 (1H, m, ArH) ppm. ^{13}C -NMR (100.6 MHz, $\text{DMSO-}d_6$) δ 55.30 (OCH₃), 101.83 (CH), 112.26 (CH), 120.02 (C), 120.73 (CH), 121.20 (C), 123.92 (CH), 124.69 (CH), 125.79 (CH), 128.63 (CH), 129.61 (CH), 131.69 (CH), 134.10 (C), 142.46 (C), 144.07 (C), 154.26 (C), 157.06 (C), 158.08 (C) ppm. MS (EI): m/z 308 (M^+ , 100), 280 ($\text{M}^+ - 28$, 59). HRMS M^+ calc. for $\text{C}_{18}\text{H}_{12}\text{O}_3\text{S}$: 308.0507, found: 308.0508.

Spectroscopic studies

Materials and methods

All the solutions were prepared using spectroscopic grade solvents and ultrapure water (Milli-Q grade). 1,2-Dipalmitoyl-*sn*-glycero-3-phosphocholine (DPPC) and 1,2-Diacyl-*sn*-glycero-3-phosphocholine from egg yolk (Egg-PC), from Sigma-Aldrich, and dioctadecyldimethylammonium bromide (DODAB), from Tokyo Kasei, were used as received (lipid structures are shown below).



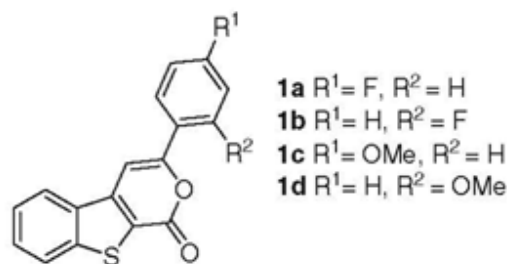


Fig. 1 Structure of 3-(aryl)benzothieno[2,3-c]pyran-1-ones

For Egg-PC vesicles preparation, defined volumes of a stock solution of lipid (34.5 mM) and compound (0.2 mM) in ethanol were injected together, under vigorous stirring, to an aqueous buffer solution (10 mM Tris, pH=7.4), at room temperature. A similar procedure was adopted for DPPC and DODAB liposomes, but the injection of the required amounts of stock solutions of lipid (50 mM for DPPC and 20 mM for DODAB) and compound in ethanol was done at 60 °C, well above the melting transition temperature of both lipids, *ca.* 41 °C for DPPC [8] and 45 °C for DODAB [9]. In all cases, the final lipid concentration was 1 mM, with compounds **1a–d**/lipid molar ratio of 1:500.

Spectroscopic measurements

Absorption spectra were recorded in a Shimadzu UV-3101PC UV-Vis-NIR spectrophotometer. Fluorescence measurements were performed using a Spex Fluorolog 3 spectrofluorimeter, equipped with double monochromators in both excitation and emission, Glan-Thompson polarizers and a temperature-controllable cuvette holder. Fluorescence spectra were corrected for the instrumental response of the system.

For fluorescence quantum yield determination, the solutions were previously bubbled for 20 min with ultrapure nitrogen. The fluorescence quantum yields (Φ_s) were determined using the standard method (Eq. 1) [10, 11]. Anthracene in ethanol ($\Phi_r=0.27$ at 25 °C [12]) and quinine sulfate in 0.05 M H₂SO₄ ($\Phi_r=0.546$ at 25 °C [13, 14]) were used as references.

$$\Phi_s = \frac{A_r F_s n_s^2}{A_s F_r n_r^2} \Phi_r \quad (1)$$

where A is the absorbance at the excitation wavelength, F the integrated emission area and n the refraction index of the solvents used. Subscripts refer to the reference (r) or sample (s) compound.

The steady-state fluorescence anisotropy, r , is calculated by

$$r = \frac{I_{VV} - GI_{VH}}{I_{VV} + 2GI_{VH}} \quad (2)$$

where I_{VV} and I_{VH} are the intensities of the emission spectra obtained with vertical and horizontal polarization, respectively (for vertically polarized excitation light), and $G = I_{HV}/I_{HH}$ is the instrument correction factor, where I_{HV} and I_{HH} are the emission intensities obtained with vertical and horizontal polarization (for horizontally polarized excitation light).

Data analysis

Solvatochromic shifts were described by the Lippert-Mataga Eq. (3), which relates the energy difference between absorption and emission maxima to the orientation polarizability, [15, 16]

$$\bar{\nu}_{\text{abs}} - \bar{\nu}_{\text{fl}} = \frac{1}{4\pi\epsilon_0} \frac{2\Delta\mu^2}{hcR^3} \Delta f + \text{const} \quad (3)$$

where $\bar{\nu}_{\text{abs}}$ is the wavenumber of maximum absorption, $\bar{\nu}_{\text{fl}}$ is the wavenumber of maximum emission, $\Delta\mu = \mu_e - \mu_g$ is the difference in the dipole moment of solute molecule between excited (μ_e) and ground (μ_g) states, R is the cavity radius (considering the fluorophore a point dipole at the center of a spherical cavity immersed in the homogeneous solvent), and Δf is the orientation polarizability given by (Eq. 4):

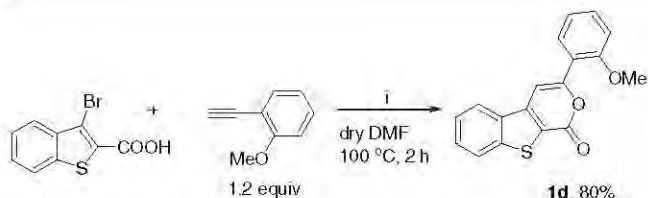
$$\Delta f = \frac{\epsilon - 1}{2\epsilon + 1} - \frac{n^2 - 1}{2n^2 + 1}, \quad (4)$$

where ϵ is the static dielectric constant and n the refractive index of the solvent.

Fluorescence anisotropy components (I_{VV} and $G \cdot I_{VH}$) were globally fitted to two sums of lognormal components (Eqs. 5 and 6) [17], each sum characterized by a fitted anisotropy value,

$$I_{VV} = \sum_i \frac{A_{1i}}{(\lambda - (\lambda_{\text{max}})_{1i} + a_{1i})} \exp(-c_{1i}^2) \exp\left\{-\frac{1}{2c_{1i}^2} \left[\ln\left(\frac{\lambda - (\lambda_{\text{max}})_{1i} + a_{1i}}{b_{1i}}\right)\right]^2\right\} + \sum_i \frac{A_{2i}}{(\lambda - (\lambda_{\text{max}})_{2i} + a_{2i})} \exp(-c_{2i}^2) \exp\left\{-\frac{1}{2c_{2i}^2} \left[\ln\left(\frac{\lambda - (\lambda_{\text{max}})_{2i} + a_{2i}}{b_{2i}}\right)\right]^2\right\} \quad (5)$$

$$G \cdot I_{VH} = \sum_i \frac{A'_{1i}}{(\lambda - (\lambda_{\text{max}})_{1i} + a_{1i})} \exp(-c_{1i}^2) \exp\left\{-\frac{1}{2c_{1i}^2} \left[\ln\left(\frac{\lambda - (\lambda_{\text{max}})_{1i} + a_{1i}}{b_{1i}}\right)\right]^2\right\} + \sum_i \frac{A'_{2i}}{(\lambda - (\lambda_{\text{max}})_{2i} + a_{2i})} \exp(-c_{2i}^2) \exp\left\{-\frac{1}{2c_{2i}^2} \left[\ln\left(\frac{\lambda - (\lambda_{\text{max}})_{2i} + a_{2i}}{b_{2i}}\right)\right]^2\right\} \quad (6)$$



i) $\text{PdCl}_2(\text{PPh}_3)_2$ (5 mol%), CuI (3 mol%), NEt_3 (3 equiv.)

Scheme 1 Synthesis of compound **1d**

where A (or A') is the maximum intensity at wavelength λ_{max} and the parameters a , b and c are given by [17]

$$c = \ln(\rho) / \sqrt{2 \ln(2)} \quad b = H \frac{\rho}{\rho^2 - 1} \exp(c^2) \quad a = H \frac{\rho}{\rho^2 - 1} \quad (7)$$

where H is the half-width of the band and ρ is the skewness. The lognormal function sums account for the vibrational structure of compound spectrum. The components (1 and 2) have two different fitted anisotropy values, r_1 and r_2 , given by

$$r_1 = \frac{A_{11} - A'_{11}}{A_{11} + 2A'_{11}} \quad \text{and} \quad r_2 = \frac{A_{21} - A'_{21}}{A_{21} + 2A'_{21}}, \quad (8)$$

due to the additivity law of anisotropy [18],

$$r = \sum_i \frac{I_i}{I_{\text{total}}} r_i \quad (9)$$

with

$$r_i = \frac{(I_i)_{\text{VV}} - G(I_i)_{\text{VH}}}{(I_i)_{\text{VV}} + 2G(I_i)_{\text{VH}}}. \quad (10)$$

Therefore,

$$A'_{11} = A_{11} \left(\frac{1 - r_1}{1 + 2r_1} \right) \quad \text{and} \quad A'_{21} = A_{21} \left(\frac{1 - r_2}{1 + 2r_2} \right). \quad (11)$$

Results and discussion

Synthesis of compound **1d**

As referred above, compound **1d** was prepared in this work for comparison with compounds **1a–c** which were already prepared by some of us in a previous work [4], using the same method (Scheme 1).

Compound **1d** was prepared in an excellent yield by a tandem one-pot Pd/Cu catalyzed Sonogashira reaction of the 3-bromobenzo[*b*]thiophene-2-carboxylic acid with the 2-methoxyphenylacetylene followed by an intramolecular cyclization on the intermediate involving the carboxyl group and the triple bond [4].

Photophysical properties of compounds **1a–d** in homogeneous solution

The absorption and fluorescence properties of compounds **1a**, **1b**, **1c** and **1d** were studied in several solvents. The maximum absorption (λ_{abs}) and emission wavelengths (λ_{em}), molar extinction coefficients (ϵ) and fluorescence quantum yields (Φ_{F}) of the four compounds are presented in Table 1. The normalized fluorescence spectra of compounds **1a–d** are shown in Fig. 2. Examples of absorption spectra are displayed as insets.

The effect of solvent in the absorption spectrum of these compounds is generally small (insets of Fig. 2 and Table 1). Despite this, a red shift of the lowest energy absorption maximum can be observed with increasing solvent polarity, thus indicating that a $\pi \rightarrow \pi^*$ transition is involved. The molar extinction coefficients at absorption maxima are high ($\epsilon > 10^4 \text{ M}^{-1} \text{ cm}^{-1}$), confirming this assumption.

In fluorescence spectra, significantly higher red shifts for all compounds can be observed from cyclohexane to more polar solvents, indicating that solvent relaxation after photoexcitation plays an important role. In polar solvents, a loss of vibrational structure is also detected (Fig. 2), more significant for compound **1c**, that presents completely non-structured emission bands in the more polar environments. This behavior is usually related to an intramolecular charge transfer (ICT) mechanism and/or to specific solvent effects [15].

The red shifts in emission are larger for the compounds with the electron-donating (EDG) OCH_3 group, especially for compound **1c** (26 nm from cyclohexane to DMSO). Compounds **1a** and **1b** exhibit smaller red shifts, which may be due to the dual character of the F atom, which is an EDG by mesomeric effect (+M) and an electron-withdrawing group (EWG) by inductive effect (-I). A similar behavior was already observed in tetracyclic lactams previously obtained by us, bearing this type of substituents [19].

The Lippert-Mataga plots (Eq. 3) for compounds **1a–d** (Fig. 3) display a high linearity for all compounds in the solvents studied. Therefore, specific solute–solvent interactions like hydrogen bonding are not detectable by deviations of linearity in the Lippert-Mataga plots.

From *ab initio* molecular quantum chemistry calculations, the cavity radius (R) and the ground state dipole moment (μ_{g}) were determined for the four compounds (Table 2), through an optimized structure provided by GAMESS software [21], using a RHF/3-21G(d) basis set [22] (Fig. 4). The optimized geometries show that molecules **1a** and **1c** are roughly planar, while in compounds **1b** and **1d** the fluorophenyl and the methoxyphenyl groups are out of the plane of the benzothienopyran-1-one moiety. The excited state dipole moments, μ_{e} , estimated from the Lippert-Mataga plots (Table 2), point to the presence of an intramolecular

Table 1 Maximum absorption (λ_{abs}) and emission wavelengths (λ_{em}), molar extinction coefficients (ϵ) and fluorescence quantum yields (Φ_{F}) for compounds **1a–d** in several solvents

Solvent	$\lambda_{\text{abs}}/\text{nm}$ ($\epsilon/10^4\text{M}^{-1}\text{cm}^{-1}$)				$\lambda_{\text{em}}/\text{nm}$				Φ_{F}			
	1a	1b	1c	1d	1a	1b	1c	1d	1a ^a	1b ^a	1c ^b	1d ^b
Cyclohexane	363 (1.23); 275 (2.03)	361 (1.57); 274 (3.16)	372 (1.70); 283 (2.88)	366 (1.36); 274 (2.57)	418	409	433	422	0.002	0.005	0.006	0.009
Dioxane	365 (1.25); 277 (2.67)	365 (2.17); 277 (4.12)	374 (1.89); 266 (3.03)	367 (1.66); 276 (2.09)	422	415	440	426	0.006	0.013	0.020	0.016
Dichloromethane	366 (1.72); 277 (3.78)	363 (1.46); 276 (3.39)	376 (1.40); 285 (2.75)	371 (1.30); 275 (2.48)	425	417	449	434	0.005	0.014	0.022	0.020
Dimethylformamide	367 (1.36) ^c	363 (1.40) ^c	378 (2.06); 286 (2.75)	370 (1.82); 278 (1.73)	427	419	456	437	0.010	0.012	0.039	0.015
Dimethylsulfoxide	369 (1.50) ^c	363 (1.70) ^c	381 (2.29); 286 (2.93)	372 (1.51); 279 (1.61)	429	420	459	438	0.012	0.016	0.068	0.030
Acetonitrilo	366 (1.04); 276 (2.06)	360 (1.29); 276 (3.39)	373 (1.23); 282 (2.61)	367 (1.71); 284 (3.41)	425	416	452	433	0.004	0.008	0.021	0.012
Ethanol	366 (1.57); 277 (3.67)	362 (1.30); 275 (2.94)	377 (1.77); 284 (3.63)	370 (1.49); 276 (2.90)	426	418	456	435	0.007	0.012	0.040	0.022
Methanol	367 (1.58); 277 (3.69)	363 (1.09); 275 (2.58)	377 (1.43); 283 (2.69)	370 (1.51); 275 (3.27)	427	420	458	437	0.006	0.012	0.047	0.023

^a Relative to anthracene in ethanol ($\Phi_{\text{r}}=0.27$ [12])

^b Relative to quinine sulfate in 0.05 M H_2SO_4 ($\Phi_{\text{r}}=0.546$ [13, 14])

^c Solvent cut-offs: Dimethylformamide: 275 nm; Dimethylsulfoxide: 270 nm

charge transfer (ICT) mechanism, especially for compound **1c**. Twisted intramolecular charge transfer states (TICT) usually exhibit higher excited state dipole moments (≥ 20 D) [23] than those here obtained.

Figure 5 reports the representation of HOMO and LUMO molecular orbitals for the four compounds. In all

compounds, the HOMO-LUMO transition causes an increase in the electronic density of the O atom of the pyranone ring, especially in the case of compound **1c**. It can be observed that the HOMO-LUMO transition of compound **1c** exhibits a charge transfer from the oxygen atom of the methoxyphenyl group to the aromatic ring system,

Fig. 2 Normalized fluorescence (at peak of maximum emission) spectra of compounds **1a–d** in several solvents: cyclohexane (---); dioxane (.....); dichloromethane (—); dimethylformamide (.....); dimethylsulfoxide (---); acetonitrile (----); ethanol (---); methanol (---). Insets: Absorption spectra of solutions of compounds **1a–d** in dichloromethane and in ethanol, as examples. **A** Compound **1a** (7×10^{-6} M solutions for fluorescence, $\lambda_{\text{exc}}=360$ nm, and 2.4×10^{-5} M for absorption); **B** Compound **1b** (4×10^{-6} M solutions for fluorescence, $\lambda_{\text{exc}}=360$ nm, and 2.5×10^{-5} M for absorption); **C** Compound **1c** (4×10^{-6} M solutions for fluorescence, $\lambda_{\text{exc}}=370$ nm, and 2×10^{-5} M for absorption); **D** Compound **1d** (4×10^{-6} M solutions for fluorescence, $\lambda_{\text{exc}}=370$ nm, and 2×10^{-5} M for absorption)

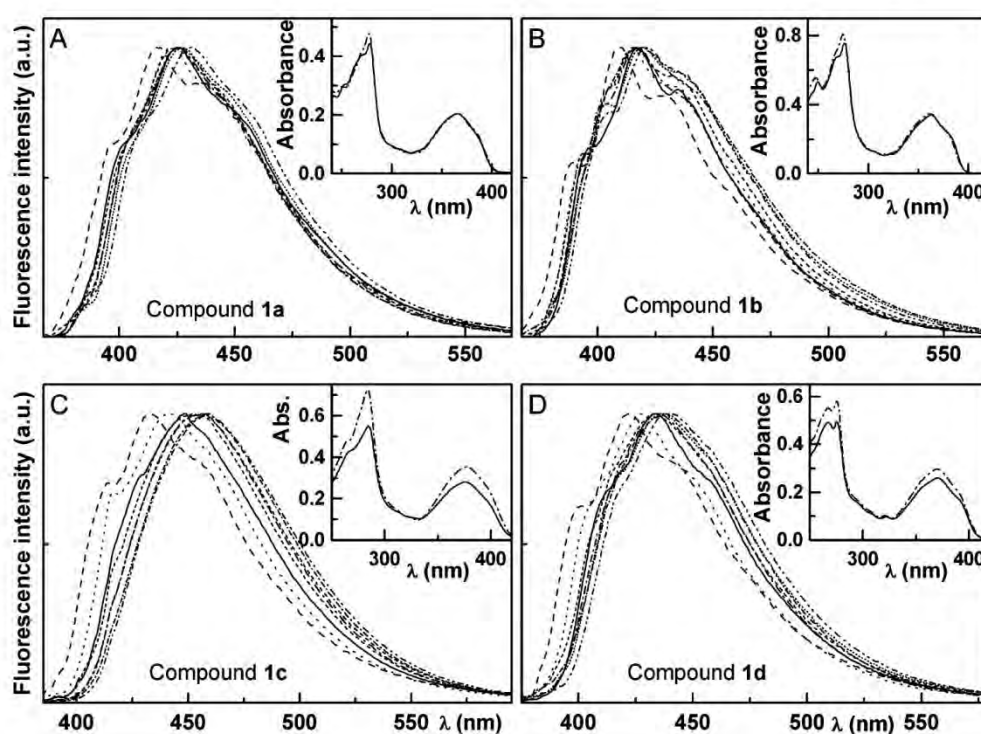
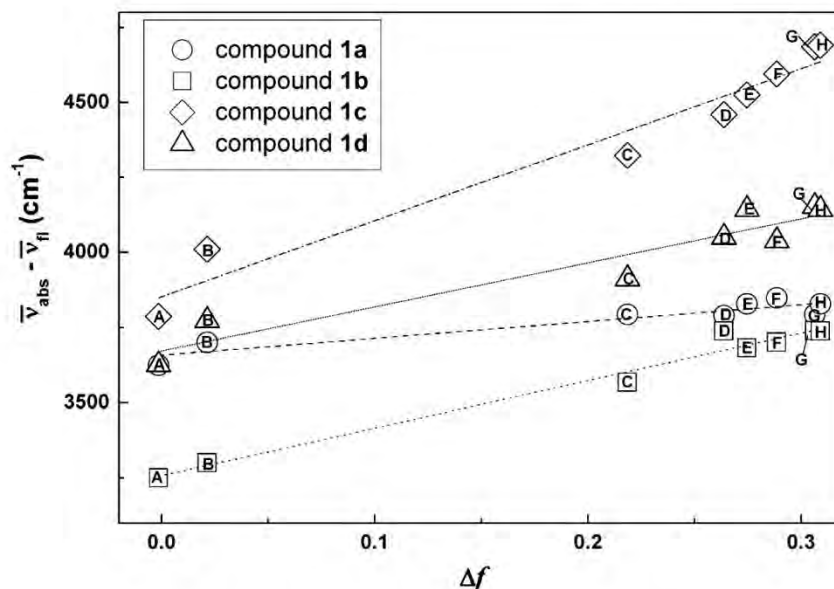


Fig. 3 Lippert-Mataga plots for compounds **1a**, **1b**, **1c** and **1d**. A: cyclohexane; B: dioxane; C: dichloromethane; D: dimethylsulfoxide; E: dimethylformamide; F: ethanol; G: acetonitrile; H: methanol (values of ϵ and n were obtained from ref. [20])

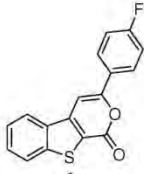
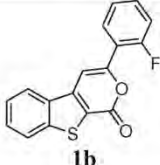
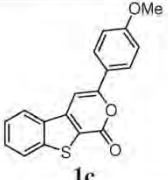
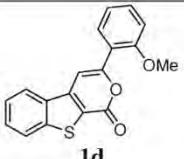


confirming the ICT character of the excited state. The effect is significantly lower for compound **1d**. Comparing compounds **1a** and **1b**, the F atom presents higher electronic density in compound **1a**, which decreases slightly upon HOMO-LUMO transition. It can also be observed that the carbon atom bound to fluorine decreases its electronic

density upon HOMO-LUMO transition in compound **1a**, the opposite occurring in compound **1b**.

All compounds **1a–d** present low fluorescence quantum yields in all solvents ($\Phi_F \leq 6.8\%$, Table 1). Fluorescence quantum yields are very low ($\Phi_F < 2\%$) for compounds with a F substituent (**1a** and **1b**). For compounds with a

Table 2 Cavity radius (R) and ground state dipole moments (μ_g), obtained from theoretical calculations, and excited state dipole moments (μ_e) calculated from the Lippert-Mataga plots

Compound	Cavity radius, R (Å)	Ground state dipole moment, μ_g (D)	Excited state dipole moment, μ_e (D)
 1a	5.3	6.1	8.9
 1b	5.8	7.6	13.1
 1c	6.3	7.9	15.8
 1d	6.1	5.1	10.8

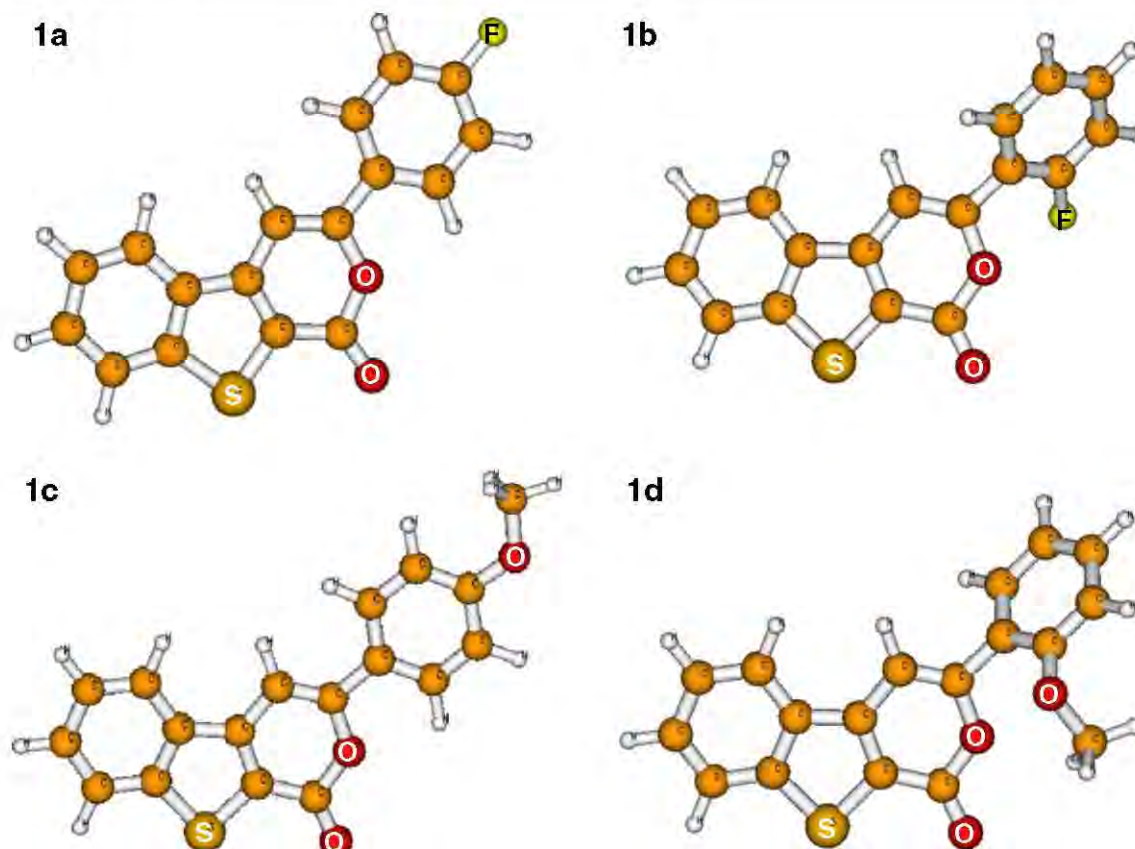


Fig. 4 Optimized structures of compounds **1a**, **1b**, **1c** and **1d** (obtained by GAMESS software), with the indication of S, O and F atoms

methoxy substituent (**1c** and **1d**), Φ_F values are generally higher, especially in polar solvents. The low values of fluorescence quantum yield observed for these compounds are due to the presence of the S atom in the thiophene ring, which may promote the intersystem crossing process by enhancement of spin–orbit coupling interaction [15, 24], as observed for other molecules which include a thiophene ring [1, 19]. The expected formation of hydrogen bonds of compounds **1a–d** with protic solvents was not inferred from deviations of the Lippert–Mataga plots (Fig. 3) and, if they occur, do not influence the Φ_F values in alcohols (Table 1).

Interaction of compounds **1a–d** with lipid membranes

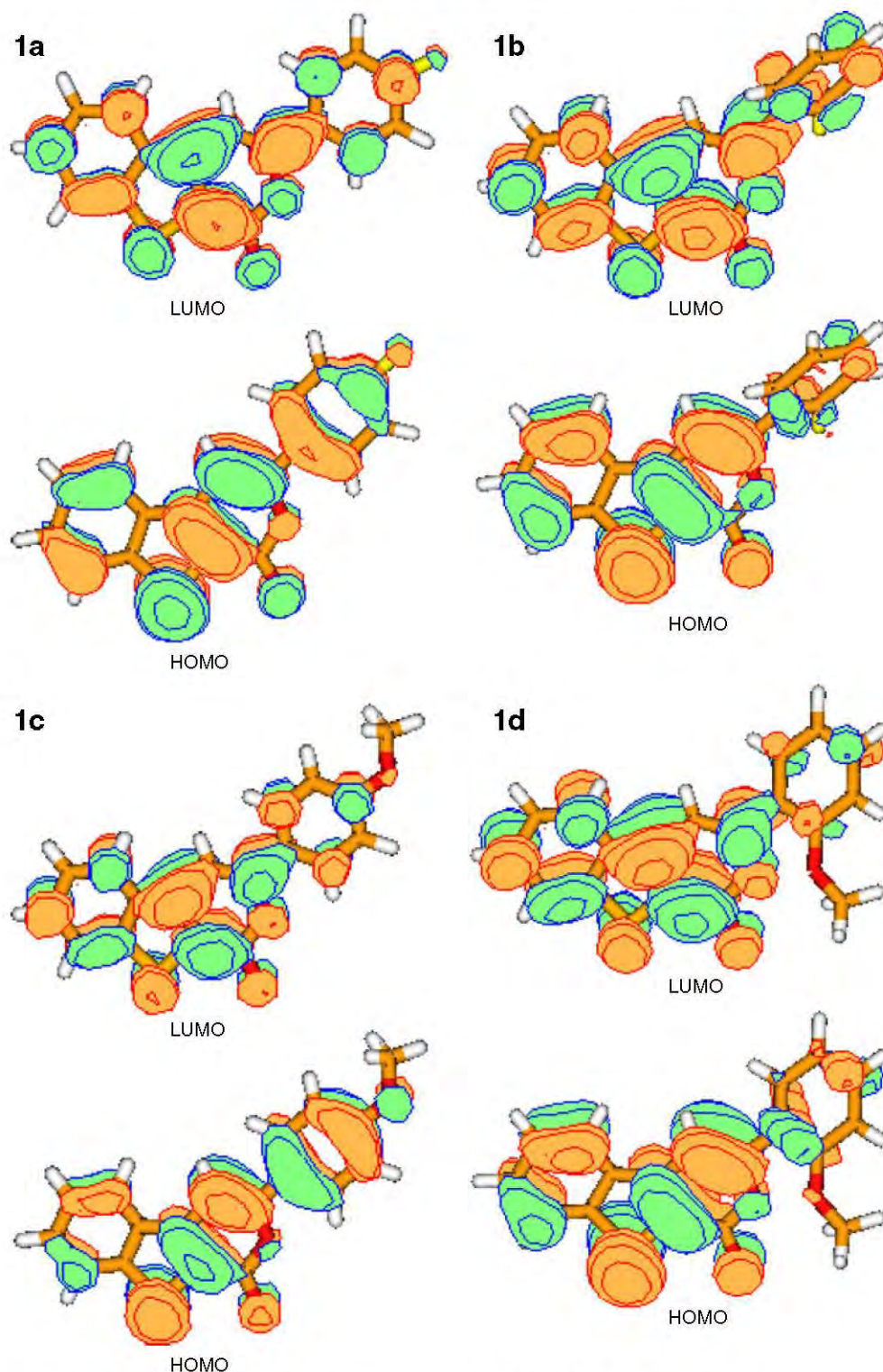
Due to their promising antitumoral activity [4], photophysical studies of compounds **1a–d** incorporated in lipid vesicles were also performed. These experiments are important to evaluate their location in liposomes pointing to drug delivery applications.

Different types of lipid molecules, Egg-PC, DPPC and DODAB, were used for the vesicles preparation. Egg-PC is a natural phospholipid mixture, where all molecules have the same polar head group (phosphatidylcholine) but several hydrocarbon chains, differing in length and degree

of unsaturation. Egg-PC main components are 16:0 PC, 18:0 PC and 18:1 PC [25]. Considering DPPC (16:0 PC) and DODAB, it is known that at room temperature, both lipids are in the ordered gel phase, where the hydrocarbon chains are fully extended and closely packed. Above the melting transition temperature, 41 °C for DPPC [8] and 45 °C for DODAB [9], these lipids attain the disordered liquid-crystalline phase.

The emission spectra of compounds **1a–d** in lipid membranes are displayed in Fig. 6. Compound **1a** (Fig. 6A) exhibits a composed spectrum in lipids at the gel phase (DODAB and DPPC at 25 °C), showing the existence of two emission bands (with maxima near 420 nm and 438 nm, Table 3), pointing to the existence of two different locations of **1a** molecules in these rigid lipid membranes. At the liquid-crystalline phase (both DPPC and DODAB at 55 °C and Egg-PC at 25 °C), only one emission band is observed, with very slight differences between the three lipids. The maximum emission wavelengths in this fluid phase (Table 3) are similar to the lower energy maximum of the compound in lipids at the gel phase. A distinct behavior is observed for compound **1b**, where the position and shape of the emission bands are similar in all lipids either at 25 °C or at 55 °C. A decrease of the shoulder at the higher energy region is

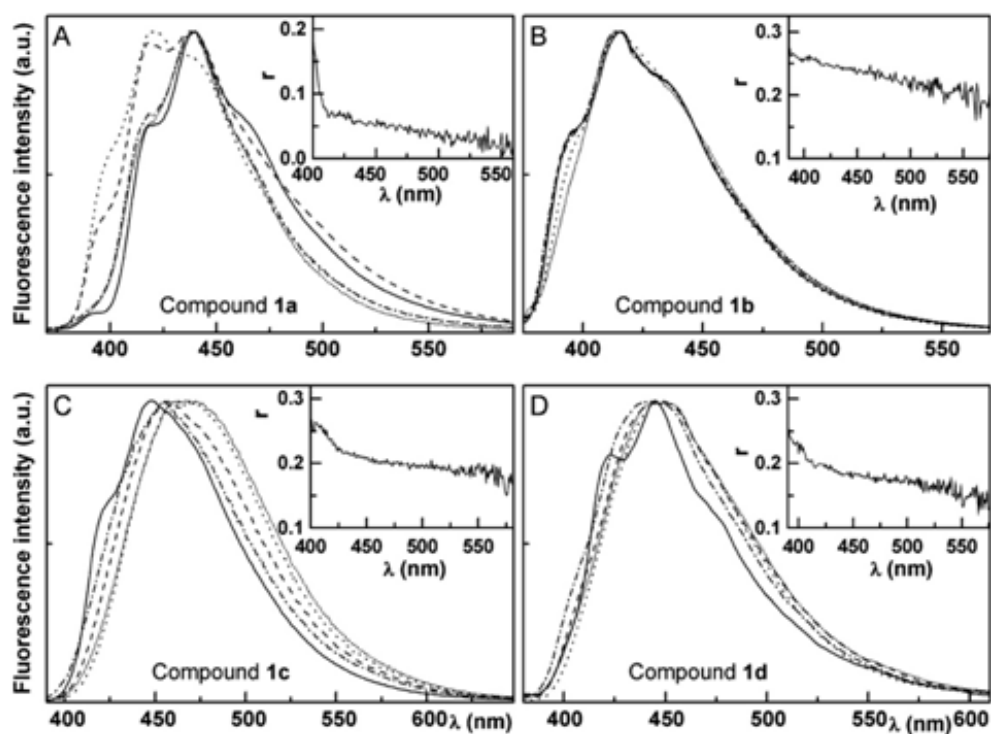
Fig. 5 Representation of HOMO (*lower*) and LUMO (*upper*) molecular orbitals of compounds **1a–d**



observed in DODAB, especially in the fluid phase (Fig. 6B). The maximum emission wavelengths indicate an environment of moderate polarity, similar to dioxane and acetonitrile (Tables 1 and 3). In homogeneous solution, the effect of the temperature increase in the fluorescence of these compounds is a *ca.* 40% reduction and a very small blue shift (1–2 nm) between 25 °C and 55 °C.

For compounds **1c** and **1d** (Fig. 6C and D, respectively) a structured emission is observed in Egg-PC, especially for compound **1d**. In DPPC and DODAB, the emission bands of both compounds are basically non-structured and, in some cases, seem clearly to be composed of two emissions. For compound **1c**, a significant spectral shift is observed between the different lipid membranes. The maximum

Fig. 6 Normalized fluorescence spectra of compounds **1a–d** in lipid membranes: Egg-PC at 25 °C (—); DPPC gel phase at 25 °C (---); DPPC liquid-crystalline phase at 55 °C (- · - · -); DODAB gel phase at 25 °C (· · · · ·); DODAB liquid-crystalline phase at 55 °C (.....). Insets: Fluorescence anisotropy spectrum of compounds **1a–d** in DPPC at gel phase (25 °C), as an example.
A Compound **1a** (λ_{exc} =360 nm); **B** Compound **1b** (λ_{exc} =360 nm); **C** Compound **1c** (λ_{exc} =370 nm); **D** Compound **1d** (λ_{exc} =370 nm)



emission wavelength in Egg-PC is similar to that in dichloromethane, while for DODAB a more hydrated environment is predicted. For compound **1d**, the emission maxima in all lipids are similar to the observed in ethylene glycol, pointing also to a hydrated location of this compound in lipid vesicles.

In order to obtain further information about the behavior of these molecules in lipid membranes, fluorescence (steady-state) anisotropy measurements were performed. The average fluorescence steady-state anisotropies (\bar{r}) and fluorescence quantum yields of the four compounds in lipid vesicles are shown in Table 3. Fluorescence anisotropy values in ethylene glycol at room temperature were also determined for comparison, being similar for all molecules. For each compound, an example of fluorescence anisotropy spectrum is displayed as inset in Fig. 6. Notable variations

with emission wavelength are observed for compound **1a** (inset of Fig. 6A), while the variations are smaller for compounds **1c**, **1d** and **1b** (inset of Fig. 6B–D). In ethylene glycol, the steady-state fluorescence anisotropy is constant with wavelength for all compounds. The behavior observed in lipid membranes points to the existence of two emitting species, corresponding to compound locations in different environments.

Figures 7 and 8 display an example of the fit of anisotropy components, I_{VV} and $G \cdot I_{VH}$ (Eqs. 5 and 6), and the fitting to the anisotropy curve, as well as the respective spectral contributions recovered from the fitting. The results are given in Table 4.

For all compounds, two components were recovered, one with higher anisotropy (r_1) and lower maximum

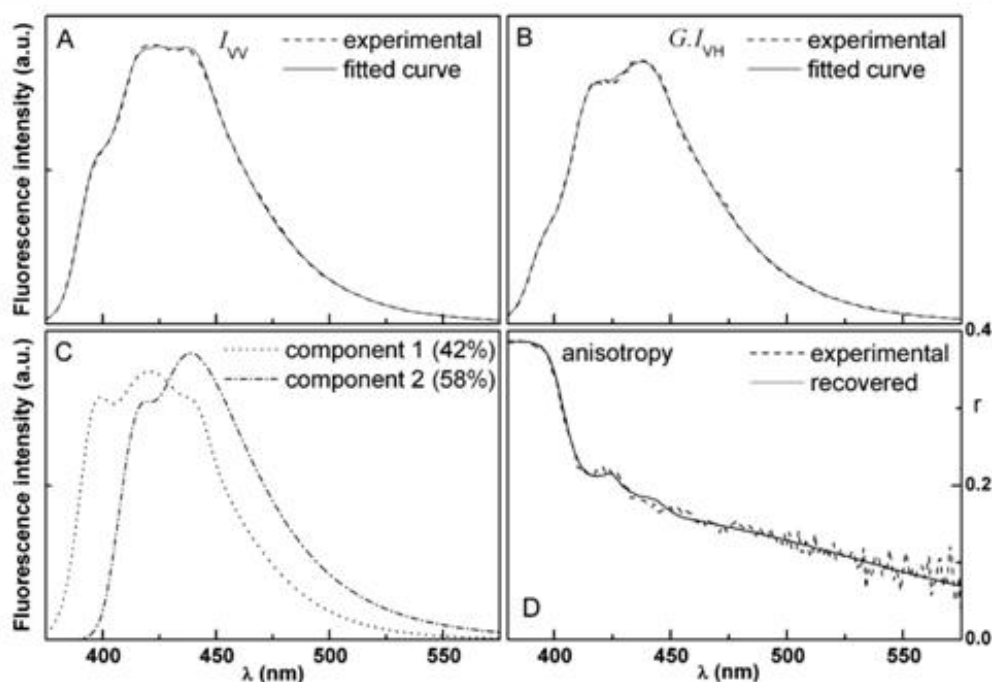
Table 3 Average steady-state fluorescence anisotropy (\bar{r}) values, fluorescence quantum yields and maximum emission wavelengths (λ_{em}) of compounds **1a–d** in lipid membranes. Values in ethylene glycol at room temperature are also shown for comparison

	Compound 1a			Compound 1b			Compound 1c			Compound 1d		
	λ_{em} /nm	Φ_F^a	\bar{r}	λ_{em} /nm	Φ_F^a	\bar{r}	λ_{em} /nm	Φ_F^b	\bar{r}	λ_{em} /nm	Φ_F^b	\bar{r}
DPPC (25 °C)	419; 438	0.034	0.089	416	0.011	0.234	459	0.042	0.203	448	0.030	0.194
DPPC (55 °C)	438	0.013	0.065	415	0.004	0.185	457	0.010	0.192	444	0.008	0.190
DODAB (25 °C)	421	0.084	0.188	415	0.013	0.210	467	0.054	0.173	449	0.031	0.189
DODAB (55 °C)	439	0.047	0.075	414	0.005	0.140	469	0.017	0.161	448	0.011	0.167
Egg-PC (25 °C)	440	0.024	0.066	416	0.006	0.231	449	0.022	0.229	424; 445	0.015	0.212
Ethylene glycol (25 °C)	431	–	0.276	421	–	0.272	465	–	0.240	444	–	0.264

^a Relative to anthracene in ethanol ($\Phi_r=0.27$ at 25 °C [12])

^b Relative to quinine sulfate in 0.05 M H₂SO₄ ($\Phi_r=0.546$ at 25 °C [13, 14])

Fig. 7 Fit of compound **1a** in DODAB gel phase (25 °C). **A** I_{VV} component and fitted curve; **B** $G \cdot I_{VH}$ component and fitted curve; **C** Recovered spectral components from the fitting procedure; **D** Fluorescence steady-state anisotropy and recovered curve (calculated from the recovered components)



emission wavelength (λ_1), corresponding to compound molecules located deeper in the lipid membrane, and another corresponding to a more hydrated environment (higher emission wavelength, λ_2 , and lower anisotropy, r_2). The fraction of the first component, f_1 (corresponding to the fraction of spectral area), is also presented. In general, the microviscosity decreases from the interface to the interior of the membrane [26, 27], with a more pronounced variation when the membrane is in the liquid-crystalline phase [27]. Thus, the recovered anisotropy values for the

two compound locations are in opposite direction to that given by the spectral band positions. This can be explained by the observed increase in the fluorescence quantum yield with solvent polarity (Table 1). The absorption spectra exhibit a very low dependence on solvent polarity (insets of Fig. 2). From the Strickler-Berg relation [18, 28], it can be concluded that the radiative lifetime, τ_r , is mainly invariant with polarity. Therefore, a higher Φ_F value results from an increase of the excited-state lifetime. This, in turn, contributes to a decrease in fluorescence anisotropy, as the excited

Fig. 8 Fit of compound **1d** in DODAB gel phase (25 °C). **A** I_{VV} component and fitted curve; **B** $G \cdot I_{VH}$ component and fitted curve; **C** Recovered spectral components from the fitting procedure; **D** Fluorescence steady-state anisotropy and recovered curve (calculated from the recovered components)

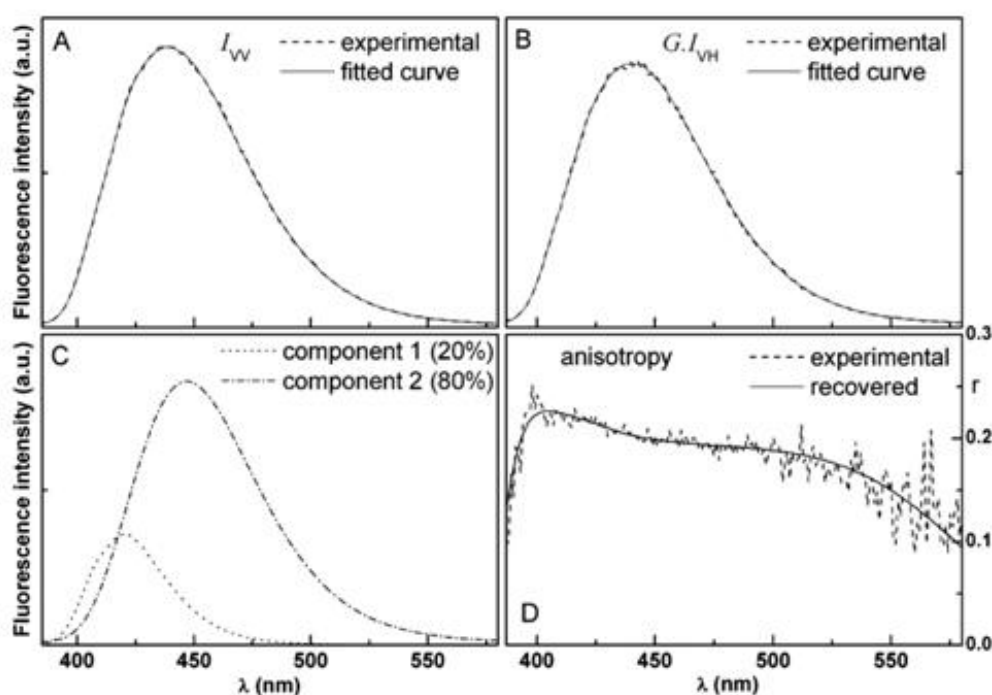


Table 4 Steady-state fluorescence anisotropy (r) of the two anisotropy components, weights of the first component (f_1) and respective maximum emission wavelengths (λ_{max}) for compounds **1a–d** in lipid membranes

	Compound 1a				Compound 1b				Compound 1c				Compound 1d							
	f_1	r_1	λ_1 (nm)	τ_2	λ_2 (nm)	f_1	r_1	λ_1 (nm)	τ_2	λ_2 (nm)	f_1	r_1	λ_1 (nm)	τ_2	λ_2 (nm)	f_1	r_1	λ_1 (nm)	τ_2	λ_2 (nm)
DPPC (25 °C)	0.38	0.147	422	0.054	448	0.58	0.256	414	0.231	442	0.27	0.260	425	0.188	455	0.19	0.230	417	0.177	446
DPPC (55 °C)	0.08	0.146	417	0.022	439	0.51	0.219	406	0.187	440	0.47	0.278	439	0.173	456	0.18	0.238	418	0.175	442
DODAB (25 °C)	0.42	0.287	422	0.057	439	0.58	0.248	410	0.190	444	0.37	0.256	429	0.164	463	0.20	0.250	420	0.194	447
DODAB (55 °C)	0.13	0.128	419	0.029	439	0.60	0.222	409	0.109	440	0.50	0.231	440	0.132	464	0.21	0.221	422	0.163	444
Egg-PC (25 °C)	0.06	0.130	417	0.014	440	0.54	0.247	414	0.229	440	0.31	0.258	424	0.238	455	0.32	0.250	420	0.228	442

compound has more time to rotate leading to a depolarization of its fluorescence.

Compound **1a** locates mainly in a very hydrated environment (λ_2 values higher than λ_{max} observed in methanol), while compound **1b** preferential location is deeper inside the lipid membrane, as the component with lower maximum emission wavelength (406–414 nm) is dominant ($f_1 > 0.50$). For compounds **1a** and **1b**, similar environments (as inferred from the maximum emission wavelengths) show very distinct anisotropy values for component 2 (Table 4), r_2 value being especially low for compound **1a**. The different geometry (vd. Fig. 4) of both compounds cannot explain this distinct behavior, as compounds **1c** and **1d** which have also different geometries do not show similar variations in anisotropy values. This peculiar behavior of compound **1a** indicates that some of its molecules locate at the outer part of the liposome interface, with a fluidity approaching that of water.

Upon transition from the gel (25 °C) to the liquid-crystalline (55 °C) phase (for DPPC and DODAB), compound **1a** relocates to a more hydrated environment, as the f_1 value strongly decreases. The opposite seems to happen for compound **1c**, where f_1 clearly increases at 55 °C. Therefore, compounds with a planar geometry (**1a** and **1c**) have higher mobility in the lipid vesicles when phase transition occurs.

Liposomes have been widely used to deliver anticancer agents, in order to reduce the toxic effects of the drugs or to increase the drug circulation time and effectiveness [29]. The studies described here are important for the incorporation of the new potential antitumoral benzothienopyran-1-ones in liposomes for future controlled drug delivery applications.

Conclusions

The four new potential antitumoral compounds, 3-arylbenzothieno[2,3-*c*]pyran-1-ones, show a solvent sensitive emission, with significant red shifts in polar solvents for the methoxylated compounds. Compound **1c** exhibits the higher fluorescence quantum yields in all solvents studied. The estimated excited state dipole moments point to an ICT character of the excited state, more pronounced for compound **1c**, confirmed by molecular quantum chemistry calculations.

Photophysical studies of the compounds incorporated in liposomes of DPPC, DODAB and Egg-PC indicate that all the compounds exhibit two different locations, one due to a deep penetration in the lipid membrane and other corresponding to a more hydrated environment. Compounds with a planar geometry (**1a** and **1c**) have higher mobility in the lipid vesicles when phase transition occurs.

Considering the already tested anti-proliferative activity of human tumor cell lines exhibited by these molecules, the

results obtained here are important for future drug delivery applications using liposomes.

Acknowledgements Foundation for the Science and Technology (FCT)—Portugal and FEDER (Fundo Europeu de Desenvolvimento Regional), for financial support through Centro de Física (CFUM) and Centro de Química (CQ-UM) of University of Minho and through the Project PTDC/QUI/81238/2006. M.S.D. Carvalho and R.C. Calheta acknowledge FCT for their PhD grants SFRH/BD/47052/2008 and SFRH/BD/29274/2006, respectively.

References

- Queiroz M-JRP, Castanheira EMS, Pinto AMR, Ferreira ICFR, Begouin A, Kirsch G (2006) Synthesis of the first thieno- δ -carboline. Fluorescence studies in solution and in lipid vesicles. *J Photochem Photobiol A: Chem* 181:290–296
- Castanheira EMS, Abreu AS, Carvalho MSD, Queiroz M-JRP, Ferreira PMT (2009) Fluorescence studies on potential antitumoral heteroaryl and heteroannulated indoles in solution and in lipid membranes. *J Fluorescence* 19:501–509
- Castanheira EMS, Abreu AS, Queiroz M-JRP, Ferreira PMT, Coutinho PJG, Nazareth N, Nascimento MS-J (2009) Fluorescence properties of a potential antitumoral benzothieno[3, 2-b]pyrrole in solution and lipid membranes. *J Photochem Photobiol A: Chem* 206:220–226
- Queiroz M-JRP, Calheta RC, Vale-Silva LA, Pinto E, Nascimento MS-J (2009) Synthesis of novel 3-(aryl)benzothieno[2, 3-c]pyran-1-ones from Sonogashira products and intramolecular cyclization: antitumoral activity evaluation. *Eur J Med Chem* 44:1893–1899
- Lasic DD (1995) In: Lasic DD, Barenholz Y (eds) *Handbook of nonmedical applications of liposomes: from gene delivery and diagnostic to ecology*, vol IV. CRC, New York, pp 1–32
- Lasic DD, Ruff D (1998) In: Lasic DD, Papahadjopoulos D (eds) *Medical applications of liposomes*. Elsevier, Netherlands, pp 353–394
- Pedroso de Lima MC, Simões S, Pires P, Faneca H, Düzgünes N (2001) Cationic lipid-DNA complexes in gene delivery: from biophysics to biological applications. *Adv Drug Deliv Rev* 47:277–294
- Lentz BR (1989) Membrane “fluidity” as detected by diphenyl-hexatriene probes. *Chem Phys Lipids* 50:171–190
- Feitosa E, Barreleiro PCA, Olofsson G (2000) Phase transition in dioctadecyldimethylammonium bromide and chloride vesicles prepared by different methods. *Chem Phys Lipids* 105:201–213
- Demas JN, Crosby GA (1971) The measurement of photoluminescence quantum yields. A review. *J Phys Chem* 75:991–1024
- Fery-Forgues S, Lavabre D (1999) Are fluorescence quantum yields so tricky to measure? A demonstration using familiar stationery products. *J Chem Educ* 76:1260–1264
- Dawson WR, Windsor MW (1968) Fluorescence yields of aromatic compounds. *J Phys Chem* 72:3251–3260
- Melhuish WH (1961) Quantum efficiencies of fluorescence of organic substances—effect of solvent and concentration of fluorescent solute. *J Phys Chem* 65:229–235
- Meech SR, Phillips D (1983) Photophysics of some common fluorescence standards. *J Photochem* 23:193–217
- Lakowicz JR (1999) *Principles of fluorescence spectroscopy*. Kluwer Academic/Plenum, New York
- Mataga N, Kubota T (1970) *Molecular interactions and electronic spectra*. Marcel Dekker, New York
- Siano DB, Metzler DE (1969) Band shapes of electronic spectra of complex molecules. *J Chem Phys* 51:1856–1861
- Valeur B (2001) *Molecular fluorescence—principles and applications*. Wiley-VCH, Weinheim
- Queiroz M-JRP, Castanheira EMS, Lopes TCT, Cruz YK, Kirsch G (2007) Synthesis of fluorescent tetracyclic lactams by a “one pot” three steps palladium-catalyzed borylation, Suzuki coupling (BSC) and lactamization. DNA and polynucleotides binding studies. *J Photochem Photobiol A: Chem* 190:45–52
- Lide DR (ed) (2002) *Handbook of chemistry and physics*, 83rd edn. CRC, Boca Raton
- Schmidt MW, Baldrige KK, Boatz JA, Elbert ST, Gordon MS, Jensen JH, Koseki S, Matsunaga N, Nguyen KA, Su S, Windus TL, Dupuis M, Montgomery JA (1993) General atomic and molecular electronic structure system. *J Comput Chem* 14:1347–1363
- Jensen F (1999) *Introduction to computational chemistry*. Wiley, West Sussex
- Grabowski ZR, Rotkiewicz K, Rettig W (2003) Structural changes accompanying intramolecular electron transfer: focus on twisted intramolecular charge-transfer states and structures. *Chem Rev* 103:3899–4031
- Turro NJ (1978) *Modern molecular photochemistry*. Benjamin/Cummings, Menlo Park
- Papahadjopoulos D, Miller N (1967) Phospholipid model membranes. I. Structural characteristics of hydrated liquid crystals. *Biochim Biophys Acta* 135:624–638
- Tilley L, Thulborn KR, Sawyer WH (1979) An assessment of the fluidity gradient of the lipid bilayer as determined by a set of n-(9-anthroyloxy)fatty acids (n = 2, 6, 9, 12, 16). *J Biol Chem* 254:2592–2594
- Bahri MA, Heyne BJ, Hans P, Seret AE, Mouithys-Mickalad AA, Hoebcke MD (2005) Quantification of lipid bilayer effective microviscosity and fluidity effect induced by propofol. *Biophys Chem* 114:53–61
- Strickler SJ, Berg RA (1962) Relationship between absorption intensity and fluorescence lifetime of molecules. *J Chem Phys* 37:814
- Banerjee R (2001) Liposomes: applications in medicine. *J Biomater Appl* 16:3–21

New potential antitumoral fluorescent tetracyclic thieno[3,2-*b*]pyridine derivatives: interaction with DNA and nanosized liposomes

Elisabete M.S. Castanheira, Maria Solange D. Carvalho, Ana Rita O. Rodrigues, Ricardo C. Calhela, Maria-João R.P. Queiroz, *Nanoscale Research Letters*, **2011**, *6*, 379-386.

My contribution to this paper was the photophysical studies in several solvents, fluorescence and DLS measurements of the compounds encapsulated in nanoliposomes and fluorescence studies of the interaction with DNA.

NANO EXPRESS

Open Access

New potential antitumoral fluorescent tetracyclic thieno[3,2-*b*]pyridine derivatives: interaction with DNA and nanosized liposomes

Elisabete MS Castanheira^{1*}, Maria Solange D Carvalho^{1,2}, Ana Rita O Rodrigues¹, Ricardo C Calhella² and Maria-João RP Queiroz²

Abstract

Fluorescence properties of two new potential antitumoral tetracyclic thieno[3,2-*b*]pyridine derivatives were studied in solution and in liposomes of DPPC (dipalmitoyl phosphatidylcholine), egg lecithin (phosphatidylcholine from egg yolk; Egg-PC) and DODAB (dioctadecyldimethylammonium bromide). Compound **1**, pyrido[2',3':3,2]thieno[4,5-*d*]pyrido[1,2-*a*]pyrimidin-6-one, exhibits reasonably high fluorescence quantum yields in all solvents studied ($0.20 \leq \Phi_F \leq 0.30$), while for compound **2**, 3-[(*p*-methoxyphenyl)ethynyl]pyrido[2',3':3,2]thieno[4,5-*d*]pyrido[1,2-*a*]pyrimidin-6-one, the values are much lower ($0.01 \leq \Phi_F \leq 0.05$). The interaction of these compounds with salmon sperm DNA was studied using spectroscopic methods, allowing the determination of intrinsic binding constants, $K_i = (8.7 \pm 0.9) \times 10^3 \text{ M}^{-1}$ for compound **1** and $K_i = (5.9 \pm 0.6) \times 10^3 \text{ M}^{-1}$ for **2**, and binding site sizes of $n = 11 \pm 3$ and $n = 7 \pm 2$ base pairs, respectively. Compound **2** is the most intercalative compound in salmon sperm DNA (35%), while for compound **1** only 11% of the molecules are intercalated. Studies of incorporation of both compounds in liposomes of DPPC, Egg-PC and DODAB revealed that compound **2** is mainly located in the hydrophobic region of the lipid bilayer, while compound **1** prefers a hydrated and fluid environment.

Introduction

Liposomes are among technological delivery developments for chemotherapeutic drugs in the treatment of cancer. This technique can potentially overcome many common pharmacologic problems, such as those involving solubility, pharmacokinetics, in vivo stability and toxicity [1-3]. Liposomes are closed spherical vesicles consisting of a lipid bilayer that encapsulates an aqueous phase in which hydrophilic drugs can be stored, while water insoluble compounds can be incorporated in the hydrophobic region of the lipid bilayer [4].

In this work, two new potential antitumoral fluorescent planar tetracyclic thieno[3,2-*b*]pyridine derivatives **1** and **2** (Figure 1), previously synthesized by some of us [5], were encapsulated in liposomes of DPPC (dipalmitoyl phosphatidylcholine), egg lecithin (phosphatidylcholine from egg yolk) and DODAB (dioctadecyldimethylammonium

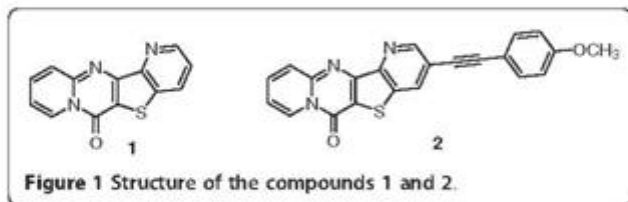
bromide). DPPC and egg lecithin [egg yolk phosphatidylcholine (Egg-PC)] are neutral components of biological membranes, while cationic liposomes based on the synthetic lipid DODAB have been used as vehicles for DNA transfection and drug delivery [6]. These studies are important keeping in mind future drug delivery applications using these compounds as anticancer drugs.

Due to the antitumoral potential of the two compounds **1** and **2**, related with their possible intercalation between the DNA base pairs, interactions with natural double-stranded salmon sperm DNA were studied. These interactions can be assessed using spectroscopic measurements, which are important tools for monitoring DNA-binding processes. The investigation based on DNA interactions has a key importance in order to understand the mechanisms of action of antitumor and antiviral drugs and to design new DNA-targeted drugs [7,8]. Small molecules are stabilized on groove binding and intercalation with DNA through a series of associative interactions such as π -stacking, hydrogen bonding, attractive van der Waals and hydrophobic interactions

* Correspondence: ecoutinho@fisica.uminho.pt

¹Centre of Physics (CFUM), University of Minho, Campus de Gualtar, Braga, 4710-057, Portugal

Full list of author information is available at the end of the article



[8]. The occurrence of intercalation seems to be an essential (but not sufficient) step for antitumoral activity [7]. Fluorescence quenching experiments using external quenchers are also very useful to distinguish between DNA binding modes [9] since intercalated molecules are less accessible to anionic quenchers due to electrostatic repulsion with negatively charged DNA [10].

Experimental

Salmon sperm DNA from Invitrogen (Carlsbad, CA, USA) and compounds stock solutions were prepared in 10 mM Tris-HCl buffer (pH = 7.4), with 1 mM EDTA. The DNA concentration in number of bases was determined from the molar absorption coefficient, $\epsilon = 6600 \text{ M}^{-1} \text{ cm}^{-1}$ at 260 nm [11]. Fluorescence spectra of several solutions with different [DNA]/[compound] ratios and constant compound concentration ($5 \times 10^{-6} \text{ M}$) were recorded. The solutions were left several hours to stabilize.

Dipalmitoyl phosphatidylcholine (DPPC), egg yolk phosphatidylcholine (Egg-PC), from Sigma-Aldrich (St. Louis, Missouri, USA), and dioctadecyldimethylammonium bromide (DODAB), from Tokyo Kasei (Tokyo, Japan), were used as received. Liposomes were prepared by the ethanolic injection method, previously used for the preparation of Egg-PC and DPPC liposomes [12-15] and DODAB vesicles [16,17]. An ethanolic solution of a lipid/compound mixture was injected in an aqueous buffer solution under vigorous stirring, above the melting transition temperature of the lipid (approx. 41°C for DPPC [18] and 45°C for DODAB [19]). The final lipid concentration was 1 mM, with a compound/lipid molar ratio of 1:500. One millilitre solutions of liposome dispersions were placed in 3 mL disposable polystyrene cuvettes for dynamic light scattering (DLS) measurements in a Malvern ZetaSizer Nano ZS particle analyzer (Worcestershire, UK). Five independent measurements were performed for each sample. Malvern Dispersion Technology Software (DTS) (Worcestershire, UK) was used with multiple narrow mode (high resolution) data processing, and mean size (nm) and error values were considered.

Absorption spectra were recorded in a Shimadzu UV-3101PC UV-Vis-NIR spectrophotometer (Kyoto, Japan) and fluorescence measurements were obtained in a Fluorolog 3 spectrofluorimeter (HORIBA Scientific,

Kyoto, Japan) equipped with Glan-Thompson polarizers. Fluorescence spectra were corrected for the instrumental response of the system. The fluorescence quantum yields were determined by the standard method [20,21], using 9,10-diphenylanthracene in ethanol as reference, $\Phi_f = 0.95$ [22]. The solutions were previously bubbled for 20 min with ultrapure nitrogen.

Results and discussion

The size and size distribution of the liposomes prepared was obtained by DLS. All the liposomes have a mean hydrodynamic radius lower than 150 nm and generally low polydispersity. For Egg-PC and DODAB liposomes, the size distributions are bimodals and broader than for DPPC liposomes, the Egg-PC being the more polydisperse (Figure 2). The ethanolic injection method was described to produce phospholipid small unilamellar vesicles (SV) [12-15]. Accordingly, DPPC and Egg-PC liposomes obtained here are in this category, with a mean diameter of around 90 nm for DPPC and 50 nm for Egg-PC. DODAB liposomes exhibit a significantly larger mean diameter (around 270 nm) than the phospholipid ones. The size of DODAB vesicles strongly depends on the preparation method, sonication and ethanolic injection giving small DODAB vesicles [17,23,24], while injection using chloroform yielded large DODAB vesicles [16]. Besides, spontaneously prepared DODAB liposomes have a much larger size

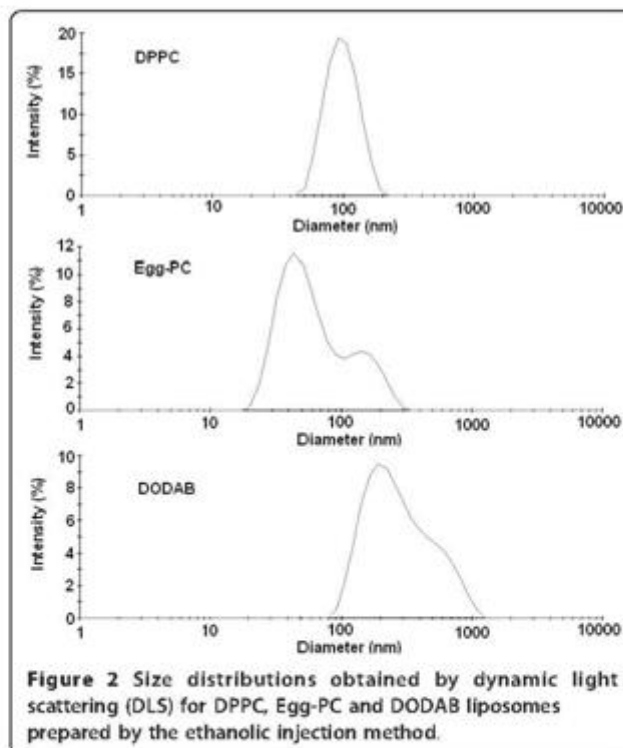


Figure 2 Size distributions obtained by dynamic light scattering (DLS) for DPPC, Egg-PC and DODAB liposomes prepared by the ethanolic injection method.

(hydrodynamic radius around 337 nm [25]), being considered giant unilamellar vesicles (GUV). The DODAB liposomes mean diameter obtained here (*ca.* 270 nm) compares well with the reported value of 249 nm for DODAB SV [16]. In all samples, no experimental evidence of the presence of open bilayer fragments (diameter lower than 10 nm [17]) was obtained (Figure 2).

The absorption and fluorescence properties of compounds **1** and **2** were studied in several solvents (Table 1). The normalized fluorescence spectra of compounds **1** and **2** are shown in Figures 3 and 4. The fluorescence emission maximum of both compounds displays a loss of vibrational structure in polar solvents together with a small red shift (Figures 3 and 4), indicating some charge transfer character of the excited state [26]. The red shifts are more significant for compound **2** (Table 1), which may be due to a higher capability of this compound to establish hydrogen bonds with protic solvents (especially with water), due to the presence of the OCH₃ group. Compound **1** has significantly higher fluorescence quantum yields (between 20 and 30%) than compound **2** (Φ_F between 1 and 5%), showing that the functionalization of the pyridine ring with a triple bond linked to a *p*-methoxyphenyl group causes a significant enhance of the non-radiative deactivation pathways. The fluorescence quantum yields of compound **1** are also higher than the ones of a benzo [*b*]thiophene derivative of the same type, a benzothienopyridopyrimidone [27], in which the benzene ring linked to the thiophene is substituted in compound **1** by a pyridine ring. The intrinsic fluorescence of

compounds **1** and **2** can be used to monitor interactions with DNA and compounds behaviour when encapsulated in liposomes.

Both compounds **1** and **2** were tested for their interaction with natural salmon sperm DNA using spectroscopic methods. For compound **1**, fluorescence intensity decreases with increasing DNA concentration, while the opposite happens for compound **2** (Figures 5 and 6). This behaviour, also previously observed for differently substituted tetracyclic lactams [28], may indicate a different type of interaction of both compounds with the DNA molecule. For the two compounds, full saturation (corresponding to spectral invariance with increasing DNA concentration) is attained at [DNA]/[compound] = 200, meaning that total binding is achieved at this ratio. The high [DNA]/[compound] ratio needed for total binding, together with the negligible changes observed in absorption spectra (not shown), point to a weak interaction of these molecules with the nucleic acid.

The intrinsic binding constants (K_i) and binding site sizes (n) were determined (Table 2) through the McGhee and von Hippel modification of Scatchard plot (Equation 1) [29],

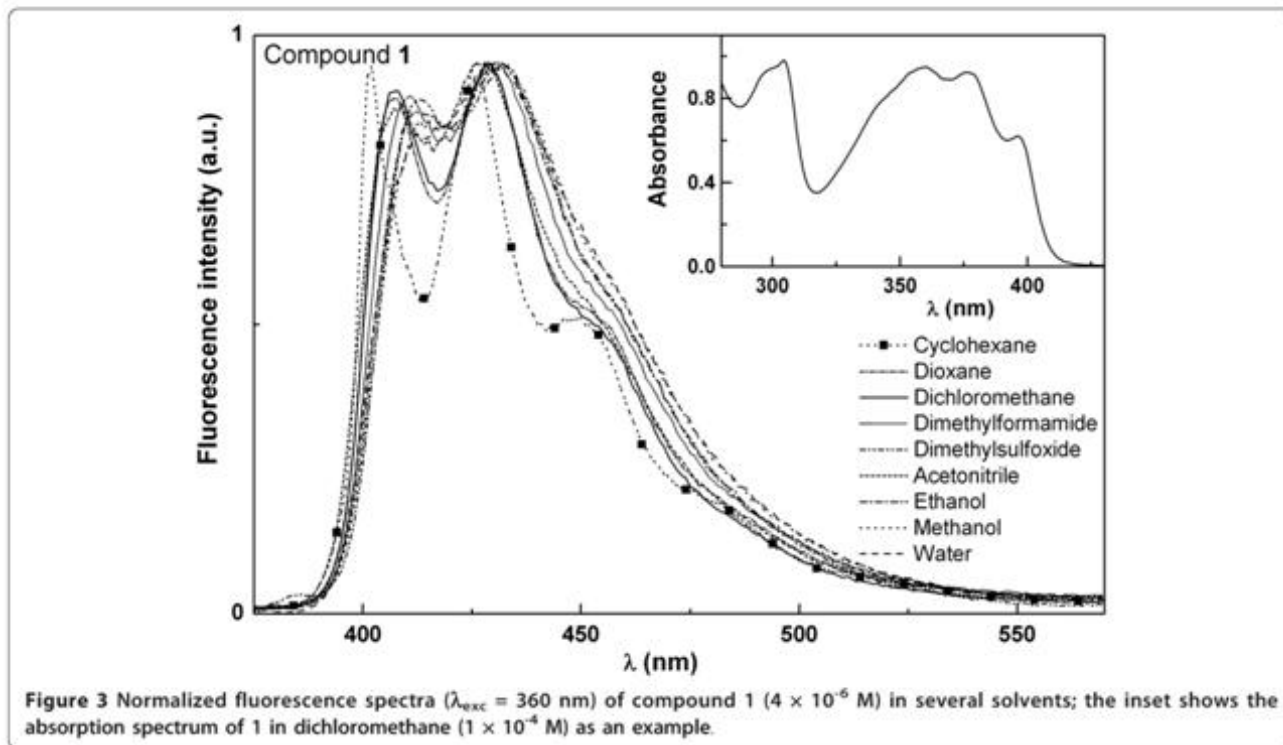
$$\frac{r}{c_f} = K_i (1 - nr) \left[\frac{1 - nr}{1 - (n - 1)r} \right]^{n-1} \quad (1)$$

where K_i is the intrinsic binding constant, n the binding site size, r the ratio $c_b/[DNA]$ and c_b and c_f the concentrations of bound and free compound, respectively, calculated by

Table 1 Maximum absorption (λ_{abs}) and emission (λ_{em}) wavelengths, molar absorption coefficients (ϵ) and fluorescence quantum yields of compounds **1 and **2** in several solvents**

Solvent	λ_{abs} (nm) ($\epsilon/10^4 M^{-1} cm^{-1}$)				λ_{em} (nm)		Φ_F	
	1		2		1	2	1	2
Cyclohexane	398 (0.84); 377 (1.24); 360 (1.27); 305 (0.95); 258 (3.93)	411 sh (0.33); 354 (2.19); 347 (2.37); 308 (1.25); 291 (1.12); 270 (1.40)	402; 426; 452 sh	417; 441	0.20	0.047		
Dioxane	398 (0.76); 377 (1.18); 359 (1.20); 305 (1.17); 258 (3.60)	411 sh (0.66); 356 (5.36); 346 (5.40); 309 (3.23); 291 (2.98); 272 (3.33)	407; 428; 455 sh	425; 449	0.29	0.054		
Dichloromethane	397 (0.58); 377 (0.91); 360 (0.93); 305 (0.97); 259 (2.70)	410 sh (0.55); 357 (4.37); 311 (2.28); 290 (2.29); 273 (2.78)	408; 429	427; 448	0.26	0.022		
Acetonitrile	395 (0.68); 376 (1.06); 358 (1.06); 304 (1.09); 256 (3.32)	409 sh (0.66); 355 (5.76); 308 (3.41); 289 (3.20); 271 (3.67)	408; 428	450	0.21	0.036		
<i>N,N</i> -Dimethylformamide ^a	397 (0.78); 377 (1.19); 360 (1.16); 305 (1.19)	411 sh (0.69); 356 (5.52); 311 (3.11); 290 (2.86)	411; 430	453	0.30	0.047		
Dimethylsulfoxide ^a	397 (0.77); 378 (1.17); 361 (1.14); 305 (1.17)	412 sh (0.61); 357 (4.70); 313 (2.52)	413; 432	455	0.28	0.048		
Ethanol	396 (0.69); 375 (1.13); 358 (1.17); 304 (1.40); 256 (3.59)	408 sh (0.72); 355 (5.50); 311 (2.95); 272 (3.69)	412; 431	452	0.27	0.041		
Methanol	395 (0.67); 374 (1.08); 358 (1.10); 304 (1.34); 256 (3.43)	408 sh (0.62); 354 (5.00); 311 (2.80); 272 (3.41)	413; 433	453	0.26	0.040		
Water	394 (0.41); 374 (0.57); 361 (0.58); 303 (0.93); 256 (2.07)	420 sh (0.26); 358 (0.87); 314 (0.94); 278 (0.97)	413 sh; 433	505	0.22	0.012		

^aSolvent cut-offs: *N,N*-Dimethylformamide: 275 nm; Dimethylsulfoxide: 280 nm; sh: shoulder.

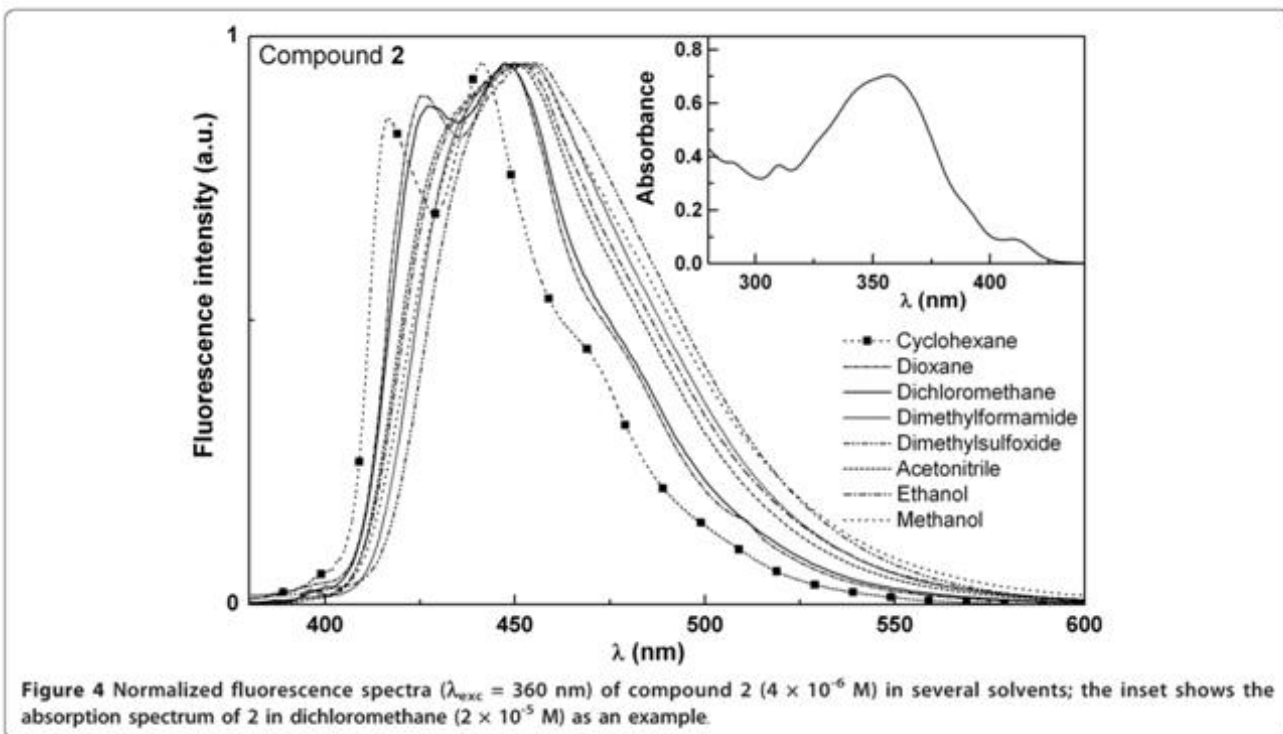


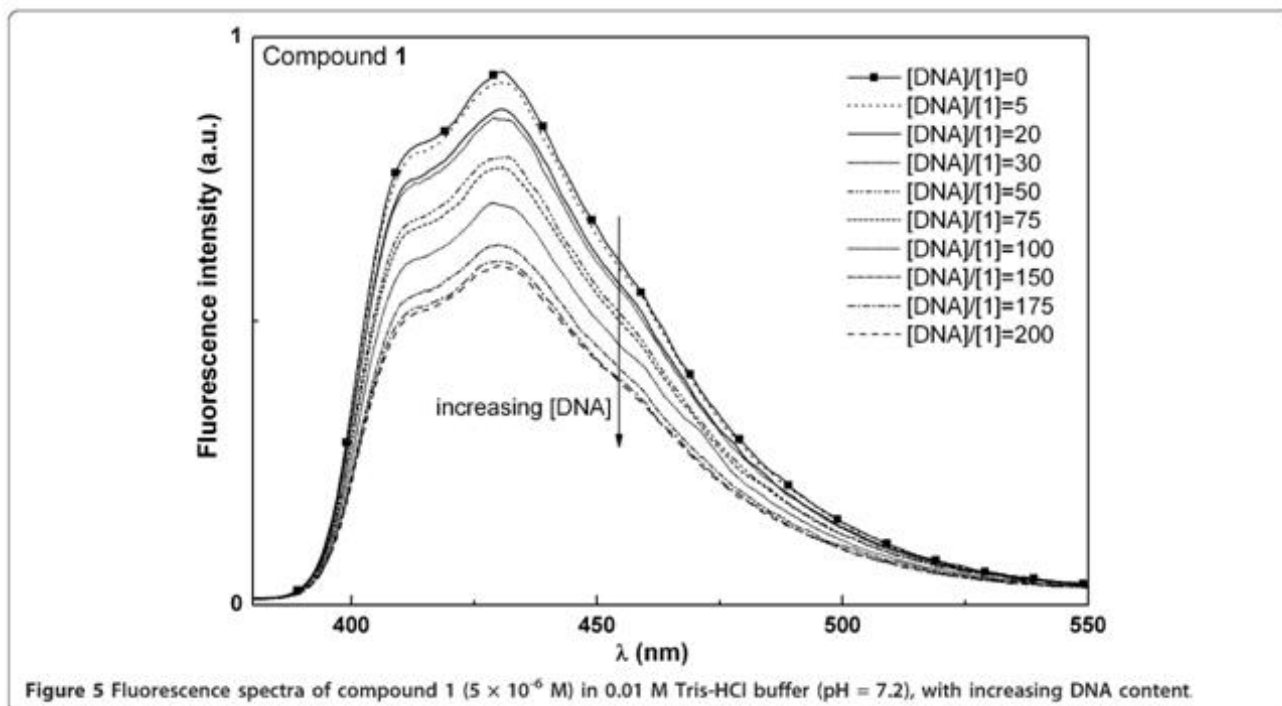
$$c_b = \frac{I_{F,0} - I_F}{I_{F,0} - I_{F,b}} \times c_{total}; \quad c_{total} = c_f + c_b \quad (2)$$

being $I_{F,0}$ the fluorescence intensity of the free compound and $I_{F,b}$ the fluorescence intensity of the bound compound at total binding. The binding constants

(Table 2) are moderately low, with a large number of base pairs between consecutive intercalated compound molecules (n).

Anionic quenchers can be useful in distinguishing between DNA binding modes [9,10]. Compounds that





are bound at the DNA surface (groove binding or electrostatic binding) are more accessible and emission from these molecules can be quenched more efficiently. Fluorescence quenching measurements using iodide ion showed that the usual Stern-Volmer plots (plots of the fluorescence intensity ratio in the absence, I_0 , and

presence, I , of quencher vs. quencher concentration) are not linear and exhibit a downward curvature (Figure 7A). This indicates that some compound molecules are not accessible to the anionic quencher, being intercalated between DNA base pairs. The modified Stern-Volmer plot [30] (Equation 3) allows the determination of

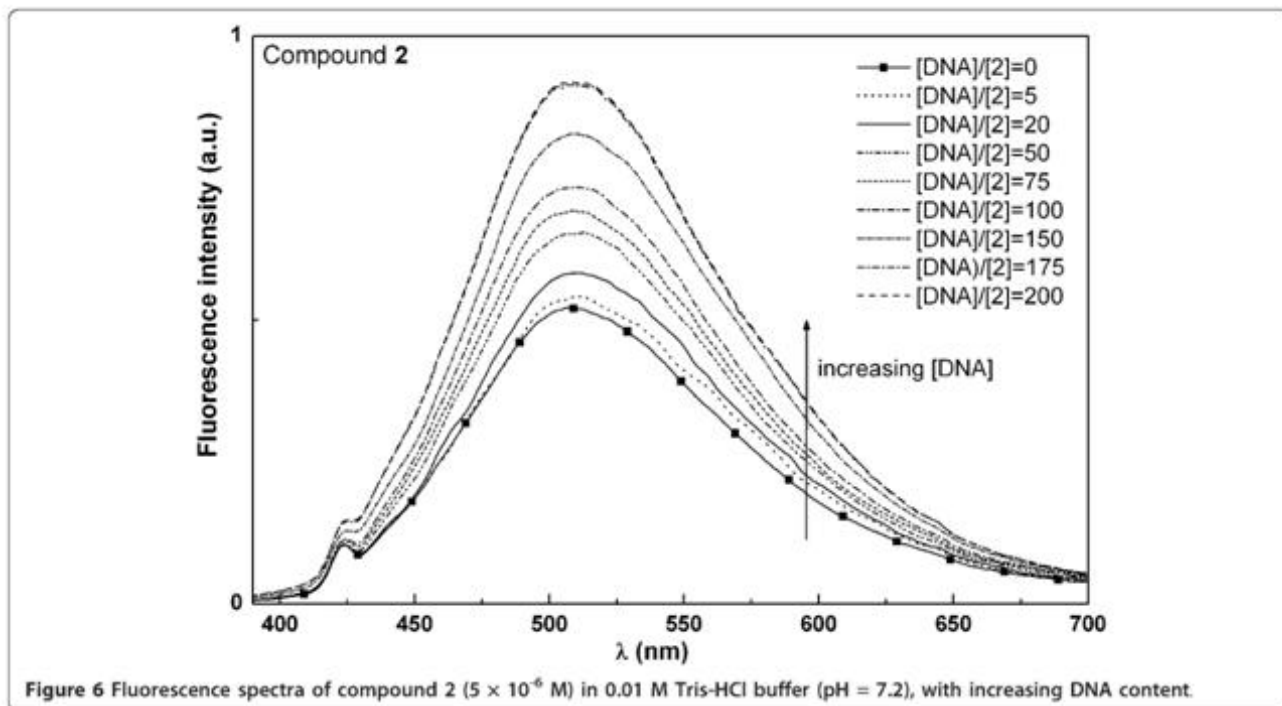


Table 2 Values of the intrinsic binding constants (K_i) and binding site sizes (n) and fraction of compound molecules accessible to external quenchers (f_a) for interaction with salmon sperm DNA

Compound	K_i (M^{-1})	n	f_a
1	$(8.7 \pm 0.9) \times 10^3$	11 ± 3	0.89
2	$(5.9 \pm 0.6) \times 10^3$	7 ± 2	0.65

the fraction of compound molecules accessible to quencher,

$$\frac{I_0}{\Delta I} = \frac{1}{f_a} + \frac{1}{f_a K_{SV} [Q]} \quad (3)$$

where I_0 is the fluorescence intensity in the absence of quencher, $\Delta I = I_0 - I$, K_{SV} the Stern-Volmer constant, $[Q]$ the quencher concentration and f_a the fraction of molecules accessible to quencher.

The representations of the modified Stern-Volmer plot are reasonably linear (Figure 7B) and the f_a values are in Table 2. Both compounds exhibit some intercalation in DNA, compound 2 being the more intercalative one, with a lower fraction (65%) of molecules accessible to anionic quencher. The higher hydrophobic character of compound 2, promoted by the functionalization of the pyridine with a triple bond linked to a *p*-methoxyphenyl group, may justify this behaviour. As both compounds 1 and 2 are neutral molecules (and electrostatic interaction with the negatively charged DNA molecule is not expected), the high f_a values indicate that the main type

of interaction with the nucleic acid must be the binding to DNA grooves [28].

Fluorescence experiments of both compounds encapsulated in liposomes of DPPC, DODAB and Egg-PC were carried out (Figure 8), in both gel (below T_m) and liquid-crystalline (above T_m) phases. The melting transition temperature of Egg-PC is very low [31] and this lipid is in the fluid liquid-crystalline phase at room temperature. Fluorescence spectra of compound 1 incorporated in liposomes (Figure 8, Table 3) are roughly similar to the one obtained in pure water, regarding the band shape and maximum emission wavelength. Compound 2 in liposomes presents emission spectra similar to those in polar solvents, significantly blue-shifted relative to water. In Egg-PC, a band enlargement is observed in the blue region, which can indicate two different locations of compound 2 in these liposomes, one deep in the hydrophobic region and another more close to the lipid polar heads.

Fluorescence anisotropy (r) measurements (Table 3) can give relevant information about the location of the compounds in liposomes, as r increases with the rotational correlation time of the fluorescent molecule (and, thus, with the viscosity of the fluorophore environment) [26]. Anisotropy values in a viscous solvent (glycerol) were also determined, for comparison. Anisotropy results (Table 3) allow to conclude that compound 2 is mainly located in the inner region of the lipid bilayer, feeling the penetration of some water molecules. The transition from the rigid gel phase to

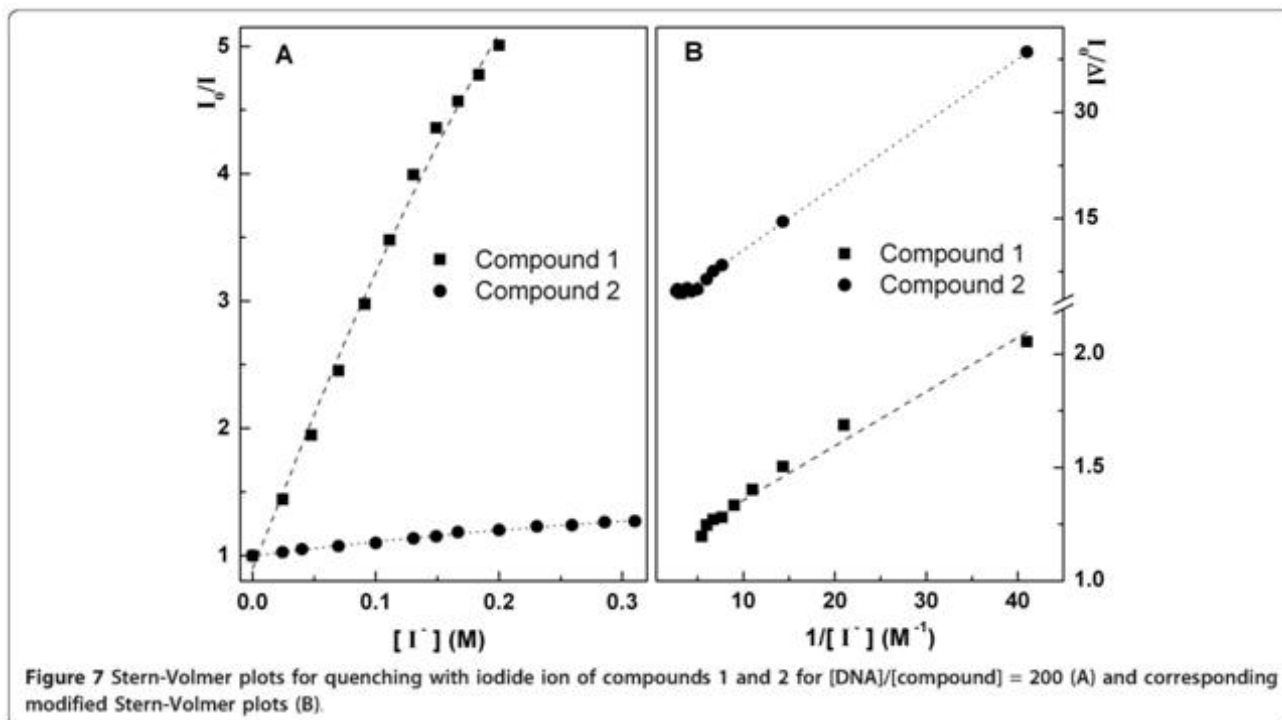


Figure 7 Stern-Volmer plots for quenching with iodide ion of compounds 1 and 2 for $[DNA]/[compound] = 200$ (A) and corresponding modified Stern-Volmer plots (B).

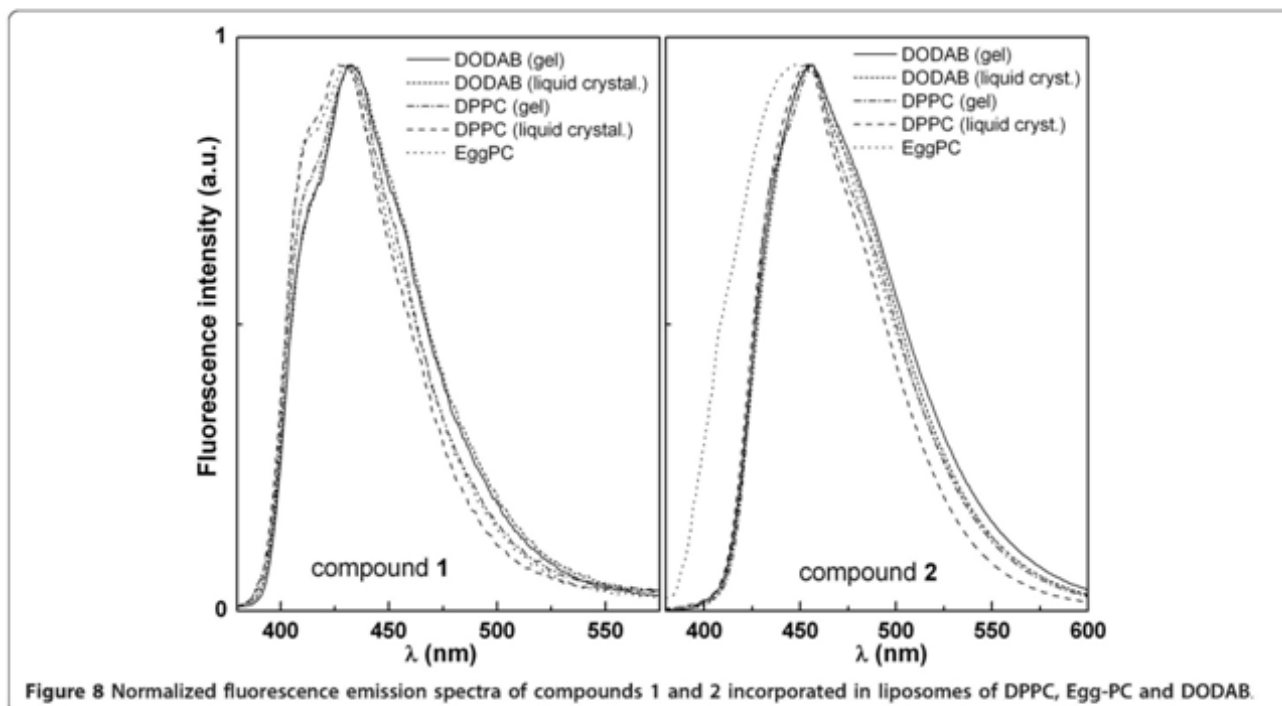


Figure 8 Normalized fluorescence emission spectra of compounds 1 and 2 incorporated in liposomes of DPPC, Egg-PC and DODAB.

the liquid-crystalline phase is clearly detected by a significant decrease in anisotropy at 55°C observed in DPPC and DODAB liposomes. Compound 1 exhibits a different behaviour and anisotropy is very low in all types of liposomes (and much lower than in glycerol, Table 3). Overall, the results indicate that compound 1 prefers a hydrated and fluid environment and the transition from the gel phase to the liquid-crystalline phase is not detected. To further clarify the location of compound 1, the solutions of liposomes with incorporated compound were passed through filters of 0.05 µm diameter. The fluorescence emission of the filtered solutions was negligible, indicating that compound 1 is mainly in the liposome aqueous interior or located at the interfaces, with a very hydrated environment. This behaviour is similar to the observed previously for a

benzothienopyridopyrimidone in lipid vesicles [27]. The encapsulation assays performed here may be important for future drug delivery applications of these potential antitumoral compounds using liposomes as drug carriers.

Conclusions

The interaction with DNA of two new potential antitumoral fluorescent planar thieno[3,2-*b*]pyridine derivatives was studied using spectroscopic methods. Compound 2 was shown to be the most intercalative compound in salmon sperm DNA (35%). The binding to DNA grooves seems to be the main type of interaction with the nucleic acid. Studies of incorporation of both compounds in liposomes of DPPC, Egg-PC and DODAB revealed that compound 2 is mainly located in the hydrophobic region of the lipid bilayer, while compound 1 prefers a hydrated and fluid environment. Our data thus suggest that both potential antitumoral compounds may be transported in liposomes for drug delivery applications.

Table 3 Steady-state fluorescence anisotropy (*r*) values and maximum emission wavelengths (λ_{em}) of compounds 1 and 2 incorporated in liposomes

	Compound 1		Compound 2	
	λ_{em}/nm	<i>r</i>	λ_{em}/nm	<i>r</i>
DPPC (25°C)	433	0.009	453	0.111
DPPC (55°C)	434	0.008	454	0.032
Egg-PC (25°C)	432	0.008	453	0.095
DODAB (25°C)	433	0.011	454	0.112
DODAB (55°C)	432	0.007	455	0.051
Glycerol (25°C)	437	0.166	472	0.202

Values in glycerol are also shown for comparison.

Abbreviations

DLS: dynamic light scattering; DODAB: dioctadecyldimethylammonium bromide; DPPC: dipalmitoyl phosphatidylcholine; DTS: Dispersion Technology Software; Egg-PC: egg yolk phosphatidylcholine; GUV: giant unilamellar vesicles; SV: small unilamellar vesicles.

Acknowledgements

This work was funded by FCT-Portugal through CFUM, CQ-UM, Project PTDC/QUI/81238/2006 (cofinanced by program FEDER/COMPETE, ref.

FCOMP-01-0124-FEDER-007467) and PhD grants of M.S.D. Carvalho (SFRH/BD/47052/2008) and R.C. Calhelha (SFRH/BD/29274/2006).

Author details

¹Centre of Physics (CFUM), University of Minho, Campus de Gualtar, Braga, 4710-057, Portugal ²Centre of Chemistry (CQ-UM), University of Minho, Campus de Gualtar, Braga, 4710-057, Portugal

Authors' contributions

EMSC conceived the study, was responsible for its coordination and for the interpretation of results, and drafted the manuscript. MSDC carried out the liposome preparation and the fluorescence studies in liposomes. AROR carried out the experimental studies of the compounds interaction with DNA. RCC carried out the synthesis, purification and characterization of the new compounds. MJRPQ supervised the organic synthesis and participated in the draft of the manuscript. All authors read and approved the final manuscript.

Competing interests

The authors declare that they have no competing interests.

Received: 28 September 2010 Accepted: 12 May 2011

Published: 12 May 2011

References

- Andresen TL, Jensen SS, Jorgensen K: **Advanced strategies in liposomal cancer therapy: Problems and prospects of active and tumor specific drug release.** *Prog Lipid Res* 2005, **44**:68.
- Ochekpe NA, Olorunfemi PO, Ngwuluka NC: **Nanotechnology and drug delivery. Part 1: Background and applications.** *Tropical J Pharm Res* 2009, **8**:265.
- Ochekpe NA, Olorunfemi PO, Ngwuluka NC: **Nanotechnology and drug delivery. Part 2: Nanostructures for Drug Delivery.** *Tropical J Pharm Res* 2009, **8**:275.
- Malam Y, Loizidou M, Seifalian AM: **Liposomes and nanoparticles: nanosized vehicles for drug delivery in cancer.** *Trends Pharmacol Sci* 2009, **30**:592.
- Calhelha RC, Queiroz M-JRP: **Synthesis of new thieno[3,2-b]pyridine derivatives by palladium-catalyzed couplings and intramolecular cyclizations.** *Tetrahedron Lett* 2010, **51**:281.
- Pedrosa de Lima MC, Simões S, Pires P, Faneca H, Düzgünes N: **Cationic lipid-DNA complexes in gene delivery: from biophysics to biological applications.** *Adv Drug Deliv Rev* 2001, **47**:277.
- Lyne PD: **Structure-based virtual screening: an overview.** *Drug Discovery Today* 2002, **7**:1047.
- Mahadevan S, Palaniandavar M: **Spectroscopic and voltammetric studies of copper(II) complexes of bis(pyrid-2-yl)-di/trithia ligands bound to calf thymus DNA.** *Inorg Chim Acta* 1997, **254**:291.
- Kumar CV, Asuncion EH: **DNA-binding studies and site-selective fluorescence sensitization of an anthryl probe.** *J Am Chem Soc* 1993, **115**:8547.
- Kumar CV, Punzalan EHA, Tan WB: **Adenine-thymine base pair recognition by an anthryl probe from the DNA minor groove.** *Tetrahedron* 2000, **56**:7027.
- Renault E, Fontaine-Aupart MP, Tfibel T, Gardes-Albert M, Bisagni E: **Spectroscopic study of the interaction of pazelliptine with nucleic acids.** *J Photochem Photobiol B Biol* 1997, **40**:218.
- Batzli S, Korn ED: **Single bilayer liposomes prepared without sonication.** *Biochim Biophys Acta* 1973, **298**:1015.
- Kremer JMH, Esker MWJvd, Pathmamanoharan C, Wiersema PH: **Vesicles of variable diameter prepared by a modified injection method.** *Biochemistry* 1977, **16**:3932.
- Nordlund JR, Schmidt CF, Dicken SN, Thompson TE: **Transbilayer distribution of phosphatidylethanolamine in large and small unilamellar vesicles.** *Biochemistry* 1981, **20**:3237.
- Cruz A, Casals C, Plasencia I, Marsh D, Pérez-Gil J: **Depth profiles of pulmonary surfactant protein B in phosphatidylcholine bilayers, studied by fluorescence and electron spin resonance spectroscopy.** *Biochemistry* 1998, **37**:9488.
- Tsunata LR, Carmona-Ribeiro AM: **Counterion effects on colloid stability of cationic vesicles and bilayer-covered polystyrene microspheres.** *J Phys Chem* 1996, **100**:7130.
- Pacheco LF, Carmona-Ribeiro AM: **Effects of synthetic lipids on solubilization and colloid stability of hydrophobic drugs.** *J Coll Interface Sci* 2003, **258**:146.
- Lentz BR: **Membrane fluidity as detected by diphenylhexatriene probes.** *Chem Phys Lipids* 1989, **50**:171.
- Feltosa E, Barreiros PCA, Olofsson G: **Phase transition in dioctadecyldimethylammonium bromide and chloride vesicles prepared by different methods.** *Chem Phys Lipids* 2000, **105**:201.
- Demas JN, Crosby GA: **Measurement of photoluminescence quantum yields - Review.** *J Phys Chem* 1971, **75**:991.
- Fey-Forgues S, Lavabre D: **Are fluorescence quantum yields so tricky to measure? A demonstration using familiar stationary products.** *J Chem Educ* 1999, **76**:1260.
- Morris JV, Mahaney MA, Huber JR: **Fluorescence quantum yield determinations - 9,10-Diphenylanthracene as a reference-standard in different solvents.** *J Phys Chem* 1976, **80**:969.
- Feltosa E, Brown W: **Fragment and vesicle structures in sonicated dispersions of dioctadecyldimethylammonium bromide.** *Langmuir* 1997, **13**:4810.
- Andersson M, Hammarström L, Edwards K: **Effect of bilayer phase-transitions on vesicle structure and its influence on the kinetics of viologen reduction.** *J Phys Chem* 1995, **99**:14531.
- Lopes A, Edwards K, Feltosa E: **Extruded vesicles of dioctadecyldimethylammonium bromide and chloride investigated by light scattering and cryogenic transmission electron microscopy.** *J Coll Interface Sci* 2008, **322**:582.
- Valeur B: **Molecular Fluorescence - Principles and Applications** Weinheim: Wiley-VCH; 2002.
- Castanheira EMS, Pinto AMR, Queiroz MJRP: **Fluorescence of a benzothienopyridopyrimidone in solution and in lipid vesicles.** *J Fluorescence* 2006, **16**:251.
- Queiroz M-JRP, Castanheira EMS, Lopes TCT, Cruz YK, Kirsch G: **Synthesis of fluorescent tetracyclic lactams by a "one pot" three steps palladium-catalyzed borylation, Suzuki coupling (BSC) and lactamization. DNA and polynucleotides binding studies.** *J Photochem Photobiol A Chem* 2007, **190**:45.
- McGhee JD, von Hippel PH: **Theoretical aspects of DNA-protein interactions - Cooperative and non-cooperative binding of large ligands to a one-dimensional homogeneous lattice.** *J Mol Biol* 1974, **86**:469.
- Lehrer SS: **Solute perturbation of protein fluorescence - quenching of tryptophyl fluorescence of model compounds and of lysozyme by iodide ion.** *Biochemistry* 1971, **10**:3254.
- Papahadjopoulos D, Miller N: **Phospholipid model membranes. I. Structural characteristics of hydrated liquid crystals.** *Biochim Biophys Acta* 1967, **135**:624.

doi:10.1186/1556-276X-6-379

Cite this article as: Castanheira et al.: New potential antitumoral fluorescent tetracyclic thieno[3,2-b]pyridine derivatives: interaction with DNA and nanosized liposomes. *Nanoscale Research Letters* 2011 **6**:379.

Submit your manuscript to a SpringerOpen® journal and benefit from:

- Convenient online submission
- Rigorous peer review
- Immediate publication on acceptance
- Open access: articles freely available online
- High visibility within the field
- Retaining the copyright to your article

Submit your next manuscript at ► springeropen.com

Fluorescence studies on potential antitumor 6-(hetero)arylthieno[3,2-*b*]pyridine derivatives in solution and in nanoliposomes

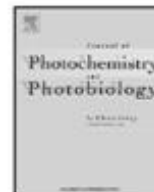
M. Solange D. Carvalho, Ana C.L. Hortelão, Ricardo C. Calhelha, Ana S. Abreu, Paulo J.G. Coutinho, Maria-João R.P. Queiroz, Elisabete M.S. Castanheira, J. *Photochem.Photobiol. A: Chem.*, **2013**, 264, 56-66.

My contribution to this paper was the photophysical studies of the compounds in several solvents, and fluorescence and DLS (size and zeta potential) measurements of the compounds encapsulated in nanoliposomes of different formulations.



Contents lists available at SciVerse ScienceDirect

Journal of Photochemistry and Photobiology A: Chemistry

journal homepage: www.elsevier.com/locate/jphotochem

Fluorescence studies on potential antitumor 6-(hetero)arylthieno[3,2-*b*]pyridine derivatives in solution and in nanoliposomes

M. Solange D. Carvalho^{a,b}, Ana C.L. Hortelão^a, Ricardo C. Calhela^b, Ana S. Abreu^{a,b}, Paulo J.G. Coutinho^a, Maria-João R.P. Queiroz^b, Elisabete M.S. Castanheira^{a,*}

^a Centro de Física, Universidade do Minho (CFUM), Campus de Gualtar, 4710-057 Braga, Portugal

^b Centro de Química, Universidade do Minho (CQUM), Campus de Gualtar, 4710-057 Braga, Portugal

ARTICLE INFO

Article history:

Received 6 February 2013

Received in revised form 15 April 2013

Accepted 30 April 2013

Available online xxx

Keywords:

Thienopyridine derivatives

Antitumor compounds

Fluorescence anisotropy

Nanoliposomes

ABSTRACT

The photophysical properties (absorption and fluorescence) of four 6-(hetero)arylthieno[3,2-*b*]pyridine derivatives, the methyl 3-amino-6-(thien-3-yl)thieno[3,2-*b*]pyridine-2-carboxylate **1**, the methyl 3-amino-6-(2,2'-bithienyl-5-yl)thieno[3,2-*b*]pyridine-2-carboxylate **2**, the methyl 3-amino-6-(thien-2-yl)thieno[3,2-*b*]pyridine-2-carboxylate **3** and the methyl 3-amino-6-(fur-3-yl)thieno[3,2-*b*]pyridine-2-carboxylate **4**, evaluated previously as potential antitumor compounds, were studied in solvents of different polarity. All compounds have reasonable fluorescence quantum yields and exhibit a solvatochromic behaviour.

The thienopyridine derivatives were incorporated in lipid membranes of neat egg-yolk phosphatidylcholine (egg-PC), dipalmitoyl phosphatidylcholine (DPPC), dipalmitoyl phosphatidylglycerol (DPPG) and dioctadecyldimethylammonium bromide (DODAB). Fluorescence measurements indicate that all compounds are mainly located in the lipid bilayer, feeling the transition from the rigid gel phase to the liquid-crystalline phase.

The most promising antitumor compounds, the thien-3-yl and the 2,2'-bithienyl-5-yl thienopyridine derivatives **1** and **2**, were encapsulated in different nanoliposome formulations, considering future drug delivery applications using liposomes as carriers. Almost all the liposomes with incorporated compounds have diameters lower than 165 nm and generally low polydispersity. The formulation DPPC:DMPG:DSPE-PEG (1:1:0.1) exhibits a small diameter (below 100 nm), low polydispersity and reasonable negative zeta-potential values for both thienopyridines **1** and **2**.

© 2013 Elsevier B.V. All rights reserved.

1. Introduction

For some years now, our research group has synthesized a large variety of new fluorescent potential antitumoral heteroaromatic compounds and studies of their incorporation in nanosized liposomes using fluorescence techniques have been performed [1–3]. These studies are very useful for drug delivery purposes, with the possibility of carrying the drug in the hydrophobic region of the liposomes.

Thienopyridine derivatives have shown interesting biological activities, including 3-amino-6-thien-2-yl-thieno[2,3-*b*]pyridin-2-yl)arylmethanones against a tumorigenic cell line [4], diarylamine derivatives of thieno[3,2-*b*]pyridines [5], substituted thieno[3,2-*c*]pyridine ureas [6] and diarylether derivatives

of thieno[3,2-*b*]pyridine phenylacetylthioureas [7] as inhibitors of the vascular endothelial growth factor receptor (VEGFR-2), related to angiogenesis and metastasis.

More recently, some of us have described the synthesis of a wide variety of 6-(hetero)arylthieno[3,2-*b*]pyridines by Suzuki-Miyaura cross-coupling of the methyl 3-amino-6-bromothieno[3,2-*b*]pyridine-2-carboxylate with several heteroaryl pinacolboranes or potassium trifluoroborates. The Suzuki coupling products were evaluated for their growth inhibitory effect on three human tumour cell lines, representing different tumour models, MCF-7 (breast adenocarcinoma), A375-C5 (melanoma) and NCI-H460 (non-small cell lung cancer). Some of the compounds showed an interesting activity against the tested cell lines, namely compound **1** (Fig. 1) presenting low growth inhibition concentration values (GI_{50}) in all the tested cells (12 μ M), and compound **2** (Fig. 1) presenting very low GI_{50} values in MCF7 and NCI-H460 cells (1 μ M) [8]. These promising results suggested us to perform fluorescence studies of incorporation of these compounds in nanoliposomes, for future drug delivery purposes.

* Corresponding author. Tel.: +351 253 604321; fax: +351 253 604061.

E-mail addresses: ecoutinho@fisica.uminho.pt, emscoutinho@gmail.com (E.M.S. Castanheira).

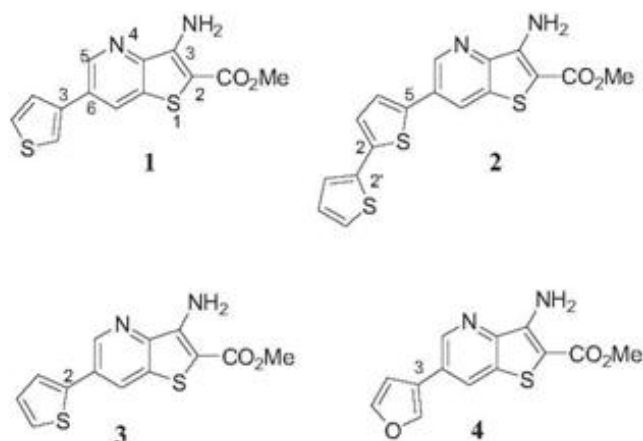


Fig. 1. Structure of the methyl 6-(hetero)arylthieno[3,2-*b*]pyridine-2-carboxylate derivatives 1–4.

Herein we report photophysical properties of four 6-(hetero)arylthieno[3,2-*b*]pyridine derivatives 1–4 (Fig. 1) in solution and in lipid bilayers of phospholipid components of biological membranes, either zwitterionic (egg-PC and DPPC) or anionic (DPPG), and also in bilayers of the cationic synthetic lipid DODAB. Fluorescence (steady-state) anisotropy measurements were also performed to obtain further information about the behaviour of the different 6-(hetero)arylthieno[3,2-*b*]pyridine derivatives in lipid membranes. These studies are very important, keeping in mind the incorporation of these compounds in liposomes for controlled drug delivery systems. Considering this possibility, the most potent antitumor compounds, particularly the thien-3-yl and the 2,2'-bithienyl-5-yl thienopyridine derivatives 1 and 2 [8] were encapsulated in different nanoliposome formulations and the mean size, size distribution, zeta potential, and stability were evaluated.

2. Experimental

2.1. Spectroscopic measurements

All the solutions were prepared using spectroscopic grade solvents and ultrapure water (Milli-Q grade). Absorption spectra were recorded in a Shimadzu UV-3101PC UV-Vis-NIR spectrophotometer. Fluorescence measurements were performed using a Fluorolog 3 spectrofluorimeter, equipped with double monochromators in both excitation and emission, Glan-Thompson polarizers and a temperature controlled cuvette holder. Fluorescence spectra were corrected for the instrumental response of the system.

For fluorescence quantum yield determination, the solutions were previously bubbled for 30 minutes with ultrapure nitrogen. The fluorescence quantum yields (Φ_s) were determined using the standard method (Eq. (1)) [9,10]. Quinine sulfate in sulfuric acid 0.05 M was used as reference, $\Phi_r = 0.546$ at 25 °C [11].

$$\Phi_s = \frac{(A_r F_s n_s^2)}{(A_s F_r n_r^2)} \Phi_r \quad (1)$$

where A is the absorbance at the excitation wavelength, F the integrated emission area and n the refraction index of the solvents used. Subscripts refer to the reference (r) or sample (s) compound. The absorbance at the excitation wavelength was always lower than 0.1 to avoid the inner filter effects.

Solvatochromic shifts are usually described by the Lippert-Mataga equation (2), where the energy difference between

absorption and emission maxima is related to the orientation polarizability [12,13],

$$\bar{\nu}_{\text{abs}} - \bar{\nu}_{\text{fl}} = \frac{1}{4\pi\epsilon_0} \frac{2 \Delta\mu^2}{hcR^3} \Delta f + \text{const} \quad (2)$$

$\bar{\nu}_{\text{abs}}$ is the wavenumber of maximum absorption, $\bar{\nu}_{\text{fl}}$ is the wavenumber of maximum emission, $\Delta\mu = \mu_e - \mu_g$ is the difference in the dipole moment of solute molecule between excited (μ_e) and ground (μ_g) states, R is the cavity radius, and Δf is the orientation polarizability given by (Eq. (3)):

$$\Delta f = \frac{\epsilon - 1}{2\epsilon + 1} - \frac{n^2 - 1}{2n^2 + 1}, \quad (3)$$

where ϵ is the static dielectric constant and n the refractive index of the solvent.

Bakhshiev proposed an alternative expression that considers the angle, γ , between the ground and excited state dipole moments of the fluorescent molecule [14,15]:

$$\bar{\nu}_{\text{abs}} - \bar{\nu}_{\text{fl}} = \frac{1}{4\pi\epsilon_0} \frac{2}{hcR^3} (\mu_g^2 - 2\mu_g\mu_e \cos \gamma + \mu_e^2) f(\epsilon, n) + \text{const} \quad (4)$$

where $\mu_g^2 - 2\mu_g\mu_e \cos \gamma + \mu_e^2$ is equivalent to $|\tilde{\mu}_e - \tilde{\mu}_g|^2$ and

$$f(\epsilon, n) = \frac{\epsilon - 1}{\epsilon + 2} - \frac{n^2 - 1}{n^2 + 2} \quad (5)$$

The steady-state fluorescence anisotropy, r , is given by

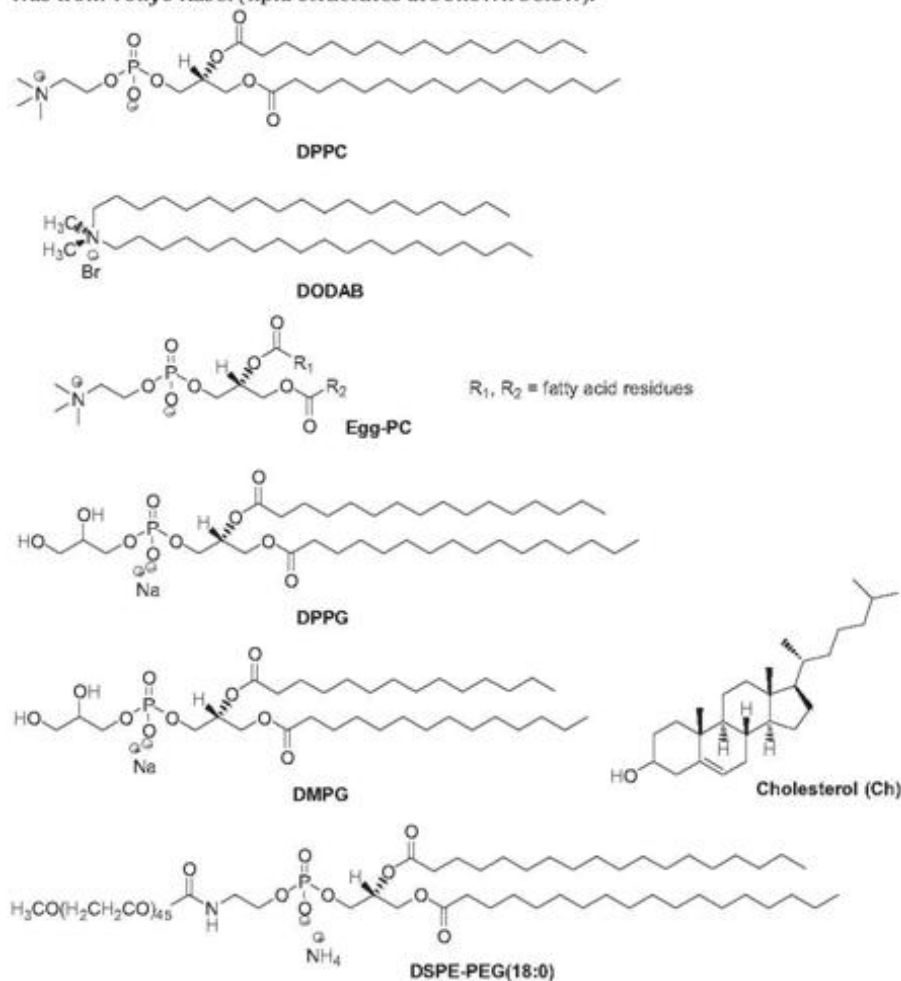
$$r = \frac{I_{VV} - GI_{VH}}{I_{VV} + 2GI_{VH}} \quad (6)$$

where I_{VV} and I_{VH} are the intensities of the emission spectra obtained with vertical and horizontal polarization, respectively (for vertically polarized excitation light), and $G = I_{HV}/I_{HH}$ is the instrument correction factor, where I_{HV} and I_{HH} are the emission intensities obtained with vertical and horizontal polarization (for horizontally polarized excitation light).

2.2. Liposomes preparation

1,2-Dipalmitoyl-*sn*-glycero-3-phosphocholine (DPPC), 1,2-diacyl-*sn*-glycero-3-phosphocholine from egg yolk (egg-PC), 1,2-dipalmitoyl-*sn*-glycero-3-[phospho-*rac*-(1-glycerol)] (sodium salt) (DPPG), 1,2-dimyristoyl-*sn*-glycero-3-[phospho-*rac*-(1-glycerol)] (sodium salt) (DMPG) and cholesterol (Ch) were obtained from Sigma-Aldrich. 1,2-Distearoyl-*sn*-glycero-3-phosphoethanolamine-*N*-[methoxy(polyethylene glycol)-2000] (ammonium salt) (DSPE-PEG) was obtained from Avanti Polar Lipids, while dioctadecyldimethylammonium bromide (DODAB)

was from Tokyo Kasei (lipid structures are shown below).



Nanoliposomes were prepared by evaporation of a mixture of lipids and compound in chloroform under vacuum for 12 h. The lipid/compound film was then hydrated with an aqueous buffer solution (10 mM Tris-HCl buffer, pH = 7.4), above the lipids melting transition temperature (*ca.* 41 °C for DPPC [16], 45 °C for DODAB [17], 40 °C for DPPG [18] and 23 °C for DMPG [19]), followed by six extrusion cycles (using a LIPEX™ extruder) through 100 nm polycarbonate membranes. Between the extrusion cycles, the solutions were allowed to equilibrate for 1 h. The final total lipid concentration was 1 mM, with a compound/lipid molar ratio of 1:333.

2.3. DLS and zeta potential measurements

Liposomes mean diameter and size distribution (polydispersity index) were measured using a Dynamic Light Scattering (DLS) equipment (NANO ZS Malvern Zetasizer), at 25 °C, using a He-Ne laser of 633 nm and a detector angle of 173°. Five independent measurements were performed for each sample. Malvern Dispersion Technology Software (DTS) was used with multiple narrow mode (high resolution) data processing, and mean size (nm) and error values were considered.

3. Results and discussion

3.1. Fluorescence studies in several solvents

The absorption and fluorescence properties of the 6-(hetero)arylthieno[3,2-*b*]pyridine derivatives **1–4** (Fig. 1) were studied in several solvents of different polarity. The maximum

absorption (λ_{abs}) and emission wavelengths (λ_{em}), molar absorption coefficients and fluorescence quantum yields of the four compounds are presented in Table 1 (compound **2** is not soluble in water). The normalized fluorescence spectra of each compound are shown in Fig. 2 (examples of absorption spectra are displayed as insets).

At the lowest energy absorption maximum, compounds **1–4** present moderate to high ϵ values, except in water ($\epsilon \geq 6 \times 10^3 \text{ M}^{-1} \text{ cm}^{-1}$) (Table 1). These four thienopyridine derivatives also exhibit very reasonable fluorescence quantum yields in several polar and non-polar solvents (attaining 30–50% for compounds **1** and **4**), but present significantly lower fluorescence in alcohols and water. Many carbonyl compounds exhibit low fluorescence quantum yields due to the low-lying $n \rightarrow \pi^*$ state. As all the thienopyridines **1–4** have a carboxylate group in their structure, it is possible that the electronic transitions $\pi \rightarrow \pi^*$ and $n \rightarrow \pi^*$ could be nearby in energy giving rise to a state-mixing [20], as already observed for other thienopyridine derivatives synthesized by our group [21,22].

The low fluorescence emission exhibited in protic solvents can be due to specific solute-solvent interactions by hydrogen bonds [12] in the excited state, namely by protonation of the N atom of the pyridine ring. A similar behaviour was already observed for the potential antitumoral methoxylated di(hetero)arylethers in the thieno[3,2-*b*]pyridine series [21] and for 1,3-diaryleureas linked to methyl 3-aminothieno[3,2-*b*]pyridine-2-carboxylate moiety, previously studied by some of us [22].

For all the four compounds, significant red shifts are observed for fluorescence emission in polar solvents (*ca.* 50 nm between

Table 1
Maximum absorption (λ_{abs}) and emission wavelengths (λ_{em}), molar absorption coefficients (ϵ) and fluorescence quantum yields (Φ_f) for 1–4 in several solvents.

Solvent	$\lambda_{\text{abs}}/\text{nm}$ ($\epsilon/10^4 \text{ M}^{-1} \text{ cm}^{-2}$)				λ_{em} (nm)				Φ_f^b			
	1	2	3	4	1	2	3	4	1	2	3	4
Cyclohexane	374 (0.65)	370 (2.13)	379 (0.92)	370 (0.75)	439	439; 458	442	436	0.05	0.30	0.09	0.17
	320 (1.16)	280 (1.12)	334 (1.78)	321 (1.18)								
	296 (3.31)		306 (3.16)	295 (3.62)								
Dioxane	377 (0.71)	374 (3.83)	380 (0.89)	372 (0.55)	457	458	458	449	0.14	0.09	0.06	0.14
	325 (1.27)	281 (1.81)	336 (1.71)	324 (0.88)								
	298 (3.23)		308 (2.82)	297 (2.42)								
			275 (1.23)	248 (0.78)								
Dichloromethane	372 (0.70)	378 (3.24)	374 (0.93)	373 (0.64)	462	476	467	459	0.09	0.12	0.02	0.05
	327 (1.25)	281 (1.67)	339 (1.71)	326 (1.06)								
	297 (2.82)		307 (2.51)	296 (2.57)								
			274 (1.27)	245 (0.97)								
Dimethylsulfoxide*	377 (0.81)	383 (3.85)	382 (1.01)	374 (0.83)	481	501	489	475	0.53	0.09	0.13	0.36
	329 (1.42)	284 (1.81)	341 (1.80)	328 (1.38)								
	301 (3.09)		312 (2.64)	300 (2.99)								
<i>N,N</i> -Dimethylformamide*	374 (0.76)	378 (3.93)	380 (0.95)	373 (1.05)	472	493	483	468	0.33	0.06	0.15	0.41
	328 (1.37)	282 (1.95)	339 (1.75)	326 (1.74)								
	299 (3.06)		310 (2.66)	298 (4.01)								
			274 (1.27)	245 (0.97)								
Acetonitrile	368 (0.78)	374 (3.71)	374 (0.91)	367 (0.72)	464	486	475	460	0.06	0.12	0.06	0.15
	325 (1.43)	279 (1.85)	338 (1.76)	324 (1.23)								
	295 (3.18)		305 (2.65)	294 (3.00)								
			245 (1.09)									
Ethanol	374 (0.65)	376 (3.47)	375 (0.90)	372 (0.91)	465	483	474	465	0.01	0.02	0.04	0.03
	327 (1.23)	281 (1.74)	338 (1.76)	326 (1.48)								
	297 (3.11)		308 (2.87)	296 (3.46)								
			274 (1.33)	248 (1.44)								
Methanol	373 (0.71)	375 (3.61)	376 (0.94)	370 (0.59)	468	487	481	467	0.004	0.01	0.02	0.02
	326 (1.31)	281 (1.91)	338 (1.77)	325 (0.99)								
	296 (3.13)		307 (2.84)	295 (2.45)								
			274 (1.42)	245 (0.94)								
Water	375 (0.22)	–	378 (0.32)	374 (0.21)	488	–	491	485	0.006	–	0.03	0.04
	336 (0.47)		340 (0.45)	331 (0.38)								
	289 (0.67)		302 (0.56)	292 (0.49)								

*Solvents cut-off: Dimethylsulfoxide: 270 nm; *N,N*-dimethylformamide: 275 nm; Relative to quinine sulfate in 0.05 M sulfuric acid ($\Phi_f = 0.546$ [11]). Error about 10%.

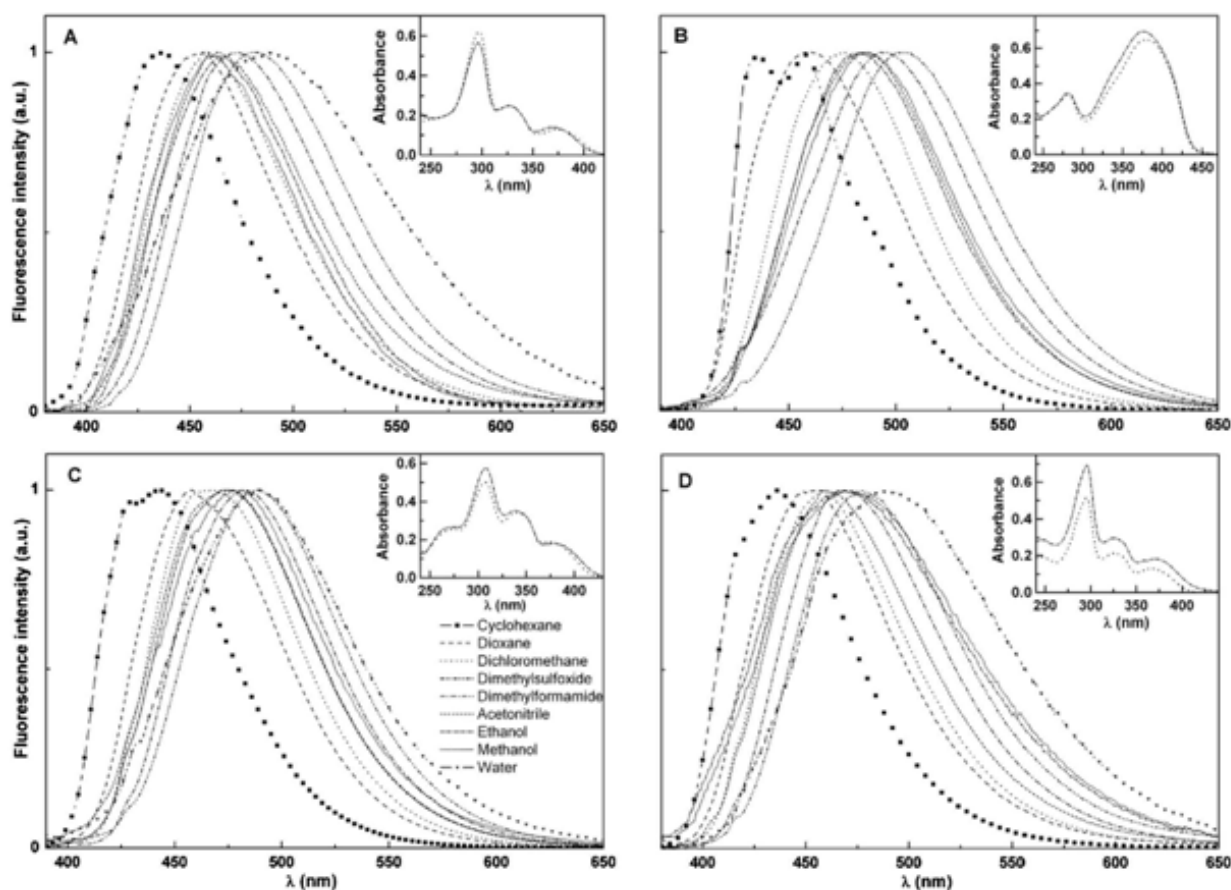


Fig. 2. Normalized fluorescence spectra (at peak of maximum emission) of 3×10^{-6} M solutions of each compound in several solvents. Insets: Absorption spectra of 2×10^{-5} M solutions of each compound in dichloromethane and ethanol, as examples (cell path = 1.0 cm). (A) compound 1 ($\lambda_{exc} = 370$ nm); (B) compound 2 ($\lambda_{exc} = 380$ nm); (C) compound 3 ($\lambda_{exc} = 380$ nm); (D) compound 4 ($\lambda_{exc} = 370$ nm).

cyclohexane and water), together with a band enlargement and loss of vibrational structure (for compounds 2 and 3) (Fig. 2). This behaviour is usually attributed to an intramolecular charge transfer mechanism or to specific solvent effects [12]. As in the absorption spectra the red shifts are negligible (Table 1), this behaviour indicates an important role for solvent relaxation after photoexcitation.

The solvatochromic plots obtained using Bakhshiev's relation (Eq. (4)) for compounds 1–4, shown in Fig. 3, are reasonably linear. Significant positive deviations are observed for the compounds in water, pointing to specific interactions by hydrogen bonding in the excited state. The slope of the plot is larger for compounds 2 and 3, showing that the presence of the 2,2'-bithienyl-5-yl or the thien-2-yl moiety in the 6-position of the thieno[3,2-*b*]pyridine causes an enhancement of the intramolecular charge transfer character of the excited state.

Using *ab initio* molecular quantum chemistry calculations, obtained with Gaussian 09 software [24] and use of a 6-311++G(d,p) basis set at the TD-SCF DFT (MPW1PW91) level of theory [25] in gas phase, the ground state dipole moment (μ_g), the excited state dipole moment (μ_e) and the cavity radius (R) were determined for these four compounds (Table 2).

The optimized geometries of the ground state of the thienopyridines 1–4 (Fig. 4), obtained with Gaussian software, show that the thiophene/bithiophene/furan moieties are completely out of the plane (but not perpendicular) of the thieno[3,2-*b*]pyridine system. In the lowest excited state, however, the ring systems of compounds 1–4 are completely planar (Fig. 4). The directions of the calculated dipole moments in the ground and excited states are also indicated in Fig. 4 (blue arrows), evidencing a change in the

excited state dipole moment vector to approximately the opposite direction relative to the ground state one. This behaviour indicates that the angle between the two dipole moment vectors must not be neglected and must be considered in the solvatochromic plots (Bakhshiev's relation).

The absolute value of the difference in the excited and ground state dipole moment vectors, estimated from the solvatochromic

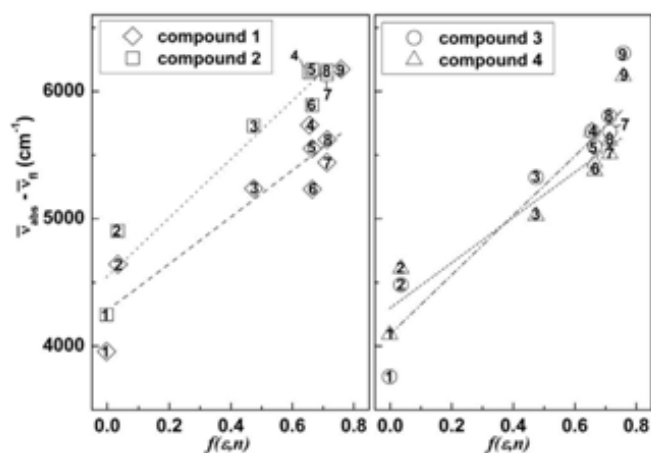


Fig. 3. Bakhshiev solvatochromic plots for compounds 1–4. Solvents: 1 – cyclohexane; 2 – dioxane; 3 – dichloromethane; 4 – dimethylsulfoxide; 5 – *N,N*-dimethylformamide; 6 – ethanol; 7 – methanol; 8 – acetonitrile; 9 – water (values of ϵ and n were obtained from Ref. [23]). Correlation coefficients: compound 1: $R^2 = 0.87$; compound 2: $R^2 = 0.94$; compound 3: $R^2 = 0.94$; compound 4: $R^2 = 0.92$.

Table 2

Cavity radius (R), ground (μ_g) and excited state (μ_e) dipole moments obtained from theoretical calculations, and absolute value of the dipole moment difference ($|\mu_e - \mu_g|$), from quantum mechanical calculations and from the solvatochromic plots.

Compound	Cavity radius, R (Å)	Ground state dipole moment, μ_g (D), from theoretical calculations	Excited state dipole moment, μ_e (D), from theoretical calculations	$ \mu_e - \mu_g $ (D) from theoretical calculations	$ \mu_e - \mu_g $ (D) from solvatochromic plots
1	5.19	2.29	3.27	5.43	5.04
2	5.88	2.79	4.57	7.29	6.81
3	5.29	2.55	3.69	6.13	5.85
4	5.06	1.90	3.29	5.08	4.78

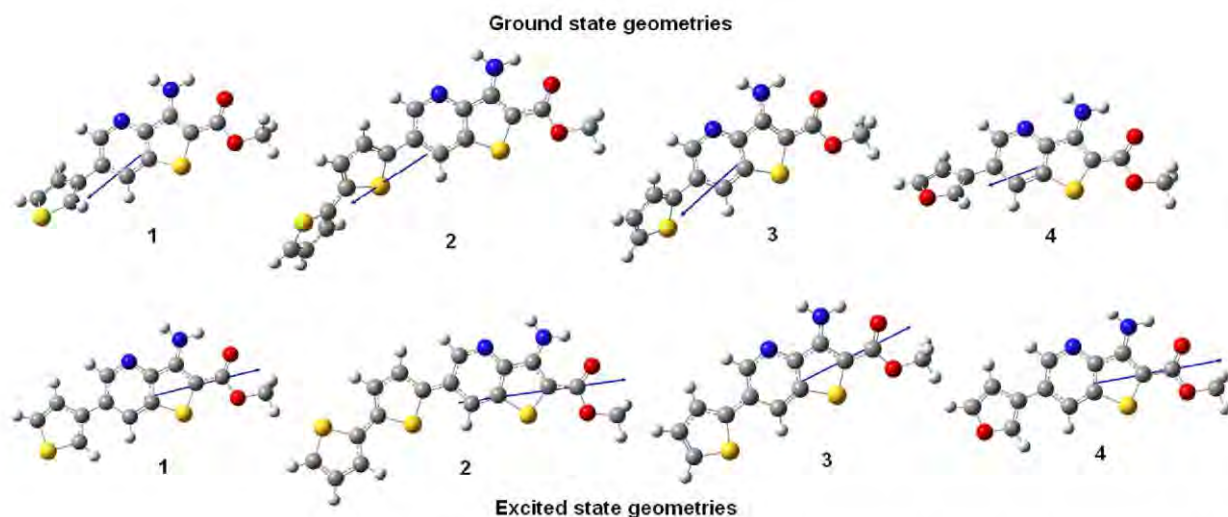


Fig. 4. Optimized geometries of compounds 1–4 obtained by Gaussian 09 software (grey: C atoms; white: H atoms; red: O atoms; blue: N atoms; yellow: S atoms). Left: ground state; Right: lowest excited singlet state. The arrows indicate the direction of the dipole moment.

plots (Fig. 3) and from the molecular quantum mechanical calculations (Gaussian software), are presented in Table 2. The $|\mu_e - \mu_g|$ values are roughly similar, the values obtained from the theoretical calculations exciding by 5–7% the ones estimated from the solvatochromic plots. Therefore, both the experimental solvatochromic plots and the theoretical calculations point to the occurrence of a significant charge transfer mechanism in the excited state, which is more pronounced for compound 2.

Fig. 5 shows the representation of electronic density difference between the lowest excited state and the ground state, for the

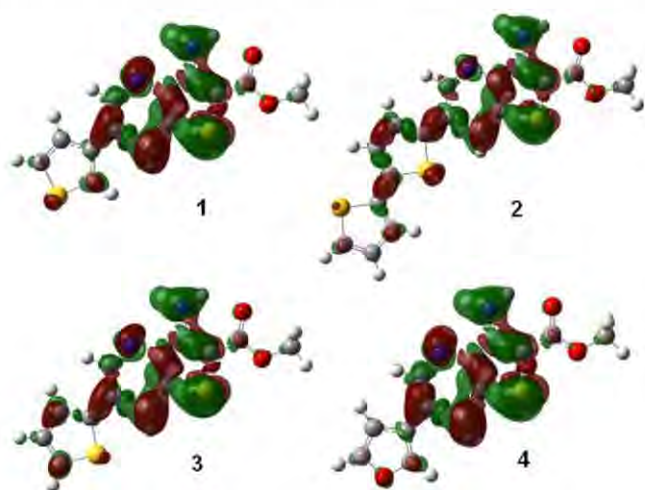


Fig. 5. Representation of the electronic density difference for compounds 1–4 (optimized geometry for the lowest excited singlet state) at an iso level of 0.001; green regions: loss of electronic density; red regions: enrichment of electronic density.

lowest excited state optimized geometry (relaxed S_1 state). In general, it can be observed that the electron density variations reside mostly on the thieno[3,2-*b*]pyridine moiety, as already reported for new 1,3-diylurea derivatives of thienopyridines [22]. Alternating increases and decreases of electronic density are observed in the π -electron system (Fig. 5). The more prominent features are an electron density transfer from the amino group linked to the thiophene ring of thienopyridine moiety and its sulfur atom to the nitrogen atom in the pyridine moiety and thiophene/bithiophene linked rings in compounds 2 and 3. This confirms the charge transfer character of the first excited state of these compounds, especially for the thieno[3,2-*b*]pyridine derivatives 2 and 3.

The representation of the energy level diagram with the transition energies for the four compounds is displayed in Fig. 6. The calculated absorption transition energies are in accordance with the maxima experimentally observed, especially for compounds 1, 3 and 4 (Table 1). These results predict Stokes' shifts of around 80 nm, coincident to those observed experimentally in dichloromethane. For these three compounds, a Stokes' shift of 86 nm for compound 1, 83 nm for compound 3 and 82 nm for compound 4 is obtained by the *ab initio* calculations. Compound 2 is the one with larger Stokes' shift (90 nm in dichloromethane). This shift is also predicted from the *ab initio* calculations (92 nm), but the calculated spectral maxima exhibit a red shift relative to those experimentally observed. As the *ab initio* calculations were performed in the gas phase, this discrepancy can be due to effects not accounted in these calculations.

In general, the photophysical behaviour of these four thienopyridine derivatives indicates that they can be considered as solvatochromic probes, compounds 1, 3 and 4 being fluorescent even in water. The significant sensitivity of the fluorescence emission to the fluorophore environment can be useful when

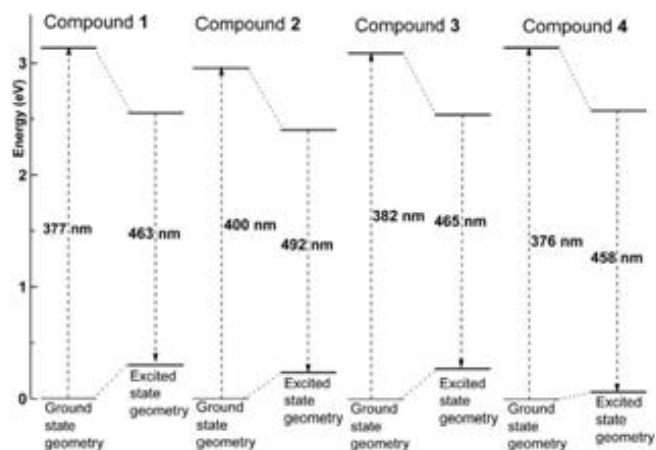


Fig. 6. Representation of the energy level diagram, with the transition energies for the four thienopyridine derivatives, obtained by molecular quantum chemistry calculations.

probing the location/behaviour of these molecules in liposomes, as described below.

3.2. Fluorescence studies in liposomes of neat lipids

Fluorescence experiments of thienopyridine derivatives 1–4 encapsulated in liposomes of several different compositions were carried out, keeping in mind future drug delivery applications of these thienopyridine derivatives as potential anticancer drugs.

First, liposomes of neat lipids, egg-PC (zwitterionic, composed of a phosphatidylcholine mixture), DPPC (16:0 phosphatidylcholine, zwitterionic), DPPG (16:0 phosphatidylglycerol, anionic), and DODAB (a cationic synthetic lipid with C₁₈ saturated chains), with encapsulated compounds 1–4, were prepared. Absorption and fluorescence emission spectra were measured in both gel (below the melting temperature, T_m) and liquid-crystalline (above T_m) phases of each lipid. At room temperature, both phospholipids DPPC and DPPG, as well as the cationic lipid DODAB, are in the ordered gel phase, where the hydrocarbon chains are fully extended and closely packed. Above the melting transition temperature (T_m = 41 °C for DPPC [16], T_m = 45 °C for DODAB [17], T_m = 40 °C for DPPG [18] and T_m = 23 °C for DMPC [19]), the lipid bilayer attains a disordered and fluid state (liquid-crystalline phase). At room temperature, egg lecithin (egg-PC) is in the fluid liquid-crystalline phase, as it is composed of molecules with the same polar head group (phosphatidylcholine) and different hydrocarbon chains (in length and unsaturation degree), the main components being 16:0 PC, 18:0 PC and 18:1 PC [26].

Fluorescence emission spectra of the thienopyridine derivatives 1–4 in liposomes of these lipids are shown in Fig. 7. Absorption spectra are presented as insets. The maximum absorption (λ_{abs}) and emission wavelengths (λ_{em}) and fluorescence quantum yields are presented in Table 3. In egg-PC, DPPC and DPPG liposomes at gel phase (25 °C), the emission spectra of compounds 1–4 are very similar to those in dichloromethane (Tables 1 and 3). This behaviour gives indication that these thienopyridines are mainly located in the lipid bilayer, experiencing the difference in fluidity between the rigid gel phase and the liquid-crystalline phase. For all the four compounds encapsulated in DODAB vesicles, the results point to a more polar and hydrated environment, near the lipid polar head groups, considering the significant red shift of the fluorescence spectra observed in these liposomes.

Relevant information about the location of these four compounds in liposomes can be obtained through fluorescence anisotropy (r) measurements. In fact, the anisotropy value increases

Table 3
Steady-state fluorescence anisotropy (r) values, maximum absorption (λ_{abs}) and emission wavelengths (λ_{em}) and fluorescence quantum yields (Φ_F) of compounds 1–4 incorporated in neat liposomes. Anisotropy values in glycerol at 25 °C are also shown, as well as the fundamental anisotropies (r₀), maximum wavelengths (λ_{0,0}) and oscillator strengths (f), obtained by theoretical calculations.

Lipid	T (°C)	1				2				3				4				
		λ _{abs} (nm)	λ _{em} (nm)	r	Φ _F	λ _{abs} (nm)	λ _{em} (nm)	r	Φ _F	λ _{abs} (nm)	λ _{em} (nm)	r	Φ _F	λ _{abs} (nm)	λ _{em} (nm)	r	Φ _F	
Egg-PC	25	376; 327; 299	458	0.122	0.09	383; 281	478	0.188	0.12	378; 341; 311; 276	477	0.180	0.06	373; 325; 297	461	0.174	0.04	
	55	372; 327; 299	460	0.216	0.09	384; 281	476	0.229	0.14	378; 340; 312; 276	475	0.215	0.04	372; 326; 296	459	0.224	0.04	
DPPC	25	372; 327; 299	460	0.168	0.02	384; 281	477	0.150	0.13	378; 340; 312; 276	479	0.146	0.03	372; 326; 296	457	0.156	0.03	
	55	372; 329; 299	470	0.223	0.08	386; 284	499	0.196	0.12	377; 344; 311; 277	488	0.193	0.04	372; 328; 295	473	0.212	0.06	
DODAB	25	372; 329; 299	475	0.158	0.04	386; 284	498	0.128	0.10	377; 344; 311; 277	486	0.120	0.03	372; 328; 295	472	0.154	0.04	
	55	371; 328; 298	460	0.093	0.02	383; 282	478	0.099	0.10	377; 340; 309; 277	474	0.095	0.02	372; 328; 295	457	0.083	0.02	
DPPG	25	371; 328; 298	459	0.071	0.01	383; 282	483	0.096	0.08	377; 340; 309; 277	477	0.064	0.01	372; 328; 295	456	0.054	0.01	
	55	371; 328; 298	459	0.332	-	383; 282	483	0.326	-	377; 340; 309; 277	477	0.327	-	372; 328; 295	456	0.324	-	
Glycerol	25	-	-	-	-	-	-	-	-	-	-	-	-	-	-	-	-	
	55	-	-	-	-	-	-	-	-	-	-	-	-	-	-	-	-	
Results from ab initio calculations		λ _{0,0} (nm)	f	r ₀	λ _{0,0} (nm)	f	r ₀	λ _{0,0} (nm)	f	r ₀	λ _{0,0} (nm)	f	r ₀	λ _{0,0} (nm)	f	r ₀	λ _{0,0} (nm)	f
S ₀ → S ₁		376	0.10	0.381	399	0.32	0.315	381	0.12	0.036	375	0.09	0.358	375	0.09	0.358	375	0.09
S ₀ → S ₂		310	0.04	-0.067	367	0.50	0.395	317	0.13	0.394	310	0.04	-0.073	310	0.04	-0.073	310	0.04
S ₀ → S ₃		295	0.55	0.296	325	0.14	0.393	304	0.51	0.319	295	0.39	0.337	295	0.39	0.337	295	0.39

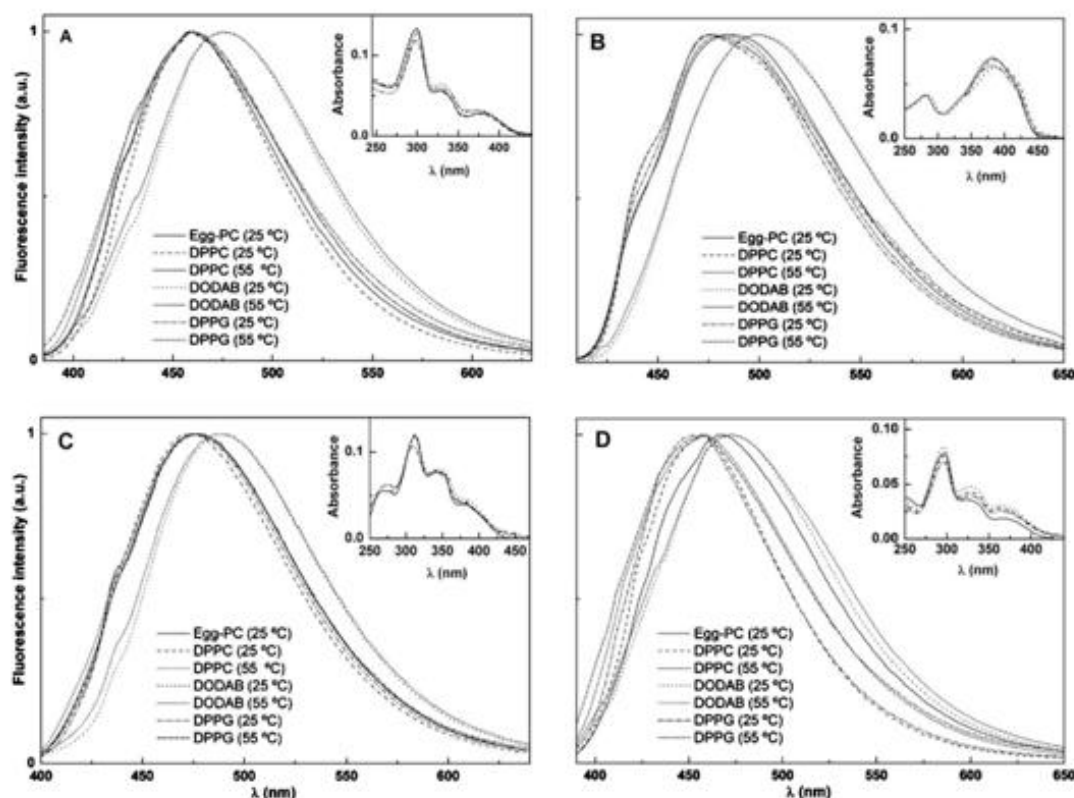


Fig. 7. Normalized fluorescence spectra of each compound in lipid membranes of egg-PC, DPPC, DPPG and DODAB. Insets: Absorption spectra at 25 °C. (A) compound 1 ($\lambda_{exc} = 370$ nm); (B) compound 2 ($\lambda_{exc} = 380$ nm); (C) compound 3 ($\lambda_{exc} = 380$ nm); (D) compound 4 ($\lambda_{exc} = 370$ nm).

with the rotational correlation time of the fluorescent molecule and, therefore, with the viscosity of the fluorophore environment (Eq. (7)) [27],

$$\frac{1}{r} = \frac{1}{r_0} \left(1 + \frac{\tau}{\tau_c} \right) \quad (7)$$

where r_0 is the fundamental anisotropy, τ is the excited-state lifetime and τ_c is the rotational correlation time.

The fluorescence steady-state anisotropies of each thienopyridine derivative in the several neat liposomes, as well as the anisotropy values in glycerol at room temperature, are shown in Table 3. The calculated fundamental anisotropy values (*ab initio* results, using S_1 state relaxed geometry), arising from photoselection by excitation to the first three electronic excited states, are also presented in Table 3, as well as the corresponding oscillator strengths, f , and transition wavelengths, λ_{0-0} . With the exception of compound 3, the fundamental anisotropy values resulting from excitation to the S_1 state are high and similar to the experimental anisotropies obtained in glycerol. For compound 3, it is upon excitation to the S_2 state that the fundamental anisotropy is high. From Tables 1 and 3, it can be observed that the thienopyridine 3 shows the smallest energy gap between S_1 and S_2 states, and also the highest difference between the experimental gap value and the calculated one (obtained in vacuum). From this, the interaction of compound 3 with solvent in the S_2 excited state is expected to be higher than in S_1 state. Thus, a significant amount of S_2 excitation is possible at the excitation wavelength used, especially in polar solvents, leading to a high fundamental anisotropy.

For all compounds, the transition from the rigid gel phase (25 °C) to the liquid-crystalline phase (55 °C) is detected by a clear reduction in anisotropy at 55 °C in the several lipid aggregates (Table 3). An increase of the steady-state anisotropy is predicted from a

diminution of the excited-state lifetime (Eq. (7)). Upon temperature increase, the excited-state lifetime is expected to decrease, due to the increment of non-radiative deactivation pathways (especially the rate constant for internal conversion $S_1 \rightarrow S_0$). Instead of an expected rise in anisotropy value (Eq. (7)), a diminution is observed, which can only be attributed to a decrease of the rotational correlation time of the fluorescent molecule, that comes from the decrease of membrane microviscosity upon changing from the gel to the liquid-crystalline phase [2,21,22].

In order to analyze the steady-state fluorescence anisotropy values at room temperature (Table 3), the Strickler–Berg equation [28], relating the radiative lifetime with the absorption intensity (Eq. (8)) could be used

$$\frac{1}{\tau_r} = 2.88 \times 10^{-9} n^2 \frac{\int F_{\nu}(\tilde{\nu}_F) d\tilde{\nu}_F}{\int \tilde{\nu}_F^{-3} F_{\nu}(\tilde{\nu}_F) d\tilde{\nu}_F} \int \frac{\varepsilon(\tilde{\nu}_A) d\tilde{\nu}_A}{\tilde{\nu}_A} \quad (8)$$

where τ_r is the radiative lifetime, n is the index of refraction, ε is the molar absorption coefficient, and $F_{\nu}(\tilde{\nu}_F)$ is the fluorescence intensity per unit wavenumber. This quantity is related to the fluorescence quantum yield [27], through

$$\int_{\infty}^0 F_{\nu}(\tilde{\nu}_F) d\tilde{\nu}_F = \Phi_F \quad (9)$$

Absorption spectra of each compound in the various lipid membranes at 25 °C (insets of Fig. 7) are roughly similar. In this case, the Strickler–Berg relation (Eq. (8)) predicts an approximately constant value for the radiative lifetime in all the lipid membranes, considering the small variations of the measured fluorescence quantum yields (an exception is compound 1 in DPPG, Table 3).

Table 4
Hydrodynamic diameter, polydispersity (PDI) and zeta potential (ζ) of several liposome formulations containing thienopyridine derivatives **1** and **2**, at 25 °C.

	Compound 1			Compound 2		
	Hydrodynamic diameter (nm) (mean \pm SD)	Polydispersity (mean \pm SD)	ζ (mV) (mean \pm SD)	Hydrodynamic diameter (nm) (mean \pm SD)	Polydispersity (mean \pm SD)	ζ (mV) (mean \pm SD)
Egg-PC:Ch (7:3)	82.2 \pm 0.9	0.194 \pm 0.008	-15.2 \pm 0.2	127.4 \pm 0.8	0.096 \pm 0.008	-10.5 \pm 0.3
Egg-PC:DSPE-PEG (9:1)	93 \pm 1	0.278 \pm 0.001	-5.25 \pm 0.04	81 \pm 2	0.33 \pm 0.04	-15.0 \pm 0.3
DPPC:DMPG (1:1)	81.7 \pm 0.5	0.47 \pm 0.023	-44.1 \pm 0.5	132.3 \pm 0.6	0.47 \pm 0.03	-39 \pm 2
DPPC:DMPG (2:1)	124.5 \pm 0.9	0.41 \pm 0.07	-46.4 \pm 0.6	122.5 \pm 0.8	0.34 \pm 0.04	-30 \pm 1
DPPC:DMPG (1:2)	59.8 \pm 0.7	0.43 \pm 0.09	-52 \pm 2	262 \pm 8	0.33 \pm 0.1	-47.4 \pm 0.4
DPPC:DMPG:DSPE-PEG (1:1:0.1)	94.6 \pm 0.2	0.264 \pm 0.004	-32.0 \pm 0.4	72 \pm 1	0.31 \pm 0.03	-22.7 \pm 0.7
DPPC:Ch:DSPE-PEG (7:2:1)	138 \pm 2	0.219 \pm 0.005	-6 \pm 1	163 \pm 1	0.23 \pm 0.02	-16.8 \pm 0.5
DPPC:DPPG:DSPE-PEG (1:1:0.1)	142 \pm 1	0.18 \pm 0.02	-25.5 \pm 0.7	96.6 \pm 0.8	0.38 \pm 0.01	-20.1 \pm 0.2

Standard deviations (SD) were calculated from the mean of the data of a series of five experiments conducted using the same parameters.

The fluorescence quantum yield and the excited-state lifetime are related by Eq. (10),

$$\Phi_F = k_r \tau \quad (10)$$

where $k_r = 1/\tau_r$ is the rate constant for radiative deactivation with fluorescence emission [27].

Taking this into account, we can conclude that the excited-state lifetimes of each compound are approximately constant for almost all the studied liposomes at 25 °C. Therefore, variations in fluorescence anisotropy at room temperature can be associated to changes in the rotational correlation time of the fluorescent compound and, thus, to changes in the microviscosity of its surrounding medium [2,29]. These considerations allow concluding that all compounds are mainly located in the inner region of the lipid membranes in the cases of egg-PC and DPPC.

The differences in anisotropy values between compounds in lipid membranes and in glycerol at room temperature can also be attributed to the distinct environment viscosities, as glycerol is much more viscous ($\eta = 993.4$ cP at 25 °C [23]) than lipid membranes (viscosities around 100–200 cP are usually reported [30,31]).

In DPPG aggregates, the anisotropy values are lower than in the other liposomes, but the maximum emission wavelengths point to an environment similar to that in egg-PC and DPPC. It may happen that some compound molecules are located at the exterior interface of the DPPG membranes, with a low anisotropy value (similar to that in water). This would facilitate hydrogen bonding between these thienopyridine derivatives and the OH groups of DPPG polar heads. In fact, in DPPG aggregates, a decrease in Φ_F values is detected (Table 3), more pronounced for compounds **1**, **3** and **4**, as observed for protic solvents (Table 1).

As referred, for the cationic lipid DODAB, a more hydrated environment is suggested from the results, probably near the lipid polar heads. The fluorescence anisotropy values in DODAB vesicles are always high at 25 °C, and this is consistent with the fact that the microviscosity decreases from the interface to the interior of the membrane [32,33], with a more pronounced variation when the membrane is in the liquid-crystalline phase [33].

3.3. Fluorescence studies in nanoliposome formulations

Considering future developments of drug delivery applications using nanoliposomes as carriers, several different liposome formulations were prepared [34–36], some of them containing cholesterol (Ch) and polyethylene glycol (PEG). The incorporation of Ch may increase the stability by modulating the fluidity of the lipid bilayer, preventing crystallization of the phospholipid acyl chains and providing steric hindrance to their movement. Recent advances in liposome research also found that PEG, while being

inert in the body, allows longer circulatory life of the drug delivery system [35].

It has been shown that the phospholipid DMPG provides the formation of pores across the lipid membrane [37], which have a promising biological relevance in applications for controlled release from nanocompartments [38]. It was also reported that DODAB-based liposomes usually exhibit very large sizes (diameter larger than 250 nm) [39–41] and, for this reason, this synthetic lipid was not used in the nanoliposome formulations studied with these compounds.

In the nanoliposome formulations prepared, the 6-(hetero)arylthienopyridine derivatives **1** and **2**, with the most promising antitumor potential [8] were encapsulated.

The size and size distribution (polydispersity index) of the prepared nanoliposomes with encapsulated antitumoral compounds **1** and **2** were obtained by Dynamic Light Scattering (DLS). Zeta-potential (ζ) values were also determined (Table 4).

All the liposomes have a mean hydrodynamic diameter lower than 165 nm, with the exception of the DPPC:DMPG (1:2) formulation with encapsulated compound **2**, that exhibits an abnormally large size (Table 4). Considering both compounds, the egg-PC:DSPE-PEG (9:1) and DPPC:DMPG:DSPE-PEG (1:1:0.1) formulations allowed us to obtain small nanoliposome diameters (below 100 nm) with lower polydispersity. The egg-PC:Ch (7:3) formulation is the one with the lowest polydispersity (Table 4), while the more polydisperse liposomes are those of DPPC:DMPG (1:1).

Zeta potential measurements are used to evaluate the relationship between surface charge and stability. The higher colloidal stability (lower aggregation tendency) is observed for DPPC:DMPG (1:2) liposomes (Table 4), that exhibit strong negative ζ -potential values. The lowest stability (higher aggregation tendency) is observed for both compounds in egg-PC/DSPE-PEG (9:1) and DPPC:Ch:DSPE-PEG (7:2:1) nanoliposome formulations, which exhibit a ζ -potential value clearly less negative than -30 mV. In general, particles with zeta potentials more positive than +30 mV or more negative than -30 mV are normally considered stable, with no tendency to flocculate. Comparing the same liposome formulation with incorporated compounds **1** and **2**, it can be concluded that the structure of the compound clearly influences both the size and zeta potential values. Liposomes with the thienopyridine **2** have a general tendency to a larger size (excluding most PEG-ylated formulations) and less negative ζ -potential. These results indicate that the encapsulated thienopyridine derivatives affect the physical characteristics of the nanoliposomes (size and surface charge).

Fluorescence emission spectra of thienopyridine derivatives **1** and **2** incorporated in nanoliposomes are displayed in Fig. 8. Both compounds **1** and **2** show significant fluorescence emission when incorporated in nanoliposomes (Fig. 8) and steady-state fluorescence anisotropy values are generally high at room temperature (Table 5).

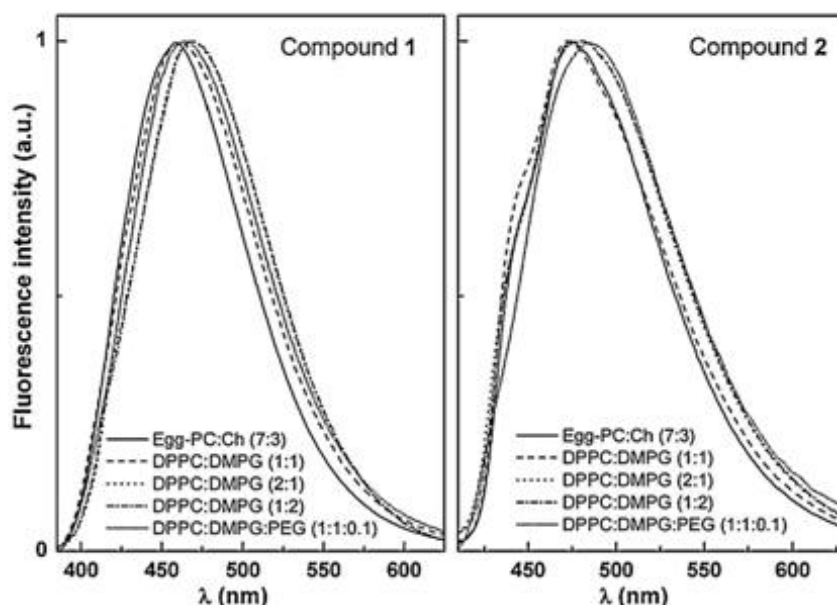


Fig. 8. Normalized fluorescence spectra of thienopyridine derivatives **1** and **2** in nanoliposomes of different compositions at room temperature.

Upon increasing temperature, both compounds exhibit a significant decrease in fluorescence anisotropy (Table 5), detecting an increase in fluidity of the nanoliposome membranes at high temperature. Therefore, both compounds are mainly located in the nanoliposome membranes. The maximum emission wavelength values (Table 5) indicate that thienopyridines **1** and **2** feel more hydrated environments in DPPC:DMPG (1:2) and DPPC:DMPG:DSPE-PEG (1:1:0.1) nanoliposomes. This can be attributed to the effect of DMPG that contributes to the formation of perforations across the lipid membranes [37,38], with a deeper penetration of water. Overall, these results indicate that both compounds can be transported in the hydrophobic region of the lipid bilayers.

Table 5

Steady-state fluorescence anisotropy (r) values and maximum emission wavelengths (λ_{em}) for compounds **1** and **2** encapsulated in nanoliposomes, at 25 °C and 50 °C.

		Compound 1		Compound 2	
		λ_{em} (nm)	r	λ_{em} (nm)	r
Egg-PC:Ch (7:3)	25 °C	457	0.239	474	0.191
Egg-PC:DSPE-PEG (9:1)	25 °C	458	0.225	475	0.221
DPPC:DMPG (1:1)	25 °C	462	0.266	473	0.258
	50 °C	463	0.159	474	0.169
DPPC:DMPG (2:1)	25 °C	465	0.253	478	0.240
	50 °C	467	0.181	477	0.181
DPPC:DMPG (1:2)	25 °C	469	0.258	481	0.257
	50 °C	468	0.166	482	0.168
DPPC:DMPG:DSPE-PEG (1:1:0.1)	25 °C	466	0.225	483	0.246
	50 °C	467	0.165	482	0.143
DPPC:Ch:DSPE-PEG (7:2:1)	25 °C	464	0.247	476	0.209
	50 °C	463	0.157	478	0.148
DPPC:DPPG:DSPE-PEG (1:1:0.1)	25 °C	456	0.258	476	0.242
	50 °C	457	0.146	477	0.169

4. Conclusions

The 6-(hetero)arylthieno[3,2-*b*]pyridine derivatives **1–4** exhibit reasonable fluorescence quantum yields and can be considered as solvatochromic probes.

Studies of incorporation of these compounds in neat lipid vesicles indicate that they are located mainly in the hydrophobic region of the lipid bilayers, experiencing the transition between the rigid gel and the fluid liquid-crystalline phases.

The potential antitumor thienopyridine derivatives **1** and **2** were also incorporated in different nanoliposome formulations, keeping in mind future drug delivery applications using liposomes as carriers. Fluorescence anisotropy values show that both compounds can be transported in the liposome bilayers. Almost all the liposomes with incorporated compounds are nanometric in size (diameter lower than 165 nm) and have generally low polydispersity. The formulation DPPC:DMPG:DSPE-PEG (1:1:0.1) allowed us to obtain small nanoliposome diameters (below 100 nm), with low polydispersity and reasonable negative zeta-potential values for both thienopyridines **1** and **2**, showing to be promising for drug delivery applications.

Acknowledgements

Foundation for the Science and Technology (FCT, Portugal), FEDER and QREN for financial support to the Research Centres, CFUM [Strategic Project PEst-C/FIS/UI0607/2011 (F-COMP-01-0124-FEDER-022711) and CQ/UM [Strategic Project PEst-C/QUI/UI0686/2011 (FCOMP-01-0124-FEDER-022716)], and to the research projects PTDC/QUI/81238/2006 (FCOMP-01-0124-FEDER-007467) and PTDC/QUI-QUI/111060/2009 (F-COMP-01-0124-FEDER-015603) also financed by COMPETE/QREN/EU. FCT, POPH-QREN and FSE are acknowledged for the PhD grant of M.S.D.C. (SFRH/BD/47052/2008) and for the Post-Doc. grants of A.S.A. (SFRH/BPD/25548/2005) and of R.C.C. (SFRH/BPD/68344/2010).

References

- [1] E.M.S. Castanheira, A.S. Abreu, M.S.D. Carvalho, M.-J.R.P. Queiroz, P.M.T. Ferreira, Fluorescence studies on potential antitumoral heteroaryl and heteroannulated indoles in solution and in lipid membranes, *Journal of Fluorescence* 19 (2009) 501–509.

- 66 M.S.D. Carvalho et al. / Journal of Photochemistry and Photobiology A: Chemistry 264 (2013) 56–66
- [2] E.M.S. Castanheira, A.S. Abreu, M.S.D. Carvalho, M.-J.R.P. Queiroz, P.M.T. Ferreira, P.J.G. Coutinho, N. Nazareth, M.S.-J. Nascimento, Fluorescence properties of a potential antitumoral benzothieno[3,2-b]pyrrole in solution and lipid membranes, *Journal of Photochemistry and Photobiology A: Chemistry* 206 (2009) 220–226.
 - [3] A.S. Abreu, E.M.S. Castanheira, M.-J.R.P. Queiroz, P.M.T. Ferreira, L.A. Vale-Silva, E. Pinto, Nanoliposomes for encapsulation and delivery of the potential antitumoral methyl 6-methoxy-3-(4-methoxyphenyl)-1H-indole-2-carboxylate, *Nanoscale Research Letters* 6 (2011), article 482.
 - [4] I. Hayakawa, R. Shioya, T. Agatsuma, H. Furukawa, Y. Sugano, Thienopyridine and benzofuran derivatives as potent anti-tumor agents possessing different structure–activity relationship, *Bioorganic & Medicinal Chemistry Letters* 14 (2004) 3411–3414.
 - [5] M.J. Munchhof, J.S. Beebe, J.M. Casavant, B.A. Cooper, J.L. Doty, R.C. Hidgon, S.M. Hillerman, C.I. Doderstrom, E.A. Knauth, M.A. Marx, A.M.K. Rossi, S.B. Sobolov, J. Sun, Design, SAR of thienopyrimidine and thienopyridine inhibitors of VEGFR-2 kinase activity, *Bioorganic & Medicinal Chemistry Letters* 14 (2004) 21–24.
 - [6] H.R. Heyman, R.R. Frey, P.F. Bousquet, G.A. Cunha, M.D. Moskey, A.A. Ahmed, N.B. Soni, P.A. Marcotte, L.J. Pease, K.B. Glaser, M. Yates, J.J. Bouska, D.H. Albert, C.L. Black-Schaefer, P.J. Dandliker, K.D. Stewart, P. Rafferty, S.K. Davidsen, M.R. Michaelides, M.L. Curtin, Thienopyridine urea inhibitors of KDR kinase, *Bioorganic & Medicinal Chemistry Letters* 17 (2007) 1246–1249.
 - [7] S. Claridge, F. Raepel, M.-C. Granger, N. Bernstein, O. Saavedra, L. Zhan, D. Llewellyn, A. Wahhab, R. Deziel, J. Rahil, N. Beaulieu, H. Nguyen, I. Dupont, A. Barsalou, C. Beaulieu, I. Chute, S. Gravel, M.-F. Robert, S. Lefebvre, M. Dubay, R. Pascal, J. Gillespie, Z. Jin, J. Wang, J.M. Besterman, A.R. MacLeod, A. Vaisburg, Discovery of a novel and potent series of thieno[3,2-b]pyridine-based inhibitors of c-Met and VEGFR-2 tyrosine kinases, *Bioorganic & Medicinal Chemistry Letters* 18 (2008) 2793–2798.
 - [8] M.-J.R.P. Queiroz, R.C. Calhelha, L.A. Vale-Silva, E. Pinto, R.T. Lima, M.H. Vasconcelos, Efficient synthesis of 6-(hetero)arylthieno[3,2-b]pyridines by Suzuki–Miyaura coupling. Evaluation of growth inhibition in human tumor cell lines, SARs and effects on the cell cycle, *European Journal of Medicinal Chemistry* 45 (2010) 5628–5634.
 - [9] J.N. Demas, G.A. Crosby, Measurement of photoluminescence quantum yields – review, *The Journal of Physical Chemistry* 75 (1971) 991–1024.
 - [10] S. Fery-Forgues, D. Lavabre, Are fluorescence quantum yields so tricky to measure? A demonstration using familiar stationary products, *Journal of Chemical Education* 76 (1999) 1260–1264.
 - [11] S.R. Meech, D. Phillips, Photophysics of some common fluorescence standards, *Journal of Photochemistry* 23 (1983) 193–217.
 - [12] J.R. Lakowicz, Principles of Fluorescence Spectroscopy, Kluwer Academic/Plenum Press, New York, 1999.
 - [13] N. Mataga, T. Kubota, Molecular Interactions and Electronic Spectra, Marcel Dekker, New York, 1970.
 - [14] N.G. Bakshshiev, Universal molecular interactions and their effects on the position of the electronic spectra of molecules in two component solutions. I Theory (liquid solutions), *Optics and Spectroscopy* 10 (1961) 379–384.
 - [15] N.G. Bakshshiev, Universal molecular interactions and their effects on the position of the electronic spectra of molecules in two component solutions, *Optics and Spectroscopy* 12 (1962) 309–313; *Optics and Spectroscopy* 13 (1962) 24–29.
 - [16] B.R. Lentz, Membrane fluidity as detected by diphenylhexatriene probes, *Chemistry and Physics of Lipids* 50 (1989) 171–190.
 - [17] E. Feitosa, P.C.A. Barreleiro, G. Olofsson, Phase transition in dioctadecyldimethyl-ammonium bromide and chloride vesicles prepared by different methods, *Chemistry and Physics of Lipids* 105 (2000) 201–213.
 - [18] J.S. Vincent, S.D. Revak, C.D. Cochrane, I.W. Levin, Interactions of model human pulmonary surfactants with a mixed phospholipid bilayer assembly: Raman spectroscopic studies, *Biochemistry* 32 (1993) 8228–8238.
 - [19] M.T. Lamy-Freund, K.A. Riske, The peculiar thermo-structural behavior of the anionic lipid DMPC, *Chemistry and Physics of Lipids* 122 (2003) 19–32.
 - [20] N.J. Turro, J.C. Scaiano, V. Ramamurthy, Modern molecular Photochemistry of Organic Molecules, University Science Books, Sausalito, CA, 2009.
 - [21] M.-J.R.P. Queiroz, S. Dias, D. Peixoto, A.R.O. Rodrigues, A.D.S. Oliveira, P.J.G. Coutinho, L.A. Vale-Silva, E. Pinto, E.M.S. Castanheira, New potential antitumoral di(hetero)arylether derivatives in the thieno[3,2-b]pyridine series: synthesis and fluorescence studies in solution and in nanoliposomes, *Journal of Photochemistry and Photobiology A: Chemistry* 238 (2012) 71–80.
 - [22] M.-J.R.P. Queiroz, D. Peixoto, A.R.O. Rodrigues, P. Mendes, C.N.C. Costa, P.J.G. Coutinho, E.M.S. Castanheira, New 1,3-diarylureas linked by C-C Suzuki coupling to the methyl 3-aminothieno[3,2-b]pyridine-2-carboxylate moiety: synthesis and fluorescence studies in solution and in lipid membranes, *Journal of Photochemistry and Photobiology A: Chemistry* 255 (2013) 27–35.
 - [23] D.R. Lide (Ed.), Handbook of Chemistry and Physics, 83th ed., CRC Press, Boca Raton, 2002.
 - [24] M.J. Frisch, G.W. Trucks, H.B. Schlegel, G.E. Scuseria, M.A. Robb, J.R. Cheeseman, G. Scalmani, V. Barone, B. Mennucci, G.A. Petersson, H. Nakatsuji, M. Caricato, X. Li, H.P. Hratchian, A.F. Izmaylov, J. Bloino, G. Zheng, J.L. Sonnenberg, M. Hada, M. Ehara, K. Toyota, R. Fukuda, J. Hasegawa, J. Ishida, T. Nakajima, Y. Honda, O. Kitao, H. Nakai, T. Vreven, J.A. Montgomery Jr., J.E. Peralta, F. Ogliaro, M. Bearpark, J.J. Heyd, E. Brothers, K.N. Kudin, V.N. Staroverov, R. Kobayashi, J. Normand, K. Raghavachari, A. Rendell, J.C. Burant, S.S. Iyengar, J. Tomasi, M. Cossi, N. Rega, J.M. Millam, M. Klene, J.E. Knox, J.B. Cross, V. Bakken, C. Adamo, J. Jaramillo, R. Gomperts, R.E. Stratmann, O. Yazyev, A.J. Austin, R. Cammi, C. Pomelli, J.W. Ochterski, R.L. Martin, K. Morokuma, V.G. Zakrzewski, G.A. Voth, P. Salvador, J.J. Dannenberg, S. Dapprich, A.D. Daniels, Ö. Farkas, J.B. Foresman, J.V. Ortiz, J. Cioslowski, D.J. Fox, Gaussian 09, Revision A.02, Gaussian, Inc., Wallingford, CT, 2009.
 - [25] F. Jensen, Introduction to Computational Chemistry, John Wiley & Sons, West Sussex, England, 1999.
 - [26] D. Papahadjopoulos, N. Miller, Phospholipid model membranes. I Structural characteristics of hydrated liquid crystals, *Biochimica et Biophysica Acta* 135 (1967) 624–638.
 - [27] B. Valeur, Molecular Fluorescence – Principles and Applications, Wiley-VCH, Weinheim, 2002.
 - [28] S.J. Strickler, R.A. Berg, Relationship between absorption intensity and fluorescence lifetime of molecules, *Journal of Chemical Physics* 37 (1962) 814.
 - [29] A.S. Abreu, E.M.S. Castanheira, P.J.G. Coutinho, M.-J.R.P. Queiroz, P.M.T. Ferreira, L.A. Vale-Silva, E. Pinto, Interaction of antitumoral fluorescent heteroaromatic compounds, a benzothienopyrrole and two thienoindoles, with DNA and lipid membranes, *Journal of Photochemistry and Photobiology A: Chemistry* 240 (2012) 14–25.
 - [30] J.N. Israelachvili, S. Marcelja, R.G. Horn, Physical principles of membrane organization, *Quarterly Reviews of Biophysics* 13 (1980) 121–200.
 - [31] D.B. Kell, C.M. Harris, On the dielectrically observable consequences of the diffusional motions of lipids and proteins in membranes. 1. Theory and overview, *European Biophysics Journal* 12 (1985) 181–197.
 - [32] L. Tilley, K.R. Thulborn, W.H. Sawyer, An assessment of the fluidity gradient of the lipid bilayer as determined by a set of *n*-(9-anthroyloxy)fatty acids (*n* = 2, 6, 9, 12, 16), *Journal of Biological Chemistry* 254 (1979) 2592–2594.
 - [33] M.A. Bahri, B.J. Heyne, P. Hans, A.E. Seret, A.A. Mouithys-Mickalad, M.D. Hoebeke, Quantification of lipid bilayer effective microviscosity and fluidity effect induced by propofol, *Biophysical Chemistry* 114 (2005) 53–61.
 - [34] M.R. Mozafari, V. Hasirci, Mechanism of calcium ion induced multilamellar vesicle DNA interaction, *Journal of Microencapsulation* 15 (1998) 55–65.
 - [35] Y. Ran, S.H. Yalkowsky, Halothane, a novel solvent for the preparation of liposomes containing 2'-4'-amino-3'-methylphenyl benzothiazole (AMPB), an anticancer drug: a technical note, *AAPS PharmSciTech* 4 (2003) (article 20).
 - [36] N. Berger, A. Sachse, J. Bender, R. Schubert, M. Brandl, Filter extrusion of liposomes using different devices: comparison of liposome size, encapsulation efficiency, and process characteristics, *International Journal of Pharmaceutics* 223 (2001) 55–68.
 - [37] K.A. Riske, L.Q. Amaral, H.-G. Döbereiner, M.T. Lamy, Mesoscopic structure in the chain-melting regime of anionic phospholipid vesicles: DMPC, *Biophysical Journal* 86 (2004) 3722–3733.
 - [38] R.P. Barroso, K.R. Perez, I.M. Cuccovia, M.T. Lamy, Aqueous dispersions of DMPC in low salt contain leaky vesicles, *Chemistry and Physics of Lipids* 165 (2012) 169–177.
 - [39] Y. Malam, M. Loizidou, A.M. Seifalian, Liposomes and nanoparticles: nanosized vehicles for drug delivery in cancer, *Trends in Pharmacological Sciences* 30 (2009) 592–599.
 - [40] L.R. Tsuruta, A.M. Carmona-Ribeiro, Counterion effects on colloid stability of cationic vesicles and bilayer-covered polystyrene microspheres, *Journal of Physical Chemistry* 100 (1996) 7130–7134.
 - [41] E.M.S. Castanheira, M.S.D. Carvalho, A.R.O. Rodrigues, R.C. Calhelha, M.-J.R.P. Queiroz, New potential antitumoral fluorescent tetracyclic thieno[3,2-b]pyridine derivatives: Interaction with DNA and nanosized liposomes, *Nanoscale Research Letters* 6 (2011), article 379.

Benzothienoquinolines: new one pot synthesis and fluorescence studies of their interaction with DNA and polynucleotides

M.Solange D. Carvalho, A. Rita O. Rodrigues, João A.V. Cardoso, Ricardo C. Calhela, Elisabete M.S. Castanheira, Maria-João R.P. Queiroz, manuscript to be submitted for publication.

My contribution to this paper was the photophysical studies in several solvents, and fluorescence studies of the interaction with DNA, including fluorescence quenching.

Benzothienoquinolines: new one-pot synthesis and fluorescence studies of their interaction with DNA and polynucleotides

M. Solange D. Carvalho,^{1,2} A. Rita O. Rodrigues,¹ João A. V. Cardoso¹, Ricardo C. Calhelha,² Elisabete M.S. Castanheira,^{1,*} Maria-João R. P. Queiroz^{2,*}

¹*Centro de Física (CFUM), Universidade do Minho, Campus de Gualtar, 4710-057 Braga, Portugal*

²*Centro de Química, Universidade do Minho, Campus de Gualtar, 4710-057 Braga, Portugal*

Manuscript to be submitted to an international journal

ABSTRACT

In this work we were able to obtain the benzothieno[3,2-*b*]quinoline **1** and benzothieno[2,3-*c*]quinoline **2** using a new one pot procedure from the reaction of the commercial available 3-bromobenzo[*b*]thiophene-2-carbaldehyde with 2-aminophenylpinacolborane under Suzuki coupling conditions using a stereochemically hindered ligand, 2-(cyclohexylphosphane)biphenyl and Ba(OH)₂·8H₂O as the base.

Fluorescence properties of the benzothieno[3,2-*b*]quinoline **1** and the benzothieno[2,3-*c*]quinoline **2** were studied in solvents of different polarity. Both compounds exhibit a solvent sensitive emission, compound **1** being less fluorescent ($\Phi_F < 0.05$) than compound **2** ($0.04 \leq \Phi_F \leq 0.10$).

The interaction of these compounds with salmon sperm DNA and synthetic double-stranded heteropolynucleotides, poly(dA-dT)·(dA-dT) and poly(dG-dC)·(dG-dC), was studied using spectroscopic methods, allowing the determination of the intrinsic binding constants and binding site sizes. The interaction of both compounds is stronger with adenine-thymine (A-T) base pairs. Compound **1** is the most intercalative in salmon sperm DNA (47%) and polynucleotides (46%-49% of intercalated molecules), while for compound **2**, 41% is intercalated in salmon sperm DNA and only 8% in poly(dG-dC)·(dG-dC). Overall, these

results point to a predominant interaction of both compounds to nucleic acids by groove binding.

KEYWORDS: Benzothieno[3,2-*b*]quinoline, Benzothieno[2,3-*c*]quinoline, DNA interaction, polynucleotides, binding constants.

1. INTRODUCTION

The investigation of the nature and dynamics of the binding of small molecules to biomacromolecules is actually an active area of research [1,2]. DNA interaction studies are important to understand the mechanism of action of antitumor and antiviral drugs and to design new DNA-targeted drugs [3,4]. Three different modes of binding to DNA have been described: intercalation into the base pairs, in the major or minorgrooves, and outside the double helix by electrostatic interactions. Small molecules are stabilized on groove binding and intercalation with DNA through a series of associative interactions such as π -stacking, hydrogen bonding, attractive van der Waals and hydrophobic interactions [4]. DNA intercalation seems to be an essential, but not sufficient, step for antitumoral activity [3].

Benzothieno[3,2-*b*]quinoline **1** [5] and benzothieno[2,3-*c*]quinoline **2** [6] are known for their anti-plasmodic and anti-infectious activities, acting mainly through intercalation between DNA base pairs when used in their salt form. Earlier synthesized by separated reactions and in several steps [5,6], in this work we were able to obtain the two compounds in a one pot procedure.

The interactions of the biologically active compounds with nucleic acids have been studied using a variety of techniques [7-11], including absorption and fluorescence spectroscopies. The binding of the fluorescent polycyclic molecules to DNA can be conveniently investigated by these methods, because their absorption and emission properties significantly change on complex formation [7,12,13]. Fluorescence quenching experiments using external quenchers have been used to establish the DNA-binding modes, since intercalated fluorophores are less accessible to anionic quenchers, due to electrostatic repulsion with the negatively charged DNA backbone [13-15].

In this work, the interaction of the synthesized benzothienoquinolines **1** and **2** with natural double-stranded salmon sperm DNA and with synthetic *ds*-polyheteronucleotides was

investigated by fluorescence emission measurements. These studies are important due to the biological relevance of both compounds as potential antitumorals.

2. EXPERIMENTAL

2.1. Synthesis

General remarks

Melting points (°C) were determined in a SMP3 Stuart apparatus and are uncorrected. ¹H and ¹³C NMR spectra were recorded on a Varian Unity Plus at 300 and 75.4 MHz, respectively. Heteronuclear correlations, ¹H-¹³C, HMQC or HMBC were performed to attribute some signals. HRMS data were recorded using a method of direct injection by EI by the mass spectrometry service of the University of Vigo, Spain. The reactions were monitored by thin layer chromatography (TLC) in aluminium plates covered with a layer of silica gel 60 (Macherey-Nagel) of 0.2 mm, with UV254 fluorescence indicator. Column chromatography was performed using silica-gel 230-400 mesh. Petroleum ether refers to the 40-60 °C boiling range fraction.

One pot synthesis of benzotieno[3,2-*b*]quinoline 1 and benzotieno[2,3-*c*]quinoline 2: To a solution of 3-bromobenzo[*b*]thiophene-2-carbaldehyde (150 mg, 0.600 mmol) in dioxane (5 mL) Pd(AcO)₂ (5 mol%), 2-(cyclohexylphosphane)biphenyl (20 mol%), Ba(OH)₂·8H₂O (3 equiv.) and 2-aniline pinacolborane (170 mg, 0.780 mmol). The mixture was heated at 100 °C for 5h. After cooling, H₂O and AcOEt were added and the phases were separated. The organic phase was dried (MgSO₄), filtered and the removal of the solvent gave an oil which was submitted to column chromatography using solvent gradient from neat petroleum ether to 20% ether/petroleum ether and the two products were separated.

Compound **1** was the major product and was isolated using 10% ether/petroleum ether (45.0 mg, 30 %), p.f. 173-175 °C [5]. ¹H NMR (CDCl₃, 300 MHz): δ 7.55-7.67 (3H, m, Ar-H), 7.74-7.81 (1H, m, Ar-H), 7.84-7.94 (2H, m, Ar-H), 8.31 (1H, d, J = 8.4 Hz, Ar-H), 8.59 (1H, s, 11-H), 8.66-8.71 (1H, m, Ar-H) ppm. ¹³C NMR (CDCl₃, 75.4 MHz): δ 123.04 (CH), 124.01 (CH), 125.08 (CH), 126.19 (CH), 126.60 (C), 127.08 (CH), 128.89 (11-CH), 129.06 (CH), 129.42 (CH), 129.90 (CH), 130.61 (C), 134.14 (C), 141.17 (C), 146.44 (C), 153.96 (C). MS

(EI): m/z (%) 235 (M^+ , 100). HRMS M^+ : Calculated for $C_{15}H_9NS$: 235.0456; Found: 235.0449.

Compound **2** was isolated using 20% ether/petroleum ether (28.0 mg, 20 %), p.f. 123-125 °C [6]. 1H NMR ($CDCl_3$, 300 MHz): δ 7.61-7.70 (2H, m, Ar-H), 7.74-7.82 (2H, m, Ar-H), 8.05-8.11 (1H, m, Ar-H), 8.30-8.36 (1H, m, Ar-H), 8.84-8.94 (2H, m, Ar-H), 9.37 (1H, s, 6-H) ppm. ^{13}C NMR ($CDCl_3$, 75.4 MHz): δ 122.92 (CH), 123.77 (CH), 125.39 (CH+C), 126.04 (CH), 127.49 (CH), 127.51 (CH), 127.76 (CH), 130.81 (CH), 133.37 (C), 135.15 (C), 135.37 (C), 141.35 (C), 145.56 (C), 145.65 (6-CH) [6b]. MS (EI): m/z (%) 235 (M^+ , 100). HRMS M^+ : Calculated for $C_{15}H_9NS$: 235.0456; Found: 235.0457.

The data for both compounds are identical to those presented in earlier works [5,6].

2.2. Spectroscopic measurements

Absorption spectra were recorded in a Shimadzu UV-3101PC UV-Vis-NIR spectrophotometer. Fluorescence measurements were performed using a Fluorolog 3 spectrofluorimeter, equipped with double monochromators in both excitation and emission and a temperature-controlled cuvette holder. For fluorescence quantum yield determination, the solutions were previously bubbled for 30 minutes with ultrapure nitrogen. Fluorescence spectra were corrected for the instrumental response of the system.

The fluorescence quantum yields (Φ_s) were determined using the standard method (equation 1) [16,17] and 9,10-diphenylanthracene in ethanol as reference, $\Phi_r = 0.95$ at 25 °C [18].

$$\Phi_s = \left[\frac{A_r F_s n_s^2}{A_s F_r n_r^2} \right] \Phi_r \quad (1)$$

where A is the absorbance at the excitation wavelength, F the integrated emission area and n the index of refraction of the solvents used. Subscripts refer to the reference (r) or sample (s) compound.

All solutions were prepared using spectroscopic grade solvents and Milli-Q grade water. Natural double-stranded salmon sperm DNA was obtained from Invitrogen, while synthetic double-stranded heteropolynucleotides, poly(dA-dT)·(dA-dT) and poly(dG-dC)·(dG-dC), were obtained from Sigma-Aldrich. Salmon sperm DNA, polynucleotides and compounds stock solutions were prepared in 10^{-2} M Tris-HCl buffer (pH=7.2), with 10^{-3} M EDTA. The purity of DNA was checked by monitoring the absorption spectrum and the ratio of the

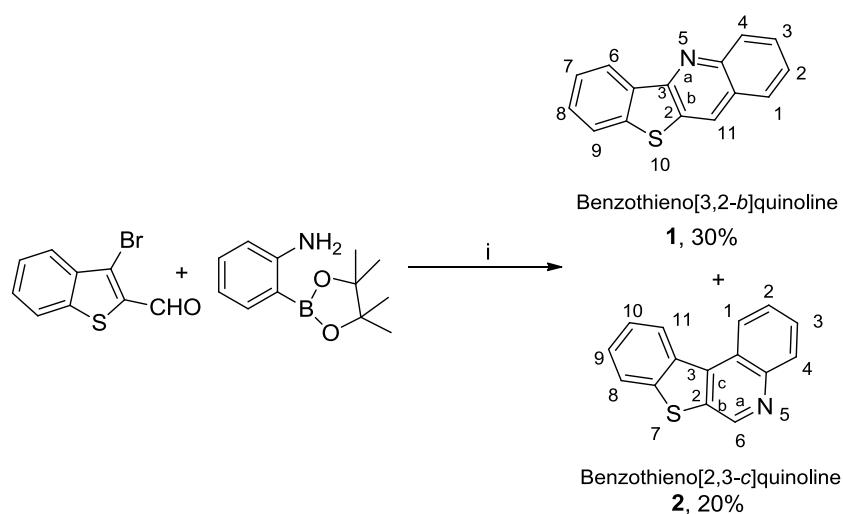
absorbance at 260 and 280 nm, $A_{260}/A_{280}=1.95$ (good-quality DNA has an A_{260}/A_{280} ratio higher than 1.8) [19]. The DNA and polynucleotide concentrations in number of bases (or phosphate groups) were determined from the molar absorption coefficients [12], $\epsilon=6600 \text{ M}^{-1} \text{ cm}^{-1}$ at 260 nm for DNA, $\epsilon=8400 \text{ M}^{-1} \text{ cm}^{-1}$ at 254 nm for poly(dG–dC)·(dG–dC) and $\epsilon=6600 \text{ M}^{-1} \text{ cm}^{-1}$ at 260 nm for poly(dA–dT)·(dA–dT).

The absorption and emission spectra of several solutions with different [nucleic acid]/[compound] ratios using the same compound concentration ($2 \times 10^{-6} \text{ M}$) were recorded. The solutions were left 24 h to stabilize. The absorbance at excitation wavelengths was always less than 0.1, in order to avoid inner filter effects. All measurements were performed at room temperature ($25.0 \pm 0.5 \text{ }^\circ\text{C}$). Binding analysis of the experimental data was performed according to McGhee and von Hippel model [20] to determine the intrinsic binding constants and the binding site sizes.

3. RESULTS AND DISCUSSION

3.1. Synthesis

The reaction of the commercial available 3-bromobenzo[*b*]thiophene-2-carbaldehyde with 2-aminophenylpinacolborane under Suzuki coupling conditions using a stereochemically hindered ligand as 2-(cyclohexylphosphane)biphenyl [21] and $\text{Ba}(\text{OH})_2 \cdot 8\text{H}_2\text{O}$ as the base, gave in a one pot procedure compounds **1** and **2** which were separated by column chromatography (**Scheme 1**).



i) $\text{Pd}(\text{OAc})_2$ (5 mol%), 2-(cyclohexylphosphane)biphenyl (20 mol%), $\text{Ba}(\text{OH})_2 \cdot 8\text{H}_2\text{O}$ (3 equiv.), dioxane, $100 \text{ }^\circ\text{C}$.

Scheme 1. One pot synthesis of benzothieno[3,2-*b*]quinoline **1** and benzothieno[2,3-*c*]quinoline **2**.

Although these compounds have already been synthesized by other authors in several steps, we were able to prepare them in a one pot procedure which is very advantageous to save reagents and time.

The synthesis of the benzothieno[3,2-*b*]quinoline **1** was unexpected using these reaction conditions. It seems that it is the result of a Pd-catalyzed C-N coupling followed by an intramolecular cyclization that may perhaps occur by nucleophilic attack of the activated *ortho* position of the diarylamine intermediate on the carbonyl of the aldehyde, after deboronation. In the synthesis of the expected compound **2**, a Suzuki cross-coupling and a nucleophilic attack of the amino group on the aldehyde occurred.

3.2. Fluorescence studies in several solvents

The absorption and fluorescence properties of compounds **1** and **2** were studied in several solvents of different polarity. The maximum absorption (λ_{abs}) and emission wavelengths (λ_{em}) and fluorescence quantum yields (Φ_{F}) of both compounds in several solvents are presented in Table 1. The normalized fluorescence spectra are shown in Figures 2 and 3 (examples of absorption spectra are also shown as insets).

Compounds **1** and **2** exhibit fluorescence emission in several polar and non-polar media, including water. Fluorescence quantum yield values are generally low, varying from 2% to 10% (Table 1), the benzothieno[2,3-*c*]quinoline **2** being the more fluorescent compound. A red-shift and loss of vibrational structure is observed for the emission in polar solvents, this effect being more pronounced for compound **1** (red shifts between cyclohexane and water are 48 nm for compound **1** and 28 nm for compound **2**). As in the absorption spectra the red shifts are negligible (Table 1), this behavior indicates that solvent relaxation after photoexcitation plays an important role, especially for the benzothieno[3,2-*b*]quinoline **1**. This predicts a higher ICT character of the excited state for the latter compound.

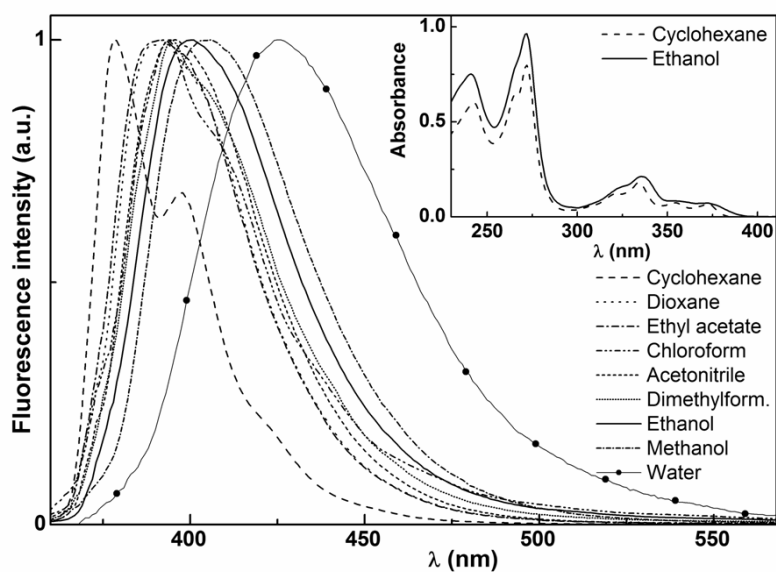


Figure 2. Normalized fluorescence spectra of solutions (3×10^{-6} M) of compound **1** ($\lambda_{\text{exc}}=335$ nm) in several solvents. Inset: absorption spectra of 2×10^{-5} M solutions of compound **1** in cyclohexane and ethanol, as examples.

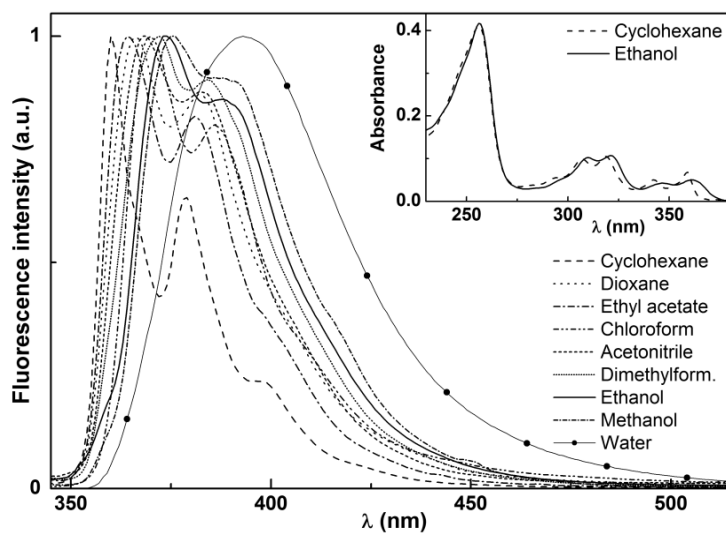


Figure 3. Normalized fluorescence spectra of solutions (3×10^{-6} M) of compound **2** ($\lambda_{\text{exc}}=325$ nm) in several solvents. Inset: Absorption spectra of 10^{-5} M solutions of compound **2** in cyclohexane and ethanol, as examples.

Table 1. Maximum absorption (λ_{abs}) and emission wavelengths (λ_{em}) and fluorescence quantum yields (Φ_{F}) of compounds **1** and **2** in several solvents.

Solvent	$\lambda_{\text{abs}}(\text{nm})$		$\lambda_{\text{em}}(\text{nm})$		$\Phi_{\text{F}}^{\text{a}}$	
	1	2	1	2	1	2
Cyclohexane	372, 354, 334, 272, 243	359, 342, 319, 307, 256	378	364	0.02	0.07
Dioxane	372, 354, 335, 272, 242	359, 343, 320, 308, 257	392	367	0.03	0.10
Ethylacetate ^b	371, 353, 334, 271	358, 342, 318, 307	393	365	0.02	0.08
Dichloromethane	372, 354, 336, 273, 243	360, 344, 321, 309, 257	392	370	0.02	0.06
Chloroform ^b	374, 356, 337, 274	361, 345, 322, 310, 258	394	372	0.02	0.04
Acetonitrile	371, 353, 334, 270, 241	358, 342, 319, 307, 255	394	369	0.02	0.05
<i>N,N</i> -Dimethylformamide ^b	372, 355, 335	360, 344, 320, 309	395	384	0.04	0.08
Dimethylsulfoxide ^b	373, 356, 337	360, 344, 322, 310	403	374	0.03	0.08
Ethanol	372, 336, 272, 241	361, 347, 321, 310, 256	401	374	0.03	0.09
Methanol	371, 336, 271, 240	361, 346, 321, 310, 256	406	375	0.02	0.07
Water	372, 336, 271, 240	362, 349, 321, 311, 255	426	392	0.01	0.06

^aRelative to 9,10-diphenylanthracene in ethanol ($\Phi_{\text{R}}=0.95$) [18]. Error about 10%.

^bSolvents *cut-off*: Chloroform: 250 nm; Ethyl acetate: 265 nm; *N,N*-dimethylformamide: 280 nm. Dimethylsulfoxide: 275 nm.

The fluorescence quantum yields in protic solvents tend to decrease with increasing solvent hydrogen bonding capability (Φ_{F} in ethanol > Φ_{F} in methanol > Φ_{F} in water), may be due to an increase of S→T intersystem crossing efficiency through H-bond formation between these quinoline derivatives and protic solvents, probably by protonation of the N atom of the pyridine moiety. A similar behaviour has been observed previously for other compounds synthesized by us and containing a pyridine ring, namely several thieno[3,2-*b*]pyridine derivatives [22-24]. The formation of hydrogen bonds between chloroform and these proton acceptor quinoline derivatives can also explain the lower fluorescence quantum yield values in this solvent [25,26].

3.3. Interaction with salmon sperm DNA and with synthetic double-stranded polynucleotides

The interaction of compounds **1** and **2** with natural double-stranded salmon sperm DNA was studied by fluorescence. Changes in absorption spectra upon DNA interaction are negligible, as previously observed for other neutral aromatic compounds already studied by some of us, namely tetracyclic lactams [27] and thieno[3,2-*b*]pyridine derivatives [24]. Figures 4 and 5 show the emission spectra of the benzothienoquinolines **1** and **2** with increasing [DNA]/[compound] ratio, where [DNA] is expressed in number of bases or

phosphate groups. For both quinoline derivatives, spectral invariance with increasing DNA concentration occurs for the ratio $[\text{DNA}]/[\text{compound}]=100$, indicating that total compound binding is achieved at this $[\text{DNA}]/[\text{compound}]$ ratio (spectra corresponding to ratio 100 and 120 are overlapped).

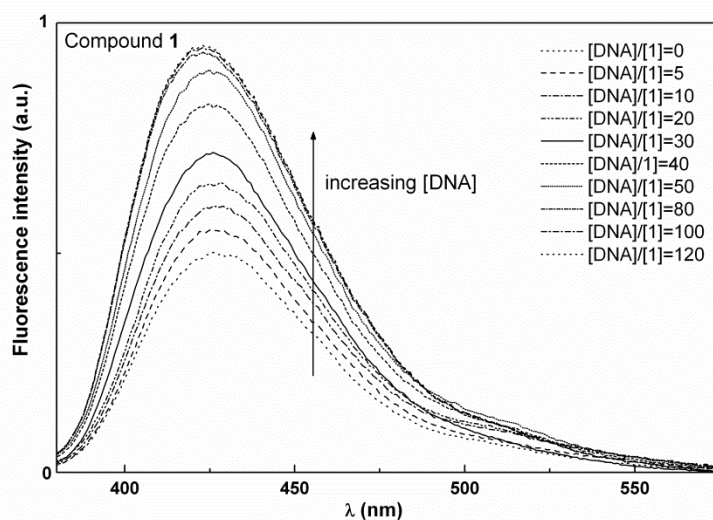


Figure 4. Fluorescence spectra of the benzothienoquinoline **1** (2×10^{-6} M) in 10 mM Tris-HCl buffer (pH = 7.2), with increasing DNA content.

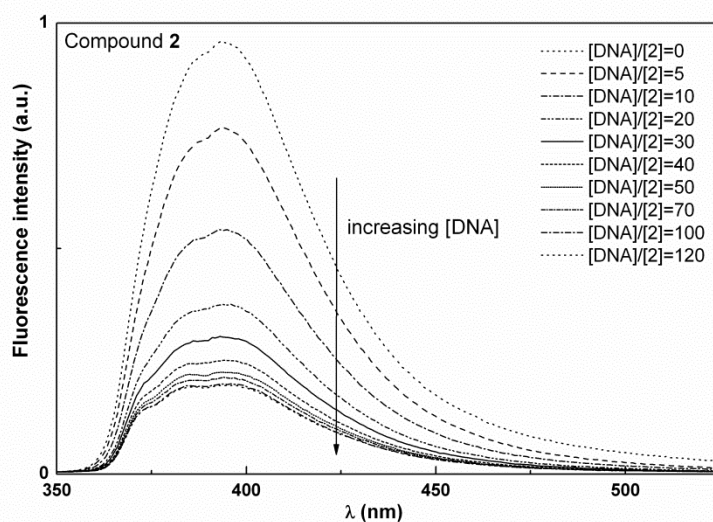


Figure 5. Fluorescence spectra of the benzothienoquinoline **2** (2×10^{-6} M) in 10 mM Tris-HCl buffer (pH = 7.2), with increasing DNA content.

An enhancement in emission intensity with increasing DNA concentration is observed for compound **1**, while the opposite occurs for compound **2** (figure 6). This may indicate a

different type of interaction of the two benzothienoquinolines with DNA bases, as already observed for other tetracyclic compounds [24,27]. The high [DNA]/[compound] ratio needed for total binding, together with the negligible changes observed in absorption spectra (not shown), point to a weak interaction of these molecules with the nucleic acid, which is also a common behavior with tetracyclic thienopyridine derivatives [24].

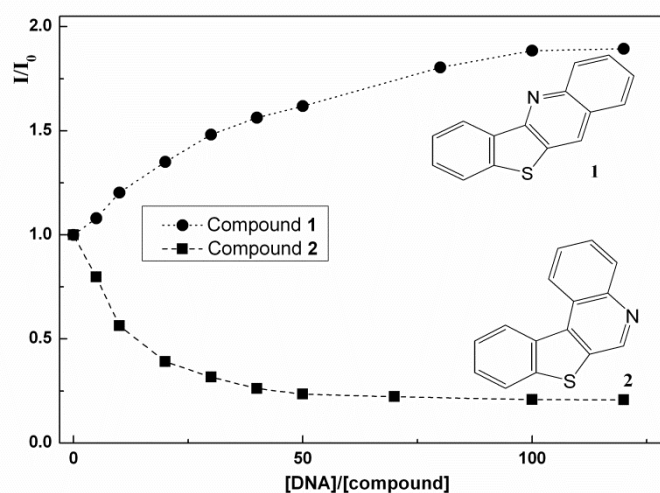


Figure 6. Fluorescence intensities ratio in the presence (I) and absence (I_0) of DNA for compounds **1** and **2** at several [DNA]/[compound] molar ratios.

To clarify the different behavior of the two quinolines, the base sequence binding preference was also investigated, using synthetic *ds*-heteropolynucleotides, poly(dA-dT)·(dA-dT) and poly(dG-dC)·(dG-dC). Figure 7 displays the ratio of maximum emission intensities in the presence (I) and absence (I_0) of *ds*-heteropolynucleotides for several [nucleic acid]/[compound] ratios, for compounds **1** and **2**, respectively. The behaviour in heteropolynucleotides is similar to that in salmon sperm DNA, with a rise in fluorescence intensity with increasing polynucleotide concentration for compound **1** and a decrease for compound **2**. However, the stabilization in emission intensity, indicative of full binding, is attained at a significantly lower molar ratio for poly(dA-dT)·(dA-dT) ([nucleotide]/[compound]=60 and 80, respectively for compound **1** and **2**). For poly(dG-dC)·(dG-dC), the stabilization is attained at a molar ratio of 100 for both quinolines, similarly to the behavior observed with salmon sperm DNA.

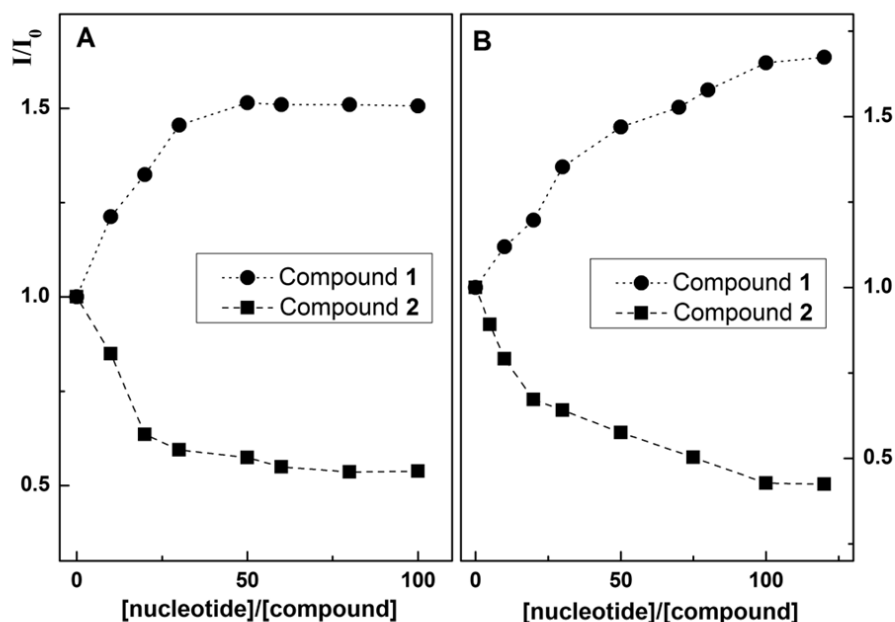


Figure 7. Fluorescence intensities ratio in the presence (I) and absence (I_0) of heteropolynucleotides for the benzothienoquinolines **1** and **2** at several [nucleotide]/[compound] molar ratios. **A:** Poly(dA-dT)·poly(dA-dT); **B:** poly(dG-dC)·poly(dG-dC).

The binding constants and binding site sizes were determined by the modified Scatchard equation, given by McGhee and von Hippel [20]

$$\frac{r}{c_f} = K_i (1 - nr) [(1 - nr) / [1 - (n - 1)r]]^{n-1} \quad (2)$$

where K_i is the intrinsic binding constant, n is the binding site size in base pairs, r is the ratio c_b /[nucleic acid], c_b and c_f are the concentrations of bound and free compound, respectively, calculated by

$$c_b = \frac{I_{F,0} - I_F}{I_{F,0} - I_{F,b}} \times c_{\text{total}} \quad ; \quad c_{\text{total}} = c_f + c_b \quad (3)$$

being $I_{F,0}$ the fluorescence intensity of the free compound and $I_{F,b}$ the fluorescence intensity of the bound compound at total binding.

The fluorescence measurements results were fitted by least squares methods to obtain the values of the binding constants (K_i) and the number of base pairs between consecutive intercalated compound molecules (n). The results are presented in Table 2.

Table 2. Values of binding constants (K_i) and binding site sizes (n) for benzothienoquinolines interaction with DNA and synthetic heteropolynucleotides.

	Nucleic acid	K_i (M^{-1})	n
Compound 1	salmon sperm DNA	$(2.6 \pm 0.3) \times 10^5$	14 ± 5
	poly(dA-dT)·(dA-dT)	$(3.0 \pm 0.4) \times 10^5$	13 ± 5
	poly(dG-dC)·(dG-dC)	$(5.9 \pm 0.6) \times 10^4$	35 ± 9
Compound 2	salmon sperm DNA	$(2.9 \pm 0.3) \times 10^5$	16 ± 6
	poly(dA-dT)·(dA-dT)	$(3.1 \pm 0.4) \times 10^5$	14 ± 5
	poly(dG-dC)·(dG-dC)	$(4.5 \pm 0.5) \times 10^4$	25 ± 9

It has already been reported that small variations in the structure of tetracyclic compounds, as differences only in the substituent groups, influence strongly the interaction with nucleic acids [13,24,27], either by changes in the main mechanism and/or by affecting the magnitude of interaction (binding constant and binding site size). As both compounds exhibit a stronger interaction with poly(dA-dT)·poly(dA-dT) than with poly(dG-dC)·(dG-dC) (higher binding constants and lower binding site sizes in the former), it can be concluded that the main interaction in DNA is established with A-T base pairs. The mechanism of photoinduced electron transfer between compounds and DNA bases is not expected to occur, as this kind of interaction depends strongly on the bases structure [28,29]. A more likely mechanism for the intercalation of these compounds in nucleic acids is the π -stacking.

Fluorescence quenching experiments with iodide ion were also performed for compounds 1 and 2 in the presence of DNA and heteropolynucleotides. The quenching data were first plotted according to the Stern-Volmer relation (equation 4) [30],

$$\frac{I_0}{I} = 1 + K_{SV}[Q] \quad (4)$$

where I_0 and I are, respectively, the fluorescence intensities in the absence and in the presence of quencher (I), K_{SV} is the Stern-Volmer constant and $[Q]$ is the quencher concentration.

In all cases, Stern-Volmer plots are non-linear (figure 8, as an example), with a downward curvature. This means that not all the fluorescent molecules are accessible to the quencher. In this case, the system contains heterogeneously emitting sites, in which some compound molecules are accessible to the quencher and other molecules are not accessible. Thus, the Stern-Volmer equation must be modified [31] as (5):

$$\frac{I_0}{\Delta I} = \frac{1}{f_a} + \frac{1}{f_a K_{SV}[Q]} \quad (5)$$

where $\Delta I = I_0 - I$, f_a is the accessibility to quencher. From the plots of $I_0/\Delta I$ vs. $1/[Q]$, it is possible to obtain the accessibilities to the anionic quencher. The results are summarized on Table 3.

Table 3. Values of the accessibilities (f_a) to the quencher (Γ) and Stern-Volmer constants for compounds **1** and **2** bound to DNA and heteropolynucleotides.

	Nucleic acid	K_{SV} (M^{-1})	f_a
Compound 1	Salmon sperm DNA	4.65	0.53
	poly(dA-dT)·(dA-dT)	9.33	0.54
	poly(dG-dC)·(dG-dC)	11.1	0.51
Compound 2	Salmon sperm DNA	8.61	0.59
	poly(dA-dT)·(dA-dT)	9.54	0.63
	poly(dG-dC)·(dG-dC)	6.1	0.92

Anionic quenchers can be used to distinguish between DNA binding modes [14,15,31]. Intercalated chromophores are less accessible to quenching by iodide ion due to electrostatic repulsion between the negatively charged DNA and iodide anion [15]. Compounds which are bound at the DNA surface (groove binding or electrostatic binding) are more accessible and, therefore, emission from these molecules can be quenched more efficiently. As these benzothienoquinolines are neutral molecules, electrostatic binding to nucleic acids is not anticipated. Therefore, the fraction of compound molecules accessible to the external quencher (f_a) should correspond to bound molecules at the grooves.

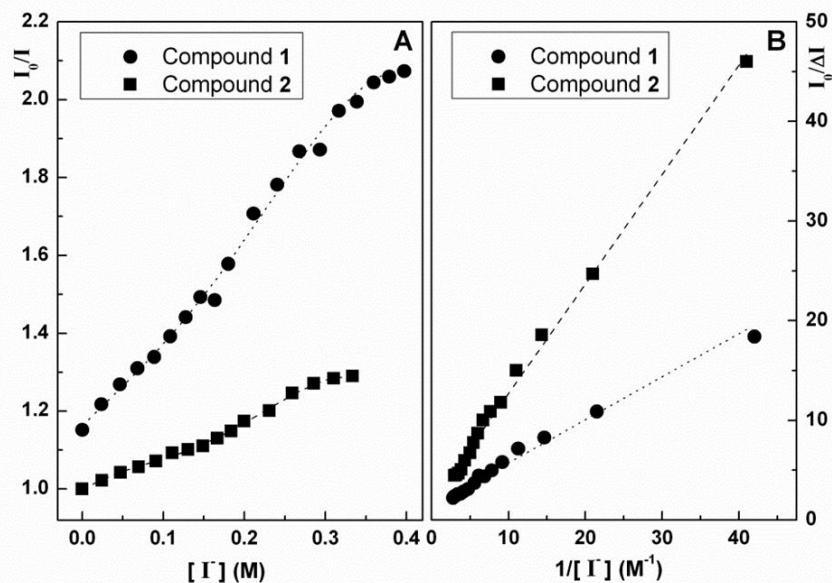


Figure 8. **A:** Stern-Volmer plots for quenching with iodide ion (I^-) for compounds **1** and **2** with salmon sperm DNA. **B:** Corresponding modified Stern-Volmer plots.

The fraction of intercalated molecules into salmon sperm DNA and heteropolynucleotides is higher for the benzothienoquinoline **1** (46% to 49%). On the contrary, compound **2** presents a very small fraction of intercalated molecules (8%) in poly(dG-dC).(dG-dC), while in poly(dA-dT).(dA-dT) the percentage is similar to the observed in natural DNA (around 40%). As both compounds are neutral molecules, the relatively high value for f_a for compounds **1** and **2** may indicate that the main type of binding of these quinoline derivatives to DNA must be the groove binding [24,27] (electrostatic interaction is not expected), being compound **1** the more intercalative one.

CONCLUSIONS

A new one pot method was achieved for the synthesis of benzothieno[3,2-*b*]quinoline **1** and benzothieno[2,3-*c*]quinoline **2** by the reaction from the reaction of the commercial available 3-bromobenzo[*b*]thiophene-2-carbaldehyde with 2-aminophenylpinacolborane under Suzuki coupling conditions using a stereochemically hindered ligand, 2-(cyclohexylphosphane)biphenyl and $Ba(OH)_2 \cdot 8H_2O$ as the base. Although the compounds have already been synthesized earlier by other authors using several steps, our methodology is advantageous saving reagents and time. Both compounds are fluorescent and present a solvent sensitive emission, despite the low fluorescence quantum yields (below 10%).

The benzothieno[3,2-*b*]quinoline **1** is the most intercalative compound in DNA and synthetic heteropolynucleotides. Both compounds exhibit a stronger interaction with A-T than with G-C base pairs, exhibiting higher binding constants and smaller binding site sizes. Fluorescence quenching measurements allowed concluding that the main mechanism of interaction of these quinoline derivatives is the binding in the DNA grooves.

ACKNOWLEDGEMENTS

Foundation for the Science and Technology (FCT, Portugal), FEDER and QREN for financial support to the Research Centres, CFUM [Strategic Project PEst-C/FIS/UI0607/2011 (F-COMP-01-0124-FEDER-022711) and CQ/UM [Strategic Project PEst-C/QUI/UI0686/2011 (FCOMP-01-0124-FEDER-022716)], and to the research project PTDC/QUI-QUI/111060/2009 (F-COMP-01-0124-FEDER-015603) also financed by COMPETE/QREN/EU. FCT, POPH-QREN and FSE are acknowledged for the PhD grants of M.S.D.C. (SFRH/BD/47052/2008) and A.R.O.R. (SFRH/BD/90949/2012) and for the Post-Doc. Grant of R.C.C. (SFRH/BPD/68344/2010).

REFERENCES

- [1] Yang, X.-L.; Wang, A.H.-J. (1999) Structural studies of atom-specific anticancer drugs acting on DNA. *Pharmacol. Ther.* 83:181-215
- [2] McGown, L. B.; Joseph, M. J.; Pitner, J. B.; Vonk, G. P.; Linn, C. P. (1995) The nucleic-acid ligand - A new tool for molecular recognition. *Anal. Chem.* 67:663A-668A
- [3] Lyne, P.D. (2002) Structure-based virtual screening: an overview. *Drug Disc. Today* 7:1047-1055
- [4] Mahadevan, S.; Palaniandavar, M. (1997) Spectroscopic and voltammetric studies of copper(II) complexes of bis(pyrid-2-yl)-di/trithia ligands bound to calf thymus DNA. *Inorg. Chim. Acta* 254:291-302
- [5] Zhu, X.Y.; Mardenborough, L.G.; Li, S.M.; Khan, A.; Zhang, W.; Fan, P.C.; Jacob, M.; Khan, S.; Walker, L.; Ablordeppey, S.Y. (2007) Synthesis and evaluation of isosters of

- N*-methylindole[3,2-*b*]quinoline (cryptolepine) as new anti-infective. *Bioorg. Med. Chem.* 15:686-695
- [6] a) McKenney, Jr., J. D.; Castle, R. N. (1987) The synthesis of [1]benzothieno[2,3-*c*]quinolines, [1]benzothieno[2,3-*c*][1,2,4]triazolo[4,3-*a*]quinoline and [1]benzothieno[2,3-*c*]tetrazolo[1,5-*a*]quinoline. *J. Heterocycl. Chem.* 24: 1525-1529. b) Zektzer, A. Z., Quast, M. J.; Linz, G. S.; Martin, G. E.; McKenney, J. D.; Johnston, Jr., M. D.; Castle, R. N. (1986) New pulse sequence for long-range two dimensional heteronuclear chemical shift correlation. *Magn. Reson. Chem.* 24:1083-1088
- [7] Dougherty, G.; Pilbrow, J.R. (1984) Physicochemical probes of intercalation. *Int. J. Biochem.* 16:1179-1192
- [8] Fritzsche, H.; Akhebat, A.; Taillandier, E.; Rippe, K.; Jovin, T. M. (1993) Structure and drug-interactions of parallel-stranded DNA studied by infrared-spectroscopy and fluorescence. *Nucleic Acid Res.* 21:5085-5091
- [9] Pang, D.; Abruna, H. D. (1998) Micromethod for the investigation of the interactions between DNA and redox active molecules. *Anal. Chem.* 70:3162-3169
- [10] Gane, P. J.; Dean, P.M. (2000) Recent advances in structure-based rational drug design. *Curr. Opin. Struct. Biol.* 10:401-404
- [11] Graves, D. E.; Velea, L. M. (2000) Intercalative binding of small molecules to nucleic acids. *Curr. Org. Chem.* 4:915-929
- [12] Renault, E.; Fontaine-Aupart, M.P.; Tfibel, F.; Gardes-Albert, M.; Bisagni, E. (1997) Spectroscopic study of the interaction of pazelliptine with nucleic acids. *J. Photochem. Photobiol. B: Biol.* 40:218-227
- [13] Queiroz, M.-J.R.P.; Castanheira, E.M.S.; Carvalho, M.S.D.; Abreu, A.S.; Ferreira, P.M.T.; Karadeniz, H.; Arzum, E. (2008) New tetracyclic heteroaromatic compounds based on dehydroamino acids: photophysical and electrochemical studies of interaction with DNA. *Tetrahedron* 64:382-391
- [14] Kumar, C.V.; Asuncion, E.H. (1993) DNA-binding studies and site-selective fluorescence sensitization of an anthryl probe. *J. Am. Chem. Soc.* 115:8547-8553
- [15] Kumar, C.V.; Punzalan, E.H.A.; Tan, W.B. (2000) *Tetrahedron* 56:7027-7040

- [16] Demas, J. N.; Crosby, G. A. (1971) Measurement of photoluminescence quantum yields – Review. *J. Phys. Chem.* 75:991-1024
- [17] Fery-Forgues, S.; Lavabre, D.J. (1999) Are fluorescence quantum yields so tricky to measure? A demonstration using familiar stationary products. *J. Chem. Educ.* 76:1260-1264
- [18] Morris, J. V.; Mahaney, M. A.; Huber, J. R. (1976) Fluorescence quantum yield determinations – 9,10-diphenylanthracene as a reference-standard in different solvents. *J. Phys. Chem.* 80:969-974
- [19] Cao, Y.; He, X.-w. (1998) Studies of interaction between Safranin T and double helix DNA by spectral methods. *Spectrochim. Acta, Part A* 54:883-892
- [20] McGhee, J. D.; von Hippel, P. H. (1974) Theoretical aspects of DNA-protein interactions – Cooperative and non-cooperative binding of large ligands to a one-dimensional homogeneous lattice. *J. Mol. Biol.* 86:469-489
- [21] Thompson, W. J.; Jones, J. H.; Lyle, P. A.; Thies, J. E. (1988) An efficient synthesis of arylpyrazines and bipyridines. *J. Org. Chem.* 53: 2052-2055.
- [22] Queiroz, M.-J. R. P.; Dias, S.; Peixoto, D.; Rodrigues, A. R. O.; Oliveira, A. D. S.; Coutinho, P. J. G.; Vale-Silva, L. A.; Pinto, E.; Castanheira, E. M. S. (2012) New potential antitumoral di(hetero)arylether derivatives in the thieno[3,2-*b*]pyridine series: Synthesis and fluorescence studies in solution and in nanoliposomes. *J. Photochem. Photobiol. A: Chem.* 238:71-80
- [23] Queiroz, M.-J. R. P.; Peixoto, D.; Rodrigues, A. R. O.; Mendes, P. M. F.; Costa, C. N. C.; Coutinho, P. J. G.; Castanheira, E. M. S. (2013) New 1,3-diarylureas linked by C-C Suzuki coupling to the methyl 3-aminothieno[3,2-*b*]pyridine-2-carboxylate moiety: synthesis and fluorescence studies in solution and in lipid membranes. *J. Photochem. Photobiol. A: Chem.* 255:27-35
- [24] Castanheira, E. M. S.; Carvalho, M. S. D.; Rodrigues, A. R. O.; Calhella, R. C.; Queiroz, M.-J.R.P. (2011) New potential antitumoral fluorescent tetracyclic thieno[3,2-*b*]pyridine derivatives: Interaction with DNA and nanosized liposomes. *Nanoscale Res. Lett.* 6:379
- [25] James, K. C.; Noyce, P. R. (1971) Hydrogen bonding between testosterone propionate and solvent in chloroform-cyclohexane solutions. *Spectrochim. Acta A* 27:691-696

- [26] Wiley, G. R.; Miller, S. I. (1972) Thermodynamic parameters for hydrogen-bonding of chloroform with Lewis bases in cyclohexane - Proton magnetic-resonance study. *J. Am. Chem. Soc.* 94:3287-3293
- [27] Queiroz, M.-J. R. P.; Castanheira, E. M. S.; Lopes, T. C. T.; Cruz, Y. K.; Kirsch, G. (2007) Synthesis of fluorescent tetracyclic lactams by a “one pot” three steps palladium-catalyzed borylation, Suzuki coupling (BSC) and lactamization. DNA and polynucleotides binding studies. *J. Photochem. Photobiol. A: Chem.* 190:45-52
- [28] Shafirovich, V. Y.; Levin, P. P.; Kuzmin, V. A.; Thorgeirsson, T. E.; Kliger D. S.; Geacintov, N. E. (1994) Photoinduced electron transfer and enhanced triplet yields in benzo[*a*]pyrene derivative-nucleic acid complexes and covalent adducts, *J. Am. Chem. Soc.* 116:63-72
- [29] Real Oliveira, M. E. C. D.; Baptista, A. L. F.; Coutinho, P. J. G.; Castanheira, E. M. S.; Hungerford, G. (2004) Fluorescence studies of the interaction of pyrenylmethyl tributylphosphonium bromide with double-strand polynucleotides. *Photochem. Photobiol. Sci.* 3:217-225
- [30] Valeur, B. (2002) *Molecular Fluorescence – Principles and Applications*, Wiley–VCH, Weinheim.
- [31] Lehrer, S.S. (1971) Solute perturbation of protein fluorescence. Quenching of tryptophyl fluorescence of model compounds and of lysozyme by iodide ion. *Biochemistry* 10:3254-3263

Chapter 6

Conclusions and future perspectives

As outlined in the Abstract the spectroscopic properties of several classes of potential antitumoral heterocyclic compounds, derivatives of indoles, benzo[*b*]thiophenes and thieno[3,2-*b*]pyridines, synthesized in our research group, were studied in different environments, like solvents of different polarity, liposomes and in the presence of nucleic acids.

All compounds exhibited a solvent sensitive emission, with red-shifts in polar solvents.

For the planar tetracyclic compounds, either derivatives of thieno[3,2-*b*]pyridines or of benzo[*b*]thiophenes, the interaction with nucleic acids, which may be important for the antitumoral activity, was also evaluated by fluorescence. Experiments of fluorescence quenching using iodide anion indicated that the groove binding is the main type of interaction, some of the compounds exhibiting also a significant intercalation.

The intrinsic fluorescence of the compounds was used to monitor the location and behaviour in nanoliposomes of neat lipids and lipid mixtures of different formulations, keeping in mind drug delivery applications using these systems as carriers.

Future work is envisaged, considering applications of the most promising compounds as antitumoral drugs:

- Evaluation of the interaction and internalization of the nanoliposomes with incorporated compounds, with human tumor cell lines.
- Development of nanoliposomes labeled with folate or transferrin in order to enhance the interaction with the tumor cells.
- Development of magnetoliposomes (liposomes entrapping magnetic nanoparticles) with incorporated antitumoral compounds. These systems allow the exact location in the therapeutic site of interest, through the use of an external magnetic field.

